LOS ANGELES PUBLIC LIBRARY

JUN 24 1960

SCIENCE & TECHNOLOGY

ARS JOURNAL

A PUBLICATION OF THE AMERICAN ROCKET SOCIETY

VOLUME 30 NUMBER 6 JUNE 1960

BIND

SURVEY ARTICLE

Physics of Artificial Electron Clouds . . . . . F. F. Marmo, L. M. Aschenbrand and J. Pressman 523

CONTRIBUTED ARTICLES

Ideal Performance of Multistage Rockets . . . . . Richard D. Geckler 531

Orbits for Planetary Satellites From Doppler Data Alone . . Armin J. Deutsch 536

Detonation Wave Hypersonic Ramjet . . . . W. H. Sargent and R. A. Gross 543

Design of UHF Multipliers for Space Probe Communications . . . . . Leonard R. Malling 550

TECHNICAL NOTES

Determination of Diffusion Coefficients From Asymmetric Concentration Profiles . . . . . A. W. Blackman 557

Angular Displacement of a Magnetized Sphere by the Terrestrial Magnetic Field During Vertical Descent . . . . . Marvin H. Hewitt 558

Calculation of Electrical Conductivity of Ionized Gases . . . . . A. Sherman 559

Approximation of Optimum Thrust Nozzle Contour . . . . . G. V. R. Rao 561

Estimating Transient Temperature Distributions During Ablation . . M. Richard Denison 562

Isentropic Compression of Shock Tube Driver Gas . . . . . R. J. Stalker 564

An Approximate Analytic Solution of Re-Entry Trajectory With Aerodynamic Forces . . . . . Kenneth Wang and Lu Ting 565

Pressure-Density-Temperature Relationship of Liquid O_2 . . . . . Eugene A. Trachenko 566

Analog Network to Convert Surface Temperature to Heat Flux . . . . . G. T. Skinner 569

Elliptical Orbit Characteristics . . . . . G. S. Gedeon and B. J. Greer 570

Comparison of Transpiration and Ablation Cooling . Curtis C. Bensman and Joel Weisman 573

Combustion Instability in Solid Propellant Rocket Motors . . . . . E. W. Price 574

DEPARTMENTS

Technical Comments 576

Book Reviews 578

Technical Literature Digest 580

FORECAST

Laboratories for space science at Martin are now studying and forecasting the physical, psychological, and biological factors that will affect man in space . . . another tremendously fascinating program which attracts persons with exceptional professional abilities. If you have these abilities, you are invited to communicate with N. M. Pagan, Director of Technical and Scientific Staffing (Dept. 4-D) The Martin Company, P. O. Box 179, Denver 1, Colorado.

MARTIN
DENVER DIVISION

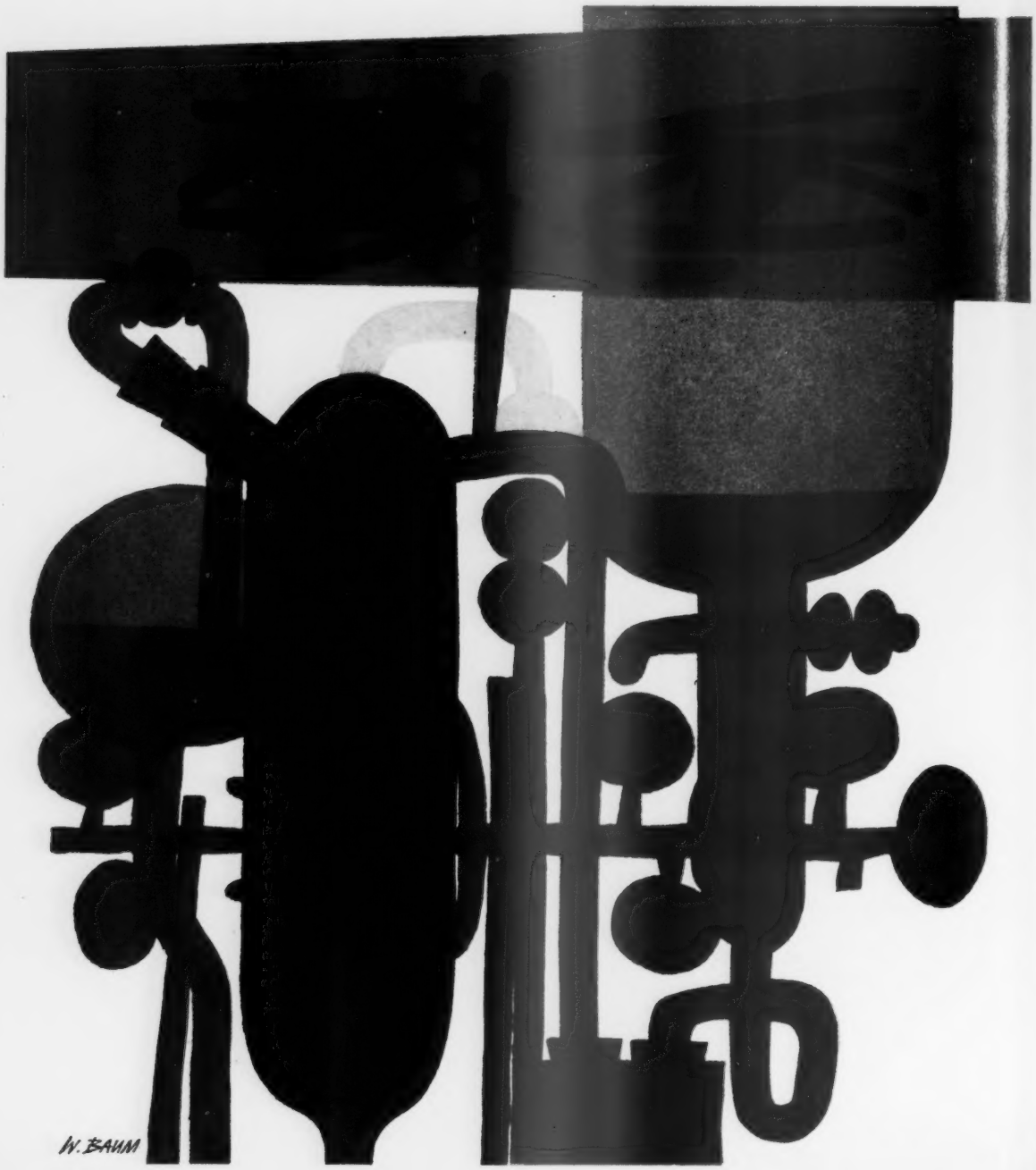

Is a FUNDAMENTAL Research Program Worthwhile?

Normal binary eutectic structure (250X)

New binary eutectic structure (250X)

We, at the Research Laboratories, are convinced that it is worthwhile. For example, one of the fundamental scientific programs being undertaken is a study of the mechanism of solidification of polyphase alloys.

This study is still in its early stages. However, we now have a better understanding of the solidification process. And we have demonstrated that the microstructure of certain eutectics can be significantly altered by controlled solidification. The contrast is illustrated above.

It is possible that these binary alloys with preferred orientation may have unusual physical and mechanical properties.

Perhaps you are interested in corporate–sponsored studies into the fundamental nature of matter. If so, we can offer a research environment that seems to stimulate scientists to extra achievement. It may be due to the way we encourage an internal cross-fertilization of ideas; or because of a unique complex of complementary services that free the scientist from routine analysis and experimental chores.

Opportunities for scientists in the physics of solids, liquids, gases, and plasmas. Current studies range from the fundamental properties of matter to the application of scientific knowledge to promising new products.

• • •

For more specific information, please write to Mr. W. F. Walsh, at the Research Laboratories.

RESEARCH LABORATORIES
UNITED AIRCRAFT CORPORATION
400 Main Street, East Hartford 8, Conn.

UAC RESEARCH

Wiley BOOKS

AERO-THERMODYNAMICS AND FLOW IN TURBOMACHINES

By MICHAEL H. VAVRA, *U. S. Naval Postgraduate School*. Designed to give an understanding of flow phenomena and to show rational methods for formulating them mathematically. This is done by using a theoretical approach stressing basic physical processes rather than empirical methods. In combining this approach with his own experience the reader will gain an idea of design possibilities.

Part I sets up basic flow relations applying to any branch of fluid mechanics. Part II covers types more closely related to flow in machines, and Part III is directly concerned with flow in machines. One of the book's most valuable features is its use of vector- and tensor-analysis to establish fundamental flow relations. *1960. 609 pages. $14.50*

THE AERODYNAMICS OF POWERED FLIGHT

By R. L. CARROLL, *Bell Aircraft Corp*. A simple, direct and new approach: 1) lift is shown to be directly dependent on power; 2) rocket power is regarded as the logical lift source; and 3) transition is made at this point to questions of powered flight with aerodynamic lift. *1960. 275 pages. $8.50.*

PHYSICS AND MEDICINE OF THE ATMOSPHERE AND SPACE

Edited by MAJ. GEN. OTIS O. BENSON, JR., *and* DR. HUBERTUS STRUGHOLD, *both of USAF Aerospace Medical Center, Brooks Air Force Base*. A symposium sponsored by the School of Aviation Medicine and arranged by Southwest Research Institute. Stresses the environment of man in space—extreme conditions of space flight and effects of gravitational, radiational, and magnetic fields. Also: space vehicles, weightlessness, and other topics. *1960. 645 pages. $12.50.*

SURFACE EFFECTS ON SPACECRAFT MATERIALS

Edited by F. J. CLAUSS, *Lockheed Aircraft Corp*. Record of a first symposium, covering methods for calculating required characteristics, available materials, laboratory techniques for measuring radiation characteristics, and effects of space environment on behavior of materials. *1960. 404 pages. $11.50.*

THEORY OF THERMAL STRESSES

By B. A. BOLEY *and* J. H. WEINER, *Columbia University*. Unites thermodynamical foundations and practical material of interest to engineers and researchers. Both thermal stress and theory of heat conduction are covered. *1960. Approx. 590 pages. Prob. $15.50*

SEND NOW FOR ON-APPROVAL COPIES

JOHN WILEY & SONS, INC.
440 PARK AVENUE SOUTH, NEW YORK 16, N. Y.

ARS JOURNAL

A PUBLICATION OF THE AMERICAN ROCKET SOCIETY

EDITOR — Martin Summerfield
ASSOCIATE TECHNICAL EDITOR — Irvin Glassman
MANAGING EDITOR — Barbara Nowak
ART EDITOR — John Culin
CONTRIBUTOR — George F. McLaughlin

ASSOCIATE EDITORS

J. George Adashko, *Russian Supplement;* Ali Bulent Cambel, *Northwestern University, Book Reviews;* Igor Jurkevich, *G. E. Space Sciences Laboratory, Russian Articles;* Charles J. Mundo Jr., *Raytheon Manufacturing Co., Guidance;* Bernard H. Paiewonsky, *Aeronautical Research Associates of Princeton, Flight Mechanics;* M. H. Smith, *Princeton University, Technical Literature Digest*

ASSISTANT EDITORS

Julie Hight, Carol Rubenstein, Estelle Viertel

ADVERTISING AND PROMOTION MANAGER

William Chenoweth

ADVERTISING PRODUCTION MANAGER

Walter Brunke

ADVERTISING REPRESENTATIVES

New York
D. C. Emery and Associates
400 Madison Ave., New York, N. Y.
Telephone: Plaza 9-7460

Los Angeles
James C. Galloway and Co.
6535 Wilshire Blvd., Los Angeles, Calif.
Telephone: Olive 3-3223

Chicago
Jim Summers and Associates
35 E. Wacker Dr., Chicago, Ill.
Telephone: Andover 3-1154

Detroit
R. F. Pickrell and Vincent Purcell
318 Stephenson Bldg., Detroit, Mich.
Telephone: Trinity 1-0790

Boston
Robert G. Melendy
17 Maugus Ave., Wellesley Hills, Mass.
Telephone: Cedar 5-6503

Pittsburgh
John W. Foster
239 4th Ave., Pittsburgh, Pa.
Telephone: Atlantic 1-2977

American Rocket Society

500 Fifth Avenue, New York 36, N. Y.

Founded 1930

OFFICERS

President — Howard S. Seifert
Vice-President — Harold W. Ritchey
Executive Secretary — James J. Harford
Treasurer — Robert M. Lawrence
General Counsel — Andrew G. Haley
Director of Publications — Irwin Hersey

BOARD OF DIRECTORS

Terms expiring on dates indicated

Ali B. Cambel	1962	William H. Pickering	1961
Richard B. Canright	1962	Simon Ramo	1960
James R. Dempsey	1961	William L. Rogers	1960
Herbert Friedman	1962	David G. Simons	1961
Robert A. Gross	1962	John L. Sloop	1961
Samuel K. Hoffman	1960	Martin Summerfield	1962
A. K. Oppenheim	1961	Wernher von Braun	1960
		Maurice J. Zucrow	1960

TECHNICAL COMMITTEE CHAIRMEN

Ali B. Cambel, Magnetohydrodynamics
William H. Dorrance, Hypersonics
James S. Farrior, Guidance and Navigation
Herbert Friedman, Physics of the Atmosphere and Space
George Gerard, Structures and Materials
Martin Goldsmith, Liquid Rockets
Andrew G. Haley, Space Law and Sociology
Samuel Herrick, Astrodynamics
Maxwell W. Hunter, Missiles and Space Vehicles
David B. Langmuir, Ion and Plasma Propulsion
Max A. Lowy, Communications
Irving Michelson, Education
Peter L. Nichols Jr., Propellants and Combustion
Eugene Perchonok, Ramjets
Richard A. Schmidt, Test, Operations and Support
John I. Shafer, Solid Rockets
C. J. Wang, Nuclear Propulsion
Stanley C. White, Human Factors and Bioastronautics
George F. Wislicenus, Underwater Propulsion
John E. Witherspoon, Instrumentation and Control
Abe M. Zarem, Power Systems

Scope of ARS JOURNAL

This Journal is devoted to the advancement of astronautics through the dissemination of original papers disclosing new scientific knowledge and basic applications of such knowledge. The sciences of astronautics are understood here to embrace selected aspects of jet and rocket propulsion, spaceflight mechanics, high speed aerodynamics, flight guidance, space communications, atmospheric and outer space physics, materials and structures, human engineering, overall system analysis, and possibly certain other scientific areas. The selection of papers to be printed will be governed by the pertinence of the topic to the field of astronautics, by the current or probable future significance of the research, and by the importance of distributing the information to the members of the Society and to the profession at large.

Information for Authors

Manuscripts must be as brief as the proper presentation of the ideas will allow. Exclusion of dispensable material and conciseness of expression will influence the Editors' acceptance of a manuscript. In terms of standard-size double-spaced typed pages, a typical maximum length is 22 pages of text (including equations), 1 page of references, 1 page of abstract and 12 illustrations. Fewer illustrations permit more text, and vice versa. Greater length will be acceptable only in exceptional cases.

Short manuscripts, not more than one quarter of the maximum length stated for full articles, may qualify for publication as Technical Notes or Technical Comments. They may be devoted to new developments requiring prompt disclosure or to comments on previously published papers. Such manuscripts are published within a few months of the date of receipt.

Sponsored manuscripts are published occasionally as an ARS service to the industry. A manuscript that does not qualify for publication, according to the above-stated requirements as to subject, scope or length, but which nevertheless deserves widespread distribution among jet propulsion engineers, may be printed as an extra part of the Journal or as a special supplement, if the author or his sponsor will reimburse the Society for actual publication costs. Estimates are available on request. Acknowledgment of such financial sponsorship appears as a footnote on the first page of the article. Publication is prompt since such papers are not in the ordinary backlog.

Manuscripts must be double spaced on one side of paper only with wide margins to allow for instructions to printer. Include a 100 to 200 word abstract. State the authors' positions and affiliations in a footnote on the first page. Equations and symbols may be handwritten or typewritten; clarity for the printer is essential. Greek letters and unusual symbols should be identified in the margin. If handwritten, distinguish between capital and lower case letters, and indicate subscripts and superscripts. References are to be grouped at the end of the manuscript and are to be given as follows. For journal articles: Authors first, then title, journal, volume, year, page numbers; for books: Authors first, then title, publisher, city, edition and page or chapter numbers. Line drawings must be clear and sharp to make clear engravings. Use black ink on white paper or tracing cloth. Lettering should be large enough to be legible after reduction. Photographs should be glossy prints, not matte or semi-matte. Each illustration must have a legend; legends should be listed in order on a separate sheet.

Manuscripts must be accompanied by written assurance as to security clearance in the event the subject matter lies in a classified area or if the paper originates under government sponsorship. Full responsibility rests with the author.

Preprints of papers presented at ARS meetings are automatically considered for publication.

Submit manuscripts in duplicate (original plus first carbon, with two sets of illustrations) to the Managing Editor, ARS JOURNAL, 500 Fifth Avenue, New York 36, N.Y.

ARS JOURNAL is published monthly by the American Rocket Society, Inc. and the American Interplanetary Society at 20th & Northampton Sts., Easton, Pa., U. S. A. Editorial offices: 500 Fifth Ave., New York 36, N. Y. Price: $12.50 per year, $2.00 per single copy. Second-class mail privileges authorized at Easton, Pa. This publication is authorized to be mailed at the special rates of postage prescribed by Section 132.122. Notice of change of address should be sent to the Secretary, ARS, at least 30 days prior to publication. Opinions expressed herein are the authors' and do not necessarily reflect the views of the Editors or of the Society.
© Copyright 1960 by the American Rocket Society, Inc.

Scientific objectivity characterizes the examination of natural forces in the experimental laboratories at Los Alamos.

Original painting by Emil Bisttram, Taos, N.M.

For employment information write: Personnel Director Division 60-51

los alamos scientific laboratory

LOS ALAMOS, NEW MEXICO

EXCELCO

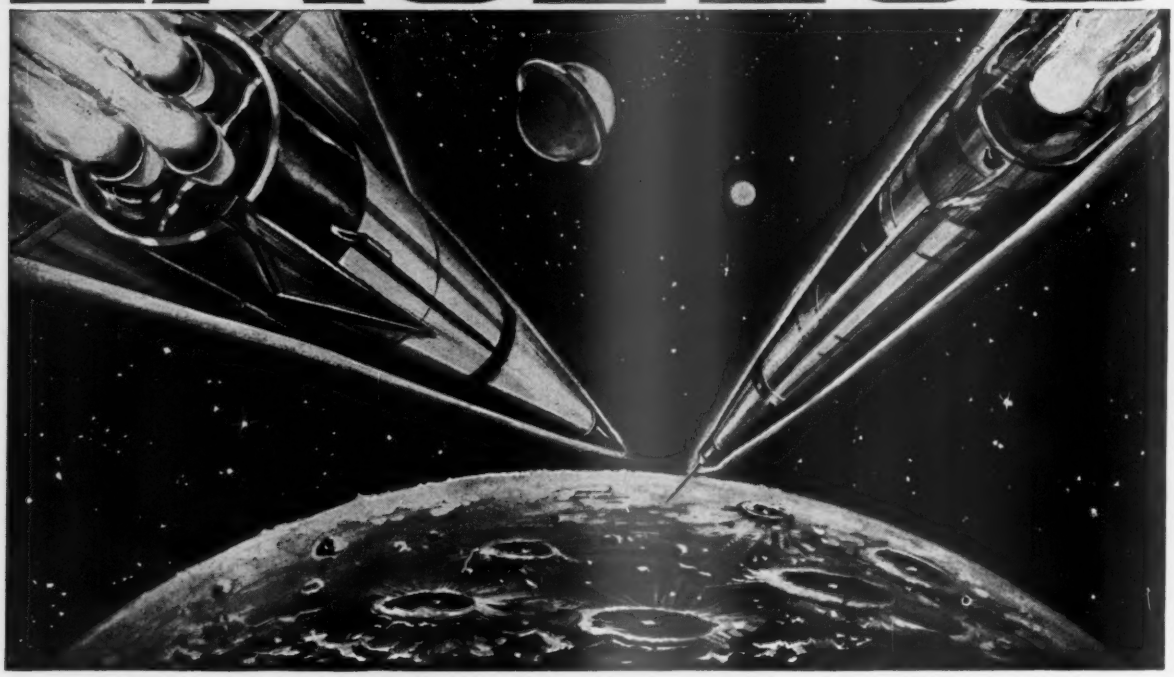

RV-A-10 • SERGEANT
AIR FORCE — RE-ENTRY X-17
POLARIS — RE-ENTRY X-36
JUPITER JR. • JUPITER SR.
POLARIS 0 • POLARIS A
POLARIS AIX • POLARIS A2-MOD 1-2-3
NIKE HERCULES • NIKE ZEUS
MINUTEMAN • PERSHING
N.A.S.A. PROGRAMS • SCOUT
LITTLE JOE

•

and many other classified projects

Builders of more large, thin wall, high strength solid propellant rocket engine cases and nozzles for development purposes than any other company in America.

A small experienced organization geared to handle your development and prototype requirements for static and flight tests in the shortest possible time.

Call or write:

EXCELCO DEVELOPMENTS

MILL STREET • SILVER CREEK, NEW YORK

CTF

ideal storable oxidizer

Investigate the many advantages of Chlorine Trifluoride (ClF_3) as a rocket fuel oxidizer!

Desirability
—Chlorine Trifluoride is one of the most powerful rocket fuel oxidizers known. Its performance compares favorably with other oxidizers far more difficult to handle.

Properties
—CTF has many characteristics desirable in a storable propellant, with a wide liquid temperature range. It has a low freezing point (—105°F) and a moderate boiling point (53°F). Vapor pressure is 80 psia at 140°F.

Storability
—Unlike most liquid propellants, Chlorine Trifluoride requires no refrigeration. It is handled and stored safely and conveniently in standard steel cylinders. No special storing precautions necessary.

Availability
—CTF has been produced commercially by General Chemical for almost 10 years. Readily available in ton and 150-lb. steel cylinders and in smaller sizes.

Stability
—CTF has very high shock resistance; is shipped nationally via common carriers. It is thermally stable up to 450°F.

Dependability
—CTF gives predictable performance. In addition, CTF is hypergolic with hydrogen fuels over a wide range of pressures and temperatures.

Flexibility
—CTF can be used under all geographic and climatic conditions. No need for fixed supply points.

Compatibility
—CTF can be used satisfactorily with properly passivated steels, nickel alloys, copper and other common metals.

Density
—CTF's high density (1.825 gm/cc at 68°F or approximately 15.3 lbs./gallon) leads to outstanding density impulse values with a variety of rocket fuels.

Write today for a free copy of our technical bulletin, "Chlorine Trifluoride." Company letterhead, please.

First in Fluorine Chemistry

Allied Chemical

GENERAL CHEMICAL DIVISION
40 Rector Street, New York 6, N. Y.

STORABILITY

Just one of the many outstanding attributes of

DIMAZINE®

unsym-Dimethylhydrazine

DIMAZINE has many characteristics that make it excel as a storable fuel.

Its remarkable stability has been proven in tests of more than two years' duration, even in mild-steel vessels. Its high thermal stability and low freezing point permit wide variations of storage temperatures. It is not shock sensitive and is unaffected by many types of accidental contamination. It is highly compatible with most metals and appropriate sealant materials.

Excellent storability, high performance, ease of handling, ample availability . . . these and many other advantages are combined in DIMAZINE, the outstanding storable fuel.

We will be pleased to assist in your evaluation of DIMAZINE and to supply detailed data on its properties and handling.

Putting Ideas to Work

FOOD MACHINERY AND CHEMICAL CORPORATION

Chlor-Alkali Division

General Sales Offices:
161 E. 42nd STREET, NEW YORK 17

Physics of Artificial Electron Clouds

F. F. MARMO,
L. M. ASCHENBRAND and
J. PRESSMAN

Geophysics Corp. of America
Boston, Mass.

THIS paper summarizes the results and analysis of seven rocket experiments designed and performed to systematically study the physics of the generation of artificial electron clouds in the upper atmosphere.

The several experiments can be discussed in four phases. For example, the first involved the daytime Aerobee rocket release of potassium at 121 km and served to establish the feasibility of solar photo-ionization generation of artificial electron clouds. The second phase was the Nike-Cajun nighttime release of cesium at 101 km to establish the role of thermochemical generation of electron clouds. The third phase was designed to study the correlation of optical and radio-radar data as obtained from a visible, photographic electron cloud. This was accomplished by the morning twilight releases of cesium and sodium at 128 and 116 km, respectively. The final phase of this series reported here involved three releases of cesium at 91, 82 and 69 km, in order to determine the altitude below which long-lived, dense artificial electron clouds cannot be generated by the techniques employed here. The results of this last phase yield valuable physical data pertinent to several of the electron decay processes dominant in the lower altitudes.

The overall analysis of the extensive optical and radar data has yielded information on the following physical parameters:

1 Chemical yield of contaminant.
2 Thermal ionization efficiency.
3 Upper atmospheric wind velocity.
4 Wind shear.
5 Optical and gaussian half-width of cloud with time.
6 Ambipolar diffusion.
7 Neutral diffusion.
8 Photo-ionization cross sections.
9 Mutual neutralization processes.
10 Rate of chemical consumption of alkali by atmospheric oxygen.

Finally, the role that artificial electron clouds can assume for practical utilization for radio-radar propagation is emphasized with some discussion indicating the extent of the available potential for this engineering purpose.

Received April 26, 1960.

[1] The original experimental work was performed while authors were associated with the Geophysics Research Directorate of the Air Force Cambridge Research Center. Most of the data analysis and interpretation presented in this survey was accomplished by the authors at their present address under the sponsorship of contracts: U. S. Army Signal Corps DA 36-039-SC-78971; U. S. Army Signal Corps DA 36-039-SC-78925.

Introduction

Artificial electron clouds are formed by the ejection of a suitable chemical contaminant at pre-selected altitudes with the generation of the electrons due to photo-ionization and/or thermal ionization. The first successful experiment on the generation of an artificial electron cloud was performed by an Aerobee rocket release of about 18 lb (275 moles) of nitric oxide gas at an altitude of 95 km (1).[2] The success of this experiment, whereby an artificial electron cloud with an initial average density of about 4×10^6 electrons per cm^3 was detected for more than 10 min by radar techniques, indicated that it would be feasible to use other contaminants to create artificial electron clouds at various altitudes with a wide range of densities, time durations, sizes, shapes and other parameters.

Since May 1957, a series of seven additional upper atmosphere rocket experiments has been performed to examine

[2] Numbers in parentheses indicate References at end of paper.

Dr. Frederick F. Marmo studied physical chemistry at Boston University, where he received the B.S. degree, Phi Beta Kappa and graduated summa cum laude in 1949. His M.S. and Ph.D. degrees in chemistry were received at Harvard University in 1951 and 1954, respectively.

Mr. Leonard M. Aschenbrand received the B.S. degree in physical chemistry from CCNY in 1947. In 1949 he was awarded an M.A. degree in chemistry from NYU.

Mr. Jerome Pressman received the B.S. degree in mathematics from CCNY in 1941. He later attended the University of Chicago and the University of Puerto Rico while taking advanced courses in meteorology and physics at NYU, 1946–1949.

From 1951 through 1958 all three scientists were involved in theoretical and experimental studies relative to the study of upper atmospheric physical processes while employed in the Photochemistry Laboratory at the Geophysics Research Directorate of the Air Force Cambridge Research Center. Dr. Marmo was chief of the Chemical Physics Branch, Mr. Aschenbrand of the Atmospheric Energy Section and Mr. Pressman of the Theoretical Photochemistry Section.

All three were responsible for initiating, planning, conducting and eventually publishing papers and reports on the program of the creation of artificial electron clouds and synthetic chemiluminescence in the upper atmosphere, using techniques of releasing chemical constituents.

these possibilities, and to ascertain the feasibility of employing these clouds as a research tool for upper atmosphere research. In addition, the possibilities of employing artificial electron clouds for propagation purposes was explored. These initial experiments established the foundation of a new technique of study of physical and chemical processes associated with Earth's upper atmosphere. A substantial amount of qualitative and quantitative data has been obtained from these experiments pertinent to the studies of upper atmospheric winds, diffusion, microscopic cross-section values (electron attachment, ion-electron recombination, charge exchange, etc.), chemical consumption, expansion of high pressure gases into an attenuated atmosphere, electromagnetic propagation research and implications, ionospheric research and thermochemical and explosive effects, to name but several. The purpose of this survey article is to briefly present the basic concepts employed, a chronological summary of experimental events, the data observed and the results of analysis of these data.

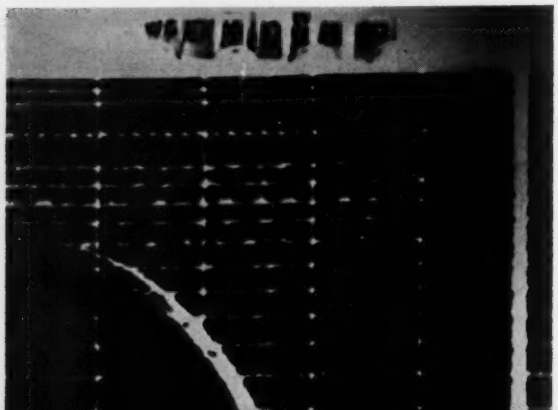

Fig. 1 Ionogram obtained 30 min after chemical release as recorded by C-3 vertical ionosonde located at White Sands Proving Ground, N. Mex., for experiment conducted in November 1957. This display depicts the slant range vs. maximum frequency. Each altitude marker represents 100 km, whereas the frequency scale goes from 1 to 25 mc per sec. The artificial cloud is shown between the normal E and F regions at about 170-km slant range. The maximum frequency return is about 8 mc per sec

The first successful experiment designed for optimum-type artificial electron clouds was accomplished by the release of atomic K from an Aerobee rocket at 121 km. This flight occurred at about 0932 MST on Nov. 19, 1957. The electron cloud formed as a result of this experiment was readily detected by conventional radar techniques. Fig. 1 depicts one of the more interesting representative pieces of radar data. This result is an ionogram obtained from a C-3 vertical ionosonde, located at White Sands Proving Grounds, N. Mex., which clearly shows the detection of the manmade electron cloud formed between the normal E and F layers (at about 170-km slant range) at 30 min after contaminant release.

Interpretation of the results pertinent to the ionized cloud which was formed in this experiment suggested that some additional process to photo-ionization was responsible for the initial electron production. The chemical nature of the experimental method indicated that the effect could be due to thermal ionization. In order to examine this important effect, an experiment was devised in which atomic Cs would be released during the nighttime hours to eliminate the role of solar photo-ionizing flux. The choice of this element arose from the consideration that, at a given temperature within the range considered, Cs should produce considerably more thermal electrons than other constituents of the alkali metal family; thus, a maximum-type effect could be anticipated. In addition, since this was to be a nighttime release, it was considered feasible to produce a cloud easily visible and, therefore, easily photographed.

Some of the obvious advantages gained by optical detection are: Accurate determination of release altitudes by triangulation optics, correlation of radar returns as a function of cloud size and shape, determination of yield and chemical rates, wind and diffusion data, and spectral characteristics of the emission. The method employed for rendering the cloud visible was to "dope" a Cs 100-km release with about 10 per cent Na so that the latter would react in a chemiluminescent manner with the ambient atomic oxygen in the upper atmosphere (maximum number density at about 100 km). Of equal importance was the fact that results of the November 17 Aerobee flight suggested the desirability of utilizing the smaller Nike-Cajun two-stage rocket. Known advantages of using the smaller rocket included lower cost, ease of handling at launching, solid fuel and superior trajectory characteristics. However, it was recognized that, for the production of maximum-type electron clouds, such utilization would incur the sacrifice of larger payload. (The Aerobee's instrumented payload is capable of carrying aloft about three times more constituent.) In spite of this, the decision was made to utilize the Nike-Cajun vehicle whenever possible.

The successful release of this Cs-Na mixture was accomplished from a Nike-Cajun rocket at an altitude of 101 km at the pre-dawn hour of 0245 MST on May 20, 1958. The electron cloud created was detected by radar; the cloud was assumed to be due to thermal ionization. It was clearly visible to the naked eye; the photographic and spectral data were obtained for as long as 6 min. Interpretation of the optical data presents the possibility of a study of the cloud dynamics vs. time, as well as information pertaining to chemical consumption, kinetics of the reactions involved and some of the physical processes previously mentioned.

The next group of experiments of the series was primarily concerned with the correlation of optical and radar data from ionized clouds as formed by solar ionization of alkali metal vapor. This could conveniently be accomplished by creating a light emitting photographic cloud, preferably one that emitted in the visible. The method of rendering the cloud visible is based upon the detectability of Na resonance radiation against a morning-twilight-sky back-

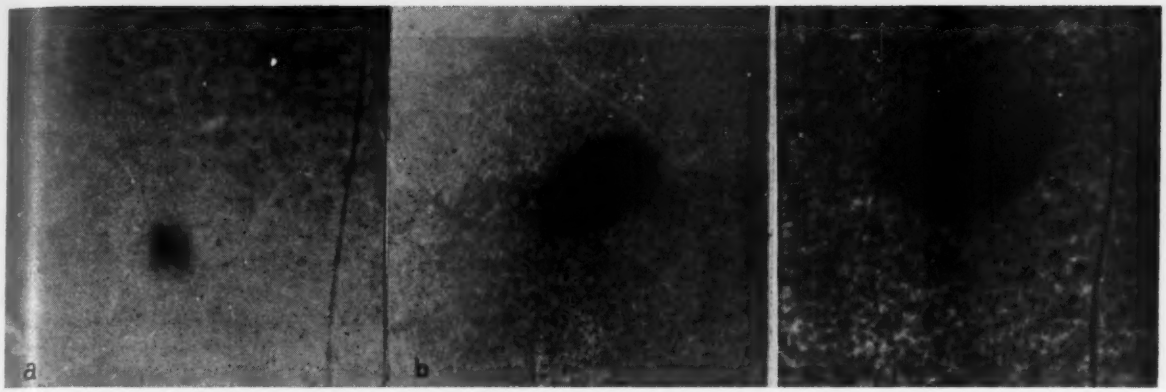

Fig. 2 Photographs taken from television screen of Lumicon depicting the dynamics of cloud formation for experiment conducted May 21, 1958. The picture (a) was obtained 2 sec after chemical release, (b) and (c) after 1 and 2 min, respectively

ground (2). Again, if we merely "doped" the chemical payload of Cs compound with a small amount of Na, an easily observable cloud would be formed. A morning-twilight release was adopted, since it was essential that the cloud be solar illuminated for an extended period, and that a reduced intensity sky background exist for the early part of the experiment. Two different experiments were performed as part of this phase of solar induced ionization. A release of a mixture of Cs and Na (2 per cent) was conducted at 128 km on May 21, 1958, and, following that, a payload consisting entirely of Na compound was released at 116 km on May 22, 1958. Both experiments were successful in that they afforded the opportunity of providing good photographic and spectral coverage for over 8 min. Fig. 2 shows a series of three pictures obtained on the May 21 experiment using a light amplifying unit (Lumicon) capable of obtaining series photographs. The first picture was obtained 2 sec after release time, and the latter two show the cloud development after 1 and 2 min, respectively.

The expansion characteristics are clearly indicated, and the utilization for data of this type is obvious (3).

The radar results from the former release provided positive results for as long as 19 min, resulting in valuable correlated radar and optical data. The results of the Na release were uniform in that all operating stations reported negative radar results. This negative result appears to be in agreement with the deduced relative photo-ionization probabilities of Cs, K and Na, namely, 6.5×10^{-4}, 1.8×10^{-5} and 1.0×10^{-5} sec^{-1}, respectively (4). This further indicates, as expected, that thermal ionization does not play an important role for Na as far as production of a detectable artificial electron cloud is concerned.

The last series of experiments reported here consisted of the daytime Cs releases at 70, 80 and 90 km. This series was conducted during September 1958 to determine the altitude below which the generation of a detectable, high density, long-lived solar induced artificial electron cloud is precluded due to the rate of photo-ionization electron production, recombination, electron attachment processes and chemical consumption of the contaminant. The basic engineering technique concerning these releases of alkali metal vapors involved a stainless steel canister so designed and constructed as to be within the requirements of payload, configuration of nose cone, high acceleration and, finally, adaptability to the rocket body and instrument package. No further details are given here, since much of the results reported here have been previously reported in a more extensive manner in a series of papers (3–8) dealing with the experimental data in detail, theoretical considerations, evaluation and interpretation, etc. Finally, the extensive radar and optical probes utilized have also been described previously (3–8).

Data Analysis and Interpretation

In addition to their use as a powerful radar propagation tool, the scientific uses of electron clouds are varied; i.e., the scientist is given a valuable research tool for the investigation of physical and chemical processes of the upper atmosphere. Many of the scientific areas explored by means of electron cloud techniques are reported here. This work is restricted to discussions of the following:

1 Thermal ionization efficiencies.
2 Chemical yield.
3 Ambipolar and neutral diffusion coefficients.
4 Horizontal wind velocities in the upper atmosphere.
5 Wind shear.
6 Chemical consumption of alkali constituent by atmospheric oxygen.
7 Lower atmospheric electron decay processes.

These do not exhaust the possible areas of investigation, but rather serve to illustrate the potential utility of artificial electron clouds as a research tool. The following sections are devoted to presenting the brief analysis on the experimental data associated with items 1 through 7.

Analysis of Thermal Release: Chemical Yield and Thermal Ionization Efficiency

A sodium-doped Cs payload was released at 101 km during a nighttime experiment to determine the magnitude of thermochemical effects upon the production of artificial electron clouds. Subsequent analysis of radio-radar and optical data pointed toward the fact that it was indeed possible to ascribe to thermal processes the generation of an ample number of electrons to account for the observed electron cloud. A thermochemical treatment of these data with application of the Saha equation suggested that values for the total number of electrons and thermal ionization probability could best be obtained from conditions wherein the temperature of reaction would be in the vicinity of 3000 K and with the canister bursting pressure range between 300 to 500 atm.

Fig. 3 was derived from the Saha relationships as applied to the specific system employed. It relates the moles reacted to the temperature of the reactants for different bursting pressures. With the aid of this figure it can be shown (6) that a chemical yield of less than 10 per cent was to be expected. This fact was further substantiated by optical and radar data from subsequent experiments in the series in which yields of between 2 to 5 per cent had been determined in an independent manner.

An initial cloud optical radius of about 300 m and an initial electron density of the order of 3×10^7 cm^{-3} were determined from an analysis of optical and radar data, respectively.

From these determinations it was experimentally concluded that the total electron content of the cloud N_e was of the order of 3×10^{21}. Theoretical evaluation of $N_e = 1 \times 10^{21}$ was determined from subsequent Cs releases; a discussion will be found in another section of this paper. An N_e value of between 1 to 3×10^{21} was adopted.

For Cs a value of 10^{-3} for the thermal efficiency c was determined from the results of this experiment in thermal release. Further, through utilization of the Cs data it was possible to extend these findings to other members of the metal alkali family. It was thus, that a corresponding value of 5×10^{-4} was estimated for potassium. These c values are employed in later data analysis.

Analysis of C-3 Radar Data: Diffusion, Chemical Yield, Ionization Efficiency

This section will outline some of the methods which were employed to analyze radar data. The results of this analysis yielded values for several important parameters.

Of all the radar data obtained, the C-3 ionosonde data were considered the most compatible to analysis. The analysis is restricted to the K and Cs releases at 121 and 128 km, respectively. It has previously been demonstrated (5,7) that for these cases, the significant factor causing a decrease in the electron concentration is diffusion. Decay processes, such as attachment, recombination and others, are not sufficiently fast for the time constants of the effects under discussion to materially affect electron concentration. Thus, considerable simplification is possible; in particular, the governing equations (7) are given by

$$\frac{dn_0}{dt} = D_n \nabla^2 n - kn \qquad [1]$$

$$\frac{dn_e}{dt} = D_a \nabla^2 n_e + kn \qquad [2]$$

where

n_0 = concentration of neutrals, cm^3
n_e = concentration of electrons, cm^3
D_n = neutral diffusion coefficient, cm^2/sec
D_a = ambipolar diffusion coefficient, cm^2/sec
k = photo-ionization probability, sec^{-1}

The solution of Equations [1 and 2] have been given elsewhere (7). The center point density solution can be written as

$$N_e(0, t) = n_{e_0} \frac{r_0^3}{m^{3/2}} + \frac{k(N + N_e - n_{e_0}\pi^{3/2} r_0^3)}{2\pi^{3/2}(D_n - D_a)} \left[\frac{1}{m^{1/2}} - \frac{\exp(-kt)}{p^{1/2}}\right] + \frac{N}{4\pi} \left(\frac{k}{D_n - D_a}\right)^{3/2} \exp\left[\frac{km}{4(D_n - D_a)}\right] \left\{ \operatorname{erf}\left[\frac{kp}{4(D_n - D_a)}\right]^{1/2} - \operatorname{erf}\left[\frac{km}{4(D_n - D_a)}\right]^{1/2} \right\} \qquad [3]$$

where

$m = (r_0^2 + 4D_a t)$
$p = (r_0^2 + 4D_n t)$
n_{e_0} = initial electron center density, which includes the initial thermal and the photo-ionization contributions

It may appear that a large degree of flexibility is available for proper fitting in view of the several parameters involved. However, this is probably not the case; in fact, the requirement of utilizing several reasonable values simultaneously for proper fit can be highly restrictive. For example, it was shown earlier that approximate N values for the cases of the Nike-Cajun Cs and Aerobee K releases should be about 1×10^{24} and 3×10^{24}, respectively. Further, it was ascertained that thermal ionization efficiencies (c values) of Cs and K are about 10^{-3} and 5×10^{-4}, respectively, for the chemical release system employed here. These values should be utilized for proper fit of the data to the theoretical curves.

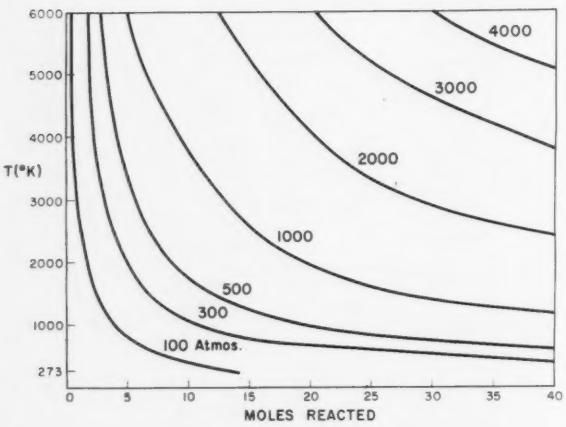

Fig. 3 Pressure within canister as a function of moles reacted and temperature of the reactants

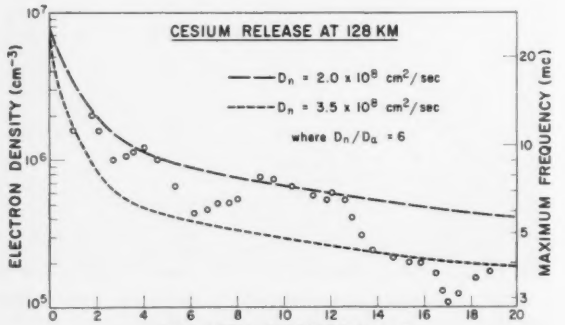
CESIUM RELEASE AT 128 KM
D_n = 2.0 x 10^8 cm^2/sec
D_n = 3.5 x 10^8 cm^2/sec
where D_n/D_a = 6
ELECTRON DENSITY (cm^{-3})
MAXIMUM FREQUENCY (mc)
TIME AFTER RELEASE (minutes)

Fig. 4 Plot of the C-3 experimental data for the release of cesium at 128 km, depicting the best fit values of the ambipolar and neutral diffusion coefficients D_a and D_n respectively. The two closely spaced curves serve to illustrate the sensitivity of the technique

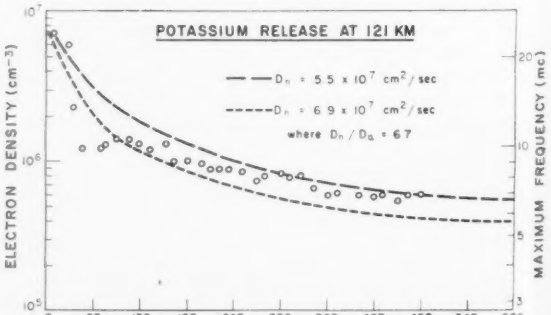
POTASSIUM RELEASE AT 121 KM
D_n = 5.5 x 10^7 cm^2/sec
D_n = 6.9 x 10^7 cm^2/sec
where D_n/D_a = 6.7
ELECTRON DENSITY (cm^{-3})
MAXIMUM FREQUENCY (mc)
TIME AFTER RELEASE (seconds)

Fig. 5 Plot of the C-3 experimental data for the release of potassium at 121 km, depicting the best fit values of the ambipolar and neutral diffusion coefficients

For the estimation of the r_0 values to be employed, optical width data were employed from the Nike-Cajun Cs and Na twilight releases at altitudes of 128 and 116 km, respectively (7). These data were then theoretically adjusted to the corresponding gaussian half-widths r_0. The r_0 values of 300 and 200 m were deduced for Cs and K, respectively. These were applied directly for data interpretation. Although some uncertainty exists in the use of this method for estimating the proper gaussian half-width, this parameter is fortunately not too sensitive to fitting.

Concerning the choices of k values, solar photo-ionization probability values of 6.5×10^{-4} sec^{-1} for Cs and 1.8×10^{-5} sec^{-1} for K were derived from published experimental data (4,9). These values were considered to be the most reliable of the several parameters employed and, as such, not subject to variation, thereby imposing an additional restriction upon the available flexibility for proper curve fitting. There now remained the problem of determining the degree of agreement achievable between the theoretical and experimental values; application of various reasonable values of D_a and D_n, the ambipolar and neutral diffusion coefficients, respectively, were used toward this end. Indeed, it was found that in both cases, D_a and D_n values and the ratio of D_n/D_a were in close agreement with theory (10). For the 128-km Cs release, the best fit values were: yield, 1×10^{24} atoms; thermal efficiency, 10^{-3}; neutral and ambipolar diffusion coefficients D_n and D_a, 2.5×10^8 cm^2/sec and 4.2×10^7 cm^2/sec, respectively. The corresponding values for the 121-km K release were 3×10^{24} atoms, 5×10^{-4} and 6.2×10^7 cm^2/sec and 9.2×10^6 cm^2/sec.

The resultant fit to experimental data using these values is indicated in Figs. 4 and 5, which include the appropriate C-3 radar experimental data. In these figures two closely spaced D_n values are shown to illustrate the sensitivity of the technique.

Optical Data: Diffusion and Chemical Yield

For obtaining diffusion and chemical yield determinations, it is assumed that the initial, very rapid, explosive expansion occurring at release leads to a gaussian cloud of half-width r_0. It is at this point that we set $t = 0$. Subsequently, the density is expected to vary with time and position in accordance with the equation

$$n(r,t) = \frac{N}{\pi^{3/2}(4Dt + r_0^2)^{3/2}} \exp\left(-\frac{r^2}{4Dt + r_0^2}\right) \qquad [4]$$

where

- $n(r,t)$ = number of particles per cm^3 at distance r from the center at time t
- N = total number of particles in cloud
- r_0 = half-width of gaussian ($1/e$ value), cm
- D = diffusion coefficient for the species at cloud height (cm^2/sec)

If luminosity is due to resonance scattered sunlight and viewed in the backscattering direction, light will, therefore, be scattered to the detector as a function of the absorption cross section σ, and in accordance with τ the number of atoms in the line of sight. The absorption cross section σ, of the Na atom and its resonance level at 5890 Å is about 10^{-11} cm^2; hence, when the number of atoms in the line of sight is about 10^{11}, this portion of the cloud may be considered as being essentially optically dense. Since at these altitudes the collisional deactivation is negligible, the optically dense portion of the cloud will have a reflectivity of unity at the characteristic wave length. Further, the total number of alkali atoms will remain constant, since the rate of chemical consumption by ambient oxygen is so slow. For example, the time for half-consumption $t_{1/2}$ is greater than 10^7 sec and is greater than 10^5 sec at 130 and 115 km, respectively. [See (4), fig. 6.]

The total number of particles in the line of sight (τ) at distance d (cm) from center is given by

$$\tau = \frac{N}{\pi(4Dt + r_0^2)} \exp\left(-\frac{r^2}{4Dt + r_0^2}\right) \qquad [5]$$

If it is assumed that the optical size of the cloud is determined by the distance from the center of that isophote for which $\tau = 1/\sigma$ (since the intensity drops rapidly for $\tau > \sigma$), we have

$$d^2 = -(4Dt + r_0^2) \ln \frac{\pi}{\sigma N}(4Dt + r_0^2) \qquad [6]$$

$$d_{\max}^2 = \frac{N\sigma}{e\pi} \qquad [7]$$

$$t_{d_{\max}} = \frac{1}{4D}\left(\frac{N\sigma}{e\pi} - r_0^2\right) \qquad [8]$$

$$t_{d=0} = \frac{1}{4D}\left(\frac{N\sigma}{\pi} - r_0^2\right) \qquad [9]$$

where

- $d_{\max}$ = maximum radius of optical radius
- $t_{d_{\max}}$ = time to achieve this maximum radius
- $t_{d=0}$ = time for cloud to disappear

To effectively relate the optical model to the observed or photographed cloud size with the contaminant density and profile throughout the cloud, requires consideration of the detector response to cloud luminosity under the varying twilight levels of background light. Many factors unite to make quantitative measurements from a photographic image difficult. Thus, for quantitative work it is necessary, in practice, to combine careful instrument calibration with meticulous densitometry techniques to plot contour lines of constant density and relate these to a theoretical model before dimensions can be accurately ascertained. This was not accomplished in the present work, and the absolute values derived suffered accordingly.

As an illustrative example of the crude optical model employed here, we analyze the Beattie-Coleman camera data for the May 21 flight (7). Here we are concerned with determining the parameters: r_0, the initial gaussian half-width; N, the number of alkali atoms; and in this case D_n, the ob-

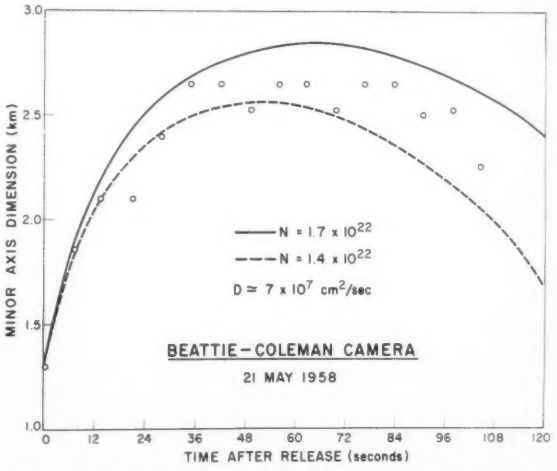

Fig. 6 The optical determination of the number of atoms N and neutral diffusion coefficient D_n. The time variation of the minor axis optical diameter is indicated by the circles. The dashed and solid curves are theoretical curves for two different yields but the same diffusion coefficients

served neutral diffusion coefficient. From Equation [6] for $t = 0$, we obtain

$$d_0^2 = r_0^2 \ln \pi r_0^2/\sigma N \qquad [10]$$

where d_0 is the initial optical radius.

Utilizing Equations [8 and 10] we obtain the fit illustrated in Fig. 6 where the size ($2d$) is plotted against the theoretical curve for two closely spaced, different values of N. This serves to show that the fit is surprisingly accurate, since small variations in both N and D_n cause large changes in the curve. The data indicate a diffusion coefficient value of $D_n = 7 \times 10^7$ cm^2/sec, and also that N is equal to 1.5×10^{22} atoms (or a sodium yield of approximately 3 per cent). The value of D_n is consistent with the theoretically extrapolated values of D_n at the altidude in question (10). Furthermore, since $t_{max} = 1/D_n$, small changes in D_n shift the maximum and the curve along the t axis in an extremely sensitive fashion.

Wind Determination: Velocity and Shear Data

The formation of a small visible photographic cloud at altitude can yield wind velocity data by means of simple optical triangulation techniques. A method of obtaining shear information from optical data is given here. In addition, a geometric method of extracting accurate horizontal wind velocity values from C-3 radar data is discussed.

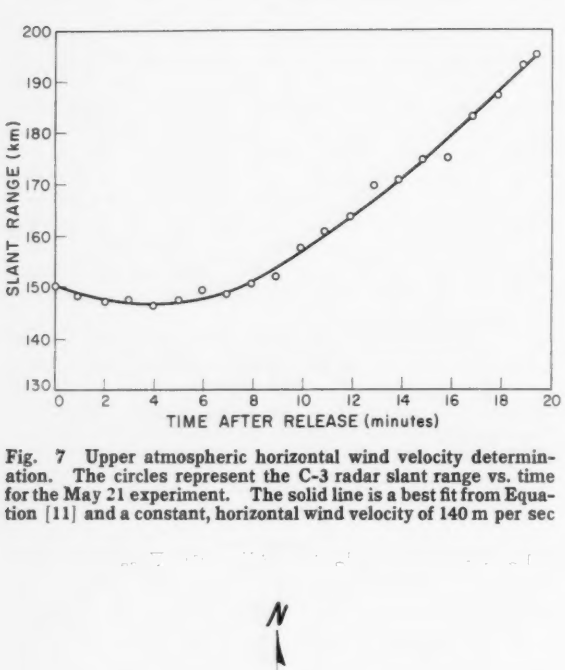

Fig. 7 Upper atmospheric horizontal wind velocity determination. The circles represent the C-3 radar slant range vs. time for the May 21 experiment. The solid line is a best fit from Equation [11] and a constant, horizontal wind velocity of 140 m per sec

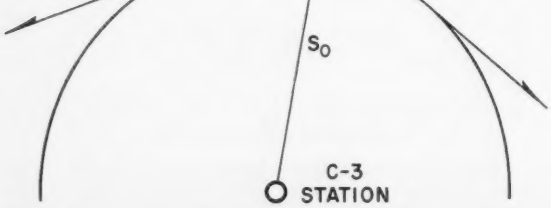

Fig. 8 Schematic representation of geometrical determination of winds from C-3 slant range vs. time plot

The pertinent radar data for obtaining horizontal wind velocities is the change in electron cloud slant range *vs.* time. The data from the C-3 ionosonde are shown as circles in Fig. 7. The smooth variation of the range with time for this 20-min period is strong support for the presence of an isolated electron cloud. From the initial slant range of about 150 km, the subsequent change in slant range in time is presumably due to ionospheric winds. The character of the curve with a shallow minimum indicates the geometry depicted in Fig. 8, in which the positions of cloud release and C-3 stations are included. This geometry can be described mathematically by the expression

$$S = [S_0^2 + wt(wt - 2S_0 \cos \theta_0)]^{1/2} \qquad [11]$$

where

S_0 = initial slant range
S = slant range between cloud trajectory and C-3 line of sight
θ = initial angle
w = wind velocity

A best fit to the data was obtained for a w value of 140 m per sec; the theoretical curve is shown as the solid line in Fig. 7. The excellent fit between the experimental points and the theoretical curve appeared to corroborate the notion of horizontal winds with a constant velocity of about 140 m per sec. This (140-m per sec) value for the velocity is considerably greater than those previously determined in a similar manner, namely, 60 and 78 m per sec at 95 km (1) and 121 km (5), respectively. Concerning wind direction, it is clear from Fig. 8 that a direction ambiguity exists on the basis of these data alone. However, in this instance visual observations dictated the choice of direction as 87 deg rather than 293 deg. This case suffices to illustrate the geometric method of obtaining wind information via these and similar data.

Wind shear in the upper atmosphere has recently been measured by a technique in which a long sodium filament is ejected into the upper atmosphere, between 70 and 200 km (11). Careful analysis of the optical data leads to accurate shear data. Clearly, in a similar manner a point release can be utilized to determine the wind shear at the release altitude. For example, photographs of the contaminant cloud indicated an initially spherical cloud becoming ellipsoidal with time due to the prevailing wind shear.

The photographed image of a cloud illuminated by resonance scattering is a complicated function of viewing angle, optical density of the cloud, film sensitivity and exposure time as well as background light intensity. Thus, for the experimental determination of shear by the employment of these clouds, a simplified model has been previously derived (7) and leads to the expression

$$L = Y[at + (1/2)bt^2] + \text{constant} \qquad [12]$$

where

a, b = constants of linearity of the shear
L = elongation, cm
Y = shear coefficient, sec^{-1}

Camera data from the May 22, 1958 flight are plotted in Fig. 9. The variation with time of the minor axis is shown on the left-hand graph, and on the right-hand graph is shown the variation with time of the major axis together with the plot of Equation [12]. From these, a shear value of $Y = 1.1 \times 10^{-2}$ sec^{-1} was obtained for the 116-km release.

Similar plots have been applied to Lumicon data (7), for which data from the May 22 flight yielded a shear constant of 1×10^{-2} sec^{-1} in agreement with the foregoing. The value obtained for the May 21 Cs release at 128 km was 6×10^{-3} sec^{-1}. These values were found to be consistent with

those obtained by sodium streamer experiments (11). It is recognized that the rate of diffusion will be a function of the cloud shape itself, but this effect is ignored in the given model. Another assumption is that shear does not affect the growth of the minor axis. Yet despite these limitations, a reasonable plot was obtained for the concomitant variation of the major and minor axes.

Low Altitude Data Analysis; Chemical Consumption, Mutual Neutralization and Other Electron Decay Processes

A series of three experiments will be discussed here, which were undertaken for the twofold purpose of studying the effect of low altitudes (below 100 km) upon the formation of artificial electron clouds and the roles of a number of electron decay processes after the generation of these clouds. It was felt that the data acquired would afford not only an investigation of the effects of individual decay processes, but would allow further investigation of an earlier conclusion (4) that there probably existed some lower altitude below which the formation of detectable, high density, long lived and solar induced artificial electron clouds could not be achieved within the framework of the experimental techniques employed in this study. More pertinent to this conclusion, however, is the fact that several electron decay processes (e.g., chemical consumption, recombination, electron attachment, etc.) predominate at low altitudes in contradistinction to other processes which exert maximum influence above the 100-km region.

For the present analysis, therefore, information was obtained concerning some of these decay processes. Of particular import was the derivation of coefficients for chemical consumption and mutual recombination.

Of the several radio-radar probes utilized in the Cs releases at 91, 82 and 69 km (8), a 40.7 pulsed radar located 15 miles east of the launch site yielded the most consistent—and therefore usable—data. The analysis applied to these data, indicated a total cloud duration (for 40.7 mc echoes) of about 70 sec at 91 km, 4.3 sec at 82 km and 1.5 sec at 69 km.

The short radar reflecting lifetimes observed for the low altitude generated clouds are due to at least two important effects: The rapid destruction of Cs atoms by chemical consumption which prevents subsequent photo-ionization, and the rapid electron destruction through attachment followed by mutual neutralization. It was found (for the types of releases discussed in this paper) that the diffusion rate of the charged particles is much too slow to account for the observed cloud history. Also, the photo-ionization production term remained, relatively, not influenced by diffusion of the neutrals, except at about 90 km.

We present here a brief summary of the mathematical model. Details have been given in a previous paper (4). We have

$$dn_e/dt = k\, n_0' \exp(-bt) - \alpha n_e^2 \qquad [13]$$

where

$n_e(0) = n_{e_0}$
b = chemical consumption rate of consumption of the cesium by atmospheric oxygen, sec^{-1}
$n_0' = n_0/(1 + \lambda)$
λ = ratio of negative ions to electrons at equilibrium

Finally

$$\alpha = \alpha_r + \lambda\alpha_i \qquad [14]$$

where

α_i = coefficient of mutual neutralization
α_r = Cs-ion recombination coefficient

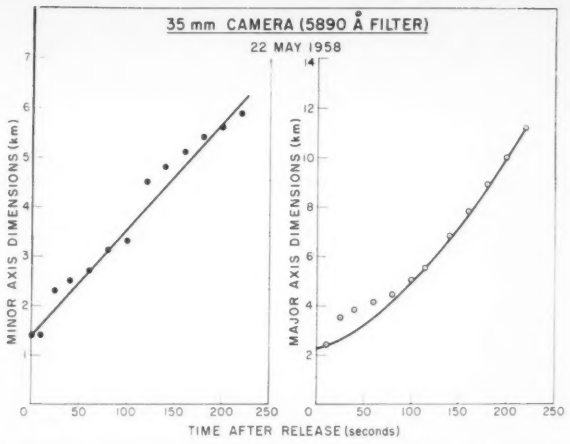

Fig. 9 Data from the May 22, 1958 flight. The solid dots and circles represent the time variation of the optical diameters of the minor and major axes, respectively. The two curves show the best theoretical fit and indicate a wind shear of 1×10^{-2} sec^{-1}

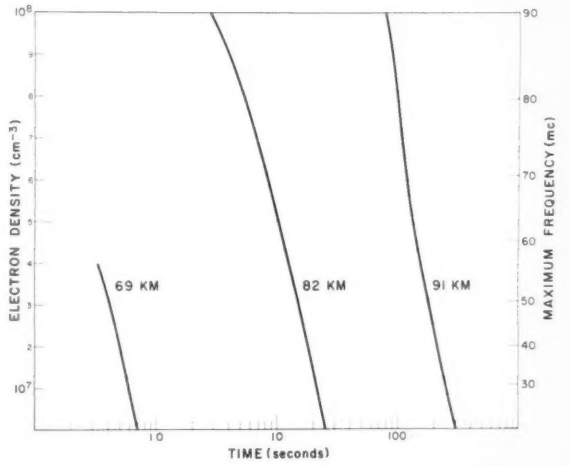

Fig. 10 Theoretical time variation of center point electron density in accordance with Equation [13] for 69, 82 and 91 km

Fortunately, this nonlinear equation is susceptible to the complete formal solution (8)

$$n_e(t) = \frac{bl}{2\alpha}\,\xi\,\frac{[I_1(l)K_1(l\xi) - I_1(l\xi)K_1(l)] + \mu[I_0(l)K_1(l\xi) + I_1(l\xi)K_0(l)]}{[I_1(l)K_0(l\xi) + I_0(l\xi)K_1(l)] + \mu[I_0(l)K_0(l\xi) - I_0(l\xi)K_0(l)]} \qquad [15]$$

where

$l = (2/b)(2k\, n_0')^{1/2}$
$\mu = 2\alpha n_e(0)/b$
$\xi = e^{-(1/2)bt}$
$y_1 = I_0(lZ)$
$y_2 = K_0(lZ)$

Both expressions for y satisfy Bessels' zero-order modified equation

$$\frac{d^2y}{dZ^2} + \frac{1}{Z}\frac{dy}{dZ} - l^2y = 0 \qquad [16]$$

and

$I_0'(Z) = I_1(Z)$
$K_0'(Z) = -K_1(Z)$

Unfortunately, the solution of Equation [15] is not susceptible to direct computation because of the large value of the arguments. However, numerical values have been obtained by the use of a variety of numerical approximations. These approximations and their range of validity are given elsewhere (8).

Fig. 10 illustrates the fit obtained with the utilization of the best values for the several parameters involved. However, it is worth noting here that the deviation between the theoretical and experimental data is greatest, as expected, at 91 km where no allowance was made for the effect of neutral diffusion on the photo-ionization term. Its direction is also as expected. Further, from the analysis it is deduced that $\alpha_i = 10^{-7} - 10^{-8}$ cm^3 sec^{-1}, in rough agreement with estimates of Bates (12) for similar processes. The value of b is in reasonable agreement with the values computed in an earlier paper (8) using the sodium rate of consumption.

Using present techniques, the lowest altitude of effective cloud duration is about 70 km. A nighttime, low altitude experiment should give an independent measure of electron attachment rate of O_2 which can be meshed with the low altitude, daytime shots to obtain a more direct value of α_i, the coefficient of mutual neutralization.

Conclusions

The foregoing is intended as a review of some of the main points in the systematic study of the physics of artificial electron clouds. Its goal is the elucidation of the basic electron creation and destruction processes.

This study has revealed that the theoretical photo-ionization cross sections are consistent with the data contained, and that cesium is the most effective of the alkali metals investigated for this purpose. It has been shown that the chemical yields have been disappointingly small, of the order of 2 to 3 per cent. Thermal ionization has been shown to be an effective process in the generation of artificial electron clouds, but, here again, thermal efficiencies of only about 0.1 per cent of the released number of atoms have been achieved.

An optical method has been devised for the successful determination of the cloud initial half-width, chemical yield, wind shear and neutral diffusion coefficients. A simple method has been used for determining (with one degree of ambiguity) the wind velocity from radar slant range data. A mathematical model has been applied to those experimental releases above 120 km in order to describe the observed electron decay history. The analysis gives measures of neutral and ambipolar diffusion, chemical yield, degree of thermal ionization and initial half-width. Reasonable correlation of radar data with the optical techniques employed has been demonstrated.

Another mathematical model has been devised and employed for the lower altitude (below 90 km) range which accounts for the dominant processes at these altitudes. These techniques also yield useful information on neutral and ambipolar diffusion, photo-ionization cross sections, mutual neutralization, thermal ionization and the chemical consumption of the alkali contaminant by atmospheric oxygen. Information on electron attachment rates should be easily available by application of similar techniques. Additional work is in progress to solve the mathematical problems in the 90 to 120-km region, where several processes are important.

Finally, the foregoing summary has made obvious the possible usage of artificial electron clouds for radar propagation purposes. In particular, a significant potential for this application is indicated by the small chemical yields and thermal efficiencies resulting from the methods employed here. Clearly, these are capable of substantial increases. A systematic chemical engineering study is being currently pursued to this end and should yield substantial improvement toward realizing the full potential of the utilization of artificial electron clouds for radio-radar propagation (13).

References

1 Marmo, F. F., Pressman, J., Aschenbrand, L. M., Jursa, A. S. and Zelikoff, M., "Formation of An Artificial Ion Cloud; Photoionization of NO by Solar Lyman Alpha at 95 km," *J. Chem. Phys.*, vol. 25, 1956, p. 187.

2 Bedinger, J. F., Manring, E. R. and Ghosh, S. N., "Study of Sodium Vapor Ejected Into the Upper Atmosphere," *J. Geophys. Res.*, vol. 63, no. 1, 1958, pp. 19–29.

3 Marmo, F. F., Aschenbrand, L. M. and Pressman, J., "Artificial Electron Clouds I: Summary Report on the Creation of Artificial Electron Clouds in the Upper Atmosphere," *Planet. Space Sci.*, vol. 1, no. 3, pp. 227–237.

4 Marmo, F. F., Pressman, J. and Aschenbrand, L. M., "Artificial Electron Clouds II: General Considerations," *Planet. Space Sci.*, vol. 1, no. 4, pp. 291–305.

5 Marmo, F. F., Aschenbrand, L. M. and Pressman, J., "Artificial Electron Clouds III: Release of Atomic Potassium at 121 km.," *Planet. Space Sci.*, vol. 1, no. 4, pp. 306–318.

6 Pressman, J., Marmo, F. F. and Aschenbrand, L. M., "Artificial Electron Clouds IV: Thermal Ionization Study, Nighttime Release of Cesium at 101 km.," *Planet. Space Sci.*, vol. 2, no. 1, pp. 17–25.

7 Marmo, F. F., Pressman, J., Manring, E. R. and Aschenbrand, L. M., "Artificial Electron Clouds V: Morning Twilight Study, Release of Cesium and Sodium at 128 and 116 km.," *Planet. Space Sci.*, vol. 2, no. 3, pp. 166–178.

8 Pressman, J., Marmo, F. F. and Aschenbrand, L. M., "Artificial Electron Clouds VI: Low Altitude Study, Release of Cesium at 69, 82, and 91 km.," *Planet. Space Sci.*, in publication.

9 Weissler, G. L., "Electron Emission Gas Discharges I," in "Handbuch der Physik Band XXI," S. Flugge, Ed., Springer-Verlag, Berlin, 1956, pp. 332–356.

10 Dalgarno, A., private communications.

11 Manning, E. R., Bedinger, J. F., Pettit, H. B. and Moore, C. B., "Some Wind Determinations in The Upper Atmosphere Using Artificially Generated Sodium Clouds," *J. Geophys. Res.*, vol. 64, no. 6, 1959, pp. 587–592.

12 Bates, D. R., "The Physics of the Upper Atmosphere," in "The Earth as a Planet," G. P. Kuiper, Ed., University of Chicago Press, Chicago, 1954, p. 618.

13 Marmo, F. F. and Engelman, A, "Artificial Ionospheres for Communications," *Special U.S. Army Space Issue of the PGMIL Trans.*, in publication.

Ideal Performance of Multistage Rockets

RICHARD D. GECKLER[1]

Aerojet-General Corp.
Sacramento, Calif.

The ideal performance of multistage rockets is presented in a graphical form especially suited for the systems designer interested in visualizing the intricate relationships between motor propellant fraction, size of the total propulsion system in relation to the payload, and burnout velocity. The effect of incremental changes in the propellant mass or inert mass of any stage and the effect of an incremental change in the payload on the final burnout velocity are derived in the form of coefficients that allow direct comparison of the relative importance of the characteristics of each stage.

THE FUNDAMENTAL equation governing the performance of an N-stage rocket in drag-free space is

$$\mathcal{V} = \ln \mathcal{R} \qquad [1]$$

where

$$\mathcal{V} = \sum_{i=1}^{N} \mathcal{V}_i \qquad [2]$$

$$\mathcal{V}_i = [v_b^{(i)} + g_i t_b^{(i)}]/c_i \qquad [3]$$

the latter being the dimensionless velocity increment of the ith stage, and

$$\mathcal{R} = \prod_{i=1}^{N} \mathcal{R}_i \qquad [4]$$

where

$$\mathcal{R}_i = M_0^{(i)}/M_b^{(i)} \qquad [5]$$

This is the mass ratio of the ith stage. These results are well known, having been derived, for example, in (1–4).[2]

The purposes of this article are first to present the fundamental performance equation in an especially useful form for the rocket systems designer and second to derive basic equations showing the change in performance associated with changes in the characteristics of the individual stages.

Referring to Fig. 1, adapted from (2), we see that the initial mass of any stage $M_0^{(i)}$ is simply the sum of the propellant mass $M_p^{(i)}$ and the empty mass $M_e^{(i)}$ of that stage plus the initial mass $M_0^{(i+1)}$ of the next stage

$$M_0^{(i)} = M_p^{(i)} + M_e^{(i)} + M_0^{(i+1)} \qquad [6]$$

The burnout mass of any stage is

$$M_b^{(i)} = M_e^{(i)} + M_0^{(i+1)} \qquad [7]$$

and the propellant mass of any stage is the difference

$$M_p^{(i)} = M_0^{(i)} - M_b^{(i)} \qquad [8]$$

Obviously the payload mass M_L is the initial mass of the $(N + 1)$ stage

$$M_L = M_0^{(N+1)} = M_e^{(N+1)} \qquad [9]$$

and

$$M_p^{(N+1)} = 0 \qquad [10]$$

If the *stage* propellant fraction ζ_i is defined by

$$\zeta_i = M_p^{(i)}/M_0^{(i)} \qquad [11]$$

so that

$$1 - \zeta_i = M_b^{(i)}/M_0^{(i)} \qquad [12]$$

then the mass ratio is given by

$$\mathcal{R}_i = 1/(1 - \zeta_i) \qquad [13]$$

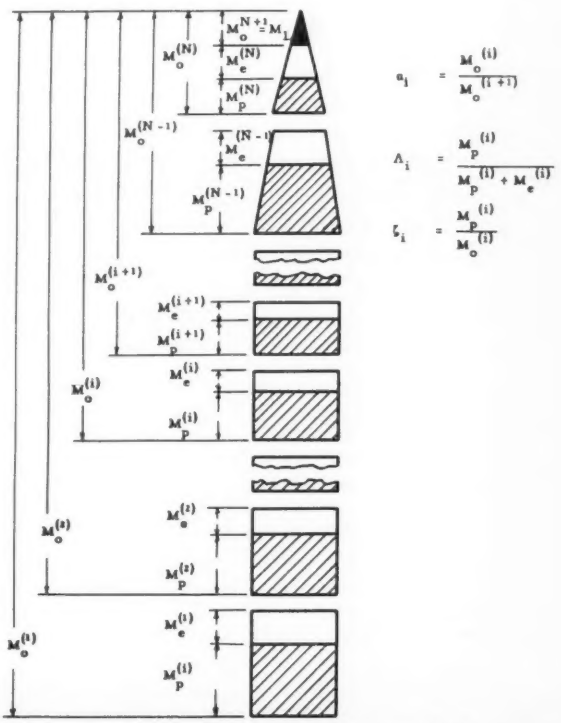

Fig. 1 Nomenclature for multistage rockets

Received Sept. 21, 1959.

[1] Vice President, Solid Rocket Plant. Fellow Member ARS.

[2] Numbers in parentheses indicate References at end of paper.

Alternatively, we may define the *motor* propellant fraction Λ_i by

$$\Lambda_i = M_p^{(i)}/[M_p^{(i)} + M_s^{(i)}] \quad [14]$$

and write the stage ratio, i.e., the ratio of the total mass of any stage to the "payload" mass of that stage, as

$$\alpha_i = M_0^{(i)}/M_0^{(i+1)} \quad [15]$$

Then the ratio of the mass of the loaded motor of any stage to the "payload" mass it carries is

$$\alpha_i - 1 = [M_p^{(i)} + M_s^{(i)}]/M_0^{(i+1)} \quad [16]$$

From Equations [14 and 16] it is apparent that the ratio of the propellant mass in any stage to the "payload" mass it accelerates is

$$\Lambda_i(\alpha_i - 1) = M_p^{(i)}/M_0^{(i+1)} \quad [17]$$

and hence from Equations [11 and 15] the stage propellant fraction is given in terms of the motor propellant fraction by

$$\zeta_i = \Lambda_i(\alpha_i - 1)/\alpha_i \quad [18]$$

Consequently, by Equation [13] the mass ratio for any stage can be written

$$\mathcal{R}_i = \left[1 - \Lambda_i\left(\frac{\alpha_i - 1}{\alpha_i}\right)\right]^{-1} \quad [19]$$

In the ideal optimum case where ζ_i, Λ_i, α_i, $\mathcal{R}_i$ and $\mathcal{V}_i$ are each constants unchanged from stage to stage, the total dimensionless velocity obtainable with a given motor propellant fraction Λ_i and a given stage ratio α_i is

$$\mathcal{V} = -N \ln\left[1 - \Lambda_i\left(\frac{\alpha_i - 1}{\alpha_i}\right)\right] \quad [20]$$

Conversely, the stage ratio needed to achieve a given dimensionless velocity when the motor propellant fraction is specified can be found by solving Equation [20] for α_i to give

$$\alpha_i = \Lambda_i/\{\Lambda_i - [1 - \exp - (\mathcal{V}/N)]\} \quad [21]$$

More important than the stage ratio is the total vehicle mass in relation to the payload mass

$$\alpha = M_0^{(1)}/M_L \quad [22]$$

which, from Equation [15], is

$$\alpha = \alpha_i^N \quad [23]$$

Hence from Equation [21] we get

$$\alpha = \left\{\frac{\Lambda_i}{\Lambda_i - [1 - \exp - (\mathcal{V}/N)]}\right\}^N \quad [24]$$

or, from Equation [20]

$$\mathcal{V} = -N \ln [1 - \Lambda_i(\alpha^{1/} - 1)/\alpha^{1N/N}] \quad [25]$$

Several interesting conclusions can be derived immediately from the last two equations. First, the minimum vehicle size in relation to the payload that is possible in the limit when $\Lambda_i \to 1$ is

$$\alpha = \exp \mathcal{V} \quad [26]$$

Conversely, the maximum velocity attainable with a given vehicle size for a given payload is

$$\mathcal{V} = \ln \alpha \quad [27]$$

These limits are independent of the number of stages. It is also apparent from Equation [24] that a lower limit to the permissible value of the motor propellant fraction that can be used to attain a specified value of the stage velocity increment $\mathcal{V}_i = \mathcal{V}/N$ is set by

$$\Lambda_i = 1 - \exp - \mathcal{V}_i \quad [28]$$

Finally, we may note that the limiting value of $\mathcal{V}$ for a given value of the motor propellant fraction Λ_i as $N \to \infty$ is

$$\mathcal{V} = \Lambda_i \ln \alpha \quad [29]$$

The most useful representation of the performance of N-stage rockets appears to be that afforded by Equation [24] which is plotted in Figs. 2–6 for $N = 1, 2, 3, 4$ and 5. These figures present, for a specified value of the total dimensionless velocity $\mathcal{V}$, the total vehicle size α in relation to the payload, as a function of the parameter of most direct concern to the rocket designer, namely the motor propellant fraction Λ_i.

Of considerable practical importance are the effects of small

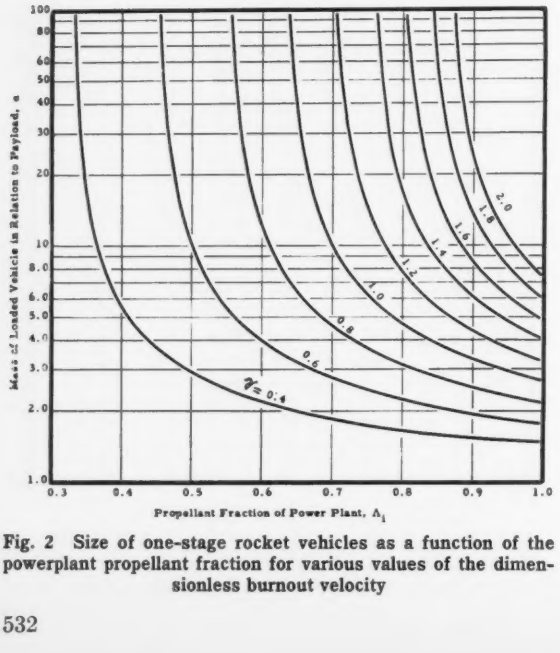

Fig. 2 Size of one-stage rocket vehicles as a function of the powerplant propellant fraction for various values of the dimensionless burnout velocity

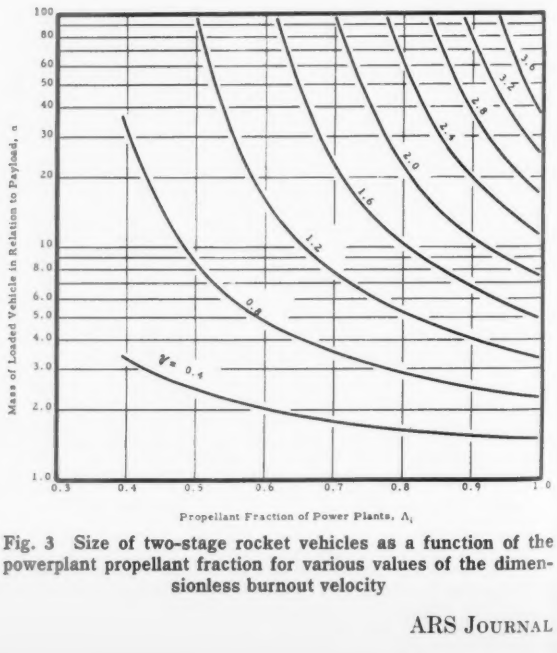

Fig. 3 Size of two-stage rocket vehicles as a function of the powerplant propellant fraction for various values of the dimensionless burnout velocity

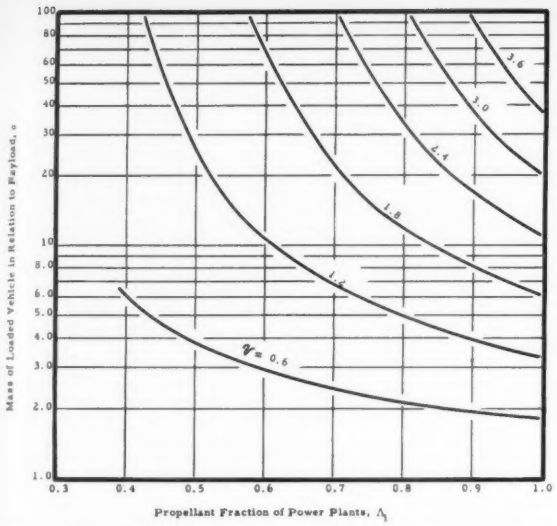

Fig. 4 Size of three-stage rocket vehicles as a function of the powerplant propellant fraction for various values of the dimensionless burnout velocity

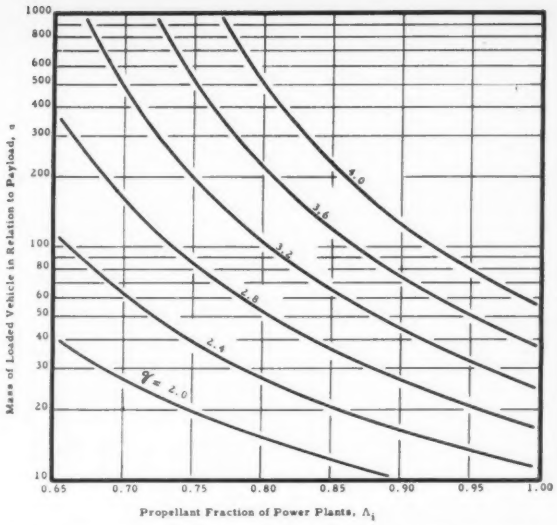

Fig. 5 Size of four-stage rocket vehicles as a function of the powerplant propellant fraction for various values of the dimensionless burnout velocity

changes in the inert parts, propellant or payload masses on the overall vehicle performance. These effects can be determined for the general N-stage rocket (where ζ_i, Λ_i, α_i, $\mathcal{R}_i$ and $\mathcal{V}_i$ are not necessarily the same for each stage) as follows. Differentiation of Equations [1 and 4] gives

$$d\mathcal{V}_i = d\mathcal{R}_i/\mathcal{R}_i \qquad [30]$$

Thus the absolute change in the dimensionless velocity increment of any stage is equal to the fractional change in its mass ratio. To put Equation [30] in terms of the actual masses involved, we start by differentiating Equation [5] to give

$$\frac{d\mathcal{R}_i}{\mathcal{R}_i} = \frac{dM_0^{(i)}}{M_0^{(i)}} - \frac{dM_b^{(i)}}{M_b^{(i)}} \qquad [31]$$

Utilizing $dM_0^{(i)} = dM_p^{(i)} + dM_b^{(i)}$ obtained from Equation [8] allows Equation [31] to be put in the form

$$\frac{d\mathcal{R}_i}{\mathcal{R}_i} = \zeta_i \left[\frac{dM_p^{(i)}}{M_p^{(i)}} - \frac{dM_b^{(i)}}{M_b^{(i)}} \right] \qquad [32]$$

We now recall that the burnout mass of the ith stage includes the propellant mass of all succeeding stages up to and including the Nth, the empty mass of the ith rocket stage and the empty mass of all succeeding rocket stages, including the $(N + 1)$ or payload stage. Hence, we may write

$$\frac{dM_b^{(i)}}{M_b^{(i)}} = \frac{\sum_{j=i+1}^{N} dM_p^{(j)} + \sum_{j=i}^{N+1} dM_e^{(j)}}{M_b^{(i)}} \qquad [33]$$

In this equation terms of the form $dM_p^{(j)}/M_b^{(j)}$ can be written

$$\frac{dM_p^{(j)}}{M_b^{(j)}} = \frac{M_p^{(j)}}{M_b^{(i)}} \frac{dM_p^{(j)}}{M_p^{(j)}} = \left(\frac{\zeta_j}{1 - \zeta_j} \right) \frac{M_0^{(j)}}{M_0^{(i)}} \frac{dM_p^{(j)}}{M_p^{(j)}} \qquad [34]$$

while

$$\frac{M_0^{(j)}}{M_0^{(i)}} = \frac{M_0^{(i+1)}}{M_0^{(i)}} \frac{M_0^{(i+2)}}{M_0^{(i+1)}} \cdots \frac{M_0^{(j)}}{M_0^{(j-1)}} = \frac{1}{\alpha_i} \frac{1}{\alpha_{i+1}} \cdots \frac{1}{\alpha_{j-1}} \qquad [35]$$

Therefore

$$\frac{dM_p^{(j)}}{M_b^{(i)}} = \left(\frac{\zeta_j}{1 - \zeta_j} \right) \left(\frac{1}{\alpha_i} \frac{1}{\alpha_{i+1}} \cdots \frac{1}{\alpha_{j-1}} \right) \frac{dM_p^{(j)}}{M_p^{(j)}} \qquad [36]$$

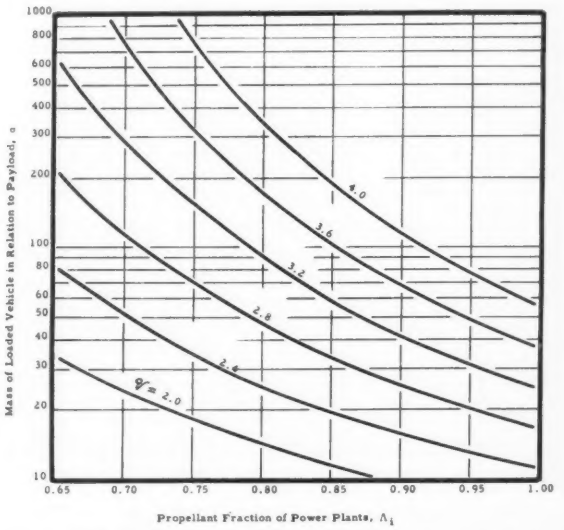

Fig. 6 Size of five-stage rocket vehicles as a function of the powerplant propellant fraction for various values of the dimensionless burnout velocity

Similarly, terms of the form $dM_e^{(j)}/M_b^{(i)}$ can be written

$$\frac{dM_e^{(j)}}{M_b^{(i)}} = \frac{dM_e^{(j)}}{M_b^{(i)}} \frac{M_e^{(j)}}{M_e^{(j)}} = \left(\frac{1 - \Lambda_j}{\Lambda_j} \right) \left(\frac{\zeta_j}{1 - \zeta_j} \right) \frac{M_0^{(j)}}{M_0^{(i)}} \frac{dM_e^{(j)}}{M_e^{(j)}} \qquad [37]$$

Therefore

$$\frac{dM_e^{(j)}}{M_b^{(i)}} = \left(\frac{1 - \Lambda_j}{\Lambda_j} \right) \left(\frac{\zeta_j}{1 - \zeta_j} \right) \left(\frac{1}{\alpha_i} \frac{1}{\alpha_{i+1}} \cdots \frac{1}{\alpha_{j-1}} \right) \frac{dM_e^{(j)}}{M_e^{(j)}} \qquad [38]$$

With these transformations, it is now possible to write Equation [33] in the form

$$\frac{dM_b^{(i)}}{M_b^{(i)}} = \sum_{j=i+1}^{N} \left(\frac{\zeta_j}{1-\zeta_i}\right)\left(\frac{1}{\alpha_i}\frac{1}{\alpha_{i+1}}\cdots\frac{1}{\alpha_{j-1}}\right)\frac{dM_p^{(j)}}{M_p^{(j)}} + \sum_{j=i}^{N+1}\left(\frac{1-\Lambda_j}{\Lambda_j}\right)\left(\frac{\zeta_j}{1-\zeta_i}\right)\left(\frac{1}{\alpha_i}\frac{1}{\alpha_{i+1}}\cdots\frac{1}{\alpha_{j-1}}\right)\frac{dM_e^{(j)}}{M_e^{(j)}} \quad [39]$$

and Equation [32] becomes

$$\frac{d\mathcal{R}_i}{\mathcal{R}_i} = \zeta_i\frac{dM_p^{(i)}}{M_p^{(i)}} - \left(\frac{\zeta_i}{1-\zeta_i}\right)\left[\sum_{j=i+1}^{N}\zeta_j\left(\frac{1}{\alpha_i}\frac{1}{\alpha_{i+1}}\cdots\frac{1}{\alpha_{j-1}}\right)\frac{dM_p^{(j)}}{M_p^{(j)}}\right] - \left(\frac{\zeta_i}{1-\zeta_i}\right)\left[\sum_{j=i}^{N+1}\zeta_j\left(\frac{1-\Lambda_j}{\Lambda_j}\right)\left(\frac{1}{\alpha_i}\frac{1}{\alpha_{i+1}}\cdots\frac{1}{\alpha_{j-1}}\right)\frac{dM_e^{(j)}}{M_e^{(j)}}\right] \quad [40]$$

This equation shows the percentage change in the mass ratio of the ith stage produced by a given percentage change in the propellant mass of that stage or any succeeding stage, or by a given percentage change in the inert mass of that stage or any succeeding stage including the payload. It should be noted that for $j = N + 1$ the factor $\zeta_j(1 - \Lambda_j)/\Lambda_j$ is unity.

The absolute change in burnout velocity of the ith stage obtained by differentiating Equation [3] is

$$dv_b^{(i)} = \mathcal{V}_i dc_i + c_i d\mathcal{V}_i - d[g_i t_b^{(i)}] \quad [41]$$

Consequently, in the most frequent circumstance where dc_i and $d[g_i t_b^{(i)}]$ are both zero, we have

$$dv_b^{(i)} = c_i d\mathcal{V}_i \quad [42]$$

and therefore, from Equations [30 and 40]

$$dv_b^{(i)} = c_i\left\{\zeta_i\frac{dM_p^{(i)}}{M_p^{(i)}} - \left(\frac{\zeta_i}{1-\zeta_i}\right)\left[\sum_{j=i+1}^{N}\zeta_j\left(\frac{1}{\alpha_i}\frac{1}{\alpha_{i+1}}\cdots\frac{1}{\alpha_{j-1}}\right)\frac{dM_p^{(j)}}{M_p^{(j)}}\right] - \left(\frac{\zeta_i}{1-\zeta_i}\right)\left[\sum_{j=i}^{N+1}\zeta_j\left(\frac{1-\Lambda_j}{\Lambda_j}\right)\left(\frac{1}{\alpha_i}\frac{1}{\alpha_{i+1}}\cdots\frac{1}{\alpha_{j-1}}\right)\frac{dM_e^{(j)}}{M_e^{(j)}}\right]\right\} \quad [43]$$

The total change in vehicle burnout velocity is found by summing Equation [43] over all stages. When rearranged the result is

$$dv_b = \sum_{i=1}^{N} p_i\frac{dM_p^{(i)}}{M_p^{(i)}} - \sum_{i=1}^{N} e_i\frac{dM_e^{(i)}}{M_e^{(i)}} - L_N\frac{dM_L}{M_L} \quad [44]$$

where the coefficients are

$$p_1 = c_1\zeta_1$$

$$p_2 = \left(1 - \frac{1}{\alpha_1}\frac{\zeta_1}{1-\zeta_1}\frac{c_1}{c_2}\right)c_2\zeta_2$$

$$p_3 = \left(1 - \frac{1}{\alpha_1}\frac{1}{\alpha_2}\frac{\zeta_1}{1-\zeta_1}\frac{c_1}{c_3} - \frac{1}{\alpha_2}\frac{\zeta_2}{1-\zeta_2}\frac{c_2}{c_3}\right)c_3\zeta_3$$

$$p_4 = \left(1 - \frac{1}{\alpha_1}\frac{1}{\alpha_2}\frac{1}{\alpha_3}\frac{\zeta_1}{1-\zeta_1}\frac{c_1}{c_4} - \frac{1}{\alpha_2}\frac{1}{\alpha_3}\frac{\zeta_2}{1-\zeta_2}\frac{c_2}{c_4} - \frac{1}{\alpha_3}\frac{\zeta_3}{1-\zeta_3}\frac{c_3}{c_4}\right)c_4\zeta_4$$

$$p_5 = \left(1 - \frac{1}{\alpha_1}\frac{1}{\alpha_2}\frac{1}{\alpha_3}\frac{1}{\alpha_4}\frac{\zeta_1}{1-\zeta_1}\frac{c_1}{c_5} - \frac{1}{a_2}\frac{1}{\alpha_3}\frac{1}{\alpha_4}\frac{\zeta_2}{1-\zeta_2}\frac{c_2}{c_5} - \frac{1}{\alpha_3}\frac{1}{\alpha_4}\frac{\zeta_3}{1-\zeta_3}\frac{c_3}{c_5} - \frac{1}{\alpha_4}\frac{\zeta_4}{1-\zeta_4}\frac{c_4}{c_5}\right)c_5\zeta_5 \quad [45]$$

$$e_1 = \left(\frac{\zeta_1}{1-\zeta_1}\right)\left(\frac{1-\Lambda_1}{\Lambda_1}\right)c_1\zeta_1$$

$$e_2 = \left(\frac{1}{\alpha_1}\frac{\zeta_1}{1-\zeta_1}\frac{c_1}{c_2} + \frac{\zeta_2}{1-\zeta_2}\right)\left(\frac{1-\Lambda_2}{\Lambda_2}\right)c_2\zeta_2$$

$$e_3 = \left(\frac{1}{\alpha_1}\frac{1}{\alpha_2}\frac{\zeta_1}{1-\zeta_1}\frac{c_1}{c_3} + \frac{1}{\alpha_2}\frac{\zeta_2}{1-\zeta_2}\frac{c_2}{c_3} + \frac{\zeta_3}{1-\zeta_3}\right)\left(\frac{1-\Lambda_3}{\Lambda_3}\right)c_3\zeta_3$$

$$e_4 = \left(\frac{1}{\alpha_1}\frac{1}{\alpha_2}\frac{1}{\alpha_3}\frac{\zeta_1}{1-\zeta_1}\frac{c_1}{c_4} + \frac{1}{\alpha_2}\frac{1}{\alpha_3}\frac{\zeta_2}{1-\zeta_2}\frac{c_2}{c_4} + \frac{1}{\alpha_3}\frac{\zeta_3}{1-\zeta_3}\frac{c_3}{c_4} + \frac{\zeta_4}{1-\zeta_4}\right)\left(\frac{1-\Lambda_4}{\Lambda_4}\right)c_4\zeta_4$$

$$e_5 = \left(\frac{1}{\alpha_1}\frac{1}{\alpha_2}\frac{1}{\alpha_3}\frac{1}{\alpha_4}\frac{\zeta_1}{1-\zeta_1}\frac{c_1}{c_5} + \frac{1}{\alpha_2}\frac{1}{\alpha_3}\frac{1}{\alpha_4}\frac{\zeta_2}{1-\zeta_2}\frac{c_2}{c_5} + \frac{1}{\alpha_3}\frac{1}{\alpha_4}\frac{\zeta_3}{1-\zeta_3}\frac{c_3}{c_5} + \frac{1}{\alpha_4}\frac{\zeta_4}{1-\zeta_4}\frac{c_4}{c_5} + \frac{\zeta_5}{1-\zeta_5}\right)\left(\frac{1-\Lambda_5}{\Lambda_5}\right)c_5\zeta_5 \quad [46]$$

$$L_N = \left(\frac{1}{\alpha_1}\frac{1}{\alpha_2}\cdots\frac{1}{\alpha_N}\frac{\zeta_1}{1-\zeta_1}\right)c_1 + \left(\frac{1}{\alpha_2}\frac{1}{\alpha_3}\cdots\frac{1}{\alpha_N}\frac{\zeta_2}{1-\zeta_2}\right)c_2 + \ldots + \left(\frac{1}{\alpha_N}\frac{\zeta_N}{1-\zeta_N}\right)c_N \quad [47]$$

It may be noted that the subscripts on p_i and e_i denote the contribution of the ith stage to dv_b, whereas the subscript on L_N denotes the total number of stages for the rocket being considered.

In the special case where the stage ratio α_i, the stage propellant fraction ζ_i and the effective exhaust velocity c_i are the same for each stage, it is apparent that the coefficient p_N, e_N and L_N all converge to definite limits when $N \to \infty$. By making use of the fact that the sum of the series $1 + x + x^2 + \ldots$ is $1/(1-x)$ when $x^2 < 1$, we find these limits to be

$$p_\infty = \left[1 - \left(\frac{1}{\alpha_{i-1}}\right)\left(\frac{\zeta_i}{1-\zeta_i}\right)\right]c_i\zeta_i \quad [48]$$

$$e_\infty = \left[\left(\frac{\alpha_i}{\alpha_{i-1}}\right)\left(\frac{\zeta_i}{1-\zeta_i}\right)\right]\left(\frac{1-\Lambda_i}{\Lambda_i}\right)c_i\zeta_i \quad [49]$$

$$L_\infty = \left(\frac{1}{\alpha_{i-1}}\right)\left(\frac{\zeta_i}{1-\zeta_i}\right)c_i \quad [50]$$

It is easy to show that p_∞ is equal to e_∞. Hence for the upper stages ($i > 3$) of a multistage rocket, increasing the propellant mass or decreasing the inert mass by the same percentage will have an approximately equal effect on the burnout velocity.

It is important to note that the coefficients p_i can never be negative, since from Equation [18]

$$\left(\frac{1}{\alpha_{i-1}}\right)\left(\frac{\zeta_i}{1-\zeta_i}\right) = \frac{\Lambda_i}{\alpha_i - \Lambda_i(\alpha_{i-1})} = \frac{1}{\alpha_i(\Lambda_i - 1)/\Lambda_i + 1} < 1 \quad [51]$$

Hence p_i is always positive. Physically this means that the increase in v_b brought about by increasing the propellant mass of the ith stage can never be offset by the decrease in v_b resulting from the associated increase in "payload" of the previous stages.

From the foregoing equations we can immediately deduce the effect of changing the propellant density in any stage. If the volume of propellant and its effective exhaust velocity are held constant in each stage so that the only change is in the propellant density ρ_i, then in [44] $dM_p^{(i)}/M_p^{(i)} = d\rho_i/\rho_i$, $dM_e^{(i)} = 0$, and $dM_L = 0$; hence

$$dv_b = \sum_{i=1}^{N} p_i \frac{d\rho_i}{\rho_i} \quad [52]$$

We may also deduce the tradeoff ratio between effective exhaust velocity and propellant density for any stage. From Equations [41 and 44] it is apparent that

$$dv_b = \sum_{i=1}^{N} \mathcal{V}_i dc_i + \sum_{i=1}^{N} p_i \frac{d\rho_i}{\rho_i} \quad [53]$$

Hence if all stages remain unchanged but one, then dv_b will be zero if

$$\frac{dc_i}{c_i} = \frac{-(p_i/c_i)(d\rho_i/\rho_i)}{\mathcal{V}_i} \quad [54]$$

Thus a given percentage increase in effective exhaust velocity must be greater than any accompanying decrease in propellant density multiplied by the factor $(p_i/c_i\mathcal{V}_i)$ in order for there to be a net increase in burnout velocity. Conversely, any attempt to increase vehicle performance by increasing the propellant density can be accompanied by a decrease in effective exhaust velocity no greater than that corresponding to Equation [54].

To illustrate the magnitudes of the coefficients p_i, e_i and L_N, let us suppose that a multistage rocket is constructed with the motor propellant fraction $\Lambda_i = 0.875$ for each stage, the stage propellant fraction $\zeta_i = 0.70$ and the stage ratio $\alpha_i = 5$. If the effective exhaust velocity is the same for each stage, then the coefficients are as follows

$$p_1 = 0.700c, \quad p_2 = 0.373c, \quad p_3 = 0.308c,$$
$$p_4 = 0.295c, \ldots, p_\infty = 0.292c$$

$$e_1 = 0.233c, \quad e_2 = 0.280c, \quad e_3 = 0.289c,$$
$$e_4 = 0.291c, \ldots, e_\infty = 0.292c$$

$$L_1 = 0.467c, \quad L_2 = 0.560c, \quad L_3 = 0.579c,$$
$$L_4 = 0.582c, \ldots, L_\infty = 0.583c$$

It is of interest to observe that in this example the effect of a given percentage increase in propellant mass is about twice as useful in the first stage as in any other stage.

To extend the usefulness of Equation [44], recall that the maximum range of a ballistic missile over a nonrotating spherical Earth is

$$R = 2r_0 \sin^{-1} v_b^2/(2gr_0 - v_b^2) \qquad 0 \le R \le \pi r_0 \quad [55]$$

where $r_0 = 2.09 \times 10^7$ ft = 3440 nautical miles is the radius of Earth. This equation may also be written

$$\frac{v_b^2}{2gr_0} = \frac{\sin(R/2r_0)}{1 + \sin(R/2r_0)} \quad [56]$$

and on differentiating gives

$$\frac{v_b dv_b}{gr_0} = \frac{\cos(R/2r_0)}{[1 + \sin(R/2r_0)]^2}\frac{dR}{2r_0} \quad [57]$$

Division of Equation [57] by [56] gives

$$\frac{2dv_b}{v_b} = \frac{dR/2r_0}{[1 + \sin(R/2r_0)]\tan(R/2r_0)} \quad [58]$$

or

$$\frac{dR}{R} = 2\left\{\frac{\tan(R/2r_0)\,[1 + \sin(R/2r_0)]}{R/2r_0}\right\}\frac{dv_b}{v_b} \quad [59]$$

This equation may be used in conjunction with Equation [44] for estimating the effect of changes in rocket characteristics on missile range.

Nomenclature

- c = effective exhaust velocity
- e = coefficient for inert parts, in Equation [44]
- g = effective component of gravitational acceleration
- L_N = coefficient for payload, in Equation [44]
- M_b = mass of vehicle at propellant burnout
- M_e = empty mass of rocket stage
- M_L = mass of payload

M_p = mass of propellant
M_0 = initial mass of vehicle stage
N = number of stages in multistage rocket
p = coefficient for propellant in Equation [44]
r_0 = radius of Earth, 2.09×10^7 ft
$\mathcal{R}$ = mass ratio, Equation [5]
R = maximum range of missile over spherical Earth
t_b = duration of burning
v_b = burnout velocity
$\mathcal{U}$ = dimensionless velocity increment, Equation [3]
α = vehicle mass in relation to payload mass, Equation [22]
α_i = stage ratio, Equation [15]
ζ_i = stage propellant fraction, Equation [11]
Λ_i = motor propellant fraction, Equation [14], = 1 − ϵ of ref. (1)
ρ = propellant density
Subscript i and superscript (i) refer to ith stage

References

1 Malina, F. J. and Summerfield, M., "The Problem of Escape from Earth by Rocket," *J. Aeron. Sci.*, vol. 14, 1947, pp. 471–480.
2 Seifert, H. S., Mills, M. M. and Summerfield, M., "The Physics of Rockets," *Amer. J. Phys.*, vol. 15, 1947, pp. 1–21, 121–140, 255–272.
3 Cleaver, A. V., "Mass Ratios," *J. Brit. Interplanet. Soc.*, vol. 8, 1949, pp. 173–179.
4 Vertregt, M., "Calculation of Step Rockets," *J. Brit. Interplanet. Soc.*, vol. 14, 1955, pp. 20–25.

Orbits for Planetary Satellites From Doppler Data Alone

ARMIN J. DEUTSCH[1]

Douglas Aircraft Co., Inc.
Santa Monica, Calif.

When an artificial satellite is put in orbit around another planet, it will be difficult or impossible from terrestrial observations to obtain its direction with sufficient precision to define its orbit. However, if the satellite carries a suitable transmitter, Doppler observations are capable of giving precise values for the line of sight component of the velocity vector. From such data alone, it is possible to obtain all the orbital elements and the mass of the planet. The analytical apparatus used by astronomers for the discussion of spectroscopic binary stars is here adapted to the interpretation of Doppler observations of a planetary or lunar satellite. An example is given of the orbit determination for a satellite of Venus.

WHEN a satellite is put in orbit around some body other than Earth, it will then become possible to ascertain for that body the same kinds of data that terrestrial satellites have recently obtained. In this way we may expect soon to map the magnetic fields of the moon and planets, and the radiation belts associated with them. We may also obtain the oblateness terms in the gravitational potentials of these bodies, the properties of their exospheres and many other results of high importance.

However, in order to achieve results of this kind, it will usually be necessary to establish the satellite orbit with considerable precision. The vehicle will be thrown into a satellite orbit by some sort of end course guidance based, presumably, upon midcourse observations of its ballistic trajectory, but it is unreasonable to expect that the end-course guidance will be sufficiently exact to yield just the desired satellite orbit. A method is therefore needed for establishing the orbital elements after the application of end-course guidance.

This requirement will not be easily satisfied by conventional methods. At planetary distances, vehicles of the expected order of size will be far too faint for optical detection by reflected sunlight. At the distance of the moon, the stellar magnitude of a perfectly reflecting sphere of 1-m diameter will be 16. But as a satellite of Venus, the same sphere will be of the 29th magnitude when Venus is near inferior conjunction, and a magnitude fainter at superior conjunction. As a satellite of Jupiter, the sphere will have a magnitude of about 37. The extreme limit of the 200-in. telescope is the 24th magnitude, and a practical working limit is the 22nd magnitude.

Although optical observations are therefore out of the question in most cases, the vehicle may nevertheless be detected by suitable radio telescopes, provided it carries a sufficiently powerful transmitter. Actually, the power requirements aboard the satellite will probably not be excessive. Rechtin[2] has recently estimated the capability of a microlock-type system in 1960 as a 30-cps information bandwidth at the distance of Mars, provided the vehicle carries a 10-w transmitter and an antenna of 16-db gain.

The detection of continuous wave signals from a planetary

Received Aug. 4, 1959.

[1] Consultant, Missiles and Space Systems Engineering; also Staff Member, Mt. Wilson and Palomar Observatories, California Institute of Technology, Pasadena, Calif.

[2] E. Rechtin, colloquium at California Institute of Technology, Pasadena, Calif., March 20, 1959.

satellite will not necessarily solve the orbit determination problem, however. Let us suppose that a vehicle is put in orbit around Venus, with a semimajor axis of order 10 per cent greater than the planetary radius. As seen from Earth, the maximum angular subtense of the semimajor axis will then be 70″; at superior conjunction it will be only 11″. In the case of a Martian satellite, these angles become 27″ at opposition and 4″ at conjunction. Now, these numbers represent the whole angular excursion of the satellite relative to the planet; to establish an orbit of any utility, we should have to require that angular measurements discern the satellite position with an accuracy at least some 10 times higher. But this requirement is far beyond the capabilities of any existing or projected high gain antenna; the Jodrell Bank paraboloid, for example, has a theoretical resolving power of 10′ at 1420 mc per sec.

Despite the evident inadequacy of angular measurements for orbit determinations of this kind, there remains the possibility that, if the satellite transmits a signal of high frequency-stability, an orbit can be accurately determined from Doppler data alone. The orbital velocities V in the examples cited previously are 23,000 fps for the Venerian satellite, and 11,000 fps for the Martian satellite. At speeds of this order, the velocity error δV that corresponds to a frequency error $\delta\lambda$ is given by the relation $\delta V/V \simeq 10^5\,(\delta\lambda/\lambda)$. For an error $|\delta\lambda/\lambda| \simeq 10^{-8}$, which appears to be a conservative figure for the frequency-stability that can be achieved, the corresponding error $|\delta V|$ amounts only to about 10 fps. In the special case of a satellite orbit that is circular around a planet of unknown mass, the measurement of V leads directly to a determination of a. Moreover, the fractional errors of a and V will be related as $\Delta a/a = 2\,|\Delta v/v|$. For a Martian satellite with $V \simeq 11{,}000$ fps, a frequency stability of 10^{-8} therefore would yield a with an error of 0.2 per cent. This is evidently quite sufficient precision for many important investigations.

An analogous problem of orbit determination is often encountered in conventional astronomical research. From the Doppler shifts of the absorption lines in stellar spectra, astronomers have determined for many stars the component of stellar velocity along the line of sight to Earth. When this velocity component is referred to an origin at rest in the sun, it is said to be the radial velocity of the star. In many stars, the radial velocity varies periodically in a way which indicates that each such star is in Kepler motion around a close companion. The companion is usually so close that the pair cannot be resolved in the sky by any existing telescope, and it is usually so faint that its light cannot be detected in the observed spectrum. Techniques have been developed for the derivation of certain orbital characteristics of such a spectroscopic binary star from its observed velocity curve. In particular, a so-called "mass function" can be obtained, which in some cases leads to a determination of the sum of masses of the two stars comprising the pair.

The techniques appropriate for the discussion of spectroscopic binaries will now be adapted for the case of a planetary satellite. We shall suppose that from pulse Doppler observations of such a satellite, it is possible to obtain a velocity curve, which gives the radial velocity of the satellite as a function of phase in its orbit. In the first instance, we shall suppose that the satellite orbit is a Kepler ellipse fixed in space relative to an inertial frame, and that Earth and planet (say, Venus) are also stationary in this frame. The Doppler effect is supposed to be measured by a stationary observer at the center of Earth, and the orbit is supposed to subtend an infinitely small angle as viewed from this position. In later sections, account will be taken of the various effects due to departures from these ideal conditions.

Doppler Orbits Observed in One Orientation

Consider the unit sphere with center O at the center of Venus. In Fig. 1, the termini are indicated for the following unit vectors:

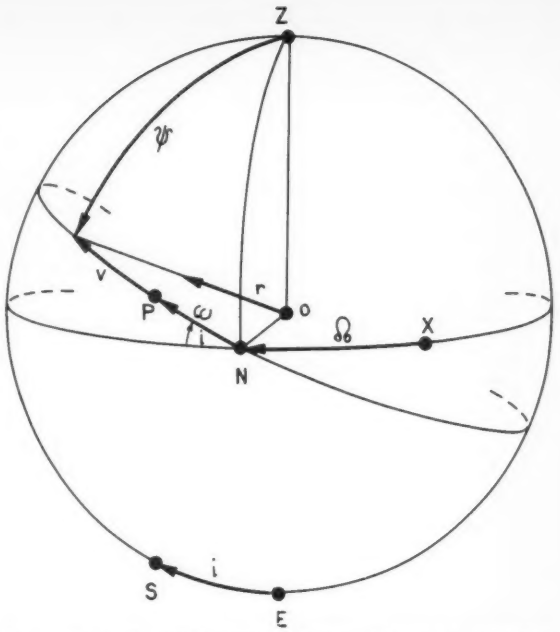

Fig. 1 Unit sphere with center at Venus. The pole of a satellite orbit lies in the direction of *S*, periplanet in the direction of *P* and Earth in the direction of *E*

- ***E***, in the direction from Venus to Earth
- ***S***, in the direction of the pole of the satellite orbit
- ***N***, in the direction of the ascending node of the satellite orbit against the plane perpendicular to ***E*** ("plane of the sky")
- ***X***, in the direction of north along the hour circle through Venus
- ***Z***, in the direction of $-\boldsymbol{E}$
- ***P***, in the direction of periplanet

To define the orbit plane, it will suffice to give the inclination i, which is the angle between ***E*** and ***S***; and the position angle of the ascending node Ω, which is the angle between ***X*** and ***N***. The orientation of the orbit in its plane is then determined by the longitude of periplanet ω, which is the angle between ***N*** and ***P***. The ranges of these three angular elements are: $0 \le i \le \pi$; $0 \le \Omega \le 2\pi$; $0 \le \omega \le 2\pi$.

Let $\boldsymbol{r}$ be the instantaneous radius vector of the satellite relative to Venus; then the true anomaly v is the angle between ***P*** and $\boldsymbol{r}$, measured in the sense of the orbital motion around ***S***. The component of $\boldsymbol{r}$ along ***Z*** is therefore seen in Fig. 1 to be

$$z = r \cos \psi \qquad [1]$$

and, by spherical trigonometry, this is easily shown to be

$$z = r \sin i \sin (v + \omega) \qquad [2]$$

As viewed from Earth, the radial component of the velocity of the satellite is then

$$\dot{z} = \dot{r} \sin i \sin (v + \omega) + r\dot{v} \sin i \cos (v + \omega) \qquad [3]$$

where the dot denotes differentiation with respect to time.

But from the theory of Kepler motion it may be shown (1)[3] that

$$\dot{r} = \frac{2\pi\, ae \sin v}{P\sqrt{1-e^2}} \qquad r\dot{v} = \frac{2\pi\, a(1+e\cos v)}{P\sqrt{1-e^2}} \qquad [4]$$

where

a = semimajor axis of the orbital ellipse
e = its eccentricity
P = orbital period

Introducing these expressions into Equation [3] and simplifying, we find that

$$\dot{z} = \mathrm{K}[e\cos\omega + \cos(v+\omega)] \qquad [5]$$

where the amplitude of velocity variation is

$$\mathrm{K} = 2\pi\, a \sin i / P\sqrt{1-e^2} \qquad [6]$$

If the distance between the observer and Venus is increasing at the constant rate γ, then this parameter will appear as an additive constant in the right member of Equation [5].

Let the time t be measured from an arbitrary origin, and let the phase Φ be defined in the relation

$$\Phi = (2\pi/P)t \qquad [7]$$

The observed velocity curve then gives $\dot{z}$ as a function of Φ. From this curve, it is possible to deduce the values of K, e, ω and γ. The techniques for obtaining these parameters are described, e.g., by Smart (1) and Aitken (2). The velocity curve also yields the epoch T of periplanet, which is an instant of minimum separation of planet and satellite. Knowing P, e and K, it is also possible to find from Equation [6] the quantity $a \sin i$.

To obtain the mass function $f(m)$ we now adduce the harmonic law

$$m = \frac{4\pi^2}{G}\frac{a^3}{P^2} \qquad [8]$$

[3] Numbers in parentheses indicate References at end of paper.

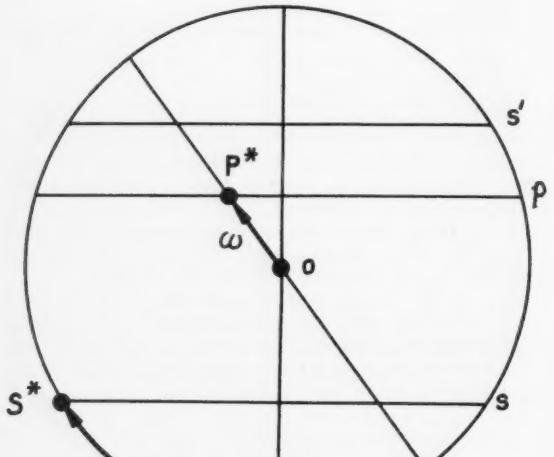

Fig. 2 Orthographic projection of the unit sphere at Venus. If the planetary mass is assumed known, then any one velocity curve for a satellite restricts S to two small circles s and s', and P to a third small circle p

In this relation, m is strictly the sum of masses of planet and satellite. For our application, it is essentially the planet mass. Again, a is strictly the semimajor axis of the satellite orbit around the planet as focus. For our application, it is essentially the same as the observed quantity, which is the semimajor axis of the satellite orbit around a focus at the center of mass of planet and satellite. The mass function may now be defined as

$$f(m) = m \sin^3 i \qquad [9]$$

and, by Equation [8] it is

$$f(m) = \frac{4\pi^2}{G}\frac{(a\sin i)^3}{P^2} \qquad [10]$$

in which the right member contains only known quantities.

When the mass may be considered known, the quantity $\sin i$ can be found directly from Equation [8] in the form

$$\sin^3 i = \frac{4\pi^2}{G}\frac{(a\sin i)^3}{m\,P^2} \qquad [11]$$

and a can then be found as well. Fig. 2 will illustrate the geometry of this case. The circle represents an orthographic projection of the unit sphere centered on Venus. Equation [11] restricts the terminus of $\boldsymbol{S}$ to the two small circles designated s and s' in Fig. 2. Similarly, the known value of ω then restricts the terminus of $\boldsymbol{P}$ to the small circle designated p. A particular case satisfying these restrictions is indicated by $\boldsymbol{S}^*$ and $\boldsymbol{P}^*$, the corresponding orbit plane being designated f.

This completes the discussion of the information that can be obtained from a velocity curve of a satellite under the assumption that its orbit is a fixed Kepler ellipse seen always in the same orientation. We shall next discuss the additional information that can be obtained when we take into account that the satellite orbit may be observed under different orientations as a consequence of the orbital motions of Earth and planet around the sun.

Doppler Orbits Observed in Diverse Orientations

Observations in Three Non Co-Planar Directions

We shall now show that if velocity curves can be obtained for a fixed Kepler ellipse as viewed from three non co-planar directions, then all the orbital elements of the ellipse are unambiguously determinate, as is the mass of the planet. In most of the foreseeable applications of Doppler techniques to satellite orbit determinations, the observations will, in fact, be very nearly confined to the plane of the ecliptic. Moreover, the principal purpose of Doppler observations is likely to be the determination of the shape, size and orientation of the satellite orbit, and for this purpose it will usually suffice to assume that the mass is known from independent astronomical determinations. Nevertheless, it will now be appropriate to consider the general non co-planar case, with unknown mass, before proceeding to the special cases which are more likely to be of early practical importance.

We shall use the same notation as in the previous section. We may take $\boldsymbol{S}$ and $\boldsymbol{P}$ to be constant vectors when referred to an inertial frame. However, due to the motion of Venus and Earth in their orbits around the sun, the vectors $\boldsymbol{E}$, $\boldsymbol{N}$ and $\boldsymbol{X}$ will vary with time. Their values at the epoch t_j will be designated $\boldsymbol{E}_j$, $\boldsymbol{N}_j$ and $\boldsymbol{X}_j$. If $\boldsymbol{E}_1$, $\boldsymbol{E}_2$, $\boldsymbol{E}_3$ are any three non co-planar unit vectors, we may write

$$\boldsymbol{S} = \sum_{j=1}^{3} \alpha_j \boldsymbol{E}_j \qquad [12]$$

But from Fig. 1, we see that

$$\boldsymbol{N}\sin i = \boldsymbol{S} \times \boldsymbol{E} \qquad [13]$$

Hence

$$\boldsymbol{N}_1 \times \boldsymbol{N}_2 \sin i_1 \sin i_2 = [(\boldsymbol{S} \times \boldsymbol{E}_1)\cdot\boldsymbol{E}_2]\boldsymbol{S} \qquad [14]$$

By Equation [12]

$$\boldsymbol{S} \times \boldsymbol{E}_1 = \alpha_2 \boldsymbol{E}_2 \times \boldsymbol{E}_1 + \alpha_3 \boldsymbol{E}_3 \times \boldsymbol{E}_1 \qquad [15]$$

Therefore

$$\boldsymbol{N}_1 \times \boldsymbol{N}_2 \sin i_1 \sin i_2 = \alpha_3[(\boldsymbol{E}_2 \times \boldsymbol{E}_1)\cdot\boldsymbol{E}_2]\boldsymbol{S} \qquad [16]$$

Moreover, Fig. 1 shows that

$$\boldsymbol{N}_1 \times \boldsymbol{N}_2 = \boldsymbol{S} \sin (\omega_1 - \omega_2) \qquad [17]$$

Hence Equation [16] yields

$$\alpha_3 = \sin (\omega_1 - \omega_2) \sin i_1 \sin i_2 / \boldsymbol{E}_3\cdot(\boldsymbol{E}_1 \times \boldsymbol{E}_2) \qquad [18]$$

and similar expressions can be obtained for α_1 and α_2 by cyclic permutation of the subscripts.

Since $\boldsymbol{S}$ is a unit vector, we find by squaring Equation [12] that

$$\sum_{j=1}^{3} \alpha_j^2 + 2 \sum_{i \neq j} \alpha_i \alpha_j \cos \Gamma_{ij} = 1 \qquad [19]$$

where Γ_{ij} is the (known) angle between $\boldsymbol{E}_i$ and $\boldsymbol{E}_j$

$$\cos \Gamma_{ij} = \boldsymbol{E}_i\cdot\boldsymbol{E}_j \qquad [20]$$

Hence Equation [19] may be written as

$$a^4 = \sum_{j=1}^{3} (a^2 \alpha_j)^2 + 2 \sum_{i \neq j} (a^2 \alpha_i)(a^2 \alpha_j) \cos \Gamma_{ij} \qquad [21]$$

and in this equation all quantities appearing in the right member may be taken as known. Having found the semimajor axis in this equation, we may now proceed to obtain $\sin i_j$ from the known values of $a \sin i_j$. Equation [18] then yields the coefficients α_j and therefore determines the vector $\boldsymbol{S}$. The α_j also determine the quadrant of each i_j, for Equation [12], and Fig. 1 gives us

$$\cos i_1 = \boldsymbol{E}_1\cdot\boldsymbol{S} = \alpha_1 + \alpha_2 \cos \Gamma_{12} + \alpha_3 \cos \Gamma_{13} \qquad [22]$$

etc., for $\cos i_2$ and $\cos i_3$.

With $\boldsymbol{S}$ known, we may now compute $\boldsymbol{N}_j$ in Equation [13]. Moreover, we see in Fig. 1 that

$$\boldsymbol{P} = \boldsymbol{N}_j \cos \omega_j + \boldsymbol{S} \times \boldsymbol{N}_j \sin \omega_j \qquad [23]$$

and this enables us to find the vector $\boldsymbol{P}$. We also have

$$\boldsymbol{E}_j \sin \Omega_j = \boldsymbol{X}_j \times \boldsymbol{N}_j \qquad \cos \Omega_j = \boldsymbol{X}_j\cdot\boldsymbol{N}_j \qquad [24]$$

and since $\boldsymbol{X}_j$ is known, these relations determine Ω_j. Finally, we may obtain the mass from the harmonic law, Equation [8]. In the practical case where m may be considered as independently known, Equations [8 and 21] provide a constraint upon the observed values of $a \sin i_j$ and ω_j. We shall see in the next section that when m is known, there is an additional constraint upon the parameters $a \sin i_j$ and ω_j that are associated with any pair of directions $\boldsymbol{E}_j$.

Observations From Co-Planar Directions

In the practically important case where the satellite orbit can only be observed from directions lying in a plane, the argument of the last section fails because $\boldsymbol{S}$ cannot in general be analyzed into components along any three $\boldsymbol{E}_j$, as in Equation [12]. To discuss this case, we define a unit vector $\boldsymbol{E}_0$ which is perpendicular to the plane of $\boldsymbol{E}_1$ and $\boldsymbol{E}_2$

$$\boldsymbol{E}_0 \sin \Gamma_{12} = \boldsymbol{E}_1 \times \boldsymbol{E}_2 \qquad [25]$$

The orbit is then never observed from the direction $\boldsymbol{E}_0$, but only from $\boldsymbol{E}_1$, $\boldsymbol{E}_2$ and (possibly) other directions in their plane.

As in Equation [18], we may then write

$$\alpha_0 = \frac{\sin (\omega_1 - \omega_2) \sin i_1 \sin i_2}{\boldsymbol{E}_0\cdot(\boldsymbol{E}_1 \times \boldsymbol{E}_2)} = \frac{\sin (\omega_1 - \omega_2) \sin i_1 \sin i_2}{\sin \Gamma_{12}} \qquad [26]$$

We also have

$$\boldsymbol{S} = \sum_{j=0}^{2} \alpha_j \boldsymbol{E}_j \qquad [27]$$

and therefore

$$\begin{aligned} \boldsymbol{E}_1\cdot\boldsymbol{S} &= \alpha_1 + \alpha_2 \cos \Gamma_{12} = \cos i_1 \\ \boldsymbol{E}_2\cdot\boldsymbol{S} &= \alpha_1 \cos \Gamma_{12} + \alpha_2 = \cos i_2 \end{aligned} \qquad [28]$$

It follows that

$$\begin{aligned} \alpha_1 \sin^2 \Gamma_{12} &= \cos i_1 - \cos \Gamma_{12} \cos i_2 \\ \alpha_2 \sin^2 \Gamma_{12} &= \cos i_2 - \cos \Gamma_{12} \cos i_1 \end{aligned} \qquad [29]$$

But the square of Equation [27] is

$$\alpha_0^2 + \alpha_1^2 + \alpha_2^2 + 2\alpha_1\alpha_2 \cos \Gamma_{12} = 1 \qquad [30]$$

and if we substitute the values of the α_j into this equation, we obtain after some simplification

$$[(2 - \sin^2 \Gamma_{12})a^4 - (A_1^2 + A_2^2)a^2 + A_1^2 A_2^2 \sin^2 (\omega_1 - \omega_2)]^2 - 4a^4 \cos^2 \Gamma_{12}(a^2 - A_1^2)(a^2 - A_2^2) = 0 \qquad [31]$$

where

$$\begin{aligned} A_1 &= a \sin i_1 \\ A_2 &= a \sin i_2 \end{aligned} \qquad [32]$$

The observed values of A_1, A_2 and $\omega_1 - \omega_2$ therefore constrain the semimajor axis a to satisfy an equation of the eighth degree, namely Equation [31]. In case we may regard m as independently known, then a follows directly from Equation [8], and Equation [31] becomes simply a constraint upon $\sin i_1$, $\sin i_2$ and $\omega_1 - \omega_2$. In either case, however, there will be two values of i_1 compatible with the observed A_1 and two values of i_2 compatible with the observed A_2. We may write these as

$$\begin{aligned} i_1 &= I_1 \quad \text{or} \quad i_1 = I_1' = \pi - I_1 \\ i_2 &= I_2 \quad \text{or} \quad i_2 = I_2' = \pi - I_2 \end{aligned} \qquad [33]$$

Suppose that when we compute (α_1, α_2) in Equations [29], we use the pair (I_1, I_2), and that this produces an (α_1, α_2) which satisfies Equation [30]. Then it is clear that (I_1', I_2') will also produce an acceptable (α_1, α_2). In general, however, the pairs (I_1, I_2') and (I_2, I_1') will then not correspond to possible solutions. It follows that the orbit plane may have one of two possible orientations, as shown in Fig. 3.

To find the effect of this ambiguity on the vector $\boldsymbol{P}$, we write it in the form

$$\boldsymbol{P} = \sum_{j=0}^{2} \beta_j \boldsymbol{E}_j \qquad [34]$$

Referring to Fig. 1, we see that

$$\begin{aligned} \boldsymbol{E}_1\cdot\boldsymbol{P} &= \beta_1 + \beta_2 \cos \Gamma_{12} = -\sin i_1 \sin \omega_1 \\ \boldsymbol{E}_2\cdot\boldsymbol{P} &= \beta_1 \cos \Gamma_{12} + \beta_2 = -\sin i_2 \sin \omega_2 \end{aligned} \qquad [35]$$

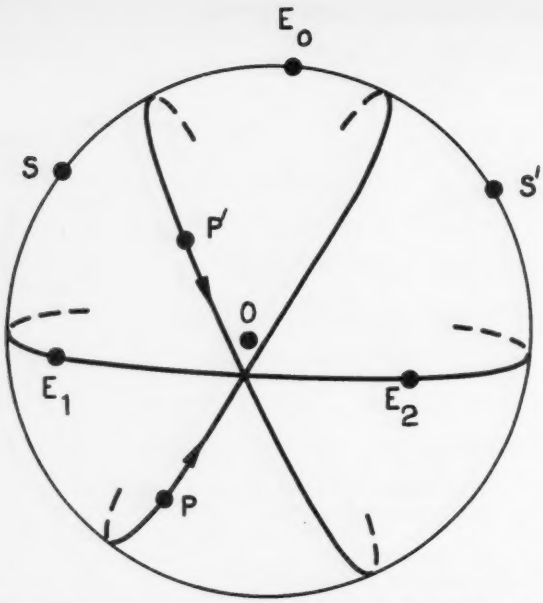

Fig. 3 Degeneracy of the solution when all observations are confined to one plane, e.g., the ecliptic. If one of the illustrated orbits satisfies the velocity curves, the other orbit will do so equally well

whence

$$\beta_1 \sin^2 \Gamma_{12} = \cos \Gamma_{12} \sin i_2 \sin \omega_2 - \sin i_1 \sin \omega_1$$
$$\beta_2 \sin^2 \Gamma_{12} = \cos \Gamma_{12} \sin i_1 \sin \omega_1 - \sin i_2 \sin \omega_2 \quad \ldots\ldots [36]$$

The ambiguities of Equations [33] therefore leave β_1 and β_2 unambiguously determined. Moreover, it is clear that

$$\boldsymbol{S} \cdot \boldsymbol{P} = 0 \qquad [37]$$

and by Equations [27 and 34] this is

$$\alpha_0\beta_0 + \alpha_1\beta_1 + \alpha_2\beta_2 + (\alpha_1\beta_2 + \alpha_2\beta_1) \cos \Gamma_{12} = 0 \qquad [38]$$

which determines β_0 and therefore $\boldsymbol{P}$, when $\boldsymbol{S}$ is known. $\boldsymbol{S}$ differs from $\boldsymbol{S}'$ only in the signs of α_1 and α_2 (see Fig. 3), and therefore β_0 reverses its sign with α_1 and α_2.

Corrections for Diurnal Motions, etc.

It is now necessary to discuss the various effects which may be produced as the result of departures from the ideal conditions specified earlier. In the first place, we note that, during one cycle of the satellite, there may be an appreciable change in that component of the observer's diurnal motion $\boldsymbol{D}$ which lies along the line of sight to the satellite. But since $\boldsymbol{D}$ is known, and also the direction $-\boldsymbol{E}$ to the satellite (or, at least, to its primary planet), it is a simple matter to remove from all the observed radial velocities the contribution $-\boldsymbol{D}\cdot\boldsymbol{E}$ of the diurnal motion.

In the idealized theory, where the observer was supposed to be at the center of an infinitely distant Earth, it was not necessary to differentiate among the following vector distances in Fig. 4:

$\rho\boldsymbol{E}$, from the center O of the primary body to the center ϵ of Earth
$\lambda\boldsymbol{F}$, from the satellite $\mathcal{S}$ to the center of Earth
$l\boldsymbol{G}$, from the satellite to the observer $\mathcal{P}$ on the surface of Earth

When the observations are sufficiently precise, however, it will be necessary to take into account that they yield the quantity $\dot{l}$. Certain small corrections must then be applied to $\dot{l}$ to obtain the quantity $\dot{z}$, for which the foregoing theory has been developed. In the case of a lunar satellite, for example, the orbit may subtend an angle of more than a degree at Earth, and the radius vector $\boldsymbol{R}$ to the observer may subtend an angle about as large at the satellite.

To find the corrections that must be applied to $\dot{l}$ in order to obtain $\dot{z}$, we note in Fig. 4 that

$$r^2 = \lambda^2 - \rho^2 - 2\rho z \qquad [39]$$

and

$$l^2 = \lambda^2 + R^2 + 2\lambda\boldsymbol{F}\cdot\boldsymbol{R} \qquad [40]$$

where the notation is the same as in the previous sections and Fig. 4. Therefore

$$\dot{z} = \frac{\lambda}{\rho}\dot{\lambda} - \left(1 + \frac{z}{\rho}\right)\dot{\rho} - \frac{r}{\rho}\dot{r} \qquad [41]$$

and

$$\dot{\lambda} = \frac{(l/\lambda)\,\dot{l} - (d/dt)(\boldsymbol{F}\cdot\boldsymbol{R})}{1 + (1/\lambda)\boldsymbol{F}\cdot\boldsymbol{R}} \qquad [42]$$

But to a close approximation, we shall always have

$$l \simeq \lambda \simeq \rho \qquad z/\lambda \ll 1 \qquad r/\lambda \ll 1$$
$$R/\lambda \ll 1 \qquad \boldsymbol{E} \simeq \boldsymbol{F} \simeq \boldsymbol{G} \quad \ldots\ldots [43]$$

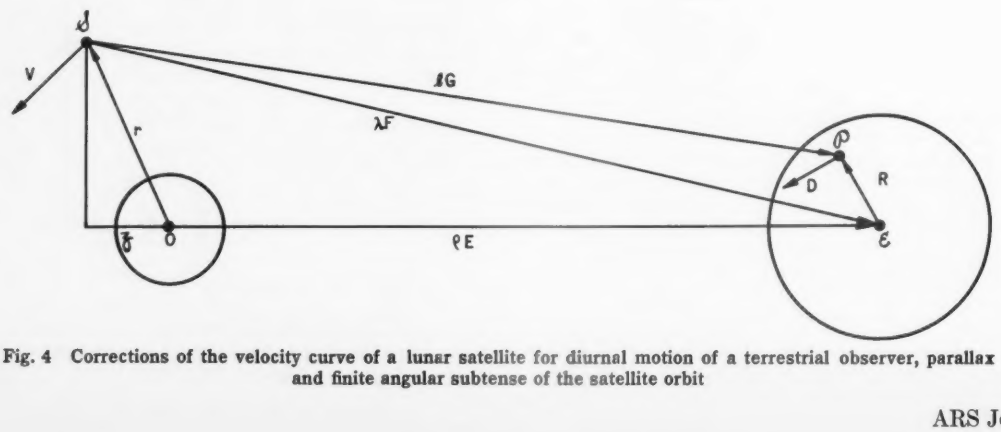

Fig. 4 Corrections of the velocity curve of a lunar satellite for diurnal motion of a terrestrial observer, parallax and finite angular subtense of the satellite orbit

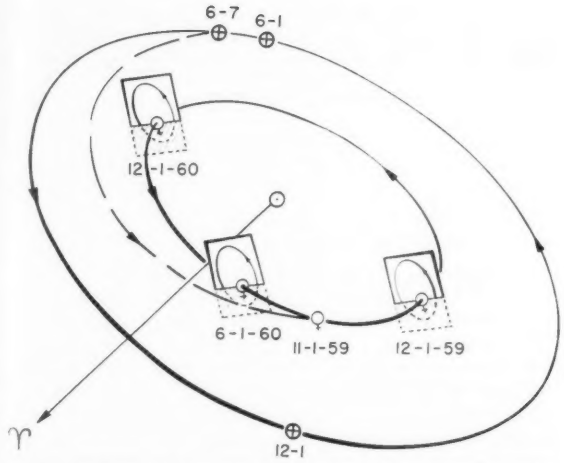

Fig. 5 Schematic representation of a Venus satellite orbit. Velocity curves are supposed to be observed on Dec. 1, 1959 and June 1 and Dec. 1, 1960. The positions of Venus and Earth on these dates are indicated, together with the transfer orbit corresponding to a launch date at Earth of June 7, 1959

Therefore a first approximation to Equations [41 and 42] yields

$$\dot{z}_1 = \dot{\lambda}_1 - \dot{\rho} \qquad \dot{\lambda}_1 = \dot{l} + (d/dt)(\boldsymbol{E}\cdot\boldsymbol{R}) \qquad [44]$$

The second of these equations gives $\dot{\lambda}$ in terms of the measured radial velocity and the (known) correction for the component of diurnal motion along the line of sight to the primary. The first equation then gives a first approximation to $\dot{z}_1$, in terms of $\dot{\lambda}_1$ and the (known) radial velocity of the primary. From $\dot{z}_1$, we may then find a first approximation to the orbital elements, by the methods detailed previously, and the corresponding approximation to r as a function of phase.

Let this approximation be designated r_1. From it, we may then compute an improved approximation of each of the following functions of time

$$\lambda_2\boldsymbol{F}_2 = \rho\boldsymbol{E} - \boldsymbol{r}_1 \qquad l_2\boldsymbol{G}_2 = \lambda_2\boldsymbol{F}_2 + \boldsymbol{R} \qquad [45]$$

$$\dot{\lambda}_2 = \frac{(l_2/\lambda_2)\,\dot{l} - (d/dt)(\boldsymbol{F}_2\cdot\boldsymbol{R})}{1 + (1/\lambda_2)\boldsymbol{F}_2\cdot\boldsymbol{R}} \qquad [46]$$

$$\dot{z}_2 = \frac{\lambda_2}{\rho}\dot{\lambda}_2 - \left(1 + \frac{z_1}{\rho}\right)\dot{\rho} - \frac{r_1}{\rho}\dot{r}_1 \qquad [47]$$

If $\dot{z}_2$ differs significantly from z_1 it is then possible to reiterate this procedure until the observations are adequately represented.

There still remain to be discussed all those effects which arise because of perturbations, i.e., because the orbit is not really a fixed Kepler ellipse. In order to view the orbit of a planetary satellite in appreciably different orientations, it will usually be necessary to wait for intervals of several months. However, during such intervals the satellite may have made a thousand cycles, and in the most interesting and

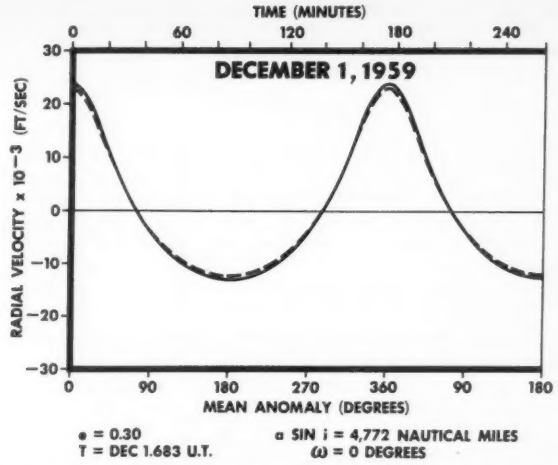

Fig. 6 Velocity curve for a satellite of Venus, Dec. 1, 1959. The dashed curve is for the image orbit

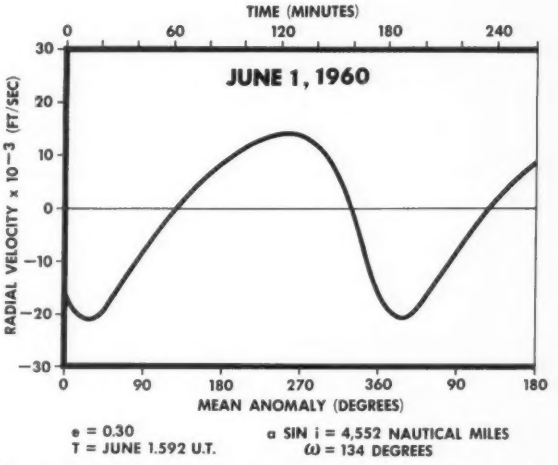

Fig. 7 Velocity curve for a satellite of Venus, June 1, 1960

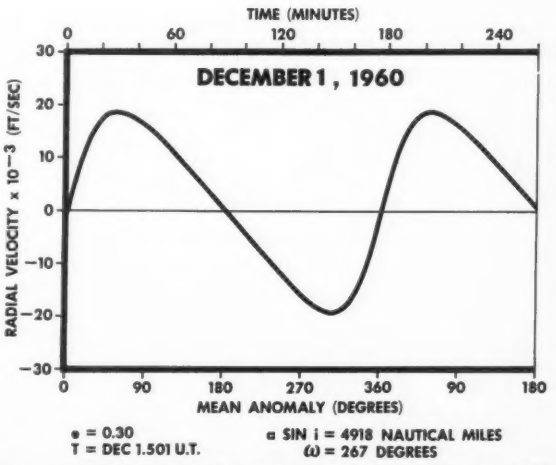

Fig. 8 Velocity curve for a satellite of Venus, Dec. 1, 1960

informative cases the orbital elements will be appreciably perturbed during these intervals. The techniques required for the analysis of perturbed satellite orbits are a natural extension of the ones developed here. They will be given in detail in a later paper.

Example: Doppler Orbit for a Satellite of Venus

To illustrate the kinds of velocity curves that will be obtained for planetary satellites, let us consider the following hypothetical example. On June 7, 1959, a vehicle is launched in a Hohmann transfer orbit to Venus, as illustrated in the schematic diagram of Fig. 5. The vehicle then arrives at Venus' orbit on Nov. 1, 1959; at this time, the last-stage motor provides an impulse sufficient to throw the probe into a satellite orbit around Venus.

The probe carries a suitable transmitter to permit Doppler measurements at a terrestrial receiver. These observations are first made on Dec. 1, 1959 (Fig. 5). After correction for the known radial velocity of Venus and for the observer's diurnal motion, the observations yield the (solid line) velocity curve of Fig. 6, with a period of 173.4 min. The other spectroscopic elements that can be deduced from this velocity curve are also indicated in Fig. 6. If we adopt the astronomically determined value for the mass of Venus, we can also obtain a and sin i. separately. In any case, the quadrant of i is indeterminate from this velocity curve, and so is the direction of the line of nodes against the plane of the sky.

Velocity curves are determined again on June 1 and Dec. 1, 1960, and the corresponding elements are found in each case, as indicated in Figs. 7 and 8. When these three sets of spectroscopic elements are analyzed with the apparatus previously described, it is found that the pole of the satellite orbit must lie in the direction of the unit vector with components

$$S_x = 0.300 \qquad S_y = 0.400 \qquad S_z = 0.866$$

The x-axis here points to the vernal equinox, as usual, and the z-axis to the north pole of the ecliptic. In addition, we find that the unit vector towards periplanet has the components

$$P_x = -0.377 \qquad P_y = 0.884 \qquad P_z = -0.278$$

The values of inclination i and position angle of the node Ω, which correspond to these values of $\boldsymbol{S}$ and $\boldsymbol{P}$, are shown with respect to the plane of the sky in the following table

	i, deg	Ω, deg
Dec. 1, 1959	67	276
June 1, 1960	119	253
Dec. 1, 1960	71	288

If these orbital elements are now referred to the plane of the ecliptic, as is customarily done for the orbital elements of planets, they are found to be

a = 5200 nautical miles = 1.55 Venus radii
e = 0.300
i = 30 deg
Ω = 143 deg
ω = 326 deg
P = 173.4 min
T = Dec. 1959, 1.683 UT

The inclination of the orbit of Venus relative to the plane of the ecliptic is only 3.4 deg, and the geocentric latitudes of the planet on the three dates of observations are, respectively, 2.2, 5.1 and 2.2 deg. The configuration is, therefore, not far from the degenerate case treated earlier, where the velocity curves are equally well satisfied by this orbit and by its mirror image in the plane of the ecliptic. To indicate, in this case, the discrimination between the true orbit and its image, the velocity curve corresponding to the image orbit has also been computed for Dec. 1, 1959, and is shown as a dashed curve in Fig. 6.

Acknowledgment

I wish to express my gratitude to R. David Lüders for a critical reading of the manuscript, and to Bernard L. Beskind for the calculations leading to the example in the last section.

References

1 Smart, W. M., "Spherical Astronomy," Cambridge Univ. Press, Cambridge, 1936, chap. 14.
2 Aitken, R. G., "Binary Stars," McGraw-Hill Publishing Co., Inc. N. Y., 1935, chap. 14.

American Rocket Society
POWER SYSTEMS CONFERENCE
September 27–30, 1960
Miramar Hotel
Santa Monica, California

Session 1—Thermoelectricity
Session 2—Thermionics
Session 3—Photovoltaic and Photoemissive Cells
Session 4—Electrochemistry
Session 5—Solar Systems—Photovoltaic nickel cadmium flight systems
Session 6—Dynamic Engines
Session 7—Nuclear
Session 8—Nuclear

The program will also include evening seminars that will deal with high temperature, high emissivity surfaces for space; condensation in gravitationless fields; and micrometeorite penetrations.

Detonation Wave Hypersonic Ramjet[1]

W. H. SARGENT[2] and R. A. GROSS[3]

Fairchild Engine and Airplane Corp. Deer Park, N. Y.

Performance of a hypersonic ramjet having a detonation wave combustion process is described. Flight speeds from Mach 2.5 to 10 are examined. Thermodynamic property changes across a detonation wave are presented. Engine cycle performance characteristics are computed including air specific impulse, specific fuel consumption and thermal efficiency. The effect of component efficiency on cycle performance is examined and the optimum place in the cycle for the detonation wave is found. The subsonic burning ramjet is shown always to have superior thermodynamic performance compared to a detonation wave engine, but the differences are often minor. Other differences and some design features are discussed.

HYPERSONIC ramjets employing a standing detonation wave were first mentioned by Roy in 1946 (1).[4] Although detonations had never been stabilized in any device at that time, their properties could be computed and potential performance assessed. Dunlap (2), Nicholls (3), Roy (4), Partel (5), Chinitz (6) and Weber (7) have recently presented papers which contain discussions of such a device.

Several years ago a number of laboratories in the United States began to explore techniques for releasing chemical energy steadily in supersonic flow. Research groups at the Fairchild Engine Division and the University of Michigan have succeeded in producing steady detonations in the laboratory. A summary of this work on stationary detonations has recently been prepared by Gross and Nicholls (8). Other pertinent work is referred to in (8, 9 and 10).

In Fig. 1 is shown a typical Schlieren photograph of a standing strong detonation wave of the type found experimentally by Gross and Chinitz (10). The detonation wave shown is a hydrogen-air reaction, stable at Mach 3.15 in a supersonic combustion research tunnel. The oblique shock waves originate from side wall wedges and, under zero fuel flow conditions, intersect in a small normal Mach reflected shock. Upon the introduction of fuel upstream, and with the proper stagnation conditions for ignition [see (10)], a strong detonation wave forms. This wave is stable, steady and reproducible. It has relatively simple properties, considering that there are large gradients in the inflowing fuel-air ratio and consequently large temperature and pressure gradients on the downstream side of the wave. The local conditions immediately across the wave are predictable using classical methods (11). The regions of stable operation are discussed in (10 and 12) and consist of the "strong" branch ($M_2 < 1$) solutions. An ignition hysteresis effect was found (10) which, although not completely understood, may permit detonation wave stabilization at low inlet stagnation temperatures.

Received July 1, 1959.

[1] This work was carried out under the sponsorship of the Air Force Office of Scientific Research under Contract no. AF 49(638)-15.

[2] Presently at Atlantic Research Corp., Alexandria, Va.

[3] Presently National Science Foundation Senior Post Doctoral Fellow, Physics Dept., University of California, Berkeley. Fellow Member ARS.

[4] Numbers in parentheses indicate References at end of paper.

With stationary stable detonations in the research laboratory and an increasing awareness and understanding of their actual properties, assessment of the performance of a propulsion device employing such a combustion system was desirable. This formed the basis and motivation for this detailed study of a detonation wave ramjet cycle.

Engine Cycle

The engine cycle which is studied here is a typical one of compression, combustion and expansion. The basic difference is the condition under which combustion takes place, namely, a standing detonation in supersonic flow.

The parameters which we determine for this cycle are: Air specific impulse, specific fuel consumption, thermal efficiency and exit to inlet area ratio.

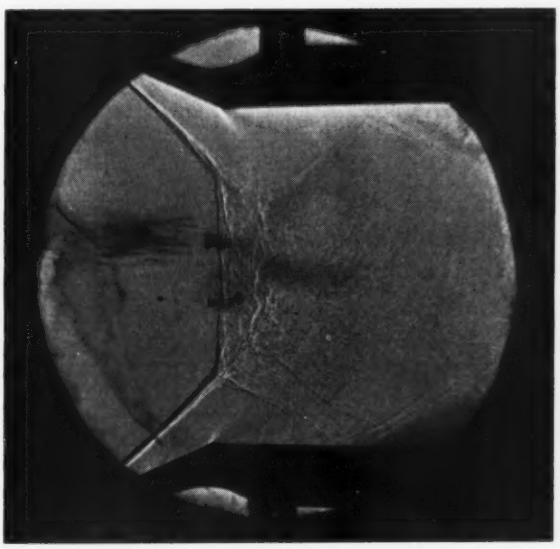

Fig. 1 Schlieren photograph, strong detonation wave. Mach 3.15, hydrogen-air, from Gross and Chinitz (10)

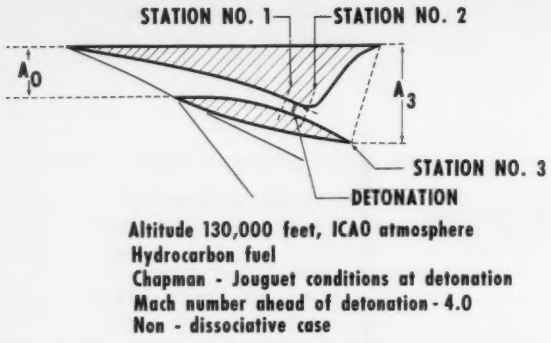

Fig. 2 Schematic of detonation wave ramjet engine, flight Mach number 6.0. Altitude 130,000 ft, hydrocarbon fuel, C-J detonation at Mach 4

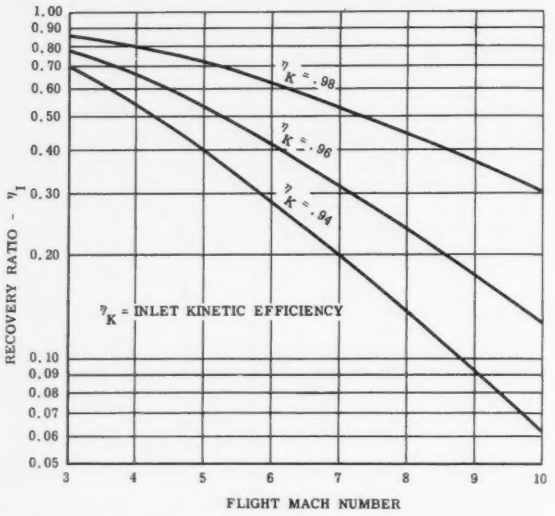

Fig. 3 Total pressure recovery vs. flight Mach number

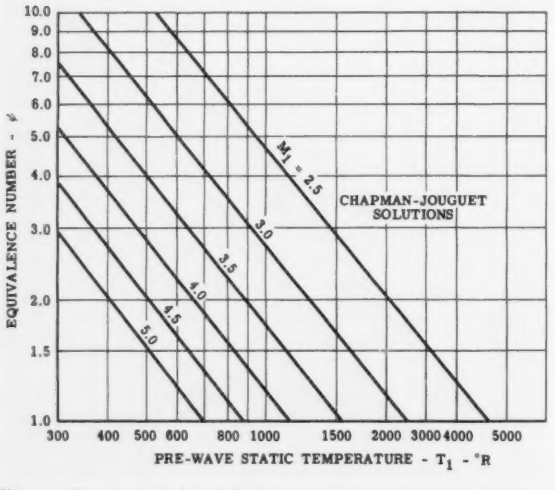

Fig. 4 Equivalence for C-J points vs. pre-wave static temperature

These parameters have been determined as a function of: Flight Mach number (2.5 to 10), detonation Mach number (2.5 to 4.0), inlet efficiency and exhaust nozzle efficiency.

The calculations were all performed for a typical hydrocarbon fuel whose heating value ΔH is 8.78×10^5 Btu/mole and for flight conditions corresponding to 130,000 ft, as defined by the ICAO atmosphere.

A typical engine configuration is shown in Fig. 2. The inlet consists of a passage in which supersonic compression of air occurs adiabatically from the flight Mach number to the combustion or detonation Mach number. The kinetic efficiency of compression η_K is defined as the ratio of the kinetic energy in the diffused stream (when that stream is isentropically expanded to ambient free stream static pressure) to the free stream kinetic energy. Values of η_K ranging from 1.0 (ideal case) to 0.94 were employed and γ_0 was treated as a constant equal to 1.4. Fig. 3 shows the total pressure recovery as a function of flight Mach number for several values of inlet kinetic efficiency.

Inlet efficiency as used in this report applies only to diffusion from flight Mach number to the pre-wave detonation Mach number. This usage is at variance with usual practice, in which the inlet efficiency refers to diffusion from free stream to a low subsonic Mach number. In our context, an inlet efficiency of 0.94 is a pessimistic assessment of performance and represents a lower boundary for design expectations. For the flight speeds from Mach 5 to 7, inlet kinetic efficiencies of approximately 0.96 to 0.98 are realistic. The static temperature at the end of diffusion and just upstream of the detonation wave is

$$T_1 = T_0 \frac{1 + [(\gamma_0 - 1)/2]M_0^2}{1 + [(\gamma_0 - 1)/2]M_1^2} \quad [1]$$

The total and static pressures are given by

$$P_{t1} = \eta_I P_0 \{1 + [(\gamma_0 - 1)/2]M_0^2\}^{\gamma_0/(\gamma_0 - 1)} \quad [2]$$

$$P_1 = P_{t1} \{1 + [(\gamma_0 - 1)/2]M_1^2\}^{\gamma_0/(1 - \gamma_0)} \quad [3]$$

where

$$\eta_I = \frac{P_0}{P_{t_0}} \left\{1 - \eta_K \left[1 - \left(\frac{P_0}{P_{t_0}}\right)^{(\gamma_0 - 1)/\gamma_0}\right]\right\}^{\gamma_0/(\gamma_0 - 1)}$$

Fuel injection is assumed to take place upstream of the inlet, so that a uniform fuel-air distribution exists at the detonation wave. Losses accruing from fuel injection have not been included in these computations. For an assessment of these losses the reader is referred to (2).

Conditions across the normal detonation wave are treated by the solution of the classical conservation equations. The methods and computer program were adapted from (11). Most of the calculations presented here employ the nondissociative case, with thermodynamic properties a function of temperature. The reactants and products of combustion result from the chemical change

$$\alpha_0 C_x H_y + \alpha_1 O_2 + \alpha_2 N_2 + \alpha_3 A \rightarrow$$

$$\beta_1 CO_2 + \beta_2 H_2O + \beta_3 O_2 + \beta_4 N_2 + \beta_5 A \quad [4]$$

and are treated as ideal gas mixtures. Combustion efficiency is assumed always to be 100 per cent. In general, it is advantageous to have detonation occur under Chapman-Jouguet conditions (7), i.e., $M_2 = 1$. For those conditions which cannot be satisfied by this requirement, a strong detonation solution is employed. The conditions across the wave that are of interest in this analysis are shown in Figs. 4 through 8.

These data represent the nondissociative solution of a hydrocarbon fuel reacting with air in one-dimensional steady flow. The nondissociative calculation is presented here in detail because of its relative simplicity and because in a comparison study it represents only a small error. In (11) dissociation as it affects the wave is discussed. The dissociative

equilibrium calculation may also be at variance with reality in that reaction rates may not permit the attainment of equilibrium. A dissociative equilibrium cycle calculation at Mach 6 gives, for example, an increase in specific fuel consumption of about 7 per cent.

In a rapidly moving gas mixture where chemical equilibrium does not exist and where the constituents are either dissociating or recombining, the extent of dissociation or recombination in an arbitrary region of the mixture will depend upon the local mean temperature of the mixture, the partial pressure of the constituents and the mean residence time of the molecular species. Since the residence time in the combustion zone in the conventional engine is far longer than in the wave engine, it might be expected that in whichever way the equilibrium is shifting, the shift will be more complete for the long residence time flow.

Figs. 6 and 7 show the variation of the wave total and static pressure ratio with respect to pre-wave static temperature. The rapid increase in the static pressure ratio should be noted in the regime of strong detonation solutions. The rise occurs because of the very rapid decay of the wave exit Mach number, as shown in Fig. 8. The total pressure ratio in the strong detonation solution region is not heavily affected by pre-wave static temperature except at the extreme Mach number conditions. It is interesting that the total pressure ratio actually moderates at the lowest pre-wave Mach number in the strong detonation solution region. In general, however, the loss increases in magnitude and gradient with increasing pre-wave Mach number.

The exhaust nozzle expands the combustion products adiabatically with a discharge coefficient C_D of either 1.0 or 0.98. The nozzle exit temperature is given by

$$T_3 = T_2(P_0/P_2)^{(\gamma-1)/\gamma} \qquad [5]$$

where

$$\gamma = [\gamma(T_2) + \gamma(T_3)]/2$$

and is computed for a gas composed of the products of combustion as specified by Equation [4]. The exit velocity is computed from

$$V_3 = C_D\sqrt{2(h_{t2} - h_3)/\bar{m}_2} \qquad [6]$$

where

$$h_{t_2} = C_{p2}T_2\{1 + [(\gamma_2 - 1)/2]M_2^2\}$$

The cycle performance can now be evaluated. The parameters of interest with their associated equations are given in the following:

Air specific impulse

$$I_A = \frac{F_N}{W_A} = \frac{V_3 - V_0}{g} \qquad [7]$$

Specific fuel consumption

$$SFC = (f/a)_S 3600/\psi I_A \qquad [8]$$

Thermal efficiency

$$\eta_{th} = \frac{V_0 I_A \psi}{(f/a)_S(\Delta H/m_f)} \qquad [9]$$

Exit to inlet area ratio

$$\frac{A_3}{A_0} = \frac{V_0\bar{m}_0 T_3}{V_3\bar{m}_3 T_0} \qquad [10]$$

Equation [7] applies for an expansion process to ambient pressure. This may be undesirable because of the large exit area and hence drag. The desired degree of expansion is a detailed question concerning an engineering balance between thrust, weight and external drag. We assume a fully expanded nozzle for comparison purposes.

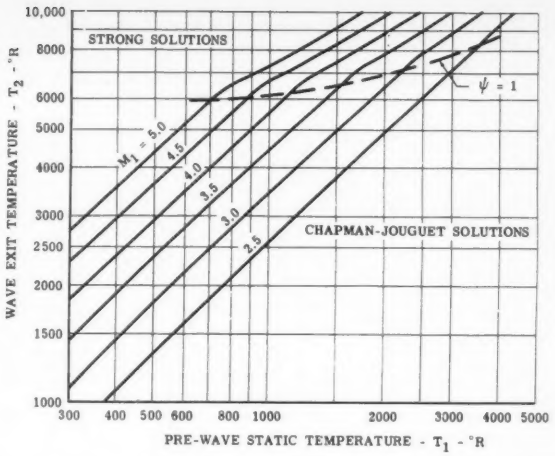

Fig. 5 Wave exit static temperature vs. pre-wave static temperature

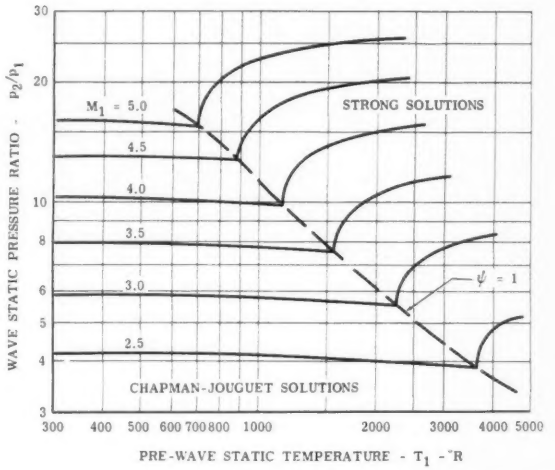

Fig. 6 Wave static pressure ratio vs. pre-wave static temperature

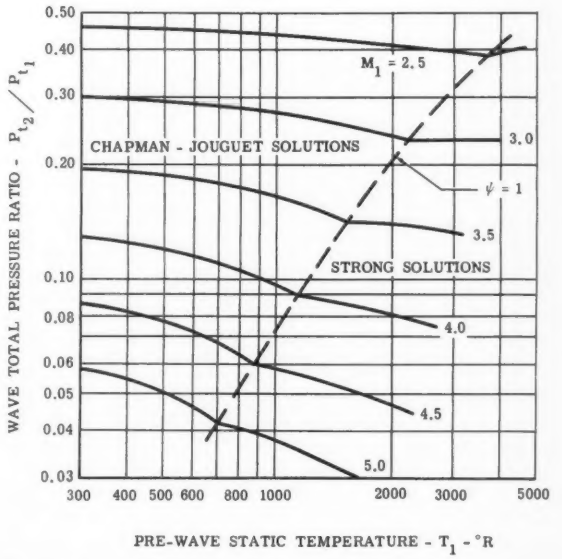

Fig. 7 Wave total pressure ratio vs. pre-wave static temperature

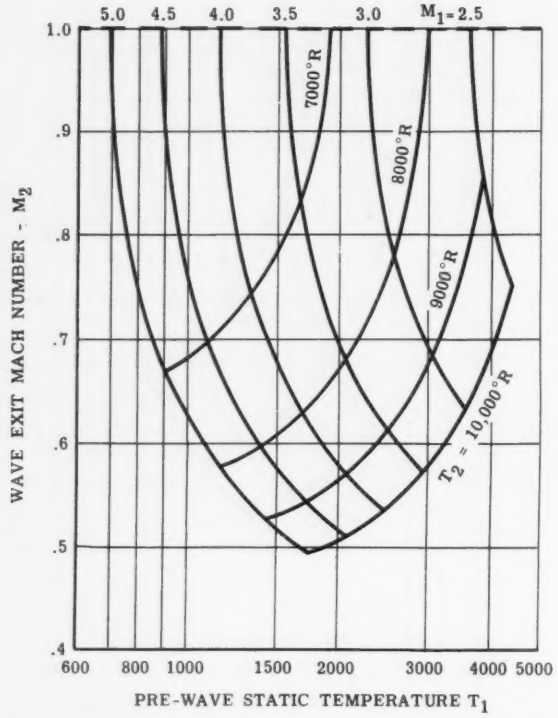

Fig. 8 Wave exit Mach number vs. pre-wave static temperature

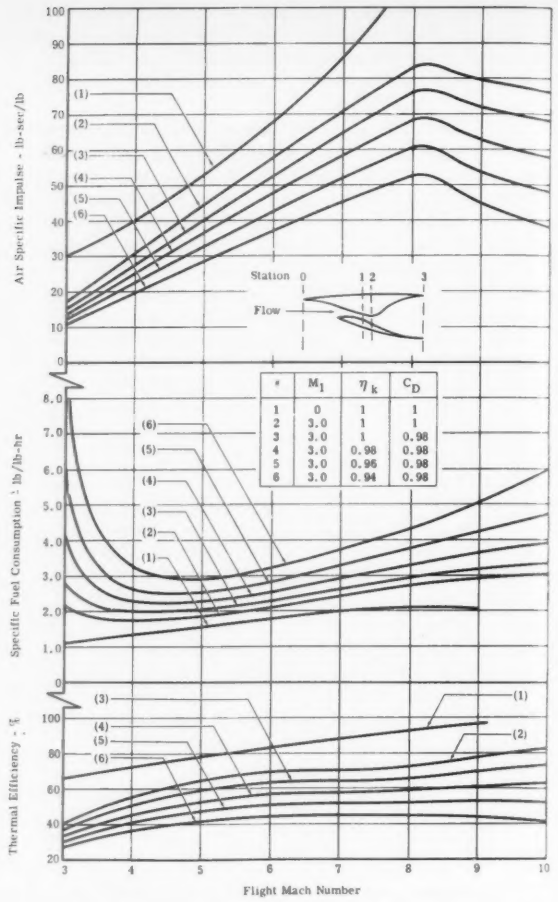

Fig. 9 Performance parameters, detonation wave ramjet, $M_1 = 3.0$

Results

Figs. 9 and 10 show some basic data for evaluating engine performance. In these plots, air specific impulse, specific fuel consumption and thermal efficiency are examined as functions of flight Mach number, pre-wave Mach number, and inlet and exhaust efficiency. In each figure where the performance characteristics for a constant pre-wave Mach number are defined, a base reference curve has been included. This curve represents the performance of an ideal conventional engine operating on the same fuel-air schedule as the associated wave engine. The ideal engine is described in a later section. At a flight Mach number of 6, the detonation wave engine makes its nearest approach to the idea engine.

In the range of pre-wave Mach numbers from 2.5 to 3.0 the difference between ideal wave and conventional engine performance becomes great. For example, at $M_1 = 2.5$ and $M_0 = 6.0$ the wave engine delivers 96 per cent of the impulse of the conventional engine, whereas at $M_1 = 3.0$ the impulse ratio falls to 87 per cent. From $M_1 = 3.0$ to $M_1 = 3.5$, approximately the same ratio between conventional and wave engine impulse is maintained. Beyond $M_1 = 3.5$ the ratio again falls rapidly to a value of 71 per cent at $M_1 = 4.0$.

Increasing the fuel-air ratio increases the specific impulse, whereas wave loss decreases the impulse. At the lowest pre-wave Mach numbers the slope of the fuel-air ratio with pre-wave Mach number is not as steep as the slope of the wave losses. This causes a rapid decline in specific impulse. In the middle region of pre-wave Mach numbers both rates of change steepen, but the fuel-air ratio is more drastically affected than the wave loss. This results in a mild impulse plateau which then drops off as the wave loss again assumes control.

The inflection of the impulse ratio is reflected in the shape of the thermal efficiency curves shown on Fig. 11. The variation of air specific impulse and thermal efficiency can be examined with respect to pre-wave Mach number. Optimum impulse at flight Mach number 4.0 is achieved with a pre-wave Mach number of 3.0. At flight Mach number 6.0, optimum impulse occurs at $M_1 = 3.75$, and at flight Mach number 8.0 the optimum point is again $M_1 = 3.0$. The shift in optimum pre-wave Mach number results from the interplay of pre-wave temperature and wave losses. At a constant pre-wave Mach number the permissible (Chapman-Jouguet) fuel-air ratio increases with increasing pre-wave temperature. At low flight speeds, if $M_0 = 4$ can be considered low, minimizing wave losses in the low fuel-air ratio range is essential. At a flight Mach number of 6.0 the optimum pre-wave Mach number is increased to take advantage of a more favorable fuel-air ratio. At a flight Mach number of 8.0 the pre-wave temperature is sufficiently high to permit a large fuel-air ratio at a reduced pre-wave Mach number, thus increasing the optimum specific impulse further.

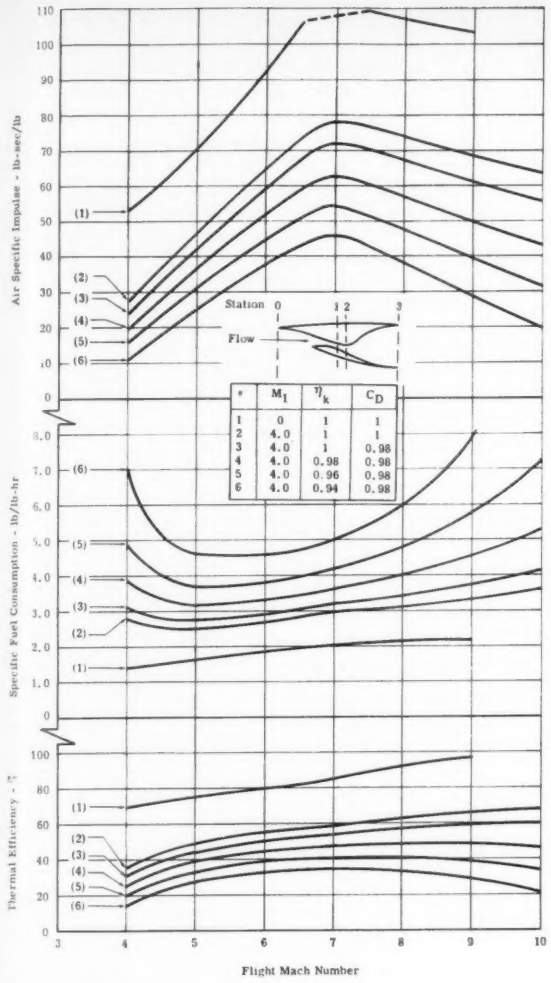
Air Specific Impulse - lb-sec/lb
Specific Fuel Consumption - lb/lb-hr
Thermal Efficiency - %
Flight Mach Number
Station 0 1 2 3
Flow
| M_1 | η_k | C_D
1 | 0 | 1 | 1
2 | 4.0 | 1 | 1
3 | 4.0 | 1 | 0.98
4 | 4.0 | 0.98 | 0.98
5 | 4.0 | 0.96 | 0.98
6 | 4.0 | 0.94 | 0.98

Fig. 10 **Performance parameters, detonation wave ramjet, $M_1 = 4.0$**

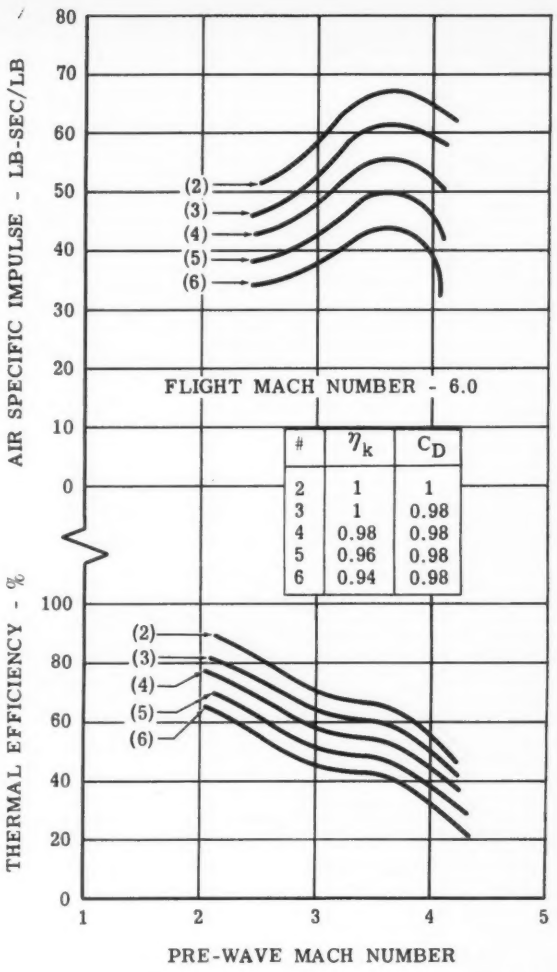
AIR SPECIFIC IMPULSE - LB-SEC/LB
THERMAL EFFICIENCY - %
FLIGHT MACH NUMBER - 6.0
PRE-WAVE MACH NUMBER
| η_k | C_D
2 | 1 | 1
3 | 1 | 0.98
4 | 0.98 | 0.98
5 | 0.96 | 0.98
6 | 0.94 | 0.98

Fig. 11 **Impulse and thermal efficiency vs. pre-wave Mach number**

Fig. 12 contains a plot of exit to inlet area ratio as a function of flight Mach number for a fully expanded nozzle. From a mechanical design standpoint this figure summarizes a very significant parameter. The conventional perfect ramjet operating at constant fuel-air ratio has an area ratio curve with a mildly negative slope. As can be seen from Fig. 12, the conventional engine operating on the wave engine fuel-air schedule has a gentle positive slope. The losses of the wave engine in conjunction with its inherent fuel schedule cause the magnitude and variation of the exit to inlet area ratio to be quite severe and from the designer's viewpoint undesirable. However, burning at higher pre-wave Mach numbers during acceleration will have the effect of easing the exit to inlet area ratio requirements. Since the losses are greater with a high pre-wave Mach number, this will require a larger exit to inlet area ratio, and it may be possible to hold the actual design area ratio to more reasonable limits. Partial expansion nozzles would probably be used.

Pre-ignition of the fuel-air mixture is a matter for concern. Fig. 13 shows a plot of pre-wave temperature vs. flight Mach number. Included is a "possible pre-ignition area," extending from 1600 to 2500 R. The reason for the uncertainty lies in the fact that time is also involved in this phenomenon. Since the fuel-air mixture is moving very rapidly, it may be able to experience temperatures which are in excess of its static ignition point and yet enter the detonation wave before undesirable effects can take place.

The inlet static pressure ratio is a function of flight Mach number. Maximum pressure ratio is reached at $M_0 = 10$ and is (at 130,000 ft-altitude) on the order of 3 to 4 atm. It is apparent that the wave engine static pressures are lower than those for the conventional engine in the inlet region. Rapid expansion following the wave will further minimize the regions of the engine experiencing high static pressure loads. The benefits of the resultant weight reduction are obvious.

Ideal Conventional Ramjet Cycle

To form a fair comparison, we have determined the performance of an ideal conventional ramjet. The same basic thermodynamic data are employed. This ideal engine consists of an isentropic inlet which diffuses, in the limit, to zero Mach number. The combustion process is at constant pressure and the exhaust nozzle is isentropic. The equations for this ideal machine are given in the following.

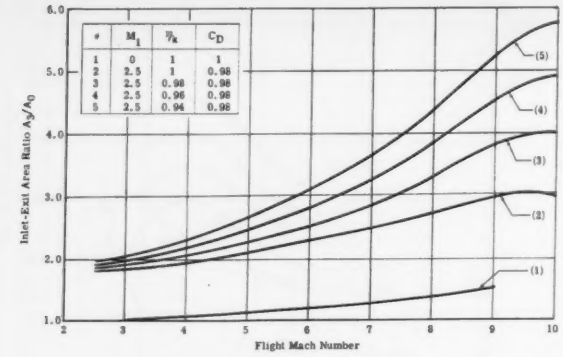

#	M_1	η_R	C_D
1	0	1	1
2	2.5	1	0.98
3	2.5	0.98	0.98
4	2.5	0.96	0.98
5	2.5	0.94	0.98

Fig. 12 Exit-inlet area ratio

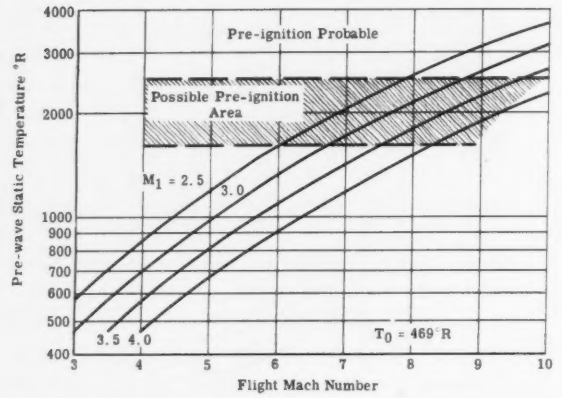

Fig. 13 Pre-wave static temperature vs. flight Mach number

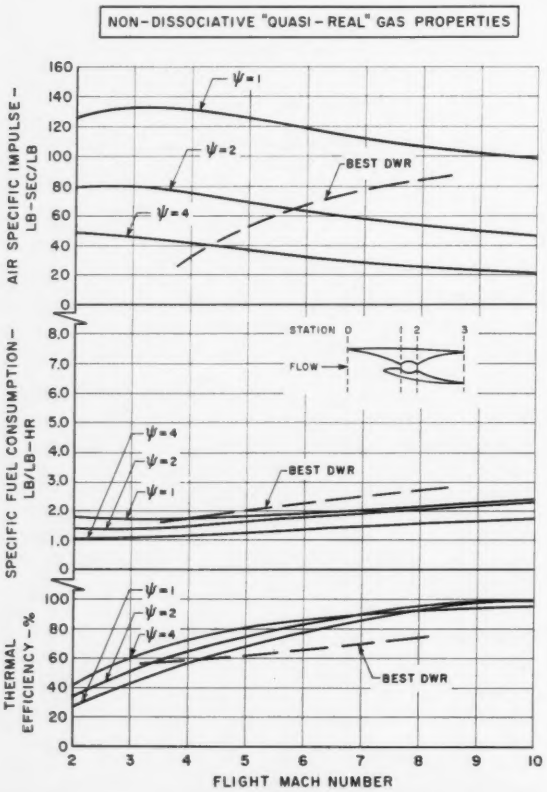

Fig. 14 Ideal ramjet performance characteristics

Burner inlet temperature

$$T_1 = \bar{m}_1 h_{t_0}/C_p \qquad [11]$$

where

$$h_{t0} = C_{p_0} T_0 \{1 + [(\gamma_0 - 1)/2] M_0^2\}$$

$$C_{p_1} = \frac{\sum \alpha_i C_{p_i}(T_1)}{\sum \alpha_i}$$

Burner inlet static pressure

$$\ln\left(\frac{P_1}{P_0}\right) = \frac{1}{\bar{R}} \int_{T_0}^{T_1} \frac{C_p}{T}\, dT \qquad [12]$$

where

$$C_p = \frac{\sum \alpha_i C_{p_i}(T)}{\sum \alpha_i}$$

Burner exit temperature

$$T_2 = \frac{h_{t_2}}{C_{p_2}} \left(\frac{2}{\gamma_2 + 1}\right) \qquad [13]$$

where

$$h_{t_2} = h_{t_0} + \frac{(f/a)_S \Delta H}{\psi\, m_f}$$

Nozzle exit temperature

$$\ln\left(\frac{P_1}{P_0}\right) = \frac{1}{\bar{R}} \int_{T_0}^{T_2} \frac{C_p}{T}\, dT \qquad [14]$$

where

$$C_p = \sum \beta_i C_{p_i}(T) / \sum \beta_i$$

Using these equations and [7 through 10], the performance of the ideal conventional engine was determined. In Figs. 9 and 10, this ideal subsonic engine follows the same fuel air schedule as the detonation wave engine. In Fig. 14 is shown the ideal subsonic engine at several different fuel-air ratios. The best detonation wave ramjet (DWR) is taken as that which has the maximum air specific impulse.

Improved Computations

As a check, a more elaborate inlet program was devised which accounts for the variation of the specific heats in the inlet resulting from the changes in temperature and the addition of fuel. In general, the results of the more exact program tend to yield static pressure ratios higher and temperature ratios lower than are derived from the original assumptions. Use of this improved supersonic inlet digital program (S. IN.) will yield a small improvement in all parameters.

As with the inlet, a more elaborated computation was derived to evaluate the expansion process. The more exact method again slightly improves the engine parameters but not to the extent achieved by the inlet program. Impetus to embark on both computer programs, supersonic inlet and supersonic expansion (S. EX.), comes from the realization that the engine parameters as computed here are based upon relatively small differences between very large numbers (i.e., inlet velocity and exhaust velocity) and hence, potentially sensitive to simplifying assumptions.

Concluding Remarks

Our results are similar to those of Weber (7) and Dunlap et al. (2), although different in detail. The results pre-

sented in (2) are strongly influenced by their arbitrary choice of a fixed pre-wave temperature. Neither of the aforementioned works considered strong detonations, since their actual existence was uncertain until recently.

Basically, the subsonic burning ramjet, when compared with a detonation wave engine, always has superior thermodynamic performance. However, the difference in some instances, such as the Mach 6 flight speed regime, are minor. The specific fuel consumption of the detonation engine is better than one might initially suspect from elementary considerations (7), because, even with large inlet and wave total pressure losses, at high Mach number the overall cycle pressure ratio is well-matched to the temperature ratios obtainable by combustion.

The results presented here are basically for design point consideration. There is, however, adequate margin for acceleration if one employs the strong detonation branch.

Experimental experience [see (10)] has shown that these detonation waves have a very wide stability range which is predictable. The chemical reaction takes place in an extremely short time, less than about 5 microsec. Combustion efficiencies, which for all engineering purposes are 100 per cent, have been achieved in flow distances less than 1 in.

The wave engine should be able to exploit the wave properties so as to achieve a shorter engine than the subsonic machine. The lower static pressures in the cycle will permit a lighter structure design. Also, these low pressures reduce the nozzle throat heat transfer, and its short length reduces drastically the heat transfer area.

The designer should take advantage of the wave properties as they feed into the exhaust nozzle. A very rapid expansion nozzle may alleviate the dissociation problem and will permit most of the nozzle interior wall surface to "see" the outside world and hence cool itself by radiation.

On the other hand, such an engine has a fuel injection problem. The seriousness of this problem has been estimated by Dunlap (2) but actual experimental experience has not yet been obtained. Both engines have a serious variable geometry problem, particularly with regard to "off design" operation, and here the detonation machine is the more serious offender. The control problem is very serious in either case, since inlet buzz and regurgitation may be disastrous at high flight speed.

Further data may be obtained from (13), of which this paper is a summary. The authors wish to acknowledge helpful discussions with J. Yampolski, C. L. Eisen and H. Van Valkenburg.

Nomenclature

V = velocity, fps
A = area, ft²
P = static pressure, lb/ft²
T = static temperature, R
γ = ratio of specific heats, C_p/C_v
R = universal gas constant, ft lb/lb-mol R
M = Mach number
ΔH = heating value of fuel, Btu/lb mol
α_i = moles of ith reactant
β_i = moles of ith product
f/a = fuel air ratio
ψ = equivalence ratio, stoichiometric fuel-air ratio/fuel air ratio
m_i = molecular weight of ith constituent
W_A = weight flow, lb/sec
$\overline{Q}$ = Q/C_pT
F_N = net thrust, lb
η_k = kinetic efficiency of inlet
η_i = inlet pressure recovery
η_{th} = thermal efficiency
C_p = coefficient of specific heat at constant pressure
Q = heat added to flow, Btu/lb sec
h = enthalpy, Btu/lb mol F
C_D = coefficient of discharge, actual velocity/ideal velocity
g = gravitational constant, 32.2 ft/sec²
C_xH_y = hydrocarbon fuel
O_2 = oxygen
N_2 = nitrogen
CO_2 = carbon dioxide
H_2O = water

Subscripts

0 = free stream
1 = wave entrance
2 = wave exit
3 = exhaust nozzle exit
t = total state
i = arbitrary constituent
f = fuel
I = inlet
K = kinetic
S = stoichiometric

References

1 Roy, M. M., *Comptes Rend. de l'Academie des Sciences*, Feb. 1, 1946. Paris.

2 Dunlap, R., Brehm, R. L. and Nicholls, J. A. "A Preliminary Study of the Application of Steady-State Detonative Combustion to a Reaction Engine," JET PROPULSION, vol. 28, no. 7, July 1958, pp. 451–456.

3 Nicholls, J. A., Wilkinson, H. R. and Morrison, R. B., "Intermittent Detonation as a Thrust Producing Mechanism," JET PROPULSION, May 1957, pp. 534–541.

4 Roy, M. M., "Propulsion Supersonique par Turboreacteurs et par Statoreacteurs," Proc. First Int. Congress Aeron. Sci., Madrid, Sept. 1958, to be published by Pergamon Press.

5 Partel, G., "General Round-up in the Ramjet Field and Its Significance to Astronautics," Ninth IAF Congress, Amsterdam, Aug. 1958, to be published.

6 Chinitz, W., "A Theoretical Analysis of a Detonation Wave Engine," M.M.E. Thesis, Polytechnic Institute of Brooklyn, June 1959.

7 Weber, R. J. and MacKay, J. S., "An Analysis of Ramjet Engines using Supersonic Combustion," NACA TN 4386, Sept. 1958.

8 Gross, R. A. and Nicholls, J. A. "Stationary Detonation Waves," Fourth AGARD Combustion and Propulsion Colloquium, Milan, April 1960, to be published.

9 Nicholls, J. A., Dabora, E. K. and Gealer, R. L., "Studies in Connection with Stabilized Detonation Waves," in "Seventh Symposium on Combustion," Butterworths Sci. Pub., London, pp. 144–150.

10 Gross, R. A. "A Study of Combustion in Supersonic Flow," *Research*, vol. 12, Oct.-Nov. 1959, pp. 381–389; *see also* Gross, R. A. and Chinitz, W., "Exploratory Studies of Combustion in Supersonic Flow," Parts I–IV, AFOSR TN 59–587, ASTIA AD 216 769, June 1959; and "A Study of Supersonic Combustion," *J. Aero/Space Sci.*, in press.

11 Eisen, C. L., Gross, R. A. and Rivlin, T. J., "Theoretical Calculations in Gaseous Detonations," *Combustion and Flame*, June 1960; *see also*, AFOSR TN 58–326, ASTIA AD 154 230.

12 Gross, R. A. and Oppenheim, A. K., "Recent Advances in Gaseous Detonation," ARS JOURNAL, March 1959, vol. 29, no. 3, pp. 173–179.

13 Sargent, W. H. and Gross, R. A., "A Detonation Wave Hypersonic Ramjet," AFOSR 59–589, ASTIA AD 216 811, June 1959.

Design of UHF Multipliers for Space Probe Communications[1]

LEONARD R. MALLING[2]

Jet Propulsion Laboratory,
California Institute of Technology
Pasadena, Calif.

The basic problem of phase stability in a correlation system is discussed, and data are included to demonstrate the design of highly stable UHF modules. It is shown that lightweight, efficient UHF cavities may be built which have a desired phase stability of better than 0.1 deg per G of vibration, an equivalent tuning stability of one part in 10^6.

THE GREATLY increased communication ranges and the antenna pointing accuracy required for present-day space vehicles have created a need for greatly improved rocket telemetry. Systems using correlation techniques based on recent advances in information theory appear to be the answer. However installation of such systems into rocket vehicles creates immediate problems. Thus, when correlation communication equipment is installed into rocket-powered space vehicles, the phase stability of the airborne units becomes a major design criterion. Although many available electronic components perform satisfactorily in the environment, it has been found that ultra high frequency (UHF) cavities of conventional design cannot be used. The essential requirements for the UHF cavities are phase stability, light weight and high efficiency.

A typical phase-coherent communication system uses phase modulation of the carrier in order to transmit intelligence over the radio link. A phase detector at the receiver accomplishes the desired demodulation. If the transmitter is to operate in the microwave region, a combination of very high, ultra high and microwave frequency multipliers may be used to obtain the desired output frequency for transmitter or local oscillator purposes. The multiplier chain is driven from a highly stable VHF oscillator source so as to insure phase coherence for the system.

Phase Stability Criterion

Mechanical vibration of components used for establishing RF resonance in a phase-coherent system produces incidental phase modulation (IPM) of the carrier or local oscillator signals, which, if sufficiently high, may seriously impair system performance. With correlation detection, these IPM signals appear as unwanted low frequency components at the output of the phase detector, with frequencies and amplitudes directly related to the rocket vibration as shown in block diagram form in Fig. 1. If vibration produces phase modulation which exceeds the 90-deg limits of the phase detector, system lock may be lost, thus, temporarily destroying the intelligence transmission capabilities of the system. Fortunately, on the premise that the rocket vibration may be assumed to have a spectral distribution similar to white noise over the band of interest, it is possible to build more sophisticated correlation systems which can extract the desired phase-modulated components in the presence of high level IPM Hence, a relatively large degree of IPM, but generally much less than 90 deg, may be tolerated without impairment of the highly accurate information such a system may normally carry. A figure of ±30-deg peak at the phase detector has been found to be acceptable, representing a level of some 3 deg per G for typical rocket environments. An RF component design, to achieve the desired phase stability, becomes most critical for a transmitter employing a large number of frequency multiplier stages because then, with the 30-deg criterion, the nth frequency multiplier may only have an IPM of $30/n$ deg (n is the ratio of the output frequency to the multiplier-module frequency). Thus, for a microwave phase-coherent system, with mechanical vibration of the order of 10 g, only phase deviations of less than 0.1 deg per G can be allowed in the early stages of the UHF multiplier band if a tolerance level of 3 deg per G at the output frequency is assumed.

The tuning stability requirements for mechanical excitation of this nature may be determined from the relationship between phase angle φ and the detuning of a resonant circuit γ (see Fig. 2). Where

$$\gamma = \frac{\text{RF input frequency}}{\text{cavity resonant frequency}} = \frac{\omega}{\omega_0} = \frac{\omega}{\omega \pm \Delta\omega} \qquad [1]$$

then

$$\varphi \approx \tan^{-1} Q(1/\gamma^2 - 1) \qquad [2]$$

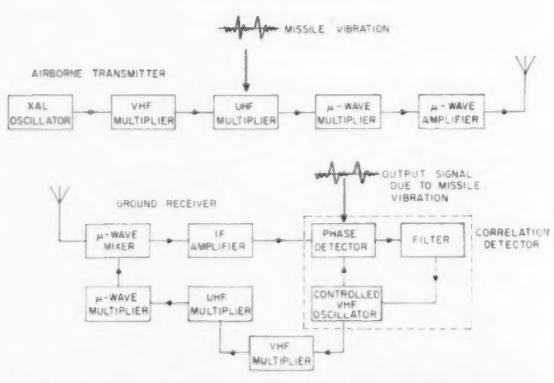

Fig. 1 Simplified coherent transmission system illustrating phase-modulation effect of missile vibration

Received March 30, 1959.

[1] This paper presents the results of one phase of research carried out at the Jet Propulsion Laboratory under Contract no. DA-04-495-Ord 18, sponsored by the Department of the Army, Ordnance Corps.

[2] Engineering Research Specialist.

an approximation for a high Q parallel resonant circuit, and $\Delta\omega$ is the detuning caused by vibration. The cavity is assumed to be in precise tune with the RF input frequency without the vibration.

For phase shifts of the order of 0.1 deg, which is well within the linear portion of the phase characteristics of a tuned circuit

$$\Delta\varphi \approx \tan^{-1}(-2Q\delta) \qquad [3]$$

where

δ = detuning caused by mechanical vibration
$\Delta\varphi$ = the corresponding phase excursions

Thus, the permissible amount of cavity detuning for a Q of 100 must be less than one part in 100,000 for a phase stability of 0.1 deg per G. This approaches the stability of a quartz crystal. The long-term frequency stability need not, of course, be of this order, since phase tracking circuits which form part of the system may readily accommodate slow phase changes produced by small order cavity tuning drifts. Expression [3] shows that the IPM will be minimized with lower Q. As thermal tuning drifts become serious with high Q cavities, a low "actively loaded" Q gives greater tuning stability, and, since the modulation techniques used in correlation systems may also require wide bandwidths, it is obviously advantageous to operate with the lowest possible loaded Q in the UHF resonant cavities consistent with efficiency. It will be shown that it is possible to design highly efficient UHF multipliers which will meet the phase stability requirements and have the desired property of low operating Q.

Payload Design Requirements

The design of a UHF frequency multiplier which will successfully meet both the system and the environmental specifications is complex, and such diverse problems as mechanical resonance with vibration, electron transit-times in vacuum tubes and the reduction of thermal gradients must be considered. Desirable properties for UHF frequency multipliers to be operated in an airborne phase-coherent system may be outlined as follows:

1 Freedom from phase modulation with vibration.
2 Lightweight and compact overall assembly.
3 High thermal stability and ability to dissipate heat directly to the payload frame.
4 High plate efficiency and maximum RF power gain.
5 Stability of tuning and ease of adjustment.
6 Adequate bandwidth for the system under consideration.
7 Minimum RF leakage and low external RF fields.
8 Ability to change tubes readily and to use tubes within the manufacturer's range of input and output capacitance variation.
9 Plate voltage requirements to be within the range of the normally available unpressurized low voltage airborne supply.
10 d-c insulation to insure freedom from voltage breakdown at high altitudes.

It will be shown that these requirements may be met by a much closer integration of mechanical and electrical design parameters than has been customary in the past. Well-established operating techniques for Class C radio-frequency multiplier operation or the basic design of coaxial cavities will not be discussed except insofar as they are related to the design of highly efficient, phase stable UHF multipliers.

Tube Considerations

Overall tube considerations for a complete multiplier chain operating from 30 mc to X-band indicate that the region between 200 and 2000 mc must be covered by coaxial-type

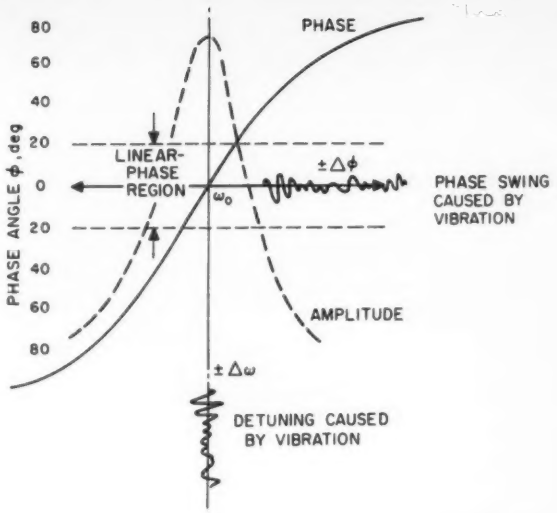

Fig. 2 Phase characteristics of tuned circuit showing incremental phase change caused by mechanical vibration

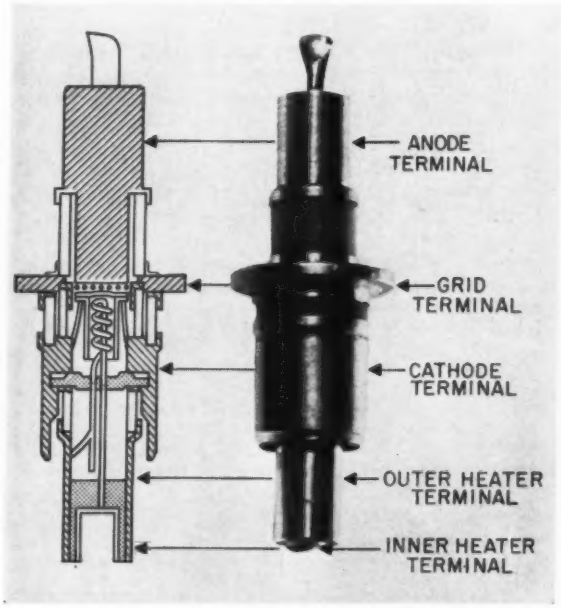

Fig. 3 UHF triode GL-6442 showing cutaway section

tubes. It is fortunate that the basic requirements for high UHF performance, fine wire grids and closely spaced rigidly supported electrodes, also produce a tube which has desirable phase stability characteristics. One UHF tube of this type which has been successfully used in missile cavities is the GL-6442. Fig. 3 is a cutaway section showing the internal structure. The manufacturer's stated characteristics are: Heater power, 5.7 w; plate dissipation, 6 w maximum; transconductance, 13,500 μmhos; and frequency multiplier operation, up to 2500 mc. Although the major electrodes of this tube are ruggedly mounted, vibration tests have disclosed that the heater is insufficiently secured within the cathode, and hence mechanical resonances cause changes in heater-to-

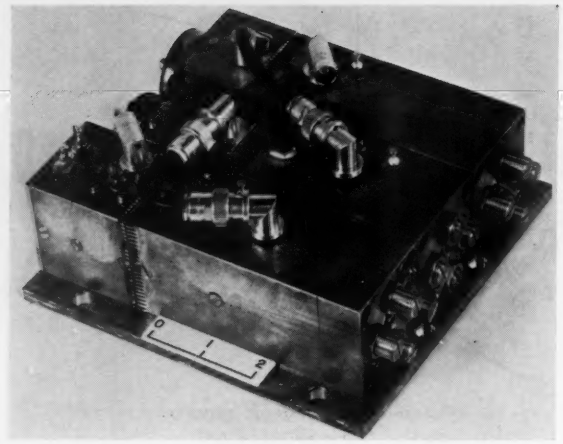

Fig. 4 x8 UHF frequency multiplier, 250–2000 mc

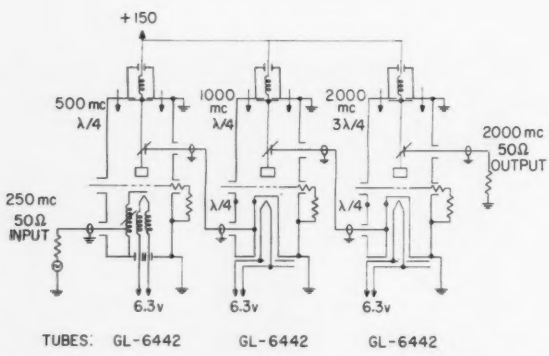

Fig. 5 Schematic of x8 UHF frequency multiplier, 250–2000 mc

cathode capacitance. Phase modulation so produced has been minimized by the use of a bifilar-heater choke that raises the heater assembly to the same RF potential as the cathode.

UHF Multiplier Module Design

A typical UHF module for a phase-coherent system operating between 200 and 2000 mc may be expected to have three cavity stages operating x3, x2, x2 or x2, x2, x2. Multiplier efficiency is generally too low for factors greater than 3.

Using lumped LC circuit constants instead of a tuned line at the lowest or input frequency, $\lambda/4$ cavities for the intermediate stages, and a $\frac{3}{4}\lambda$ cavity, by necessity, at the 2000-mc output frequency, an overall length of the order of 6 in. may be obtained for the three multiplier stages. Fig. 4 shows the overall assembly of an x8 UHF multiplier, and Fig. 5 is the corresponding simplified schematic.

A high degree of mechanical stability combined with adequate conduction cooling is obtained by constructing the cavity bodies from rectangular blocks. Holes bored into the blocks form the outer conductor of the coaxial resonators. Having thus secured a rigid outer coaxial construction, the problems of phase stability now become directed at the inner coaxial assembly, i.e., the mounting of the tube and inner coaxial conductors, the contacts to the tube elements and the methods employed for cavity tuning.

The internal construction of a cavity is determined largely by the circuit arrangements, which inevitably form part of the basic mechanical structure at ultra high frequency. The only logical RF circuit for a UHF triode is the grounded-grid configuration. By adopting an end-to-end assembly for the associated plate and cathode cavities, and by making these two sub-units completely independent, mechanically and electrically, the tube grid flange, which is at RF ground, may be clamped rigidly between the two independent structures with a strong flat spring interposed to grip the tube flange. The grid electrode and, thus, the tube are now rigidly clamped to the basic structure. Mica spacers may be interposed to allow for grid biasing. For the other tube electrodes, considerable success has been achieved by fabricating the contact springs from a solid beryllium-copper rod, slotting and re-

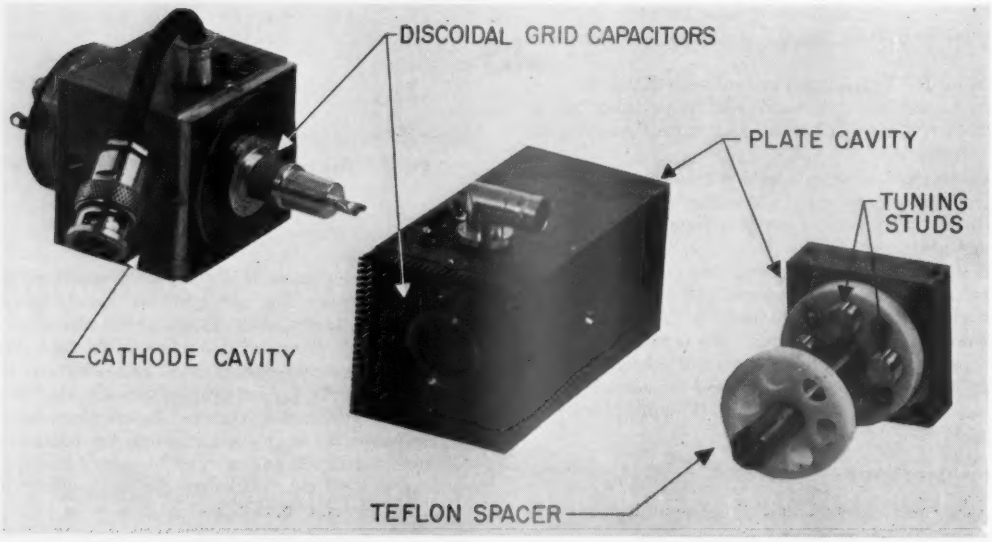

Fig. 6 1000- to 2000-mc cavity multiplier internal assembly showing construction and plate cavity tuning studs

moving metal as required in order to provide long, parabolically curved springs which form, simultaneously, the inner coaxial conductors and the tube electrode contacts. Where the length requires additional support, a Teflon spacer, inserted so as to preserve the constant characteristics of the coaxial resonator, provides increased mechanical rigidity. Fig. 6 illustrates the construction of the inner coaxial assembly.

Cavity Tuning

Cavity tuning is required to provide desirable system frequency adjustments and to cover tube-capacitance variations. The relationship between electrical length θ, coaxial line impedance Z_0, and tube or terminating capacitance C, which determine cavity resonance, is given by the transcendental equation

$$\tan \theta = X_C/Z_0 \qquad [4]$$

Tuning may obviously be accomplished by a variation of any one of the three parameters, and accepted methods of tuning vary either the capacitive reactance or the electrical length. Neither of these methods were considered sufficiently stable for the considered environment. Instead, a tuning method which varied the Z_0 was evolved. The possible tuning range is more limited because of mechanical considerations, by this means, but it has the consequent advantage of being more stable. In order to insure sufficient tuning range the electromechanical design is held to tight tolerances; then, with median capacity tubes, the cavities will tune to the desired median frequency. Also, the coaxial cavity is assumed to terminate at the tube grid flange instead of at the anode, and the outer cavity diameter is regulated to avoid the pronounced discontinuities normally associated with the tube. The required variation of Z_0 may now be obtained to maximum advantage by the insertion of a number of adjustable screws into the shorted or high current end of the cavity, which effectively control Z_0. As the mean impedance of the resonant line is changed, the electrical length is varied, as shown by Equation [4]; hence, the resonant frequency is varied. Tuning by this means gives accurate, stable and noncritical tuning control.

Plate Cavity Design

The requirement for UHF cavities of high plate efficiency is inextricably bound up not only with the parameters enumerated in the introduction, but also with freedom from voltage breakdown, adequate bandwidth, maximum RF power gain and low plate operating potential.

The overall efficiency of a tube-driven UHF multiplier plate tank circuit is

$$n_{\text{overall}} = n_1 \cdot n_2 \cdot n_3 \cdot n_4 \qquad [5]$$

where

n_1 = efficiency of the cavity
n_2 = efficiency of the tube as a Class C amplifier
n_3 = efficiency of the tube as a Class C multiplier
n_4 = efficiency of the tube as a function of frequency

The cavity efficiency

$$n_1 = (Q_u - Q_L)/Q_u \qquad [6]$$

where Q_u and Q_L are the unloaded and loaded Q of the plate cavity, respectively. An unloaded Q of well over 1000 may be expected; whereas, the desired loaded Q is of the order of 100, which gives an efficiency of 0.90. The Class C amplifier efficiency n_2 may be expected to be of the order of 0.75, a median figure for Class C operation. The multiplier efficiency n_3 represents the efficiency with which the tube extracts the harmonic component from the highly nonlinear fundamental frequency tube current. A figure of 0.65 for the second harmonic and 0.40 for the third represent typical operation based on unity for Class C fundamental frequency operation (3).[3] The parameter n_4 is a function which is dependent on the electron transit time between the grid and plate electrodes of the tube and is related to frequency. Bunched electrons at the grid plane arrive at the plate at different times as a result of velocity differences caused by the finite time of travel from cathode to grid. As a result of the different arrival times, the plate current pulse is broadened (1), and, thus, the efficiency of multiplication is reduced. This electron debunching or dispersion is illustrated in Fig. 7. Neglecting n_4, the expected efficiency for a doubler, n_{total} is 0.90, 0.75, 0.65 = 0.44. Transit time debunching may reduce this overall efficiency to 0.15 for a UHF doubler operating with an output frequency of 2000 mc. This would make n_4 equal to 0.34, which at 2000 mc would thus become the dominant term.

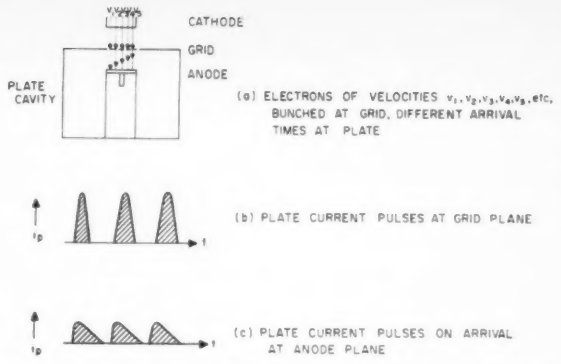

Fig. 7 Effect of grid-plate transit time on shape of current pulse applied to cavity showing electron debunching

With the efficiency considerations established, it can be seen that the external cavity bodies may be constructed, for example, from aluminum with considerable weight saving, paying only a slight penalty for its somewhat low conductivity.

Input and Output Coupling

It must be assumed that for any type of Class C operation, the drive to the tube, the coupling and the d-c plate potential are all optimized. Failure to optimize coupling with resultant mismatch will exact penalties not only in efficiency, but also in reduced bandwidth and tuning stability. Optimum output match is obtained when the load impedance is made to present an impedance equal to the effective tube impedance seen as a generator of harmonic components, which is considerably higher than when the tube is used as an amplifier. With optimum coupling, optimum bandwidth and thus desirable low Q for phase stability are simultaneously realized. The bandwidth, however, is also dependent on the terminating capacitance C_t of the coaxial line and the line impedance Z_0 (2) as shown by the following

$$B = 2\Delta f = \frac{f_0}{Q} = \frac{1}{2\pi C_t \cdot R_t} \qquad [7]$$

$$Q = \frac{1}{2}\left(\omega C_t \cdot R_t + \frac{\theta}{\sin^2 \theta} \cdot \frac{R_t}{Z_0}\right) \approx \frac{\pi}{4} \cdot \frac{R_t}{Z_0} \qquad [8]$$

which is an approximation for the equivalent lumped circuit. Therefore, in order to insure maximum bandwidth, C_t must be minimized and Z_0 maximized. C_t may be minimized

[3] Numbers in parentheses indicate References at end of paper.

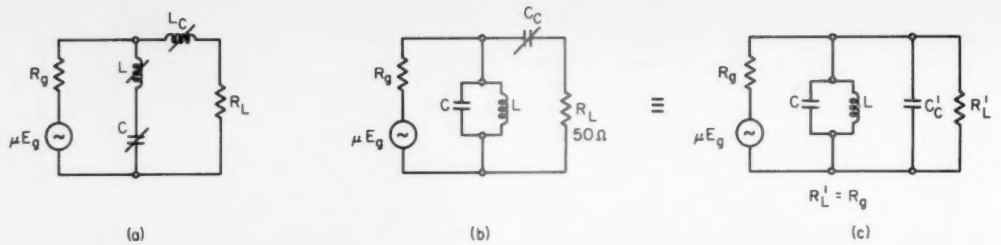

Fig. 8 Matching of plate cavity to 50-ohm load using direct capacity coupling. L_C **represents resonant cavity;** R_g **is effective tube impedance as a harmonic generator.** (a) **Conventional low-frequency circuit;** (b) **UHF equivalent circuit of** (a); (c) **impedance transformation of load at UHF**

by making the internal plate-grid capacitance of the tube the only major discontinuity in the coaxial structure, and Z_0 may be maximized by making the energy storage in the distributed line capacitance a minimum, that is, by increasing the ratio of outer-to-inner conductors.

The commonly used loop-coupling to cavities presents many difficulties with tandem operation of tube multipliers. A more effective and also simpler method of coupling is a capacitive coupling to the inner coaxial conductor. This may be compared to the impedance-transformation method commonly used at broadcast frequencies, as shown in Fig. 8. The capacitive coupling, which is more suited to UHF operation, enables a precise exact match to be made to the generator impedance and, at the same time, gives the required open circuit d-c return for multistage operation. A direct tap into the cathode line of the following multiplier is almost essential to insure an accurate match into the low impedance of the grounded-grid input circuit. Fig. 8 also shows the equivalent circuit for impedance transformation of R_L to match the effective impedance of the tube as a harmonic generator

$$R_L' = (R_L^2 + X_{C_C}^2)/R_L \qquad [9]$$

with R_L small as compared with X_{C_C}

$$R_L' \approx X_{C_C}^2/R_L \qquad [10]$$

Design of Input Cavity

If Q of a cavity is sufficiently low, and the mechanical dimensions are accurately maintained, a relatively wide band of operation may be obtained without recourse to adjustable tuning means. Thus, the input cavities, which are terminated with the low input impedance of a grounded-grid tube have a low Q and can be fixed tuned. At UHF, the input cavity terminating impedance also has an additional shunt component due to the transit time of the electrons in the cathode-to-grid space. That is, the input admittance is

$$Y_1 = Y_T + G_T \qquad [11]$$

where

Y_T = tube input admittance
G_T = conductance term resulting from transit time loading

For small signal inputs, the input admittance of a grounded-grid amplifier, neglecting transit time loading is

$$Y_1 = Y_T = (1 + \mu)/(r_p + Z_L) \qquad [12]$$

where

μ, r_p = tube parameters
Z_L = impedance in the plate circuit

As Z_L is essentially zero for a multiplier, Y_T would be expected to approximate the g_m of the tube for a high μ triode. Class C operation makes this quite inaccurate. The parameter Y_T can be approximated for high level, nonlinear operation by determining the average loading of the tube over the operating cycle. This may be simplified by assuming a linear transfer function for the e_g/i_p characteristics and a linear relationship between g_m and i_p. This is illustrated in Fig. 9. The plate current pulse for Class C operation may be regarded as a clipped sine wave, for which the average value from Fourier analysis is

$$i_{avg} = \frac{i_{max}}{\pi} \cdot \left[\frac{\sin(\theta/2) - (\theta/2)\cos(\theta/2)}{1 - \cos(\theta/2)}\right] \qquad [13]$$

where θ is the angle of current flow. The maximum g_m may be determined at i_{max} from the tube characteristics. For the GL - 6442, assuming a maximum g_m of 16,000 μmhos and a pulse length of 120 deg, the average g_m will be 3500 μmhos.

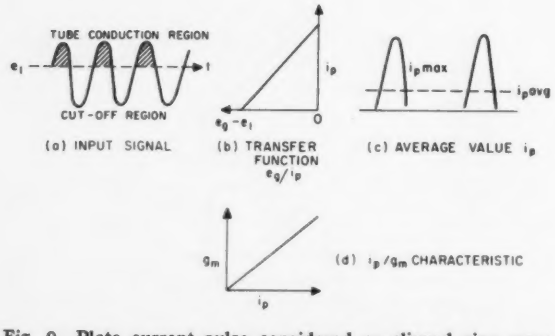

Fig. 9 Plate current pulse considered as clipped sine wave with linear e_g/i_p **and** g_m/i_p **characteristics**

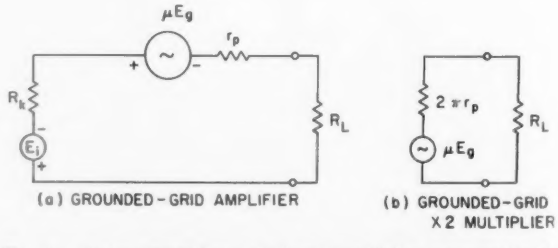

Fig. 10 Output impedance of Class C multiplier compared with small signal grounded-grid amplifier

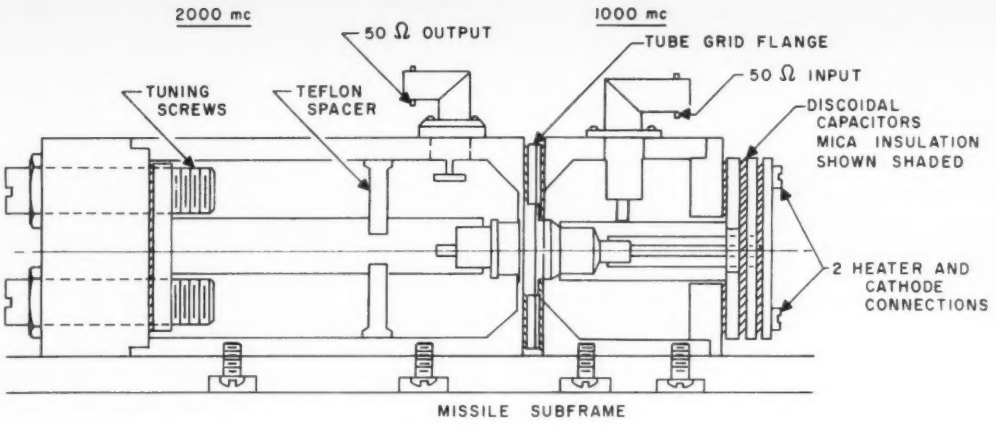

Fig. 11 Cross section of UHF cavity multiplier

The input conductance resulting from transit time loading is

$$G_T = g_m(\omega t)^2/20 \qquad [14]$$

where t is the transit time of the electrons from cathode to grid.

For the GL-6442 at 1000 mc, G_T is 2.5×10^{-3} mhos, so that from Equation [11]

$$Y_i = 3.5 \times 10^{-3} + 2.5 \times 10^{-3} \text{ mhos} = 6 \times 10^{-3} \text{ mhos}$$

Thus, using Equation [7], with a tube input capacity of 5.5 $\mu\mu$f, the expected Q will be 5.7 giving a 3-db bandwidth of 175 mc. This Q is sufficiently low to permit accurate matching over a wide band using a fixed tuned cavity.

The output impedance of the tube for the highly nonlinear operation of frequency multiplication may be arrived at by an analysis similar to the one used for the determination of the input impedance. For a small signal grounded-grid amplifier

$$Z_{out} = R_p + (\mu + 1)R_k \qquad [15]$$

where R_k is the equivalent input impedance, approximating zero for multiplier operation (see Fig. 10). The average tube conductance, where $G_{avg} = 1/R_p$ avg, for a half-sine wave is given by

$$G_{avg} = G_{max}/\pi \qquad [16]$$

based on a tube resistance which varies in a half sinusoidal manner over the operating cycle. The tube impedance for second harmonic pulse-type operation is thus approximated

$$r_{pavg} \approx 2\pi r_p \qquad [17]$$

giving an equivalent generator impedance R_g of 22,000 ohms for the GL-6442. The tuning and coupling arrangements are illustrated in Fig. 11.

d-c Plate Voltage

For RF power outputs of a few hundred milliwatts and highly efficient cavity operation, d-c plate potentials of the order of 150 v become possible, so that pressurization for high altitude operation in Earth's atmosphere is not required. The inefficiencies which may arise from too high a voltage are readily seen from Fig. 12, which illustrates that with a low plate voltage swing, the continuous dissipated power is held to a high level. However, too low a plate voltage may give an insufficiently high ratio of plate current to grid current and will also increase transit time losses

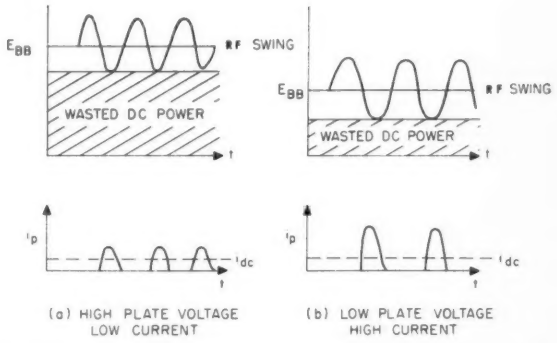

Fig. 12 Illustration of importance of matching plate voltage to RF voltage swing in order to minimize plate dissipation and increase efficiency with Class C multipliers

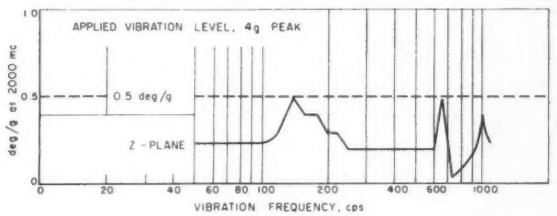

Fig. 13 Environmental performance data, vibration of x12 UHF cavities

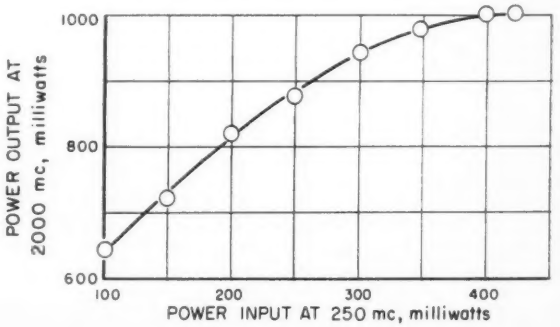

Fig. 14 Electrical performance x8 UHF multiplier

resulting from lower electron velocities. In addition, for emission-limited tubes of the type used, the plate voltage must always be maintained in order to secure the required RF power output at the higher operating frequencies without exceeding the average emission capabilities of the planar cathode.

Thermal Considerations

With the tube operation adjusted for maximum efficiency, the power to be dissipated by heat conduction to the missile subframe becomes established. A steady heat flow to the missile subframe will insure minimum operating temperatures for the cavities. However, the required circuit d-c isolation of the tube elements necessitates the insertion of insulation materials between the high temperature electrodes of the tubes and the cavity body. Heat conduction between two parallel faces is determined by

$$\frac{Q}{T} = -KA\frac{d\theta}{dx} \qquad [18]$$

where

Q/T = amount of flow in a given time
$d\theta/dx$ = temperature gradient over the spacing x
K = thermal conductivity
A = surface area in contact

Obviously, minimum operating temperatures are obtained when contact areas are maximized and insulation kept at a minimum thickness. Also, for airborne application, it is highly desirable that the insulation should be so inserted that all external parts of the cavities are at low d-c potential. These d-c, RF and thermal insulation requirements are best met at UHF by discoidal-type capacitors having a plate diameter approaching the maximum cross-sectional dimensions of the cavity. A capacitor of this type has sufficiently low reactance to replace the conventional resonant line short circuit and thus allow the external cavity bodies to be at d-c ground potential. Accurate machining of all contact surfaces and the use of thin sheet mica as a dielectric reduce estimated and measured thermal gradients to a few degrees. The advantages of mica insulation are high heat conduction, mechanical rigidity in compression, high dielectric constant and low RF losses. Fig. 11 shows the manner in which the discoidal capacitors are built into the UHF cavity.

Performance

UHF multipliers constructed in accordance with the design criteria outlined here have demonstrated their ability to operate successfully in an airborne phase-coherent system.

Table 1 Performance data of x8 UHF multiplier

RF input	
frequency	250 mc
power	300 mw
RF output	
frequency	2000 mc
power	0.95 w
Overall power gain	4–8 db
Total d-c plate input	
voltage	150 v
current	75 ma
power	11.2 w
Overall plate efficiency	8.5%
Overall bandwidth	10 mc
Total weight	5.75 lb
Total d-c power input	28.2 w
Overall efficiency[a]	3.3%

[a] Includes heater power.

Fig. 13 shows the results of an environmental test with an applied vibration level of 4 g/rms. An IPM of less than 0.5 deg per G was observed at the output frequency using a specially developed IPM instrumentation system. The wide band, low frequency peak at 150 cps is the result, almost entirely, of residual IPM from the heater-to-cathode vibration of the tube. Table 1 gives the pertinent performance data, and the curve in Fig. 14 illustrates the input-output characteristics. In estimating overall efficiency, heater power is taken into account. Several successful flights have been obtained in which these UHF cavities have operated satisfactorily as an integral part of a phase-coherent system. It is not considered that the design illustrated is optimum either in weight or performance, but it is believed to point out a new direction which the design of such components must take if success is to be achieved in the penetration of some of the new space frontiers.

References

1 Dow, W. G., "Transit-Time Effects in Ultra-High Frequency Class-C Operation," Proc. IRE, vol. 25, Jan. 1947, pp. 35–42.

2 Herold, E. W. and Malter, L., "Some Aspects of Radio Reception at Ultra-High Frequency," Proc. IRE, vol. 31, Aug. 1943, pp. 423–438.

3 Terman, F. E., "Class C Amplifiers and Harmonic Generators," in "Radio Engineers Handbook," McGraw-Hill Book Co., Inc., N. Y., 1943, section 5, paragraphs 21 and 23.

Technical Notes

Determination of Diffusion Coefficients From Asymmetric Concentration Profiles

A. W. BLACKMAN[1]

Research Laboratories, United Aircraft Corp., East Hartford, Conn.

IN THE investigation of mixing problems which occur in rockets, ramjets and turbojets, e.g., those associated with fuel injection and combustion chamber cooling by the injection of cool gases adjacent to the walls, it is sometimes necessary to calculate the rate of change of asymmetric concentration profiles when diffusion coefficients are known, or alternately to determine diffusion coefficients from measured asymmetric concentration profiles a known distance apart. A procedure is here developed for the calculation of these quantities.

Considering a control surface of height dy and length dx with unit width in the z direction, combination of the diffusion equations with a material balance for one of the components in the stream results in the following equation

$$\rho \frac{\partial}{\partial x}(fU_x)dxdy + \rho \frac{\partial}{\partial y}(fU_y)dxdy = \rho D_y \frac{\partial}{\partial y}\left(\frac{\partial f}{\partial y}\right) \times dxdy + \rho D_x \frac{\partial}{\partial x}\left(\frac{\partial f}{\partial x}\right) dxdy \quad [1]$$

Assuming that the volume of material entering the control surface is to equal the volume leaving during the same period, then

$$\frac{\partial U_x}{\partial x} + \frac{\partial U_y}{\partial y} = 0 \quad [2]$$

Neglecting diffusion in the axial direction and combining Equations [1 and 2] yields

$$U_x \frac{\partial f}{\partial x} + U_y \frac{\partial f}{\partial y} = D_y \frac{\partial^2 f}{\partial y^2} \quad [3]$$

Neglecting the y component of velocity and replacing f by a new variable defined by

$$F \equiv (f - f_0)/f_0 \quad [4]$$

Equation [3] is transformed to

$$\frac{d^2F}{\partial y^2} - \frac{U_x}{D_y} \cdot \frac{\partial F}{\partial x} = 0 \quad [5]$$

Boundary conditions will be specified as

at $x = 0$ $F = F(y)$
at $x \to \infty$ $F \to 0$

A solution of Equation [5] satisfying these boundary conditions can be written as

$$F = \exp\left[-\frac{n^2\pi^2 x}{h^2}\left(\frac{D_y}{U_x}\right)\right] \sum_{n=1}^{j} A_n \sin\frac{n\pi y}{h} \quad [6]$$

This sine series will vanish at the end points $y = 0$ and $y = h$, but will represent $F(y)$ in the interval $0 < y < h$ if a sufficient number of terms is taken. $F(y)$ at $x = 0$ can be determined from a measured concentration profile and a mass balance of the injected flows, and the constants A_n can be found by solving Equation [6]. A convenient way of solving the resulting set of equations is to arrange them in matrix form. Expansion of Equation [6] at $x = 0$ into six terms, for example, would give the following set of equations for six values of F measured at equal intervals of y

$$\begin{aligned} A_1y_{11} + A_2y_{12} + \ldots A_6y_{16} &= F_1 \\ &\cdot \\ &\cdot \\ &\cdot \\ A_1y_{61} + A_2y_{62} + \ldots A_6y_{66} &= F_6 \end{aligned} \quad [7]$$

which can be written in matrix form as

$$\begin{bmatrix} y_{11}\ y_{12} \ldots y_{16} \\ \cdot \\ \cdot \\ \cdot \\ y_{61}\ y_{62} \ldots y_{66} \end{bmatrix}^{-1} \begin{bmatrix} F_1 \\ \cdot \\ \cdot \\ \cdot \\ F_6 \end{bmatrix} = \begin{bmatrix} A_1 \\ \cdot \\ \cdot \\ \cdot \\ A_6 \end{bmatrix} \quad [8]$$

The inverse matrix can be determined by the method of triangulation[2] and the constant A_1, $A_2 \ldots A_6$ can be determined for different initial profile shapes by multiplying the matrices, provided the measured values are always taken at the same points.

Diffusion coefficients can be determined by solving Equation [6] utilizing values of F measured at two stations a known distance apart; or alternately, if the diffusion coefficient is known, Equation [6] can be solved for the rate of change of a known initial concentration distribution with distance.

Nomenclature

A = constant
D = diffusivity
f = weight fraction of diffusing species
h = height of duct in y direction
U = velocity
x = variable axial distance
y = variable vertical distance
ρ = weight density of stream

Subscripts

x = x direction
y = y direction

Received Jan. 14, 1960.

[1] Supervisor, Chemical Kinetics Group, Propulsion Section. Member ARS.

[2] Dwyer, P. S., "Linear Computations," John Wiley and Sons, N. Y., 1951, p. 183.

EDITOR'S NOTE: The Technical Notes and Technical Comments sections of ARS JOURNAL are open to short manuscripts describing new developments or offering comments on papers previously published. Such manuscripts are usually published without editorial review within a few months of the date of receipt. Requirements as to style are the same as for regular contributions (see masthead page).

Angular Displacement of a Magnetized Sphere by the Terrestrial Magnetic Field During Vertical Descent

MARVIN H. HEWITT[1]

The Martin Co., Denver, Colo.

The angular displacement bounds of a sphere with a magnetic dipole field are given for free-fall vertical descent in Earth's gravitational and magnetic fields. Effects of the atmosphere are neglected, and Earth is assumed spherical. The terrestrial magnetic field is treated as the field from a dipole situated at Earth's center.

A SPHERE in free-fall vertical descent has a magnetic dipole field. The torque acting on this sphere in Earth's magnetic field is given by

$$L = -MH \sin \beta \qquad [1]$$

where the minus sign indicates that the torque is in such a direction as to decrease β, the angle between the axis of the dipole and Earth's field and

L = the torque on the sphere
M = the sphere's dipole moment
H = Earth's magnetic field

The sphere's center of gravity is taken coincident with its geometric center and the dipole is centered there. Let the magnetic axis of the sphere be initially along the gravitational plumb line. The Earth's dipole field has moment a and is considered to be situated at Earth's origin and parallel to the axis through the poles.

Let

$H = a\phi/r^3$
r = central distance to sphere
$\phi = (1 + 3 \sin^2 \theta)^{1/2}$
θ = latitude

Consequently

$$L = -(Ma\phi/r^3) \sin \beta \qquad [2]$$

Also, let α be the angle between the line of magnetic force and the plumb line. We obtain for vertical descent

$$\sin \alpha = \cos \theta/\phi = \text{constant} \qquad [3]$$

Recalling the definition of β, we obtain

$$\alpha - \beta = \delta \qquad [4]$$

where δ is the angle between the sphere's magnetic axis and the plumb line. Therefore

$$\sin (\alpha - \delta) = \sin \beta \qquad [5]$$

$$L = -(Ma\phi/r^3) \sin (\alpha - \delta) \qquad [6]$$

The sphere's angular momentum A yields

$$dA/dt = L \qquad [7]$$

where the point 0 about which the moment is taken is at the center of gravity of the sphere. Consequently

$$(d/dt)I\omega = L \qquad [8]$$

where

I = constant moment of inertia of the sphere
ω = the body's angular speed

We now obtain

$$\frac{d\omega}{dt} = \frac{Ma\phi}{Ir^3} \sin (\alpha - \delta) \qquad [9]$$

Moreover

$$\frac{d^2\delta}{dt^2} = \frac{Ma\phi}{Ir^3} \sin (\alpha - \delta) \qquad [10]$$

Equation [10] yields

$$\delta = \iint \frac{Ma\phi}{Ir^3} \sin (\alpha - \delta) dt^2 \qquad [11]$$

where the integration is over the time of descent.

It is apparent that the maximum value of $|\phi \sin (\alpha - \delta)/r^3|$ is given by

$$\left| \frac{\phi \sin (\alpha - \delta)}{r^3} \right| \leq \frac{2}{R^3} \qquad [12]$$

where R is Earth's radius. Also, t here is a continuous variable of limited total variation; therefore

$$\delta < Mat_d^2/IR^3 \qquad [13]$$

Initial values of ω and δ have been taken equal to zero. The moment of inertia of a sphere about a diameter is

$$I = (2/5)mb^2 \qquad [14]$$

where b is the radius of the sphere. We obtain the bound

$$\delta < 5Mat_d^2/2mb^2R^3 \qquad [15]$$

If an iron sphere with a magnetic moment of 3×10^8 gauss-cm^3 and a radius of 50 cm, fell for 10^2 sec in Earth's dipole field (8.06×10^{25} gauss-cm^3), δ would be less than 0.2 deg.

Deflection δ can be given a sharper bound than that given by [15] if $\alpha - \delta$ is small (large latitudes). Then, since sin $(\alpha - \delta)$ is a weak function of time

$$\delta = \frac{Ma(\alpha - \delta)}{I} \iint \frac{\phi}{r^3} dt^2 \qquad [16]$$

We obtain

$$\delta < Ma(\alpha - \delta)t_d^2/IR^3 \qquad [17]$$

For a sphere [17] becomes

$$\delta < 5Ma(\alpha - \delta)t_d^2/2mb^2R^3 \qquad [18]$$

Inequality [18] may be put in the form

$$\delta < \frac{\alpha(5Mat_d^2/2mb^2R^3)}{1 + (5Mat_d^2/2mb^2R^3)} \qquad [19]$$

where the bound on δ is exhibited as a function of latitude through α. It is apparent that bound [19] has sharpened the range of δ under, of course, the restriction on latitude that has been imposed.

Received Jan. 5, 1960.

[1] Design Engineer, Applied Research Section. Member ARS.

Calculation of Electrical Conductivity of Ionized Gases

A. SHERMAN[1]

General Electric Co., Flight Propulsion Laboratory, Cincinnati, Ohio

IN ANY practical application of magnetohydrodynamic concepts a knowledge of the electrical conductivity of the working fluid is essential. Unfortunately, however, for an ionized gas of varying pressure and temperature the evaluation of this property by experiment or analysis is, at best, a difficult task. Some experimental measurements have been made (1,2,3),[2] but, in general, they are not easily carried out, since there is no readily available method of containing uniform samples of extremely high temperature gases for reasonable lengths of time. In order to avoid this experimental problem, at least temporarily, it would be very desirable to have some accurate analytical method for electrical conductivity calculations. The purpose of this note is to review existing methods and call attention to a general calculation procedure.

A large number of theoretical investigations presented in recent years deal with the question of electrical conductivity of ionized gases, but none treat the problem completely. That is, a number of authors have derived equations for conductivity assuming a slightly ionized gas, and others have done the same for a completely ionized gas. There have been no basic investigations of the conductivity of a gas with an arbitrary degree of ionization.

A careful analysis of conductivity for a slightly ionized gas is given by Chapman and Cowling (4). They consider a binary mixture of neutral particles and electrons and show the electrical conductivity to be

$$\sigma = (n_e e^2/kT) D_{12} \qquad [1]$$

where

n_e = electron number density
e = electronic charge
T = absolute temperature
k = Boltzmann constant
D_{12} = diffusion coefficient

The diffusion coefficient is derived for a binary mixture of rigid elastic spheres in which one species is much lighter and much less plentiful than the other. It is found to be

$$D_{12} = \frac{3.396\pi}{8 n_0 Q} \left[\frac{kT}{2\pi m_e}\right]^{1/2} \qquad [2]$$

where

n_0 = original particle number density $\cong (n_e + n_n)$
n_n = neutral number density
Q = collision cross section $= \pi\sigma_{12}^2$
σ_{12} = radius of collision cylinder
m_e = electron mass

Combining this with Equation [1] gives Chapman and Cowling's formula

$$\sigma = 0.532 \frac{\alpha e^2}{(m_e kT)^{1/2}} \frac{1}{Q} \qquad [3]$$

where

$$\alpha = \text{degree of ionization} = n_e/n_0$$

This equation is valid for a gas which is so little ionized that the influence of the ions is small, and the ions may be counted as neutrals. That is, the ion number per unit volume is so small that an electron rarely collides with one, and such collisions are unimportant.

Two different theoretical approaches have been used in the derivation of formulas for the electrical conductivity of a fully ionized gas. The first assumes the Boltzmann equation to be valid and solves it by the Enskog procedure. Using this method a number of calculations have been made (5,6,7). A result typical of the rest is found by Burgers (7) and is given

$$\sigma = 0.582 \frac{(kT)^{3/2}}{m_e^{1/2} e^2} \frac{1}{\ln \Lambda} \qquad [4]$$

where

$$\Lambda = \frac{3}{2e^3} \left(\frac{k^3 T^3}{\pi n_e}\right)^{1/2}$$

On the other hand, when the forces between the components of the gas are Coulomb forces, it becomes harder to justify the basic assumption underlying the Boltzmann equation. That is, the ratio of the time spent during a collision to the time spent between collisions is very small. In a fully ionized gas, a charged particle will experience many small deflections rather than several sudden collisions. As a result a fresh approach to the problem was developed by Spitzer (8,9), and has been used by him as well as Allis (10) to derive an equation for electrical conductivity of fully ionized gases. A summary of their results is given

$$\sigma = 0.591 \frac{(kT)^{3/2}}{m_e^{1/2} e^2} \frac{1}{\ln \Lambda} \qquad [5]$$

where Λ takes on different values. From (8) we have

$$\Lambda_1 = \frac{3}{2} \frac{1}{e^3} \left(\frac{k^3 T^3}{\pi n_e}\right)^{1/2}$$

and from (9) we find

$$\Lambda_2 = \frac{1}{\sqrt{2}} \frac{3}{2} \frac{1}{e^3} \left(\frac{k^3 T^3}{\pi n_e}\right)^{1/2} = \frac{\Lambda_1}{\sqrt{2}}$$

finally, from Allis (10)

$$\Lambda_3 = \left(\frac{1}{2}\right) \frac{3}{2} \frac{1}{e^3} \left(\frac{k^3 T^3}{\pi n_e}\right)^{1/2} = \frac{\Lambda_1}{2}$$

The equation derived by Spitzer (8) is exactly that given by Burger except for the constant.

It is of interest to note that Equations [4] or [5] are independent of the nature of the gas. In addition, the conductivity depends weakly on n_e, through the logarithmic term, and strongly on the temperature. Actually, if T is high enough to have a fully ionized gas, then σ will increase with gas pressure. At lower temperatures the reverse is true, since α, the degree of ionization, depends very strongly on pressure and increases with decreasing pressure.

One approximate procedure for calculating the electrical conductivity of a gas of arbitrary degree of ionization has been developed by Lin, Resler and Kantrowitz (1). They state that the resistance (electrical) due to neutral particles, and the resistance due to ionized particles, should be additive. Thus they write

$$\frac{1}{\sigma} = \frac{1}{\sigma_n} + \frac{1}{\sigma_i} \qquad [6]$$

and using Equation [3] for σ_n while taking Equation [5] for σ_i with Λ from (9) this becomes

$$\sigma = \left[1.88 \frac{(m_e kT)^{1/2} Q_n}{(n_e/n_0) e^2} + 1.69 \frac{m_e^{1/2} e^2}{(kT)^{3/2}} \ln \Lambda\right]^{-1} \qquad [7]$$

Received Jan. 18, 1960.

[1] Senior Engineer, Magnetogasdynamics, Applied Research Operation. Member ARS.

[2] Numbers in parentheses indicate References at end of paper.

where

$$\Lambda = \frac{3}{2\sqrt{2}e^3}\left(\frac{k^3T^3}{\pi n_e}\right)^{1/2}$$

and Q_n refers to the collision cross section for collision of electrons with neutral atoms or molecules.

General Calculation Procedure

Another approach to obtaining a formula valid for arbitrary degrees of ionization, the so-called "free path kinetic theory," has been employed by a number of authors. The basis of this theory is that the particles of a gas are assumed to make instantaneous collisions with each other but move freely between collisions. This differs from the more refined approaches in that it does not inquire into the actual form of the forces acting between the particles (ion, electron, neutral atom). However, it does have the virtue of greater generality.

If the electron mean free time τ is assumed to be constant for all electrons under given conditions of pressure and temperature, the following formula can be derived (11)

$$\sigma = (n_e e^2/m_e)\tau \qquad [8]$$

where τ is given by

$$\tau = \frac{\lambda}{\bar{C}} = \frac{\lambda}{(8kT/\pi m_e)^{1/2}} \qquad [9]$$

and where

λ = electron mean free path
$\bar{C}$ = average electron velocity suitable for a Maxwellian distribution [for τ = constant, it can be shown (11) that the distribution function for electrons is indeed Maxwellian]

In the development of Equation [8] the ionic current, pressure and temperature diffusion phenomena, and the influence of a magnetic field have been neglected. These could be included but really constitute a separate investigation. Finally, in order to bring Equation [8] into agreement with Equation [3] for a slightly ionized gas we write

$$\sigma = 0.85(n_e e^2/m_e)\tau \qquad [10]$$

Before use can be made of Equation [10] we need some way of evaluating λ for gas mixtures. An expression for this quantity is derived by Jeans (12) from free path theory and is

$$\lambda = 1/\sum_j n_j Q_j \qquad [11]$$

where

n_j = number density of neutrals or ions
Q_j = cross section for collision of electrons with neutrals or ions

As far as neutral species are concerned, considerable experimental data are available and are summarized by Massey and Burhop (13). A collision cross section for electrons and ions can be obtained if we consider a fully ionized gas and compare our present equation to Equation [5] with Λ obtained from (9). The justification for this choice for Λ is the experimental evidence with argon (1). Making the comparison gives

$$Q_{ei} = 0.90\left(\frac{e^2}{kT}\right)^2 \ln\left[\frac{1.5}{\sqrt{2}e^3}\left(\frac{k^3T^3}{\pi n_e}\right)^{1/2}\right] \qquad [12]$$

If the collision cross sections for neutrals are obtained from Ramsauer-type experiments, then a suitable average cross section is given by (1).

$$Q_n(T) = \frac{kT/m_e}{\int_0^\infty \frac{C}{Q_n(C)}\, e^{-m_e C^2/2kT}\, dC}$$

where C is the electron speed. When the cross sections are obtained from electron diffusion experiments, this averaging is unnecessary.

Next, in order to calculate σ we have to calculate n_e. For the special case of a monatomic gas at temperatures low enough so that electronic excitation above the ground level may be neglected, the Saha equation may be used to obtain n_e. For other situations more complex calculations are necessary.

One final point would be worth discussing. It is often stated that the terms in λ, Equation [11], due to electrons colliding with neutral particles ($\sum_i n_i Q_{ni}$) can be neglected compared with the electron-ion term ($n_e Q_i$) if the degree of ionization is only a per cent or so. As an example of one case in which such a statement is incorrect we consider mercury vapor (14) at 1-atm pressure. In this case, we find that the two terms in λ are *equal* at 7400 K and 2.7 per cent degree of ionization. However, the contribution due to ionic interactions is larger by a factor of 10 only at 10,200 K and 38.3 per cent degree of ionization. Thus, if the relation for a fully ionized gas, Equation [5], has been used to compute the conductivity of mercury vapor at 1 atm and 7400 K, the calculated value would be too large by a factor of 2. The assumption which we have just shown to be in error in general is, however, more accurate when the gas being considered ionizes at a lower temperature and when its electron neutral cross section is small. In other words, lower pressures and/or lower ionization potentials tend to make such an approximation more valid.

References

1 Lin, S. C., Resler, E. L. and Kantrowitz, A., "Electrical Conductivity of Highly Ionized Argon Produced by Shock Waves," *J. Appl. Phys.*, vol. 26, 1955, p. 95.

2 Lamb, L. and Lin, S. C., "Electrical Conductivity of Thermally Ionized Air Produced in a Shock Tube," Avco Research Lab. RR5, Everett, Mass., 1957.

3 Blackman, V. H., "Magnetohydrodynamic Flow Experiments of a Steady State Nature," ARS preprint no. 1007-59, 1959.

4 Chapman, S. and Cowling, T. G., "The Mathematical Theory of Non-Uniform Gases," University Press, Cambridge, England, 1952.

5 Cowling, T. G., "Electrical Conductivity of an Ionized Gas in a Magnetic Field with Applications to the Solar Atmosphere and the Ionosphere," Proc. Roy. Soc., vol. A 183, 1945, p. 453.

6 Landshoff, R., "Transport Phenomena in a Completely Ionized Gas in the Presence of a Magnetic Field," *Phys. Rev.*, vol. 76, 1949, p. 904; vol. 82, 1951, p. 442.

7 Burgers, J. M., "Application of Transfer Equations to Calculation of Diffusion, Heat Conduction, Viscosity, and Electric Conductivity," Univ. of Maryland, TN-BN-124a.

8 Spitzer, L., Jr., "Physics of Fully Ionized Gases," Interscience Publishers, Inc., N. Y., 1956.

9 Spitzer, L., Jr. and Härm, R., "Transport Phenomena in a Completely Ionized Gas," *Phys. Rev.*, vol. 89, 1953, p. 997.

10 Allis, W. P., "Motion of Ions and Electrons," MIT Research Lab. of Electronics, Cambridge, Rep. no. 299, June 1956.

11 Shockley, W., "Electrons and Holes in Semiconductors," Van Nostrand Co., Inc., Princeton, N. J., 1950.

12 Jeans, J., "An Introduction to the Kinetic Theory of Gases," University Press, Cambridge, England, 1952.

13 Massey, H. S. W. and Burhop, E. H. S., "Electronic and Ionic Impact Phenomena," Clarendon Press, Oxford, England, 1952.

14 Sherman, A. and Martinek, F., "Thermodynamic and Electrical Properties of Mercury Vapor at Pressures below Atmospheric and High Temperatures," GE-AFOSR Phys. Chem. in Aerodynamics and Space Flight Symposium, Univ. of Penn., Sept. 1959. See also General Electric Co., TIS R59FPD771, Oct. 1959.

Approximation of Optimum Thrust Nozzle Contour

G. V. R. RAO[1]

Rocketdyne Div., North American Aviation, Inc., Canoga Park, Calif.

FOR A prescribed length and area ratio the nozzle contour producing maximum thrust can be uniquely determined (1,2).[2] The thrust performance of such optimum contoured nozzles, for various area ratios and lengths, was discussed in (3). Even though such nozzle contour is unique, determination of it is by the method of characteristics and requires the use of high speed computing machines (1,2). Besides the nozzle thrust, a design engineer would like to know its weight and cooling requirements to enable him to make the proper choice. For this purpose an approximation to the optimum thrust contour is enough, and a simple geometric method is described here.

The first step in defining a nozzle contour is the description of the throat region. After a certain amount of initial expansion along the prescribed throat wall, the contour is so formed as to turn the expanding gases to a near axial direction. For the family of nozzle contours considered here and in (3), the throat region is assumed given by two circular arcs as shown in Fig. 1. With these initial throat conditions, let us consider a nozzle having a certain area ratio A_e/A_t and length ratio L/R_t. The nozzle contour optimized for thrust will have unique values for θ_M, the wall slope at the inflection point M, and θ_E, the wall slope at the end point E. These values of θ_M and θ_E can be evaluated directly (3) prior to computing the contour itself, and are shown in a parametric form in Fig. 2. For the sake of clarity, even values for θ_M and odd values for θ_E are indicated in the figure. The nozzle end point given by $(R_E/R_t, L/R_t)$ and the respective values of θ_M and θ_E are sufficient to describe a parabola. In Fig. 1 is shown a simple geometric construction for the parabolic contour. Through the nozzle end point E, line EQ is drawn inclined at an angle θ_E to the nozzle axis. Line MQ is drawn inclined at an angle θ_M to the nozzle axis and tangent to the prescribed wall profile in the throat region. The line segments MQ and QE are then divided into an equal number of parts by points a, b, c and e, f, g, respectively. The required parabola is the envelope of lines joining a to e, b to f and c to g. If necessary, further subdivision of the line segments MQ and QE can be made to obtain closer tangent points. The parabola thus constructed yields a close approximation to the contour computed by the method of characteristics. For example, in the case of a nozzle of area ratio 25:1 and length ratio 12:1, the parabolic approximation does not differ from the computed contour (3) by more than 3 per cent in radial dimension. The maximum deviation in this example occurs at one third of the distance from throat to the exit.

The values of θ_M and θ_E shown in Fig. 2 are the results of calculations using $\gamma = 1.23$ and throat conditions such as shown in Fig. 1. A different value of γ does not appear to appreciably change the nozzle contour when the area ratio and length are prescribed (3). Similarly, one can expect that minor changes in the throat region would not cause large changes in the contour. Hence, the values shown in Fig. 2 and the parabolic contours can be used in general to approximately describe the optimum thrust nozzle contours.

Received Jan. 4, 1959

[1] Senior Technical Specialist. Member ARS.

[2] Numbers in parentheses indicate References at end of paper.

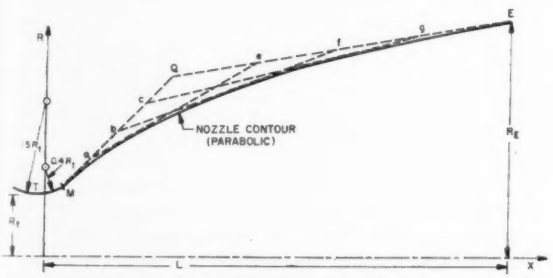

Fig. 1 Sketch of a nozzle showing nomenclature and construction of the parabola

References

1 Guderley, G. and Hantsch, E., "Beste Formen für Achsensymmetrische Uberschallschubdusen," *Zeitschrift für Flugwissenschaften*, vol. 3, no. 9, Sept. 1955, pp. 305-313.

2 Rao, G. V. R., "Exhaust Nozzle Contour for Optimum Thrust," JET PROPULSION, vol. 28, no. 6, June 1958, pp. 377-382.

3 Rao, G. V. R., "Optimum Thrust Performance of Contoured Nozzle," Bull. of first meeting JANAF Liquid Propellant Group, Johns Hopkins University, Md., Nov. 1959.

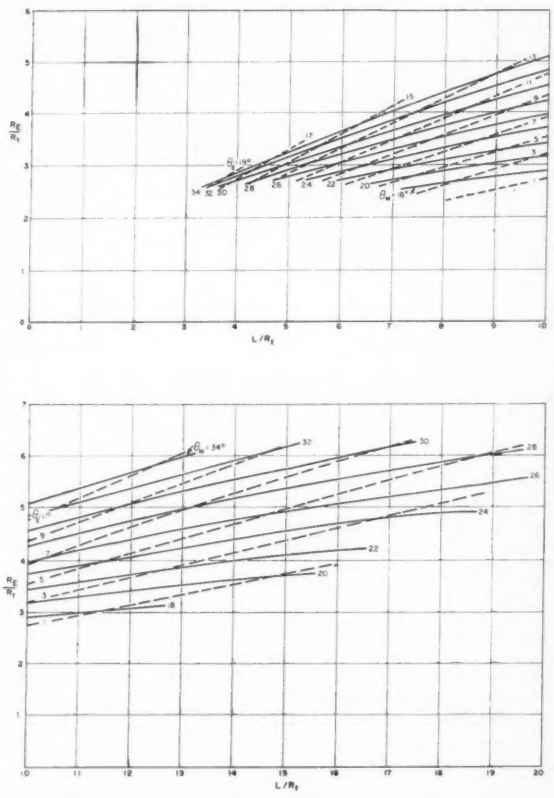

Fig. 2 Parametric values of θ_M and θ_E corresponding to various exit radius ratios and nozzle length ratios

Estimating Transient Temperature Distributions During Ablation

M. RICHARD DENISON[1]

Aeronutronic Div., Ford Motor Co., Newport Beach, Calif.

IT IS often important to investigate the penetration of heat in a solid whose surface experiences ablation. Because of the removal of material, a simple transient heat conduction analysis may lead to over-conservative estimates of the penetration distance. Integral methods similar to those of boundary layer theory have been used recently to solve the steady two-dimensional conservation equations for an ablating material with a liquid layer (1, 2).[2] Also, these methods have been applied to transient one-dimensional heat conduction (3–5). In this note it is shown that the integral technique is suitable for studying the combination of these effects. In addition, the heat penetration distance is computed for a simple special case which may be useful for design purposes.

The important physical regions which take part in the ablation process are illustrated in Fig. 1. In this note, attention is focused on the condensed phases. When the liquid layer is present, the thermodynamic change of phase from solid to liquid may play a minor role in condensed-phase heat and mass transfer phenomena. Instead the liquid layer may be defined as a region in which the velocity parallel to the surface decreases, due to the strong increase of liquid viscosity with temperature drop, from its value at the interface u_i to zero. The normal mass flux relative to the surface at the cooler boundary of the liquid layer is $\dot{m}_\delta$. The difference between $\dot{m}_\delta$ and the mass flux $\dot{m}_i$ at the gas-liquid interface represents a liquid runoff rate. The thermal layer extends from the liquid-gas interface where the temperature is T_i to the undisturbed solid where the temperature is T_0. Attention is restricted to cases in which the heat does not penetrate to the back surface. Chemical reactions and heat of fusion in the condensed phase are neglected.

Integral equations for conservation of mass and energy on two-dimensional or axisymmetric bodies are given by

$$\rho \frac{\partial}{\partial x} r_0^k \int_0^{-\delta} u dy + (\dot{m}_\delta - \dot{m}_i) r_0^k = 0 \qquad [1]$$

$$\rho c r_0^k \frac{\partial}{\partial t} \int_0^{-\delta_T} (T - T_0) dy + \rho c \frac{\partial}{\partial x} r_0^k \int_0^{-\delta} u T dy + r_0^k c(\dot{m}_\delta T_0 - \dot{m}_i T_i) + r_0^k q_i = 0 \qquad [2]$$

Conservation of momentum is represented by the assumption that the shear is constant across the liquid layer. For several materials the variation of viscosity with temperature can be represented by

$$\mu = \beta e^{\xi} \qquad \xi = A/T \qquad [3]$$

where β and A are constants. If, in addition, the liquid layer δ is considerably thinner than the thermal layer δ_T, a linear temperature distribution in the liquid layer is adequate. Under these circumstances a velocity distribution with respect to temperature in the liquid layer can be obtained

$$u = \frac{\tau_i K}{q_i \beta} \int_{T_\delta}^{T} e^{-A/T} dT \qquad [4]$$

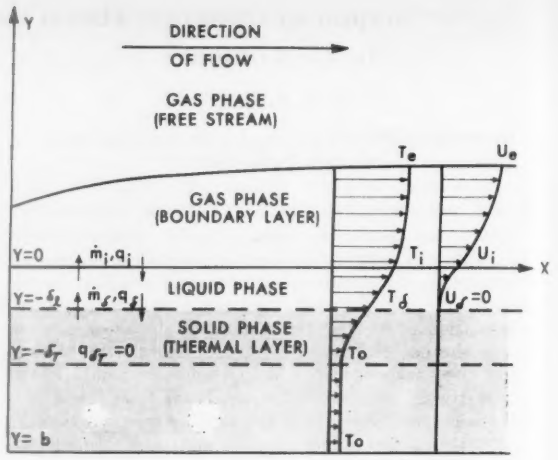

Fig. 1 Physical model

Successive integration by parts results in the asymptotic expansion

$$u = -\frac{\tau_i T_i K}{\mu_\delta q_i} \xi_i e^{(\xi_i - \xi)} \sum_{n=1}^{N} (-1)^n \frac{n!}{\xi^{n+1}} \qquad [5]$$

For purposes of describing the temperature distribution in the thermal layer, similar profiles which satisfy the boundary conditions may be applicable. In this case

$$\frac{T - T_0}{T_i - T_0} = f\left(\frac{y}{\delta_T}\right) \qquad [6]$$

Use of the distributions of Equations [5 and 6] in the conservation Equations [1 and 2], leads to the following expressions

$$\dot{m}_\delta - \dot{m}_i = \frac{\rho}{r_0^k} \frac{\partial}{\partial x} r_0^k \frac{\tau_i}{\mu_i} \left(\frac{T_i K}{q_i}\right)^2 F_1(T_i) \qquad [7]$$

$$q_i = c(\dot{m}_i T_i - \dot{m}_\delta T_0) + c T_i (m_\delta - \dot{m}_i) F_2(T_i) + c\rho \frac{\tau_i}{\mu_i} \left(\frac{K T_i}{q_i}\right)^2 F_1(T_i) \frac{\partial}{\partial_x} T_i F_2(T_i) + \rho c a_1 \frac{\partial}{\partial t} (T_i - T_0)\delta_T \qquad [8]$$

where

$$F_1(T_i) = \sum_{n=1}^{N} \sum_{m=1}^{M} (-1)^{n+m} \frac{n!\,(n+m+1)!}{(n+2)!\,\xi_i^{n+m}}$$

$$F_2(T_i) = [F_1(T_i)]^{-1} \sum_{n=1}^{N} \sum_{m=1}^{M} (-1)^{n+m} \frac{n!\,(n+m+2)!}{(n+3)!\,\xi_i^{n+m}}$$

$$a_1 = -\int_0^{-1} f d(y/\delta_T)$$

In general, Equations [7 and 8] must be matched to solutions of the gas-phase boundary layer equations. If A/T_i is sufficiently large, $F_2(T_i)$ is approximately unity. This condition applies fairly well, for example, to the ablation of silica. The third term on the right-hand side of Equation [8], which involves the x gradient of temperature, is zero at a stagnation point and sometimes may be neglected in other regions. Then Equation [8] becomes identical to that which would be obtained if the heat convected parallel to the surface in the liquid layer were neglected. Under these circumstances, if T_i and $\dot{m}_\delta$ are known functions of time, Equation [8] alone is sufficient for estimating the depth of penetra-

Received Jan. 15, 1960.

[1] Manager, Fluid Dynamics and Advanced Propulsion Section.

[2] Numbers in parentheses indicate References at end of paper.

tion δ_T as a function of time. Because of the similarity assumption of Equation [6], the heat flux q_i is related to the surface temperature and δ_T through

$$q_i = a_2 K(T_i - T_0)/\delta_T \qquad [9]$$

where $a_2 = f'(0)$.

If a simple parabolic temperature distribution is assumed, the boundary conditions are satisfied by

$$\frac{T - T_0}{T_i - T_0} = 1 + 2\left(\frac{y}{\delta_T}\right) + \left(\frac{y}{\delta_T}\right)^2 \qquad [10]$$

Therefore

$$a_1 = 1/3 \qquad a_2 = 2 \qquad [11]$$

Sometimes the surface temperature T_i quickly rises to a rather constant value determined by vaporization conditions. If, in addition, the mass flux $\dot{m}_\delta$ is constant, Equation [8] can be solved analytically. The result is

$$-\ln\left(1 - \frac{\dot{m}_\delta c \delta_T}{a_2 K}\right) - \frac{\dot{m}_\delta c \delta_T}{a_2 K} = \frac{\dot{m}_\delta^2 ct}{a_2 a_1 \rho K} \qquad [12]$$

For small values of time or low ablation rate, retention of only the leading term in a series expansion of the left-hand side of Equation [12] and use of Equation [9] for a parabolic temperature distribution results in

$$\frac{q_i}{T_i - T_0} = \sqrt{\frac{K\rho c}{3t}} \qquad [13]$$

The exact solution yields (6) under these conditions

$$\frac{q_i}{T_i - T_0} = \sqrt{\frac{K\rho c}{\pi t}} \qquad [14]$$

In the steady state, Equation [12] becomes

$$\dot{m}_\delta c(T_i - T_0)/q_i = 1 \qquad [15]$$

Equation [15] is identical with the exact solution, whereas Equation [13] differs only by $\sqrt{3/\pi}$. A comparison between the approximate and exact solutions for the entire range of time is shown in Fig. 2. It can be seen that the maximum deviation is on the order of 10 per cent. In order to get an indication of the adequacy of the thermal thickness δ_T as determined by the approximate method, the temperature rise at the location δ_T was computed from the exact solution. The result is also shown in Fig. 2. The temperature rise varies from about 2 to 13 per cent. Therefore, in the case studied, the simple parabolic distribution for determining δ_T is fairly good. However, when similarity is not valid, e.g., in cases in which a material is first heated then cooled, a modification of the method should be developed.

Some general conclusions can be drawn from Fig. 2 which may be useful for design purposes. The dimensionless parameter $\dot{m}_\delta^2 ct/\rho K$ plays a role analogous to that of the Fourier number for transient heat conduction in a finite slab. If $\dot{m}_\delta^2 ct/\rho K > 3$, then steady-state ablation conditions hold, and δ_T is approximately equal to $2K/\dot{m}_\delta c$. On the other hand, if $\dot{m}_\delta^2 ct/\rho K < 0.01$, ablation does not affect the temperature distribution, and δ_T is approximately equal to $2\sqrt{3Kt/\rho c}$.

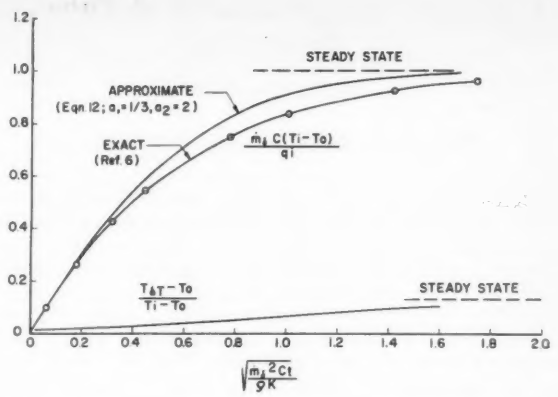

Fig. 2 Comparison of approximate and exact solutions

Nomenclature

- c = specific heat
- f = temperature distribution function (see Eq. [6])
- k = unity for axisymmetric and zero for two-dimensional bodies
- K = thermal conductivity
- $\dot{m}$ = mass flux per unit surface area
- q = $K(\partial T/\partial y)$, heat flux
- r_0 = distance from axis of symmetry to body surface
- t = time
- T = temperature
- T_0 = undisturbed temperature
- u = velocity parallel to surface
- x = distance along surface
- y = distance normal to surface in outward direction
- δ = thickness of liquid layer
- δ_T = thickness of thermal layer
- μ = viscosity
- ξ = A/T (see Eq. [3])
- ρ = density
- τ = $\mu(\partial\mu/\partial y)$, shear stress

Subscripts

- i = gas-liquid interface condition
- δ = condition at inner edge of liquid layer
- δ_T = condition of inner edge of thermal layer

References

1 Lees, L., "Similarity Parameters for Surface Melting of a Blunt Nosed Body in a High Velocity Gas Stream," ARS JOURNAL, vol. 29, no. 5, May 1959, pp. 345–353.

2 Bethe, H. A. and Adams, M. C., "A Theory for the Ablation of Glassy Materials," *J. Aero/Space Sci.*, vol. 26, no. 6, June 1959, pp. 321–328.

3 Goodman, T. R., "The Ablation of Melting Bodies With Heat Penetration Into the Solid," AFOSR-TN 58-789, AD 202-115, ARDC, Aug. 1, 1958.

4 Reynolds, W. C. and Dalton, T. A., "The Use of Integral Methods in Transient Heat Transfer Analysis," TR no. 36, Dept. of Mech. Engng., Stanford University, Sept. 1, 1958.

5 Roberts, L., "An Approximate Analysis of Unsteady Vaporization Near the Stagnation Point of Blunt Bodies," NASA TN D-41, Sept. 1959.

6 Baer, D. and Ambrosio, A., "Heat Conduction in a Semi-Infinite Slab With Sublimation at the Surface," Space Technology Laboratories, Inc., Pasadena, TR-59-0000-00610, Feb. 24, 1959.

Isentropic Compression of Shock Tube Driver Gas

R. J. STALKER[1]

National Research Council, Ottawa, Canada

USING the constant area shock tube, with air as a test gas, it has usually been found convenient to heat the driver gas in order to substantially exceed a shock Mach number of 12 (1).[2] This heating has generally been effected by combustion or by electrical means, but may, of course, result from isentropic compression immediately prior to initiation of the shock tube flow. The present note is intended to draw attention to a method of doing this, and considers the resulting shock tube performance when helium is used as driver gas.

The apparatus involved is represented schematically in Fig. 1. The method of compression, following a technique used in fundamental physical studies of gases at high pressures and temperatures (2), employs a free piston driven by air pressure into a cylinder containing the gas to be compressed. The piston is released at station A, accelerates, and comes to rest again at station B when all the energy imparted to the piston by the air from the reservoir has passed into the compressed gas. If the volume of the reservoir is sufficient for the pressure therein to change negligibly during the compression process, and the maximum velocity of the piston is so low that not only is the gas compressed isentropically, but the pressure driving the piston remains approximately equal to the reservoir pressure, then

$$\frac{P_R}{P_A}\left(1 - \frac{\rho_A}{\rho_B}\right) = \frac{1}{\gamma - 1}\left[\left(\frac{\rho_B}{\rho_A}\right)^{\gamma-1} - 1\right]$$

For large compression ratios $\rho_A/\rho_B \ll 1$ and therefore

$$\left(\frac{P_B}{P_A}\right) = \left(\frac{a_B}{a_A}\right)^{\frac{2\gamma}{\gamma-1}} = \left(\frac{\rho_B}{\rho_A}\right)^{\gamma} = \left[1 + (\gamma - 1)\frac{P_R}{P_A}\right]^{\frac{\gamma}{\gamma-1}}$$

which enables the state of the driver gas at peak pressure to be determined from its initial state and the initial pressure ratio across the piston. Arranging so that the diaphragm ruptures near the peak pressure, and that the mass of the piston is such that the time rate of pressure variation is small near this value, the subsequent unsteady flow may be taken to be identical with that in a conventional shock tube, and the performance computed on this basis.

Results of such computations, based on perfect gas assumptions, with helium as driver and air as test gas, are shown in Fig. 2. Two intersecting sets of curves are presented; one set displays the variation of the velocity behind the shock wave with the overall pressure ratio P_R/P_1 for differing volumetric compression ratios ρ_B/ρ_A, and the other shows the same variation for selected values of the maximum diaphragm pressure ratio P_B/P_1.

The curves indicate that, using this technique, high shock Mach numbers may be obtained. However, it must be pointed out that in an apparatus of practical dimensions, the large ratio between the volume of the compression cylinder and that of the driver section of the shock tube implies that the driver section must be short, and therefore that the associated test time of steady flow between the passage of the shock wave and the contact surface is limited. For example, using a 3-in. diam compression tube 10-ft long, with a volumetric compression ratio of 75 and a 1-in. diam shock tube, the theoretically available test time at $M_s = 25$ is approximately 50 microsec, when the air in the low pressure section is at 5 mm Hg and allowance is made for real gas effects on the density ratio across the shock wave.

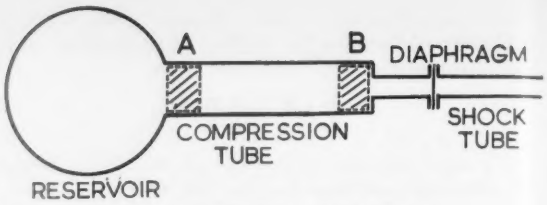

Fig. 1 Compression shock tube

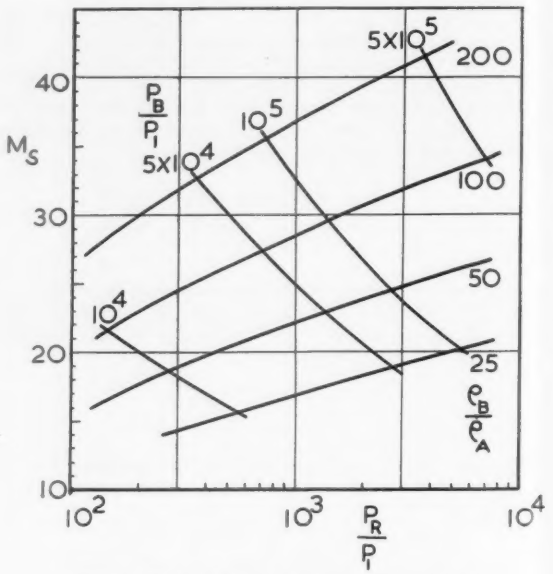

Fig. 2 Shock tube performance, helium - air

Nomenclature

P = pressure
ρ = density
a = speed of sound
γ = ratio of specific heats in driver gas
P_R = reservoir pressure
P_1 = initial pressure of test gas in shock tube
M_s = shock Mach number

Subscripts

A = conditions in driver gas before compression
B = conditions in driver gas at peak pressure

References

1 Glass, I. I., "Shock Tubes, Part I, Theory and Performance of Simple Shock Tubes," Univ. of Toronto, Canada, Inst. Aerophysics, Rev. no. 12, 1958.

2 Longwell, P. A., Reamer, H. H., Wilburn, N. P. and Sage, B. H., "Ballistic Piston for Investigating Gas Phase Reactions," *Ind. Engng. Chem.*, vol. 50, no. 4, April 1958, p. 603.

Received Feb. 1, 1960.

[1] Assistant Research Officer, Division of Mechanical Engineering. Member ARS.

[2] Numbers in parentheses indicate References at end of paper.

An Approximate Analytic Solution of Re-Entry Trajectory With Aerodynamic Forces[1]

KENNETH WANG[2] and LU TING[3]

Polytechnic Institute of Brooklyn, Freeport, N. Y.

THE PROBLEM of re-entry trajectory for space vehicles with aerodynamic forces has been investigated by Lees, Hartwig and Cohen.[4] In Lees' paper an analytic solution is obtained when the entry angle is small and the entry velocity is close to the circular satellite velocity (26,000 fps).

In this note, the method of Lees et al. is modified so that an approximate analytic solution is obtained without the restriction on the entry velocity. Numerical results are computed for entry velocity equal to 35,000 fps and compare favorably with the machine solution presented in Lees' paper.

Most of the nomenclature used in this paper is the same as in Lees et al.

The equations of motion in the directions tangential and normal to the trajectory, as shown in Fig. 1, are

$$\frac{dV}{dt} = -\frac{D}{m} + g \sin \vartheta \qquad [1]$$

$$V \frac{d\vartheta}{dt} = -\frac{L}{m} + \left(g - \frac{V^2}{r}\right) \cos \vartheta \qquad [2]$$

In deriving these equations, g is assumed constant and the velocity of air due to the rotation of the Earth is neglected.

For most entry trajectories, ϑ is small, and these equations may be simplified

$$\frac{dV}{dt} = -\frac{D}{m} = -\frac{\rho V^2 C_D A}{2m} \qquad [3]$$

$$V \frac{d\vartheta}{dt} = -\frac{L}{m} + \left(g - \frac{V^2}{r}\right) = -\frac{\rho V^2 C_L A}{2m} + \left(g - \frac{V^2}{r}\right) \qquad [4]$$

Terms in the parentheses in Equation [4] were neglected in the analysis of Lees et al., for the case where the entry velocity is close to the circular satellite velocity.

Equations [3 and 4] yield

$$d\vartheta = \frac{C_L}{C_D}\frac{dV}{V} - \frac{2mg}{C_D A}\frac{dV}{\rho V^3} + \frac{2m}{C_D A}\frac{dV}{r\rho V} \qquad [5]$$

From the exponential approximate atmosphere $\rho = \rho_0 \exp(-\beta h)$, the following relation is obtained by differentiation with respect to time

$$d\rho/dt = \beta \rho V \vartheta \qquad [6]$$

With Equation [3] it follows

$$\frac{dV}{V} = -\frac{C_D A}{2m\beta}\frac{d\rho}{\vartheta} \qquad [7]$$

and Equation [5] becomes

$$\vartheta d\vartheta = -\frac{C_L A}{2m\beta} d\rho - \left(\frac{1}{r\beta} - \frac{g}{\beta V^2}\right)\frac{d\rho}{\rho} \qquad [8]$$

The change in velocity from the entry to the peak acceleration has been shown to be moderate.[4] Furthermore, the quantities in parentheses in Equation [8] represent the terms due to gravitation and centrifugal force. They are predominant only at the earlier stage of entry and become relatively insignificant as compared to the lift term as the velocity decreases. Therefore, a good approximation is achieved by replacing the velocity V in the gravitation term with the entry velocity V_e. Since r remains practically constant, Equation [8] may now be integrated with C_L held constant.

$$\vartheta = \left[\vartheta_e^2 - \frac{C_L A}{m\beta}(\rho - \rho_e) - \left(\frac{2}{r\beta} - \frac{2g}{\beta V_e^2}\right)\ln\frac{\rho}{\rho_e}\right]^{1/2} \qquad [9]$$

For C_L varying as a function of ρ, Equation [9] may be modified. The acceleration vector felt by the pilot, in gravitational units g, is given by Lees et al. as

$$G = \frac{\rho V^2 C_D A}{2mg}\sqrt{1 + \left(\frac{C_L}{C_D}\right)^2} \qquad [10]$$

Thus, the condition for the peak acceleration or G_m for constant C_D is

$$\vartheta_m = (C_D A/m\beta)\rho_m \qquad [11]$$

Equation [9] together with Equation [11] gives the density ρ_m and the angle ϑ_m at the peak acceleration. Equation [7] may be integrated using Equation [9]. At the peak acceleration it becomes

$$\ln\frac{V_e}{V_m} = \frac{C_D A}{2m\beta}\int_{\rho_e}^{\rho_m}\frac{d\rho}{\vartheta(\rho)} \qquad [12]$$

Note here that the integrand has $\vartheta(\rho)$ as the denominator. The integral depends predominantly on the minimum value of $\vartheta(\rho)$ which is ϑ_m at $\rho = \rho_m$. Hence, the term $\ln(\rho/\rho_e)$ in $\vartheta(\rho)$ or Equation [9] is expanded in terms of ρ/ρ_m. By retaining only the first two terms in the expansion, the integral in Equation [12] may be evaluated

$$\ln\frac{V_e}{V_m} = \frac{C_D A}{2m\beta\sqrt{C}} \times \ln\left[\frac{\sqrt{A + B\rho_m + C\rho_m^2} + \sqrt{C}\rho_m + (B/2\sqrt{C})}{\sqrt{A + B\rho_e + C\rho_e^2} + \sqrt{C}\rho_e + (B/2\sqrt{C})}\right] \qquad [13]$$

Received Jan. 27, 1960.

[1] This research was supported by the United States Air Force through the Air Force Office of Scientific Research, Air Research and Development Command, under contract no. AF 49(638)-445, project 9781, under the supervision of Professor Antonio Ferri, to whom the authors are indebted for his invaluable discussion.

[2] Research Associate, Aerodynamic Laboratory.

[3] Research Associate Professor, Aerodynamic Laboratory.

[4] Lees, L., Hartwig, F. W. and Cohen, C. B., "The Use of Aerodynamic Lift During Entry Into the Earth's Atmosphere," ARS JOURNAL, vol. 29, no. 2, Sept. 1959, pp. 633–641.

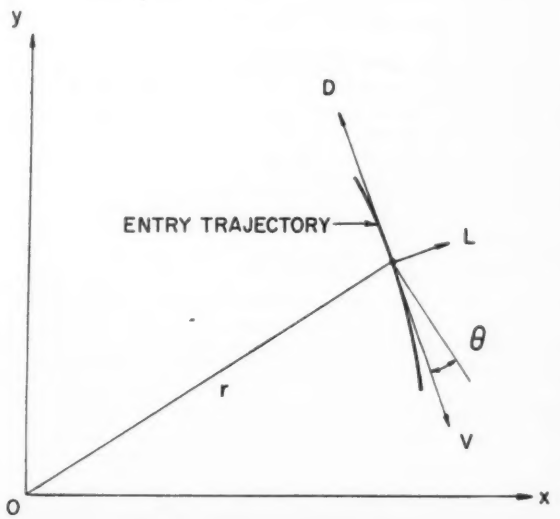

Fig. 1 Inertial coordinate system

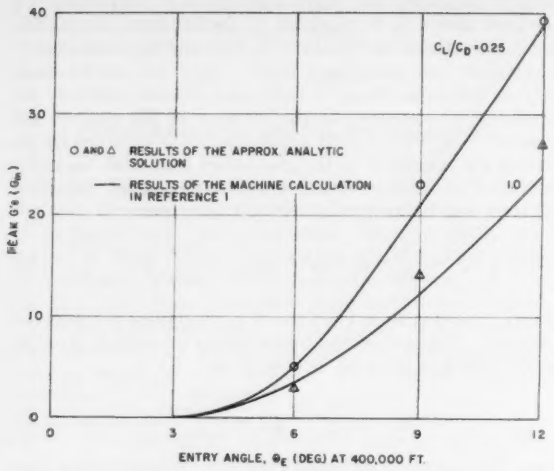
C_L/C_D = 0.25
1.0
O AND Δ RESULTS OF THE APPROX. ANALYTIC SOLUTION
RESULTS OF THE MACHINE CALCULATION IN REFERENCE 1
PEAK G's (G_m)
ENTRY ANGLE, θ_E (DEG) AT 400,000 FT.

Fig. 2 Peak acceleration with constant C_L/C_D. V_e = 35,000 fps

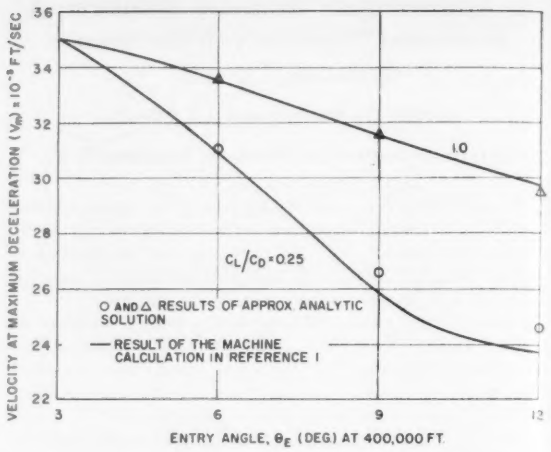
VELOCITY AT MAXIMUM DECELERATION (V_m) x 10^{-3} FT/SEC
1.0
C_L/C_D = 0.25
O AND Δ RESULTS OF APPROX. ANALYTIC SOLUTION
RESULT OF THE MACHINE CALCULATION IN REFERENCE 1
ENTRY ANGLE, θ_E (DEG) AT 400,000 FT.

Fig. 3 Velocity at peak acceleration. V_e = 35,000 fps

where

$$A = \vartheta_e^2 - \left(\frac{1}{r\beta} - \frac{g}{\beta V_e^2}\right)\left(2 \ln \frac{\rho_m}{\rho_e} - 3\right) + \frac{C_L A}{m\beta} \rho_e$$

$$B = -\left[\frac{C_L A}{m\beta} + \frac{4}{\rho_m}\left(\frac{1}{r\beta} - \frac{g}{\beta V_e^2}\right)\right]$$

$$C = \frac{1}{\rho_m^2}\left(\frac{1}{r\beta} - \frac{g}{\beta V_e^2}\right)$$

In Figs. 2 and 3, the values of the peak acceleration and the velocity, respectively, for C_L/C_D = (1/4) and 1 are compared with those in Lees' paper[5] for the case of V_e = 35,000 fps.

Applications and generalizations of present analytic solution will be presented in a later report.

[5] These data are obtained from an ASME preprint, no. 59-V-36 of the foremention paper by Lees, Hartwig and Cohen.

Pressure-Density-Temperature Relationship of Liquid O_2

EUGENE A. TKACHENKO[1]

Rocketdyne Div., North American Aviation, Inc., Canoga Park, Calif.

Two methods, one based on thermodynamics the other on a generalized equation of state, are employed in conjunction to calculate the pressure-density-temperature relationship of liquid oxygen in the temperature range of 110 to 210 R, and in the pressure range of saturation conditions to 2500 psia. Since no compressibility data for liquid oxygen are available at temperatures higher than 160 R, the results of this investigation should be of special use in rocket engine applications, where the temperature interval 160 to 210 R is of greatest interest. The pressure-density-temperature relationship of liquid oxygen is presented in tabular form, whereas the coefficient of isothermal compressibility is shown graphically, and is compared with previous calculated values.

THE EXTENSIVE use of liquid oxygen as a rocket propellant places special emphasis on knowledge of its volumetric properties. To date, no measurements of the pressure-density-temperature relationship in the liquid region of oxygen have been made except at saturation conditions, although a definite need exists for such data for large temperature and pressure ranges. In order to furnish liquid oxygen volumetric data for rocket applications which require better accuracy than the assumption of an incompressible liquid, certain basic thermodynamic relationships together with a generalized equation of state were employed, resulting in a refinement and extension of previous analytical results (3).[2]

The two methods which were employed conjunctly may be described in short as follows. One method requires saturation liquid density, vapor pressure, liquid enthalpy at saturation conditions and sonic velocity as functions of temperature. By means of basic thermodynamic relationships the coefficient of isothermal compressibility is obtained from these properties. The pressure-density-temperature relationship, in turn, may be computed on the assumption that the coefficient of isothermal compressibility is independent of pressure, or on the basis that it varies with pressure characteristic of normal liquids. The second method requires the following minimum number of physical properties: The three critical constants, the normal boiling point and the density of the saturated liquid at two temperatures. This method is formulated in an equation of state of the Van der Waals type based on a modification of the principle of corresponding states, and was developed by Hirschfelder and coworkers (6). This equation of state is semi-empirical in

Received Jan. 25, 1960.

[1] Research Engineer. Present address: St. John's University, Long Island, N. Y.

[2] Numbers in parentheses indicate References at end of paper.

nature, with constants which can be determined from generalization of empirical data for many substances, or from experimental properties of the substance studied.

Method 1

Utilizing certain thermodynamic relationships it is possible to arrive at isobaric and isothermal conditions from saturation states

$$D = f(T, P)$$

$$dD = \left(\frac{\partial D}{\partial T}\right)_P dT + \left(\frac{\partial D}{\partial P}\right)_T dP$$

$$\alpha \equiv -\frac{1}{D}\left(\frac{\partial D}{\partial T}\right)_P \qquad \beta_T \equiv \frac{1}{D}\left(\frac{\partial D}{\partial P}\right)_T$$

$$\alpha = \beta_T \frac{dP}{dT} - \frac{1}{D}\frac{dD}{dT}$$

..... [1]

$$H = f(T, P)$$

$$dH = \left(\frac{\partial H}{\partial T}\right)_P dT + \left(\frac{\partial H}{\partial P}\right)_T dP$$

$$C_P \equiv \left(\frac{\partial H}{\partial T}\right)_P \qquad \left(\frac{\partial H}{\partial T}\right)_P = \frac{1}{D}(1 - \alpha T)$$

$$C_P = \frac{dH}{dT} - \frac{1}{D}(1 - \alpha T)\frac{dP}{dT} \qquad [2]$$

From thermodynamics

$$\beta_T = \frac{1}{Dc^2} + \frac{T\alpha^2}{C_P D} \qquad [3]$$

From Equations [1, 2 and 3] the value of β_T is

$$\beta_T = \frac{(1/Dc^2)(dH/dT) - (1/D^2c^2)(dP/dT) - (T/D^2c^2)(dP/dT)(dD/dT) + (T/D^3)(dD/dT)^2}{(dH/dT) - (1/D)(dP/dT) + (T/D^2)(dP/dT)(dD/dT) - (T/D^2c^2)(dP/dT)^2}$$

It is possible to arrive at a pressure-density-temperature relationship by assuming that

$$\beta_T \neq f(P)$$

$$\beta_T \equiv \frac{1}{D}\left(\frac{\partial D}{\partial P}\right)_T \qquad [4]$$

and integrating at constant temperature

$$\Delta D = D_1(e^{\beta_T \Delta P} - 1) \qquad [5]$$

If the substance studied can be considered a normal liquid the following relationship (5) can be employed

$$(\partial \ln \beta_T/\partial P)_T \cong -10\beta_T \qquad [6]$$

Integrating at constant T

$$\beta_T = (10P + C)^{-1} \qquad [7]$$

Substituting Equation [7] in Equation [4] and integrating

$$\Delta D = D_1[(10P_2 + C/10P_1 + C)^{1/10} - 1] \qquad [8]$$

Method 2

The development and some applications of Method 2 are described in (6 and 7). Rather than recapitulate the details of Method 2, only essential equations and comments will be presented

$$p_I = -[k_0 + (\beta + k_0)t^{-1}]\rho^2 - [(1/2)(1 - k_0 - \alpha_1 + 2\beta)(1 - t^2)]\,\rho^3 t + 1 + \beta\rho^2 + (8.44 + 4.50\beta - 0.363\beta^2)(\rho - 1)^5(1/\rho) + (p - 1)^2(t - 1)[\rho^{-1}(h_0 t^{-1} - h_1) + h_2 t^{-1} + h_3] \qquad [9]$$

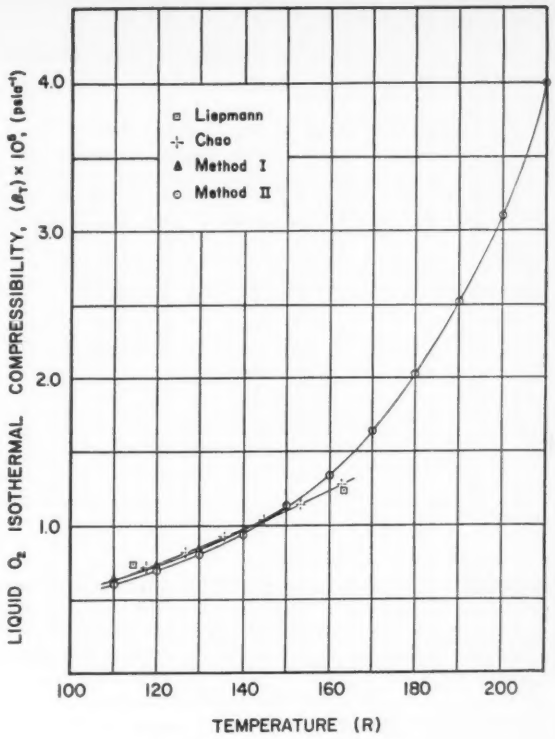

Fig. 1 Liquid O_2 compressibility

$$p_{II}(\rho, t) = p_I(\rho, t) - p_I[\rho_l(t), t] + p_v(t) \qquad [10]$$

where subscript I signifies the dense gas region and II describes the liquid region, and

$$\beta(3\beta - 1)(1 - \beta)^{-3} = (P_c/RT_cD_c) = Z_c \qquad [11]$$

k_0, β, α, h_0, h_1, h_2 and h_3 are constants characteristic of a pure substance and are best evaluated from empirical data. Since Method 2 is based on the principle of corresponding states, the variables, pressure, density and temperature are expressed in the reduced form. The reduced saturated liquid density ρ_l and the reduced vapor pressure p_v may be expressed in any accurate functional or tabular form convenient for computing purposes.

Equation [10], a generalized equation, quite useful for the representation and prediction of volumetric properties in the liquid region, is of a form suitable for computing by high speed digital computers.

Application of Method 1 and Method 2

At present the need for liquid oxygen volumetric data for rocket applications extends over an approximate temperature

Table 1 Pressure-density-temperature relationship of liquid O_2

	Liquid O_2 density, lb/ft³											
Temp, R →	110	120	130	140	150	160	170	180	190	200	210	Pressure, psia
	80.14	78.53	76.98	75.33	73.63	71.87	70.05	68.09	66.05	63.93	61.81	saturation
	80.16	78.56	77.01	75.36	73.66	71.91	70.09	68.11	...	...	...	50
	80.19	78.59	77.04	75.40	73.70	71.96	70.14	68.18	66.12	...	...	100
	80.24	78.64	77.10	75.47	73.79	72.05	70.26	68.31	66.29	64.16	62.00	200
	80.28	78.70	77.16	75.54	73.87	72.15	70.37	68.44	66.45	64.36	62.23	300
	80.33	78.75	77.23	75.61	73.95	72.24	70.48	68.57	66.60	64.54	62.46	400
	80.38	78.81	77.29	75.68	74.03	72.33	70.58	68.70	66.75	64.73	62.67	500
	80.43	78.86	77.35	75.75	74.11	72.43	70.69	68.83	66.90	64.90	62.88	600
	80.48	78.92	77.41	75.81	74.19	72.52	70.79	68.95	67.04	65.07	63.07	700
	80.52	78.97	77.47	75.88	74.27	72.61	70.90	69.07	67.18	65.23	63.26	800
	80.57	79.02	77.53	75.95	74.34	72.69	71.00	69.19	67.32	65.39	63.45	900
	80.61	79.07	77.59	76.02	74.42	72.78	71.10	69.30	67.46	65.55	63.62	1000
	80.85	79.34	77.88	76.35	74.79	73.20	71.58	69.85	68.09	66.27	64.43	1500
	81.08	79.59	78.16	76.67	75.15	73.61	72.03	70.36	68.66	66.91	65.15	2000
	81.30	79.84	78.44	76.98	75.50	73.99	72.46	70.84	69.19	67.50	65.79	2500

range of 160 to 210 R, and over a pressure range of saturation conditions to 1000 psia. Method 1 requires sonic velocity, experimental values of which are available in the range of only 108.8 to 162.8 R (9). In order to arrive at the desired pressure-density-temperature relationship one of two approaches may be followed. It is possible to extrapolate sonic velocity to the desired temperature and employ the equations of Method 1, or use only the experimental points of sonic velocity, arrive at the pressure-density-temperature relationship by Method 1, and utilize these results to evaluate the constants of Method 2, by means of which the relationship for the entire range of interest can be evaluated.

Applying experimental sonic velocity data in Method 1, the relationship can be computed considering $\beta_T \neq f(P)$ or $\beta_T = f(P)$. The assumption $\beta_T \neq f(P)$ is fairly good at low temperatures and in a wide pressure range above 7000 psia (2), but it does not hold for low pressures and high temperatures. Saturation β_T increases rapidly with temperature and is infinite at the critical point. Thus at temperatures near 260 R, in the case of liquid oxygen, at a pressure of 1000 psia, $(\partial D/\partial T)_P$ becomes positive, giving unrealistic density values, if β_T is considered independent of pressure. If one considers $\beta_T = f(P)$, as given by Equation [6], an improved relationship is obtained. The procedure followed in this investigation was to employ Method 1 with $\beta_T = f(P)$ in the temperature range 110 to 160 R and to use the resulting pressure-density-temperature values to evaluate the constants of Method 2.

Experimental Data on Which Table 1 Is Based

The data presented in Table 1 are based on graphically smoothed density values stemming from (1 and 10), on the critical constants recommended in (8), vapor pressure data presented in (8), enthalpy of the saturated liquid as given in (11) and heat capacity data presented in (4). The temperature dependence of sonic velocity originates from (9 and 12).

Acknowledgment

The aid of the following individuals is appreciatively cited: H. K. Georgius for his valuable suggestions, and E. C. Orr and G. J. Spencer for their work in the computation.

Nomenclature

D	=	density
dD/dT	=	slope of density vs. temperature at saturation conditions
α	=	coefficient of thermal expansion
β_T	=	coefficient of isothermal compressibility
dP/dT	=	slope of vapor pressure vs. temperature
H	=	enthalpy
dH/dT	=	slope of enthalpy vs. temperature at saturation conditions
C_P	=	specific heat at constant pressure
c	=	sonic velocity
p	=	P/P_c, reduced pressure
ρ	=	D/D_c, reduced density
t	=	T/T_c, reduced temperature
α_1	=	dp_v/dt, slope of reduced vapor pressure vs. reduced temperature at the critical point
ρ_l	=	reduced density of saturated liquid
p_v	=	reduced vapor pressure
P_c, D_c, T_c	=	critical pressure, density and, respectively, temperature

References

1 Baly, E. C. C. and Donnan, F. G., "The Variation With Temperature of the Surface Energies and Densities of Liquid Oxygen, Nitrogen, Argon, and Carbon Monoxide," *J. Chem. Soc.*, vol. 81, 1902, p. 907.

2 Bridgeman, P. W., "The Physics of High Pressure," G. Bell and Sons, Ltd., London, 1952.

3 Chao, G. T. Y., "Isothermal Compressibility of Liquid Oxygen and RP-1," ARS JOURNAL, vol. 29, no. 3, 1959, pp. 199–203.

4 Giauque, W. F. and Johnston, H. L., "The Heat Capacity of Oxygen from 12 K to Its Boiling Point and Its Heat of Vaporization," *J. Amer. Chem. Soc.*, vol. 51, 1929, p. 2300.

5 Hildebrand, J. H. and Scott, R. L., "The Solubility of Nonelectrolytes," Reinhold Publishing Co., N. Y., 1950, p. 139.

6 Hirschfelder, J. O., Buehler, R. I., McGee, H. A., Jr. and Sutton, J. R., "Generalized Equation of State for Both Gases and Liquids," University of Wisconsin Naval Research Laboratory, Rep. WIS-OOR15, 1956.

7 Hirschfelder, J. O., Buehler, R. I., McGee, H. A., Jr. and Sutton, J. R., "Generalized Equation of State for Gases and Liquids," *Ind. Engng. Chem.*, vol. 50, 1958, p. 375.

8 Hoge, H. J., "Vapor Pressure and Fixed Points of Oxygen and Heat Capacity in the Critical Region," Nat. Bur. Standards Research Paper RP 2081, 1950.

9 Liepmann, H. W., "Die Schallgeschwindigkeit in Flüssigem Sauerstoff als Funktion der Siedetemperatur bei Frequenzen von 715 und 1.5 × 10^6 Hz," *Helvetica Physica Acta*, vol. 11, 1938, p. 381.

10 Mathias, E. and Onnes, H. K., "The Rectilinear Diameter for Oxygen," *Communications from Kammerlingh Onnes Laboratory of the University of Leiden*, Netherlands, no. 117, 1911.

11 Millar, R. W. and Sullivan, J. D., "Thermodynamic Properties of Oxygen and Nitrogen," U. S. Bureau of Mines, Tech. Paper no. 424, 1928.

12 Van Itterbeek, A. and DeBock, A., "Velocity of Sound in Liquid Nitrogen," *Physica*, vol. 15, 1949, p. 624.

Analog Network to Convert Surface Temperature to Heat Flux[1]

G. T. SKINNER[2]

Cornell Aeronautical Laboratory, Inc., Buffalo, N. Y.

A simple analog network has been devised, for use with thin film resistance thermometers, which carries out the mathematical operation of transforming surface temperature into heat flux. The method is applicable to shock tube and shock tunnel work. A calibration unit completes the system which eliminates the necessity for complicated computational procedures.

IN A recent review article by Hall and Hertzberg[3] surface temperature thermometry was discussed and an outline was given of the data reduction procedure. With sometimes as many as 24 thin film resistance thermometers on a model in a hypersonic shock tunnel, data reduction becomes a major problem, and has raised the question of whether a suitable analog network could be devised to convert the gage output voltage, which is proportional to surface temperature, into a voltage proportional to heat flux per unit area. The conversion is usually carried out by some sort of numerical program which solves the one-dimensional heat flux equation

$$Q(t) = \sqrt{\frac{Kc\rho}{\pi}}\left[\frac{F(+0)}{\sqrt{t}} + \int_0^t \frac{F'(t-\tau)}{\sqrt{\tau}}\,d\tau\right] \qquad [1]$$

where

$Q(t)$ = heat flux per unit area
$F(t)$ = surface temperture
$F'(t)$ = surface temperature derivative
K, c, ρ = thermal conductivity, specific heat and density of the material on which the gage is plated

Using lower case letters to denote Laplace transforms of Q and F, Equation [1] becomes

$$q(s) = \sqrt{Kc\rho}\,\sqrt{s}\,f(s) \qquad [2]$$

The analog network required to solve the problem is simply a filter whose steady-state response (by substituting $j\omega$ for s) is proportional to $\sqrt{j\omega}$. That is, the amplitude response is proportional to $\sqrt{\omega}$ and the filter has a constant phase shift of 45 deg, or in other words a 3-db/octave filter. Over any finite range of frequencies, the $\sqrt{s}$ response can be approximated by a transfer function

$$g(s) = \frac{(s+a_1)(s+a_2)\ldots(s+a_n)}{(s+b_1)(s+b_2)\ldots(s+b_n)} \qquad [3]$$

where the constants $a_1, b_1, a_2, b_2, \ldots, b_n$ are separated by octave intervals.

In practice, a better approximation results if a small overshoot is allowed at each end, and, if there are more than three pairs of terms, this is done by extending a_1 and b_n one half an octave. By experiment it has been determined that a five-section filter is most satisfactory. With fewer sections accuracy suffers, and with more sections the signal-to-noise ratio becomes poor. The transfer function used is

$$g(s) = \frac{(s+0.692)(s+4)(s+16)(s+64)(s+256)}{(s+2)(s+8)(s+32)(s+128)(s+739)} \qquad [4]$$

When the resistors and capacitors have been determined, it is a simple matter to adjust these to obtain suitable input and output impedance levels, and to shift the response to the desired position on the frequency axis. The network shown in Fig. 1 has been designed for use on a hypersonic shock tunnel where the maximum anticipated duration of a run is 10 millisec. The starting transients affect the results; therefore, the optimum positioning in frequency has been determined experimentally. Amplitude response is within 0.1 db from 200 cps to 2 kc per sec, and within 1 db from 2.8 cps to 12 kc per sec, while the phase shift is within 1 deg from 22 cps to 1.6 kc per sec. Those familiar with hot wire anemometry may recognize the similarity to a very common compensator for

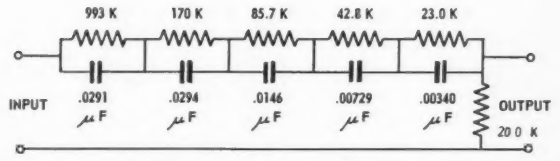

Fig. 1 Five-section network (for 10-millisec maximum run)

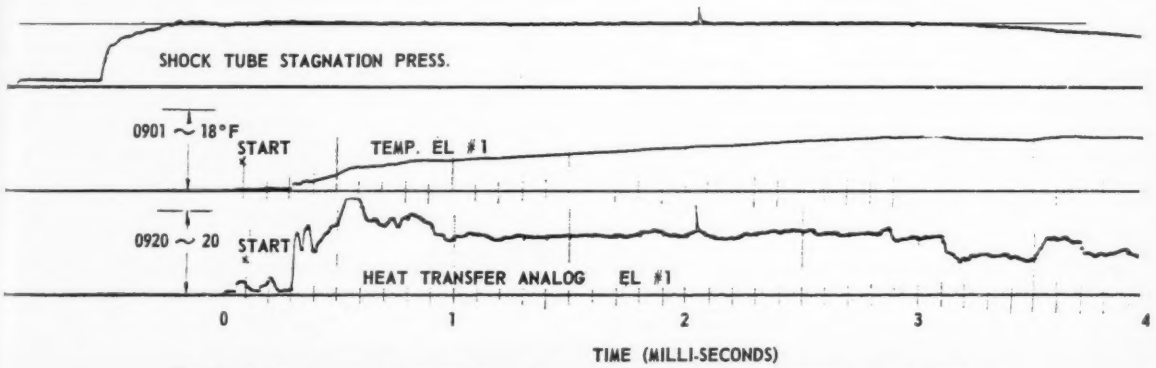

Fig. 2 Typical pressure, temperature and heat flux record from the hypersonic shock tunnel

Received Jan. 13, 1960.
[1] This work was supported as part of the Internal Research Program at the Cornell Aeronautical Laboratory, Inc.
[2] Principal Aerodynamicist.
[3] Hall, J. G. and Hertzberg, A., "Recent Advances in Transient Surface Temperature Thermometry," JET PROPULSION, vol. 28, no. 11, Nov. 1958, pp. 719–723.

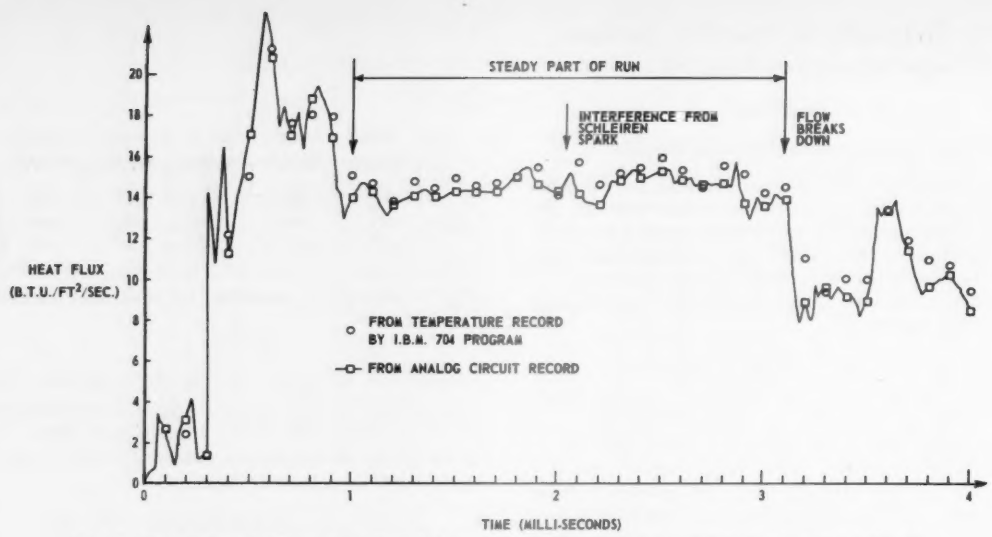

Fig. 3 Comparison between heat flux data from computer program and data from analog network

thermal lag, where only a single section is used in the approximation.

One of these filters is used as a feedback network to carry out the inverse operation on a step (of amplitude proportional to the gage current) and provide a calibration signal which, when passed through the amplifier containing the analog network, gives rise to a step output. A tuning fork oscillator provides an accurate spot check on the calibrator.

The complete system, which has now been thoroughly tested, will be described in detail in a forthcoming Cornell Aeronautical Laboratory report.[4] A typical record of a hypersonic shock tunnel run is shown in Fig. 2, where tunnel stagnation pressure, model surface temperature and analog output are reproduced. The stagnation pressure shows clearly the steady portion of the run. The surface temperature record shows a rise approximately proportional to $(\text{time})^{1/2}$ during this steady part. The analog network, operating on this temperature function, shows the constant rate of heat transfer during this steady part. Fig. 3 shows the comparison between the heat flux as computed from the temperature record of Fig. 2 by the standard IBM 704 program currently in use, and the heat flux obtained by reduction of the heat flux record of Fig. 2 using the reference amplitude provided by the calibrator unit. Discrepancies are well within the reading errors.

[4] This report is now published: Skinner, G. T., "Analog Temperature to Heat Flux," Cornell Aeronautical Laboratory Rep. no. CAL-100, Feb. 1960.

Elliptical Orbit Characteristics

G. S. GEDEON[1] and B. J. GREER[2]

Chance Vought Aircraft, Inc., Dallas, Texas

To expedite satellite feasibility studies, the well-known orbital equations are presented in the form of convenient charts. These charts permit the establishment of the permanent characteristics of the orbit and also allow following the change of the variable elements along the orbit.

TWO WORKING charts[3] are presented which permit the establishment of the orbital characteristics of a satellite after initial launch or after transfer from another orbit. The curves presented in these charts are based on two-body equations and cover a range limited by the apogee radius equal to not more than twice the perigee radius.

The charts present six basic parameters of an orbit which are defined on Fig. 1a. Knowing any two of these parameters, the remaining four may be read from the charts, and the effects of changing one of them may be readily determined. Thus, the charts serve as a simple and rather accurate way to minimize the time-consuming calculations connected with orbits.

To maintain the accuracy of four significant digits, which can be read from the charts, it is assumed that a desk calculator will be used to convert to and from the unitless quantities.

The equations defining the relationships among the variables which are plotted in Fig. 1a are as follows:

Radius ratio

$$\frac{r}{R_p} = \frac{2 - (V/V_e)^2}{1 - e}$$

Extremicity

$$x = (1 + e)/(1 - e)$$

where

$$e = \sqrt{1 - \left(\frac{V}{V_e}\right)^2 \left[2 - \left(\frac{V}{V_e}\right)^2\right] \cos^2 \phi} \quad = \text{eccentricity}$$

See (1).[4]

Received May 4, 1959.

[1] Senior Specialist; presently Head, Astrodynamics Astro Systems and Research Laboratories, Norair Div. of the Northrop Corporation.

[2] Associate Aerodynamics Design Engineer; presently Mathematician, Technical Staff, Land-Air Inc.

[3] A limited number of detailed charts are available on request from the Chance Vought Research Center, Dallas 22, Texas.

[4] Numbers in parentheses indicate References at end of paper.

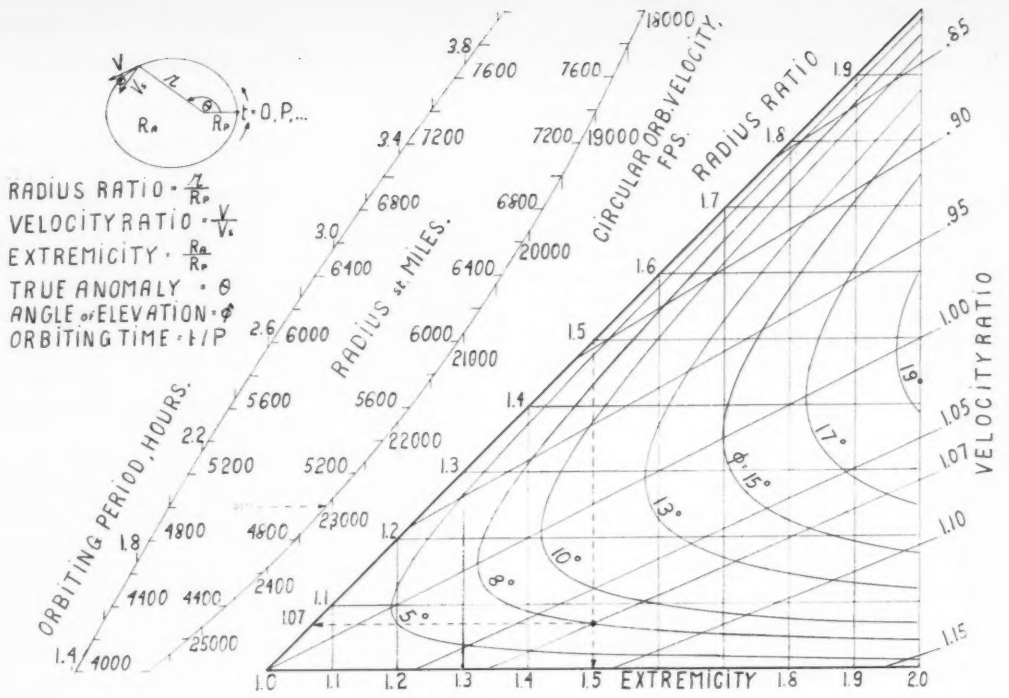

Fig. 1a

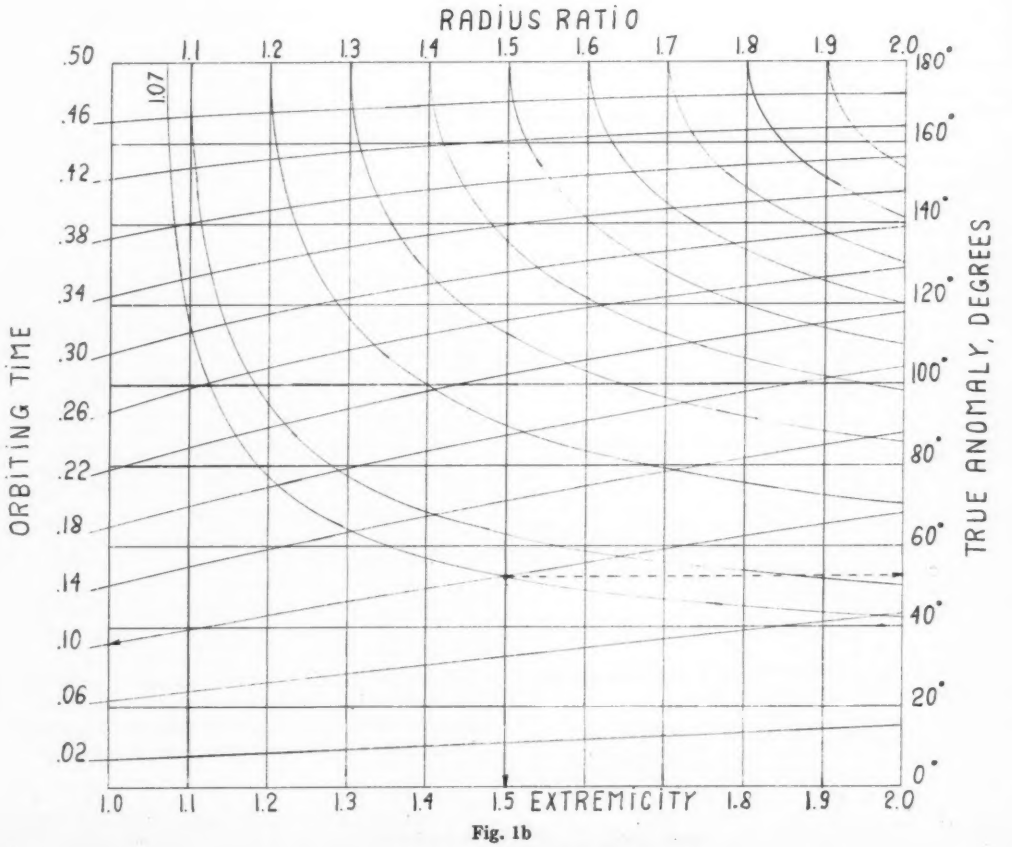

Fig. 1b

Elliptical orbit characteristics

Fig. 1a was obtained by assuming a set of (V/V_s) values for a constant ϕ and calculating the corresponding (r/R) and x values. Now plotting (r/R) against x, a constant ϕ curve is obtained, on which the defining points are labeled according to the assumed (V/V_s) values. Having drawn in this manner the constant ϕ curves, the points of equal (V/V_s) can also be connected to yield the constant (V/V_s) lines.

Fig. 1a serves to establish the orbit from the burnout conditions (launch or transfer), or to obtain the burnout conditions for achieving a required orbit. Note that the line segment corresponding to an extremicity value represents the orbit. Any point on this line segment yields the radius, the velocity and the angle of elevation of the orbit if the perigee radius is already known.

The plot of Fig. 1b was made by assuming constant (r/R_p) values and by varying e, calculating θ from the following equation for the true anomaly

$$\theta = \cos^{-1}\left[\frac{1}{e}\left(\frac{1+e}{r/R_p} - 1\right)\right]$$

Then θ was plotted against x (converted from e) and the curve was labeled according to the assumed (r/R_p) value. The second set of curves plotted on Fig. 1b was obtained by assuming constant t/P values, and by again varying e, calculating E from the following formula

$$E = 2\pi\frac{t}{P} + e\sin 2\pi\frac{t}{P} + \frac{e^2}{2!}\sin 4\pi\frac{t}{P} + \frac{e^3}{3!\,2^2}\left[3^2\sin 6\pi\frac{t}{P} - 3\sin 2\pi\frac{t}{P}\right] +$$
$$\frac{e^4}{4!\,2^3}\left[4^3\sin 8\pi\frac{t}{P} - 4\cdot 2^3\sin 4\pi\frac{t}{P}\right] + \frac{e^5}{5!\,2^4}\left[5^4\sin 10\pi\frac{t}{P} - 5\cdot 3^4\sin 6\pi\frac{t}{P} + 10\sin 2\pi\frac{t}{P}\right] + \ldots = \text{eccentric anomaly}$$

See (2).

From E and e, θ was calculated by the following equation for the true anomaly

$$\theta = \cos^{-1}[(\cos E - e)/(1 - e\cos E)]$$

Finally θ was plotted against x (converted from e) and labeled according to the assumed t/P value.

Fig. 1b is convenient for finding the time necessary to arrive at a certain point on the ellipse which is specified by a true anomaly, or vice versa. The initial anomaly can be found by transferring from Fig. 1a to Fig. 1b with the same radius ratio and extremicity values.

In order to eliminate the necessity of calculating the circular orbit velocity and the period of an orbit, Fig. 1a is equipped with two additional curves which are based on the following equations

$$V_s = R_0\sqrt{g_0/r}$$
$$P = 2\pi r_{mean}/V_s$$

where

g_0 = 32.146 ft per sec^2
R_0 = 20,926,083 ft
V_s = taken for $(r = r_{mean})$

Both figures represent only one half of the orbit. Due to symmetry, the second half can be handled by reversing the direction of motion. This will produce negative values for the anomaly, angle of elevation, and orbiting time.

Sample Problem

Determine the orbital characteristics of a launched satellite which had the following burnout conditions:

r_0 = 5000 miles V_0 = 24,706 fps ϕ_0 = 8 deg

Solution:

Using Fig. 1a and r_0 = 5000 miles, read $(V_s)_0 = 23{,}090$.

Calculate: $(V/V_s)_0 = 24{,}706/23{,}090 = 1.07$.

For $(V/V_s)_0 = 1.07$ and $\phi_0 = +8$ deg, read $(r/R_p)_0 = 1.07$ and $x = 1.5$.

Calculate

$$R_p = 5000/1.07 = 4673$$
$$R_A = 4673 \times 1.5 = 7010$$
$$r_{mean} = (4673 + 7010)/2 = 5842.$$

For this value of r_{mean}, read $P = 2.52$ hr.

Using Fig. 1b and $(r/R_p)_0 = 1.07$ and $x = 1.5$, read $\theta_0 = 52.5$ deg and $(t/P)_0 = 0.10$.

Since the angle of elevation was positive, the (zero) perigee passage of the orbit is $t_0 = 0.10 \times 2.52 = 0.252$ behind the burnout point.

It is assumed that a retrorocket which produces a velocity decrement of 900 fps will be fired 1.26 hr after burnout. Find the characteristics of the new orbit.

First calculate

$$\left(\frac{t}{P}\right)_1 = \frac{0.252 + 1.26}{2.52} = 0.60 \text{ after the zero perigee}$$

$$0.60 - 1.00 = -0.40 \text{ before the first perigee passage}$$

For this value and $x = 1.5$, one can read from Fig. 1b $\theta_1 = -155$ deg and $(r/R_p)_1 = 1.465$ and from Fig. 1a $\phi_1 = -6$ deg and $(V/V_s)_1 = 0.91$.

Thus the radius at the control point is

$$r_1 = 1.465 \times 4673 = 6846$$

The corresponding circular velocity is

$$(V_s)_1 = 19{,}730$$

and the actual velocity is

$$V_1 = 0.91 \times 19.730 = 17{,}954$$

The retrorocket decreases the velocity to

$$V_1' = 17{,}054$$

which yields

$$\left(\frac{V}{V_s}\right)_1' = \frac{17{,}054}{19{,}730} = 0.8644$$

For this $(V/V_s)_1'$ and $\phi_1 = -6$ deg the following values can be read

$$x' = 1.745 \qquad (r/R_p)_1' = 1.72$$
$$\theta_1' = -164 \text{ deg} \qquad (t/P)_1' = -0.425$$

The new perigee radius is then

$$R_p' = 6.846/1.72 = 3980$$

The mean radius of the new orbit is

$$r_{mean} = \frac{x' + 1}{2} R_p' = \frac{1.745 + 1}{2} \times 3980 = 5463$$

For this mean radius the new period is $P' = 2.28$.

Remarks

Since the submission of this paper, a new set of detailed charts have been worked out to extend the eccentricity range up to 5. These are also available on request from Chance Vought Research Center, Dallas 22, Texas.

References

1 Gedeon, G. S., "Orbital Mechanics of Satellites," in "Advances in Astronautical Sciences," vol. 3, paper 13, Plenum Press, N. Y., 1958.

2 Moulton, R. F., "An Introduction to Celestial Mechanics," MacMillan Co., N. Y., second revised edition, p. 169.

Comparison of Transpiration and Ablation Cooling

CURTIS C. BEUSMAN[1] and JOEL WEISMAN[2]

Nuclear Development Corp., White Plains, N. Y.

RECENT summaries of ablation and transpiration methods for providing thermal protection of re-entry satellites have pointed out the importance of the heat blocking effect, commonly called the transpiration factor, in increasing the effective heat capacity of a given coolant material. Adams (1)[3] presented data comparing the effectiveness of Teflon, fiber glass and foam quartz in providing protection and insulation for a recoverable satellite exposed to a rather moderate heat load during re-entry. Scala (2) on the other hand, presented ablation and transpiration data applicable to the higher heat transfer rates occurring during a ballistic missile re-entry. In relation to this study, Scala considered liquid air as a transpiration coolant and a quartz-like refractory oxide as the ablative shield. For all values of the ballistics factor W/C_DA in the range 50 to 200, Scala concluded that ablation is more effective than transpiration cooling on a coolant mass consumption basis.

We have investigated these conclusions, and extended the calculations to include other more promising transpiration coolants, i.e., water and lithium, to illustrate the added significance of the molecular weight of the transpiration coolant as well as the coolant heat of vaporization. Although the use of liquid air as a transpiration coolant does provide for important analytical simplification in the boundary layer analysis, the added engineering complexity and system weight of a cryogenic coolant storage system seems unwarranted. In view of the experimentally verified effectiveness of water (3) as a transpiration coolant, its application in this instance could prove fruitful.

Ballistic Re-Entry Comparisons

Scala expresses the mass transfer rate of the coolant m as

$$m = \frac{Q_{aero} + Q_{rad}}{(h_w - h_{res}) + \Delta Q/\Delta m}$$

where

Q_{aero} = aerodynamic heat transfer rate
Q_{rad} = radiative heat transfer rate
h_w = enthalpy of the coolant at wall conditions
h_{res} = enthalpy of the coolant at reservoir conditions
$(\Delta Q/\Delta m)$ = "effectiveness quotient" representing the heat blocking effect, caused by boundary layer thickening

Using the values of m, Q_{aero}, Q_{rad} and the wall and reservoir temperatures given by Scala for liquid air transpiration cooling, the values of $(\Delta Q/\Delta m)$ used may be computed. The computed values of the heat blocking effect (up to 17,000 Btu per lb) are appreciably greater than the enthalpy rise $(h_w - h_{res})$ for either liquid air cooling ($h_w - h_{res}$ = 1100 Btu per lb) or water with a reservoir temperature of 100 F ($h_w - h_{res}$ = 2500 Btu per lb). This fact would indicate that the choice of coolant is relatively unimportant, a fact observed early in the study of transpiration cooling (3). However, this ignores the enhancement of the "effectiveness quotient" through a reduction in the molecular weight of the coolant gas. Adams (1) points out that the blocking effect is inversely proportional to the coolant molecular weight to about the one third power.

The effect of the increased enthalpy rise and lower molecular weight for water cooling is shown in Fig. 1. It is seen that the coolant requirements are reduced nearly 30 per cent below the requirements of liquid air cooling. This system is thus more nearly competitive with the low gasification ratio (Γ) materials, e.g., quartz discussed by Scala. (The gasification ratio represents the fraction sublimed of the total material ablating from the re-entry body.)

As a further extension of this approach, lithium has also been studied as a transpiration coolant. Lithium is attractive because its lower molecular weight further reduces heat transfer to the re-entering body and its very high enthalpy of vaporization provides an additional energy sink. The required mass transfer rate for lithium cooling (based on a reservoir temperature of 400 F) is also shown in Fig. 1. It is seen that the coolant requirements are less than one third those needed when liquid air is used. Lithium weight requirements are even less than those of low gasification ratio ablative materials.

Both water and lithium can undergo chemical changes in the dissociated boundary layer; i.e., water can dissociate and lithium can react with dissociated oxygen at the wall. These additional effects have not been analyzed. In the case of water, the additional heat sink represented by dissociation (~20 per cent at 3500 R) can improve the performance of water in this instance (4). Lithium combustion could be included; if the blowing rate is high enough, no additional heat load is anticipated (5). In addition, ionization of the lithium can be significant, both from a cooling and from a telemetry standpoint.

Recoverable Satellite Re-Entry

We can also estimate the heat shield weight for satellite recovery using water as a transpiration coolant. For the case presented by Adams, severe weight penalties were incurred in ablative shields of quartz or fiber glass because of the insulation required to keep inner temperatures sufficiently low to avoid damage to the payload. In transpiration cooling, the countercurrent coolant flow prevents heat from penetrating through the porous skin (6) except for the outermost portion of the re-entry surface.

For this example (a satellite entering the atmosphere at 2 deg from the horizontal and subjected to a total heating of 7650 Btu per ft²) with an assumed outer wall temperature of 800 F, the required weight of water coolant is 1.1 lb per ft². This weight includes insulation in the sense that transpiration cooled surfaces do not require added interior thermal protection. In Table 1 the weight requirement noted is compared with the ablative insulation schemes discussed by Adams. On this basis, the transpiration cooling scheme is the most effective of those considered.

This estimate neglects the weight of the porous surface, as well as the supply reservoir and distribution system. Simple lightweight distribution schemes have been designed (7) to provide structural strength for a thin porous sheath, as well

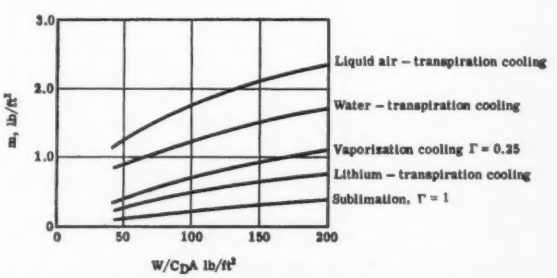

Fig. 1 Coolant mass required at stagnation point of re-entry satellite

Received Jan. 8, 1960.

[1] Manager, Special Problems Section; presently at Curtis Instruments Co., Mt. Kisco, N. Y.

[2] Development Engineer.

[3] Numbers in parentheses indicate References at end of paper.

Table 1 Weight comparison of thermal protection schemes

Material	$T_{surface}$, F	Total weight, lb/ft² (ablation and insulation)
fiber glass	~3600	15.5
foam quartz	3600	8.5
Teflon	800	4.2
water (transpiration cooling)	800	1.1

as adequate flow control for various re-entry trajectories. Other schemes, using capillary action to provide coolant distribution or self-regulation of coolant injection via gels, can be presented. The present direct comparison on the basis of total mass jettisoned during re-entry is believed to be fair since both the direct ablative as well as the transpiration methods require added material to insure structural integrity at the conclusion of re-entry.

References

1 Adams, M. C., "Recent Advances in Ablation," ARS JOURNAL, vol. 29, no. 9, Sept. 1959, pp. 625–632.

2 Scala, S. M., "Thermal Protection of a Re-Entry Satellite," ARS JOURNAL, vol. 29, no. 9, Sept. 1959, pp. 670–672.

3 Jakob, M. and Fieldhouse, I. B., "Cooling by Forcing a Fluid through a Porous Plate in Contact with a Hot Gas Stream," Proc. 2nd Symposium on Heat Transfer and Fluid Mechanics, ASME, 1949, p. 191.

4 Sänger-Bredt, I., "The Characteristics of Hydrogen and Water as Working Gases for Reactor-Heated Rocket Motors," *Astronautica Acta*, vol. 3, no. 4, 1957.

5 Sutton, G. W., "Adiabatic Wall Temperature Due to Mass Transfer Cooling With a Combustible Gas," ARS JOURNAL, vol. 29, no. 2, Feb. 1959, pp. 136–137.

6 Grootenhuis, P., "The Mechanism and Application of Effusion Cooling," *J. Royal Aero. Soc.*, vol. 63, pp. 73–89.

7 Beusman, C. C., "Feasibility Study of Transpiration Cooling for the Mark II Polaris Re-Entry Body," Lockheed Missile and Space Division, Palo Alto, Calif., NDA-2110-6, May 1959.

Combustion Instability in Solid Propellant Rocket Motors

E. W. PRICE[1]

U. S. Naval Ordnance Test Station, China Lake, Calif.

IN A Technical Comment by Green and Nachbar (1),[2] the subject of burning rate of solid propellants during high frequency oscillatory combustion was discussed further, and objections were raised to a comparison [by Price and Sofferis in (2)] of experimental work with earlier statements [by Green in (3)]. The purpose of the present note is to cite new experimental data on this problem and to clarify, if possible, the sources of controversy in (1 and 2). A more detailed version of the present note is presented in (4).

New Experimental Results

The new experimental results were obtained in a continuation of the program described in (2), and the details of the experimental procedure will not be repeated here. Tests have now been made on a wide range of double-base and composite propellants, totaling about 800 firings on 15 different propellants. Of the results obtained *with conventional propellants*,[3] the following generalizations relevant to the Green-Nachbar theory can be made:

1 Burning rate of propellants always increases during oscillatory burning, as indicated by the accompanying increases in pressure (Fig. 1).

2 Partially burned charges show that the greatest increase in burning rate is in the region where the amplitude of the velocity oscillations of the gas is a maximum (Fig. 2).

3 The observed increase in burning rate during oscillatory burning exhibits no dramatic dependence on composition of propellant or on frequency of the oscillatory behavior (investigated for one propellant over a frequency range of 1500 to 6500 cps). It has further been observed [the results reported in (2) and cited by Green and Nachbar in (1)] that consistently different behavior is exhibited by the family of mesa-burning double-base propellants.[4]

4 With these propellants, the burning rate (averaged over the charge surface) *decreases* during oscillatory burning [(5); also Fig. 3].

5 The maximum decrease in burning rate occurs in the region where the amplitude of the tangential velocity oscillation of the gas is a minimum.

Comparison With Green-Nachbar Theory and Earlier Notes

With respect to the items listed, the following comments are made:

1 A wide variety of propellants was tested, with varying degrees of sensitivity of burning rate to oscillatory behavior. However, all conventional propellants exhibited appreciable *increases* in burning rate. The observation of Green and Nachbar (1,6), that instances must be expected of no change or of decreases in burning rate, was not borne out in the present work. In the face of difficulties in performing quantitative measurements of pressure oscillations in rocket motors, and in the face of the possibility of other mechanisms producing pressure peaks, it is doubtful that severe rate changes and pressure peaks are ever caused directly by low amplitude gas oscillations.

2 The occurrence of enhanced burning rates predominantly in regions of severe velocity oscillations is suggestive of

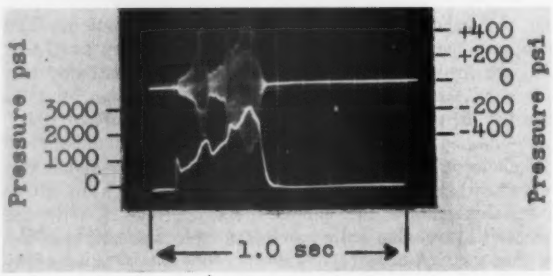

Fig. 1 Pressure-time record for firing with severe oscillatory combustion, showing variation in pressure (lower trace) with amplitude of pressure oscillations (upper trace). Conventional ($r = cp^n$) propellant. The pressure would normally increase gradually during burning even without instability, because of the increase in burning surface of the internal burning charge. The irregular increases in pressure are due to combustion instability

Received May 15, 1959.

[1] Physicist, Head, Aerothermochemistry Group, Research Department. Member ARS.

[2] Numbers in parentheses indicate References at end of paper.

[3] Meaning here propellants having an $r = cp^n$ type dependence of burning rate on pressure.

[4] Propellants characterized by negative pressure exponents of the burning rate over a limited range of pressure. Three mesa propellants were tested.

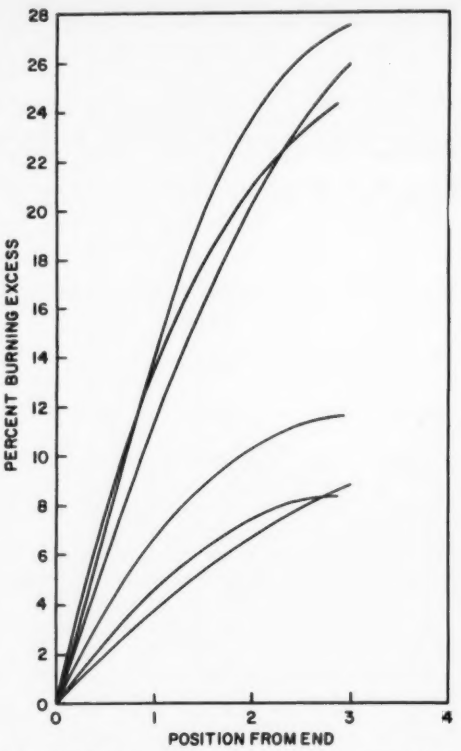

Fig. 2 Variation in burning rate with position along the charge as determined from interrupted burning tests. The ordinate is distance burned into the charge web minus distance burned in at the end of the charge (velocity node, stagnation point), divided by the distance burned in at the end. The abscissa is distance from the end of the charge. JPN (conventional) propellant

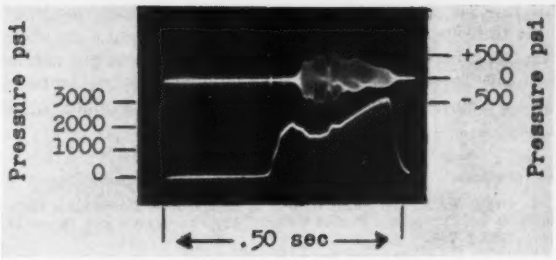

Fig. 3 Pressure-time record for firing with severe oscillatory combustion, showing evidence of decreased burning rate of mesa propellant during oscillatory combustion (pressure rises when severity of oscillations decreases). In the absence of instability, this test would show a smoothly progressive pressure-time curve corresponding to an internal burning circular cylindrical charge

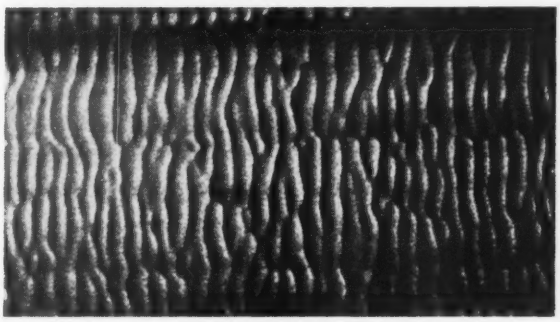

Fig. 4 Surface ripples typical of a mesa propellant recovered by interrupted burning during oscillatory combustion. Gas flow and gas oscillation were oriented in a horizontal direction in the figure. Distance between crests of ripples is about 0.06 in. (wave length of the gas oscillation was about 24 in., displacement of the gas during a cycle of oscillation was about 4 in.)

an erosion-like mechanism, and does not appear to be consistent with the Green-Nachbar theory of (1 and 7). Further scrutiny of the theory on this score (4) leads the writer to the conclusion that, contrary to (1), the theory provides no basis for an unequivocal statement as to where the largest increases in burning rate should occur on the propellant charge. Instead, the location where the burning rate is changed most by oscillatory behavior depends upon design, fluid dynamic and propellant variables, and even changes during a single test (according to the theory). This is hard to reconcile with the experimental observation in partial burning tests that the greatest amount burned from the charge web was always at the velocity antinode, no matter what conventional propellant was used or when burning was interrupted during the test.

3 In the series of tests with different charge lengths, a rather large range of oscillation frequencies was represented, with all other variables being the same at some times during each test. No singular dependence of burning rate on frequency of oscillation was evident. This result also appears to be inconsistent with the Green-Nachbar theory, and suggests the relevance of a mechanism similar to erosive burning.

4 The results obtained with mesa propellants are probably not relevant to the Green-Nachbar theory, because of the complicated solid-phase decomposition process and because of the characteristic severe rippling of the burning surface during oscillatory combustion (Fig. 4). Thus, the decreased burning rate exhibited during oscillatory combustion is probably not a valid demonstration of the decreased burning rate predicted by Green and Nachbar (1). The example of reduced burning rate reported in (2) as an exception to the theory, and subsequently interpreted by Green and Nachbar in support of their theory (1), was a result observed with a mesa propellant. Thus, the results of (2) are probably an exception to the theory as originally reported, but do not necessarily represent an irreconcilable contradiction to the theory, provided that the theory is suitably restricted.

5 In view of the remarks 2 and 4, the arguments by Green and Nachbar (1) comparing theory with the results of (2) seem to be invalid with respect to the site of maximum burning rate change as well as to the occurrence of decreases in burning rate.

Conclusions

In summary, the experimental results of the present program suggest that the burning rate increases during oscillatory combustion reflect a mechanism much like the more familiar erosive burning phenomenon of steady-state burning. The present results do not preclude the possibility of other mechanisms. However, they do seem to be in contrast to any theory that predicts critical sensitivity of burning rate to gas oscillation frequency or other propellant and environmental variables. It is suggested that the critical conditions predicted by the Green-Nachbar theory of resonance burning may be a consequence of the unsophisticated model of burn-

ing rate response to temperature and of the linear model of heat transfer from flowing gas to solid propellant. As such, the critical conditions predicted by the theory might not be relevant to severe instability and could not be identified unless quantitative tests with low amplitude instability were made.

References

1 Green, L., Jr. and Nachbar, W., "A Comment on Combustion Instability in Solid Propellant Rocket Motors," JET PROPULSION, vol. 28, no. 11, Nov. 1958, p. 769.

2 Price, E. W. and Sofferis, J. W., "Combustion Instability in Solid Propellant Rocket Motors," JET PROPULSION, vol. 28, no. 3, March 1958, pp. 190–192.

3 Green, L., Jr., "Studies on the Reaction Stability of Solid Propellant Charges," Aerojet-General Corp., Azusa, Calif., Rep. 1077, AFOSR-TN-56-10, 1956.

4 Price, E. W., "Combustion Instability in Solid Propellant Rocket Motors," U. S. Naval Ordnance Test Station, China Lake, Calif., NavOrd Rep. 7023 (NOTS 2389), Dec. 21, 1959.

5 Price, E. W., "Combustion Instability in Solid Propellant Rocket Motors," *Astronautica Acta*, vol. 4, fasc. 1, 1959, p. 63.

6 Green, Leon, Jr., "Observations on the Irregular Reaction of Solid Propellant Charges," JET PROPULSION, vol. 26, no. 8, Aug. 1956, pp. 655–659.

7 Nachbar, W. and Green, L., Jr., "Analysis of a Simplified Model of Solid Propellant Resonant Burning," *J. Aero/Space Sci.*, vol. 26, no 8, Aug. 1959, pp. 518–526.

Technical Comments

Closure by W. Nachbar[1] and L. Green Jr.[2]

EXAMINATION of the new experimental data to which Price refers in the preceding Technical Note shows that the source of the difficulties, which have been encountered in applying the model of his Reference (7)[3] to the interpretation of these experiments, is in the linearization which was performed on the equations. The analysis of (7), p. 519 specifically assumed small amplitude sinusoidal perturbations from steady-state values. Since only terms linear in ΔT_s and ΔF are retained in the expansions, it then follows that there is no predicted change in mean burning rate with these small perturbations [(7), p. 520: This is easily seen by averaging Eq. (5f) over one cycle]. The only way in which finite amplitude changes in surface temperature and finite changes in mean burning rate could arise from this linearized analysis is if operating conditions are at or very close to the predicted critical values. Under these conditions, even small (infinitesimal) amplitude oscillations of chamber pressure could give rise to finite changes in mean burning rate. Because of the limitations of the linearization, however, the amplitude of the mean burning rate at critical frequency could not be determined.

The conditions of oscillatory burning under which Price has reported sizable mean burning rate changes are not those which were assumed in the analysis of (7). Price's experimental results, reported in detail elsewhere, have shown that sizable mean burning rate changes occur in his self-excited burner only with measured peak-to-peak amplitudes of pressure oscillation of the order of the mean chamber pressure.

The predicted behavior of the linearized model is similar to that which had been observed in conventional solid rocket motors with internal burning tubular charges by experimenters before Price (6). Price's experimental results, at least those which have so far been reported, are in apparent disagreement with this earlier evidence, and, indeed, by implication they contradict the fundamental premise on which the linearized model is based. The occurrence and the amplitude of abnormal burning rates are correlated in every instance with the occurrence and the amplitude of chamber pressure oscillations (sonance). No critical or "resonance" conditions of burning are found. This experimental conclusion is corroborated by the recently reported work of Brownlee.[4]

The experiments of Price and Brownlee have all apparently been performed with great care and with superior instrumentation. However, there still appears to be some conflict between these results (see Price's generalization and comment 3) and what has been reported elsewhere as solid rocket motor experience. It is not appropriate here to enter further into discussion of this, except to point out the possibility that these experiments may involve an artificially created situation not present in actual motor designs, a situation in which the acoustic damping has been so much reduced that high frequency oscillations of finite amplitude readily occur.

Price's comments 1 and 4 are in no way surprising or in contradiction to the theory, for Price has not given any data for his propellants from which the algebraic sign of $[(E/2RT_{so}) - 1]$ can be precisely determined. Therefore, no theoretical prediction can be made relevant to his tests. However, rough estimates of typical values[5] ($E = 20$ kcal per mole, $T_{so} = 1200$ K) will clearly indicate that, for conventional propellants, this quantity will be positive, and thus conventional propellants will be expected to undergo an in-

Received Dec. 1, 1959.

[1] Staff Scientist, Lockheed Missiles and Space Division, Lockheed Aircraft Corp., Palo Alto, Calif.

[2] Senior Staff Member, Space Technology, Aeronutronic, a Division of Ford Motor Co., Newport Beach, Calif. Member ARS.

[3] Numbers in parentheses refer to the References in the preceding Technical Note by E. W. Price titled "Combustion Instability in Solid Propellant Rocket Motors," pp. 574–576.

[4] Brownlee, W. C., "An Experimental Investigation of Unstable Combustion in Solid Propellant Rocket Motors," Doctoral Thesis, California Institute of Technology, Pasadena, Calif., 1959.

[5] Summerfield, M., Sutherland, G. S., Webb, M. J., Taback, H. J. and Hall, K. P., "Burning Mechanism of Ammonium Perchlorate Propellants," ARS preprint 737–58, Nov. 1958.

crease in mean burning rate in oscillatory burning [see (7), p. 524]. This behavior may be different for mesa-type propellants. At least the theory allows for the possibility of this difference, although we have no data on which to base a numerical prediction.

As to comments 2 and 5, the controversy which has arisen here is the responsibility of the present authors, who in (1 and 7) drew one conclusion which overextended the applicability of the linearized theory. No prediction can be made from this linearized theory regarding the location of the site of maximum burning rate change with respect to the standing wave of velocity perturbations. Consequently, the conclusion we reached, that the maximum burning rate change necessarily occurs at the nodes of the velocity oscillation, is admittedly wrong, and we are indebted to Price for questioning this point.

Visual Sensitivity of Residents of Other Planets

ALLEN E. FUHS[1]

Space Technology Laboratories, Inc., Los Angeles, Calif.

RECENTLY it was announced (1)[2] that a search would be made for radio signals from other planets. Naturally this implies the existence of intelligent beings on other planets. One might speculate as to the nature of the eyes of these beings. Basic for the speculation are several facts about the eyes of human beings as they have evolved on Earth. The human eye as evolved on Earth is the result of the interplay of two factors which are illustrated in Fig. 1. There are several windows in Earth's atmosphere, one of which coincides with the peak of the spectral distribution curve of radiation from the sun. The eye is sensitive to radiation that is at the peak of solar radiation and at this window of the atmosphere.

Consider the planet of an M star in the Harvard spectral sequence (2). M stars have temperatures in the range 2500–3200 K, so that the peak radiation will occur in the range 0.94–1.20 μ. If the planet in the M star system has an atmosphere similar to Earth, i.e., similar concentrations of CO_2, H_2O, CH_4, etc., then the inhabitants will probably have eyes which have maximum sensitivity at 1 μ. There is a "window" near 1 μ, as can be seen in Fig. 2 which is based on the results of Gebbie et al. (3). Both Earthmen and residents of the M star planet could see; however each would observe the other at different wave lengths. This is illustrated in Fig. 3.

Next consider the planet of a late O star, when peak radiation occurs at 0.3 μ. Assuming that the atmosphere of this planet is similar to Earth, then its people should have similar eyes except for greater sensitivity for violet.

It is conceivable that the atmosphere of a planet in some other "stellar" system differs from Earth's atmosphere; in fact, it probably does differ. If there were strong absorption in wave length range from 0.4 to 0.75 μ, the beings of that planet would probably have sensitivity to radiation in one of that planet's windows. Hence an Earthman would be blind on that planet whereas the local residents could see. This is the condition prevailing on some of the other planets of the stellar system; however there probably are not any "local residents."

Received Feb. 1, 1960.

[1] Physical Research Laboratory. Member ARS.

[2] Numbers in parentheses indicate References at end of paper.

References

1 Science and the Citizen, "Spacious Talk," *Scientific American*, Jan. 1960, pp. 74–79.

2 Aller, L. H., "Astrophysics, The Atmosphere of the Sun and Stars," Ronald Press, N. Y., 1953, chap. 1.

3. Gebbie, H. A. Harding, W. R., Hilsun, C., Pryce, A. W. and Roberts, V., "Atmospheric Transmission in the 1 to 14μ Region," Proc. Royal Soc., vol. A 206, 1951, p. 87.

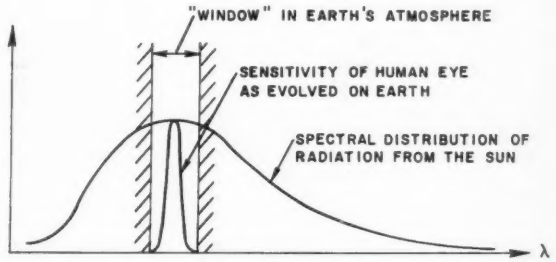
"WINDOW" IN EARTH'S ATMOSPHERE
SENSITIVITY OF HUMAN EYE AS EVOLVED ON EARTH
SPECTRAL DISTRIBUTION OF RADIATION FROM THE SUN
λ

Fig. 1 Maximum sensitivity of human eye occurs at the peak of solar radiation

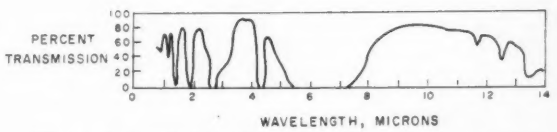

Fig. 2 Transmission of Earth's atmosphere at sea level

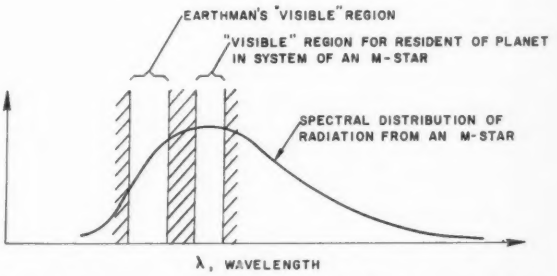
EARTHMAN'S "VISIBLE" REGION
"VISIBLE" REGION FOR RESIDENT OF PLANET IN SYSTEM OF AN M-STAR
SPECTRAL DISTRIBUTION OF RADIATION FROM AN M-STAR
λ, WAVELENGTH

Fig. 3 Maximum radiation occurs at a longer wave length. There is a window at the same wave length

Book Reviews

Ali Bulent Cambel, Northwestern University, *Associate Editor*

Feedback Control Systems, by J. C. Gille, M. J. Pelegrin and P. Decaulne, McGraw-Hill Book Co., Inc., New York, 1959, xx + 793 pp. $16.50.

Reviewed by G. J. MURPHY
Northwestern University

According to the authors, this book is intended both as a textbook for seniors and first-year graduate students and as a reference book for the engineer working in the field of automatic control. The aim of the authors is: "By progressing from the elements of the subject to provide in a single book a treatment both of the overall theory of feedback control systems and of their components."

The text is divided into five parts, titled in sequence: Dynamics of Linear Systems, Linear Servo Systems, Nonlinear Servo Systems, Components of Servo Systems and Basic Design of a Servo System. The major concepts are presented very clearly, and the entire volume is written in a literary style that is unusually good.

There are numerous references to significant French, German, Russian, English and American papers. In several instances in which different methods have been proposed for solving a given problem, the different methods are compared, and their relative merits are discussed.

For some reason, the authors chose to employ standard symbols in nonstandard manner (e.g., $r(t)$ for output, instead of input; $e(t)$ for input, instead of error), and this may be disturbing to the engineer accustomed to thinking in terms of the standard definitions.

Another item to which many readers will take exception is the attitude expressed (on p. 126) in the last sentence of the following passage: "One can study the $H(j\omega)$ function, i.e., the behavior of $H(s)$ on the imaginary axis in the Laplace plane. This is the *harmonic* approach.... Conversely, one can study the singularities of $H(s)$, that is, study the locations of its poles and zeros in the Laplace plane. This is the *pole-zero-configuration* approach.... Technically speaking, the harmonic approach is more general in its application."

Similarly, there will be many who disagree with the statement "flow graphs involve more advanced thinking than do block diagrams," which implies a nonexistent essential difference between the signal flow graph and the conventional block diagram.

The accent throughout the book is on the *application* of control theory, rather than on the theory itself. There are numerous practical examples of considerable value. However, the details are often lacking. One receives the impression that, in spite of the large number of pages in the book, the treatment of many topics is somewhat superficial. Inexplicably, an extended treatment (45 pages) is given to first-order and second-order systems.

Further evidence of the greater interest in applications than in theory is the scarcity of proofs, the weakness of many of the proofs that are presented, and the general lack of rigor in mathematical statements. For example, on p. 116 one reads, "When the transfer function of a system S has a single pole equal to zero, it can be written in the form $H(s) = P(s)/sQ_1(s)$, where $Q_1(0) \neq 0$," no mention being made of a similar restriction on $P(0)$.

Perhaps more serious is the following misleading statement, made on p. 166, in reference to Routh's criterion: "*If all the coefficients in a row are zero,* this indicates that there are two equal and opposite roots, in particular, two conjugate roots which are purely imaginary; i.e., the system is *just oscillatory.*"

Also serious is the failure to distinguish between a stationary random process and an ergodic random process. This failure is followed naturally by erroneous statements, such as: "If $y(t)$ is a stationary random function, its autocorrelation function $\phi(\tau)$ is defined as the mean value of the product $y(t)\ y(t + \tau)$. This definition leads to the equation

$$\phi(\tau) = \lim_{T \to \infty} \frac{1}{2T} \int_{-T}^{T} y(t)\, y(t + \tau)\, dt$$

which is independent of the sample used."

The value of this book is enhanced by the inclusion of some topics that are unusual in a book on automatic control. Among these are a treatment of transfer matrices, as a generalization of transfer function, and Tsypkin's method for studying oscillations in relay control systems, which is shown to be a generalization of the describing-function method of Kochenburger. In addition, the book is accompanied by a set of very useful graphs, including Bode gain-and-phase curves for first-order systems and (with damping ratio as a parameter) for second-order systems, and a Nichols chart. Numerous other graphs useful in design are included within the text.

The material on components is largely qualitative and hence of limited value. However, an extended treatment of the design of servo motors is included.

Without doubt, the book is impressive. Most control engineers will find in it something of value, and it will probably be used widely as a handbook.

Advanced Propulsion Systems, edited by Morton Alperin and George P. Sutton, Pergamon Press, New York, London, 1959, 237 pp. $6

Reviewed by A. K. OPPENHEIM
University of California

The book represents the proceedings of the unclassified portion of a symposium organized by the Directorate of Advanced Studies of the Air Force Office of Scientific Research in December 1957. It contains a good deal of information of current interest on advanced propulsion systems. All of the papers are concerned with the fundamental aspects, and the exposition is quite elementary, so that an uninitiated reader can follow the text without much difficulty. The subject matter is, of course, quite speculative in nature and consequently the book is full of imaginative but, as yet, untried concepts.

Since each paper represents essentially an entirety of its own, the best way to describe the book is by a résumé of its contents. The basic features of ion propulsion systems are reviewed by S. Naiditch, and design aspects of the ion rocket engine are described by Robert H. Boden. Some results of experimental studies on the thrust from a continuous plasma jet are reported by Gordon Cann, Adriano Ducati and Vernon Blackman; the general subject of thrust from plasma is covered by Winston H. Bostick. Krafft A. Ehricke presents a comprehensive comparison of various advanced propulsion systems; Rolf D. Buhler and Peter J. Gingo discuss the potential aircraft applications of closed gas cycle nuclear power plants; and R. A. Koehler reports on speculations about future trends in light weight electric equipment. The problem of direct power conversion is presented by John H. Huth and George Safonov. The electrostatic generators applicable to advanced propulsion systems are described by A. John Gale; their magnetohydrodynamic counterpart is elucidated by Richard J. Rosa. The status quo of liquid propellants is summarized by John F. Tormey. The particular features of the ozone-fluorine system are discussed by Edward N. Hall, metals and metal hydrides by James M. Carter, the problem of stabilized free radicals by Julius L. Jackson, and the research on free radicals as rocket propellants by George Moe and Don L. Armstrong. The book contains, also, a paper by Homer J. Stewart on human hazards of space flight, and one on system considerations affecting new propulsion applications, by Allen F. Donovan.

Quantitative Molecular Spectroscopy and Gas Emissivities, by S. S. Penner, Addison-Wesley Publishing Co., Inc., Reading, Mass., 1959, xv + 587 pp. $15.

Reviewed by A. G. GAYDON
Imperial College, London

In the period between the two World Wars, the emphasis in spectroscopic research was on the determination of atomic and molecular structures. This involved analyses of spectra in order to build up energy level schemes and their quantum mechanical interpretation. This phase in research, at least in regard to the simpler

atoms and molecules, is nearing completion, and the emphasis is now increasingly on the quantitative use of spectroscopic data. The lead for this type of work has come from astrophysics, detailed studies of intensity and line contour being used to calculate the physical and chemical constitution of stellar atmospheres. Similar calculations are, however, necessary in other fields, including the spectroscopic study of combustion processes, temperature measurements of plasma, study of radiation from shock heated gases and radiative heat transfer to space vehicles on re-entry.

Underlying the whole subject is a treatment of the profiles of spectrum lines. These profiles are the result of a combination of the natural (uncertainty) line width with Doppler broadening, collision broadening, self-absorption, and with instrumental resolving power and slit width. Professor Penner deals thoroughly with this subject; he goes on to discuss emissivities of hot gases; there is an especially long (92-page) chapter on infrared measurements; the emissivity of heated air is dealt with fully, as this is relevant to the re-entry problem; the chapter on emissivity of hydrogen atoms is mainly of astrophysical interest. The three final chapters are of especial value for combustion and rocketry; they are on measurement of flame temperature, on radiation, heat transfer and burning rates of solid propellants, and on liquid-fuel rocket motors.

This is an advanced monograph, assuming a good knowledge of molecular spectroscopy and quantum mechanics. There is very little overlap with standard books on these subjects. As Penner says, the selection of subject matter has been strongly biased by the researches of his own group, which have, of course, been most valuable. Thus, the infrared work is well treated, both theoretically and experimentally.

The discussion of electronic transitions is much less complete; there is only a casual reference to Hund's coupling cases, and rotational intensity factors are not given explicitly.

The book is not limited entirely to molecular spectroscopy; the other subjects include photo-detachment of electrons, the continuous spectra produced by ion recombination and by free-free transitions, and optical dispersion.

Penner tends to gloss over the underlying physical principles and to concentrate on the mathematical formulation of the problems. This may add to the precision but certainly not to the clarity of the treatment, and the reviewer, whose background contains mostly experimental work, has found the book very heavy reading and has failed to understand many sections of it. A major weakness is the inadequate subject index; with a more detailed index, the book would have been much more useful for reference work.

There is a recent tendency to publish research papers, especially those with aeronautical applications, in obscure reports of research organizations and universities, rather than in established scientific journals. These reports are usually not abstracted and are not available in small libraries. Penner has apparently had access to a large number of these reports and has made good use of them, the book making readily available for the first time many new results and detailed calculations. There are few references to Russian work, though; and in some sections, e.g., the calculation of vibrational overlap integrals, the bibliography is incomplete.

From what has been said, it will be clear that the book is at an advanced level, and the statement on the dust cover that it is written on the advanced undergraduate level is not true. However, for the specialist in the field, with adequate spectroscopic and mathematical background, the book will be valuable.

Absorption Spectrophotometry, by G. F. Lothian, Macmillan Co., New York, 1958, viii + 246 pp. $10.75.

Reviewed by A. E. Fuhs
Space Technology Laboratories, Inc.

In the last two decades absorption spectrophotometry has increased in its usefulness as a research tool. New instruments have been developed, numerous significant papers have appeared in the literature, and new applications have evolved. In "Absorption Spectrophotometry," which is a second edition of a previous book "The Practice of Absorption Spectrophotometry," these topics are concisely discussed. The author has divided the book into three parts.

Part I deals with the laws and principles of the subject. Integrated band intensities, pressure broadening, effects of finite slit-width, scattered radiation and absorption measurements on diffusing materials are among the principles presented in detail.

Part II considers applications. In this part of the book, problems which have been attacked successfully by absorption techniques are briefly outlined. The results of several papers specifically concerned with the application are then discussed. Typical absorption spectra are frequently given as illustrations. If the reader has a deeper interest in a particular problem, sufficient references are provided to guide additional study. Many of the applications are chosen from the fields of biochemistry and metallurgy and, hence, consider complex molecules. In the usual jet propulsion and astronautical problems, the engineering scientist is primarily concerned with monatomic, diatomic and a few triatomic molecules. Although the book does not discuss specific applications selected from aeronautical and space sciences, it does clearly demonstrate the principles and techniques.

Part III is concerned with the techniques. To cover wavelengths from 0.1 to 100μ requires a wide variety of instruments; these instruments are discussed. The principles of operation of modern instruments are described. Accessories such as cells, light sources, and standard reference substances are included in Part III.

The cross references between different parts do enhance the value of the book in spite of the many shifts from page to page required to fully utilize the cross referencing. Although the book is primarily descriptive, formulae are brought into the discussion as necessary. Units and symbols are clearly stated and defined. In reading the book, the reviewer noticed very few typographical errors. Drawings and plates are used generously throughout the book.

Books Received

Advanced Magnetism and Electromagnetism, edited by Alexander Schure, John F. Rider, N. Y., 1959, 104 pp., $2.25.

First Colloquium on the Law of Outer Space (The Hague 1958 Proceedings), edited by Andrew G. Haley and Welf Heinrich, Prince of Hanover, Springer Verlag, Germany, 1959, 126 pp., DM 15.20.

Moon Base—Technical and Psychological Aspects, T. C. Helvey, John F. Rider, N. Y., 1960, 80 pp., $1.95.

On Mathematics and Mathematicians, Robert Edouard Moritz, Dover Publication, N. Y., 1958, 410 pp., $1.95.

Philosophy and the Physicists, L. Susan Stebbing, Dover Publication, N. Y., 1958, 295 pp., $1.65.

Technical Literature Digest

M. H. Smith, *Associate Editor*
The James Forrestal Research Center, Princeton University

Propulsion and Power (Combustion Systems)

Experimental Investigation in an Altitude Test Facility of Burning of Excess Combustibles in a Rocket Engine Exhaust, by Harry E. Bloomer, Paul E. Renas and Robert J. Antl, *NASA TN* D-200, Jan. 1960, 25 pp.

Full-Scale Propulsion Testing in Wind Tunnels, by R. W. Hensel and H. K. Matt, *Arnold Engng. Dev. Center,* AEDC-TR-59-9, May 1959, 80 pp.

Combustion and Propulsion, Third AGARD Colloquium (Palermo, 1958); **Noise-Shock Tubes—Magnetic Effects—Instability and Mixing,** Pergamon Press, N. Y., 1958, 614 pp.

Development Problems in Large Liquid Rocket Engines, by R. S. Levine, pp. 3–13.

Propulsion by Air Breathing Engines, by A. A. Lombard, pp. 24–41.

Effects on Turbojet Combustors and Afterburners of Other Engine Components, by J. H. Child, pp. 55–77.

The Problem of the Ducted Rocket, by E. Le Grivzés, pp. 86–113. (In French.)

Jet Engine Noise Reduction, by N. D. Sanders and W. J. North, pp. 185–196.

Some Thought on Noise Suppression Nozzle Design, by E. J. Richards, pp. 197–222.

Muffling of Aviation Engine Stands; Technical, Financial, and Physiological Aspects, by P. Ducrot, A. Riehn, G. Roumilhac and H. Souvras, pp. 224–262. (In French.)

Role of Fundamental Research in the Study of Inlets, by C. Fouré, pp. 333–358. (In French.)

Some Problems of Providing for Scientific Research on Rockets, by A. A. Blagonravov, ARS JOURNAL, vol. 30, Jan. 1960, pp. 22–26.

Analysis of Ramjet Engine Performance Including Effects of Component Changes, by Richard J. Weber and Roger W. Luidens, *NACA Res. Mem.* E56D2-, Oct. 1956, 46 pp. (Declassified from Confidential by authority of *NASA TPA* 8, 7-22-59.)

Effect of Immersed Surfaces in Combustion Zone on Efficiency and Stability of 5-inch-diameter Ram-jet Combustor, by Thaine W. Reynolds and Donald W. Male, *NACA Res. Mem.* E54C25, June 1954, 35 pp. (Declassified from Confidential by authority *NASA TPA* 8, 7-22-59.)

Development Problems of Rocket Engines for Ballistic Missiles, by T. F. Dixon, *Interavia,* vol. 14, July 1959, pp. 818–819.

Propulsion and Power (Non-Combustion)

Some Remarks Concerning a Magnetohydrodynamic Method of Propulsion, by Rudolf X. Meyer, *Space Tech. Labs., Inc., Phys. Res. Lab.,* GM-TR-0165-00544, Dec. 1958, 16 pp.

Use of Energy Storage in Low Thrust Spaceflight, by Morton Camac, ARS JOURNAL, vol. 30, Jan. 1960, pp. 54–65.

Propulsion System for Rendezvous, by Charles J. Kaplan and D. P. Buergiss, *Astron. Sci. Rev.,* vol. 1, Oct.-Dec. 1959, pp. 11–12.

Orbital Propulsion Systems (PROFAC), by Sterge T. Demetriades, *Astron. Sci. Rev.,* vol. 1, Oct.-Dec. 1959, pp. 17–18.

Simulating Nuclear Power Systems, by B. Ya. Kogan, Yu. A. Nechaev and F. E. Tranin, *Automation & Remote Control (trans. of Avtomatika i Telemekhanika),* vol. 20, March 1959, pp. 334–339.

Beamed Electromagnetic Power as a Propulsion Energy Source, by Martin I. Willinski, ARS JOURNAL, vol. 29, Aug. 1959, pp. 601–603.

Utilization of Stored Energy in Solid Material as an Added Energy Source, by John J. Newgard, ARS JOURNAL, vol. 29, Aug. 1959, pp. 603–604.

Research on Controlled Thermonuclear Reactions in the USSR, by L. S. Artsimovich, *Soviet Physics-Uspekhi,* vol. 1 (Russian vol. 66), no. 2, Nov.-Dec. 1958, pp. 191–207.

The Characteristics of Hydrogen and Water as Working Gases for Reactor Heater Rocket Motors, by Irene Säuger-Bredt, (transl. from *Astronautica Acta,* vol. 3, no. 4, 1957, pp. 241–280), *NASA,* TT F-1, Aug. 1959. 51 pp.

The Plasma Jet and its Application, by Gabriel M. Giannini, *Giannini Res. Lab.,* Aug. 2, 1957, 23 pp. (*AFOSR-TN*-57-520; *ASTIA AD*-136,505.)

The Direct Conversion of Thermonuclear Energy to Electrical Power in the Stabilized Pinch, by R. J. Bickerton and J. D. Jukes, *J. Nuclear Energy,* vol. 8, no. 4, Jan. 1959, pp. 206–214.

On the Possibility of Neutrons Producing Secondary Interactions in High Energy Showers, by P. K. Aditya, *Nuovo Cimento,* vol. 11, no. 6, March 16, 1959, pp. 872–875.

Muon Capture in Certain Light Nuclei, by A. Fujii and H. Primakoff, *Nuovo Cimento,* vol. 12, no. 4, May 16, 1959, pp. 327–368.

Augmentation of Nuclear Rocket Specific Impulse Through Mechanical-electrical Means, by Martin Goldsmith, ARS JOURNAL, vol. 29, Aug. 1959, pp. 600–601.

Injection into Thermonuclear Machines Using Beams of Neutral Deuterium Atoms in the Range from 100 Kev to 1 Mev, by G. Gibson, W. A. S. Lamb and B. J. Lauer, *Phys. Rev.,* vol. 114, May 15, 1959, pp. 937–940.

Plasma Propulsion Devices for Space Flight, by M. Camac, A. Kantrowitz and H. E. Petschek, *Avco Mfg. Corp., Res Rep.* 45, Feb. 1959, 40 pp.

Thrust Optimization of a Nuclear Rocket of Variable Specific Impulse, by C. J. Wang, G. W. Anthony and H. R. Lawrence, ARS JOURNAL, vol. 29, May 1959, pp. 341–344.

Analytical Investigation of the Effect of Turbopump Design on Gross-Weight Characteristics of a Hydrogen-Propelled Nuclear Rocket, by Harold E. Rohlik and James E. Crouse, *NASA Memo* 5-12-59E, June 1959, 37 pp.

Nuclear Magnetic Shielding at Large Distances of a Hydrogen Atom in an Electric Field, by H. F. Hameka, *Nuovo Cimento,* vol. II, no. 3, Feb. 1, 1959, pp. 395–399.

Electric Propulsion Systems, by Victor P. Kovacik and Daniel P. Ross, *SAE Preprint* 63S, March 31-April 3, 1959, 6 pp.

Measurements of Velocity and Momentum with a Pulsed T-tube Plasma Generator, by B. Gorowitz and B. Harned, *General Electric Co., Missile & Space Vehicle Dept., Rep.* R59SD314, Feb. 20, 1959, 35 pp.

Electric Propulsion Measurements with a Small Thrust Plasma Generator, by B. Gorowitz and B. W. Harned, *SAE Preprint* 63 T., March 31-April 3, 1959, 14 pp.

Nuclear Rockets for Interplanetary Propulsion, by Frank E. Rom and Paul G. Johnson, *SAE Preprint* 63 R., March 31-April 3, 1959, 14 pp.

Jet Sources for Photon Propulsion, by E. Sänger, *Astronautica Acta,* vol. 5, no. 1, 1959, pp. 15–25.

Nuclear Rockets, by John T. Newgard and Myron Levoy, *Scientific American,* vol. 200, May 1959, pp. 46–51.

Ion Rockets for Small Satellites, by Russell N. Edwards and Harold Brown, *ARS Preprint* 789–59, April 30-May 1, 1959, 27 pp.

Arc Heated Plasma Thrust Chamber, by Mac C. Adams and Morton Camac, *ARS Preprint* 791–59, April 30-May 1, 1959, 7 pp.

Effect of Dissociation on the Performance of Working Fluids for Nuclear Propulsion, by J. G. Logan and E. L. Colichman, ARS JOURNAL, vol. 29, June 1959, pp. 409–413.

Electrical Propulsion Systems in Space Flight, by L. R. Shepherd, *Astronautica Acta,* vol. 5, no. 2, 1959, pp. 144–157.

Energy Levels of Light Nuclei, VI, by F. Ajzenberg-Selove and T. Lauritsen, *Nuclear Phys.,* vol. 11, no. 1, May 2, 1959, pp. 1–340.

Propellants and Combustion

On the Stability of Laminar Flame Fronts, by Wiktor Eckhaus, *Mass. Inst. Tech., Fluid Dynamics Res. Group,* Rep. no. 59–41, May 1959, 94 pp. (*AFOSR TN* 59–562; *ASTIA AD*-216,757.)

Determination of Turbulence Characteristics of Solid Particles in a Two Phase Stream by Optical Auto-Correlation, by S. L. Soo, C. L. Tien and V. Kadambi, *Project Squid Tech. Rep.* PR-84-P (*ASTIA AD* 206,249), Oct. 1958, 14 pp. (Available only on microcards.)

EDITOR'S NOTE: Contributions from Professors E. R. G. Eckert, J. P. Hartnett, T. F. Irvine Jr. and P. J. Schneider of the Heat Transfer Laboratory, University of Minnesota, are gratefully acknowledged.

A General Method for Calculating the Equilibrium Compositions and Temperatures and the Thermodynamic Performance Parameters, by Paul C. Hanzel, *Calif. Inst. Tech., Jet Propulsion Lab.*, Rep. 30-3, April 15, 1959, 17 pp.

Theoretical Performance of Liquid Hydrogen with Liquid Oxygen as a Rocket Propellant, by Sanford Gordon and Bonnie J. McBride, *NASA Memo* 5-21-59E, June 1959, 139 pp.

Thermodynamic Properties of Products of Combustion of Hydrogen with Air for Temperatures of 600° to 4400°R, by Robert E. English and Cavour H. Hauser, *NACA RM* E56G03, Oct. 12, 1956, 85 pp.

Approximate Composition and Thermodynamic Properties on Non-ionized Nitrogen-oxygen Mixtures, by Richard A. Hord, *NASA TN* D-2, Aug. 1959, 54 pp.

Optimum Proportioning of Two Propellants to Obtain Maximum Burnt Velocity, by R. H. Olds, ARS JOURNAL, vol. 29, Aug. 1959, pp. 598-600.

Adsorption of Halogenated Fire-extinguishing Agents on Powders, by Allen J. Barduhn, Bhailal S. Patel, Walter Meyer and Bronislaw B. Smura, *NASA Tech. Rep.* R-51, 1960, 62 pp.

Computation of Complicated Combustion Equilibria on a High-speed Digital Computer, by D. S. Villars, *U.S. Naval Ordnance Test Station*, Nov. 1959, 29 pp. (*NOTS TP* 2354.)

Combustion and Propulsion, Third AGARD Colloquium (Palermo, 1958); **Noise—Shock Tubes—Magnetic Effects—Instability and Mixing,** Pergamon Press, N. Y., 1958, 614 pp.

Study of an Aerodynamic Combustion Process, by J. Bertin and B. Salmon, pp. 555-580. (In French.)

Recent Work on Mixing at the Polytechnic Institute of Brooklyn, by L. G. Napolitano, P. A. Libby and A. Ferri, pp. 118-147.

Shock Wave and Flame Interactions, by G. Rudinger, pp. 153-176.

Some Thoughts on Flame Theory, by D. B. Spalding, pp. 269-297.

Review of Some Recent Combustion Experiments, by M. Gerstein, pp. 307-325.

Studies of the Decomposition Mechanism, Erosive Burning Sonance and Resonance for Solid Composite Propellants, by R. Schultz, L. Green Jr. and S. S. Penner, pp. 367-420.

A Review of Flame Stabilization by Means of Gaseous Jets, by A. B. Cambel, pp. 541-553.

Flame Stabilization in Boundary Layers, by Tau-Yi Toong, pp. 581-597.

Uncertainty in a Calculated Specific Impulse Due to an Uncertainty in the Heat of Formation of the Propellant, by L. J. Gordon, ARS JOURNAL, vol. 30, Jan. 1960, p. 115.

Formation of a Shock Discontinuity Ahead of a Flame Front, by G. D. Salamandra and O. A. Tsukhanova, ARS JOURNAL, vol. 30, Jan. 1960, pp. 66-72.

Interaction between a Flame and a Shock Discontinuity, by G. D. Salamandra, ARS JOURNAL, vol. 30, Jan. 1960, pp. 73-75.

Measurement of the Speed of Propagation of Turbulent Combustion, by K. I. Shchelkin, ARS JOURNAL, vol. 30, Jan. 1960, pp. 76-77.

Connection between the Flame Temperature Measured by Optical Means and by Other Methods, by K. P. Vlasov, ARS JOURNAL, vol. 30, Jan. 1960, pp. 83-85.

Theory of Flame Propagation in Solid Nitrogen at Low Temperatures, by S. G. Reed and C. M. Herzfeld, *J. Chem. Phys.*, vol. 32, Jan. 1960, pp. 1-2.

Burning Rates of Solid Propellants, by Gerald Rosen, *J. Chem. Phys.*, vol. 32, Jan. 1960, pp. 89-92.

Effect of Ambient and Fuel Pressure on Spray Drop Size, by S. M. DeCorso, *J. Engng. for Power* (*Trans. ASME*), vol. 82, Jan. 1960, pp. 10-18.

Temperature-regulated Ignition Source, by John Preston and Leland E. Ashman, *Rev. Sci. Instr.*, vol. 31, Jan. 1960, pp. 53-58.

NMR Study of Bonding in Some Solid Boron Compounds, by A. H. Silver and P. J. Bray, *J. Chem. Phys.*, vol. 32, Jan. 1960, pp. 288-292.

Analysis of a Simplified Model of Solid Propellant Resonant Burning, by W. Nachbar and L. Green Jr., *J. Aero/Space Sci.*, vol. 26, Aug. 1959, pp. 518-526.

Flame Stability Effect of Gases Ejected into a Stream from a Bluff-body Flameholder, by Edgar L. Wong, *NASA TN* D-128, Aug. 1959, 26 pp.

Aerodynamics of Flame Stabilization, by H. H. Chiu (Fourteenth Quarterly Progress Report for the Period Feb. 16, 1959 to May 15, 1959), *Princeton Univ., Aeron. Engng. Dept., Rep.* 335-n, July 1959, 30 pp.

Further Studies on the Light Scattering Technique for Determination of Size Distributions in Burning Sprays, by R. A. Dobbins, *Princeton Univ., Aeron. Engng. Dept., Rep.* 463, April 1959, 37 pp.

Combustion, by Raymond Friedman and J. H. Grover, *Ind. Engng. Chem.*, vol. 51, no. 9, Sept. 1959, Part 2, pp. 1067-1072.

Impact Sensitivity of Organic Materials on Exposure to Liquid Oxygen, by D. E. Clippinger and G. J. Morris, *Aircr. Engng.*, vol. 31, July 1959, pp. 204-214.

Precision High-velocity Detonating Cord, by G. R. Abrahamson and G. B. Huber, *Stanford Res. Inst., Poulter Labs., TR* 006-59, June 1959, 11 pp.

Exploratory Studies of Combustion in Supersonic Flow, III: Chemical Reactions in Supersonic Boundary Layer, IV: Supersonic Flame Stabilization, by Wallace Chinitz and Robert A. Gross, *Proj. Squid. Tech. Rep.* FED-1-R-P (*ASTIA AD* 217,765), June 1959, 23 pp. (Available only on microcards.)

Burning Rates of Solid Propellants, by Gerald Rosen, *Princeton Univ., Proj. Squid. Tech. Rep.* PR-95-P (*ASTIA AD* 218,687), July 1959, 20 pp. (Available only on microcards.)

A Summary of Preliminary Investigations into the Characteristics of Combustion Screech in Ducted Burners, by Lewis Lab. Staff, *NACA Rep.* 1384, 1958, ii, 18 pp.

Generalization of the Laminar Flame Action Principle for Arrhenius-type Rate Functions, by Gerald Rosen, *Princeton Univ., Proj. Squid. Tech. Rep.* PR-94-P (*ASTIA AD* 218,686), July 1959, 4 pp. (Available only on microcards.)

A Comparison of Ionization and Electronic Excitation in Flames, by I. R. King, *Proj. Squid. Tech. Rep.* EXP-8-P (*ASTIA AD* 215,360), May 1959, 3 pp. (Available only on microcards.)

Recent Advances in Solid Propellant Grain Design, by Jean A. Vandenkerckhove, ARS JOURNAL, vol. 29, July 1959, pp. 483-491.

The Useful Life of Solid Propellants at Very High Temperatures, Part I, by M. Visnov, ARS JOURNAL, vol. 29, July 1959, pp. 500-504.

Investigation of Flame Holders, by G. A. Agoston, R. H. Eustis, A. W. Noon and T. D. Witherly, *Wright Air Dev. Center, TN* 56-316, Part III, Sept. 1958, 38 pp. (*ASTIA AD* 211,846.)

Analysis of a Fuel-air Combustion Mixture by Infrared Spectroscopy, by J. S. Whittick and R. F. Muraca, *Calif. Inst. Tech., Jet Prop. Lab., Progr. Rep.* 30-9, May 21, 1959, 8 pp.

The Infrared Spectrum of the Gaseous LiF Molecule, by Guido L. Vidale, *General Electric Co. Missile and Space Vehicle Dept., Tech. Info. Series* R59SD359, May 1959, 21 pp. (Aerophys. Res. Mem. 32.)

Evaluation of Some Analytical Procedures for Solid-rocket Oxidants, Part II, by Eugene A. Burns and Ralph F. Muraca, *Calif. Inst. Tech., Jet Prop. Lab., Mem.* 20-173, Oct. 1, 1958, 11 pp.

Development of T34 Propellant: An Improved Nitroguanidine Composition, by Russell L. Trask and David J. Zauder, *Picatinny Arsenal, Tech. Rep.* 2629, July 1959, 37 pp.

Probability Studies on the Incendivity of Permissible Explosives and Effect of Small Percentages of Sodium Chloride, by N. E. Hanna, G. H. Damon and R. W. Van Dolah, *Bureau of Mines, Rep. of Investigations*, no. 5463, 1959, 22 pp.

Non-linear Theory of Combustion Instability for Liquid Propellant Rocket Motors, by T. Paul Torda and Samuel Z. Burstein, *Brooklyn Polytech. Inst., Propulsion Res. Lab., TN*-58-1, Dec. 1, 1958, 98 pp. (*ASTIA AD* 209,491.)

Combustion Instability in Liquid Propellant Rocket Motors, *Princeton Univ., Aeron. Engng. Dept.*, (27th Quart. Progr. Rep. for the period Nov. 1, 1958-Jan. 31, 1959), *Aeron. Engng. Rep.* 216-aa, May 1959, 25 pp.

Experimental Altitude Performance of JP-4 Fuel and Liquid-oxygen Rocket Engine with an Area Ratio of 48, by Anthony Fortini, Charles D. Hendrix and Vearl N. Huff, May 1959, *NASA Mem.* 5-14-59E, 27 pp.

Materials and Structures

Principles of Design of Dynamically Similar Models for Large Propellant Tanks, by Paul E. Sandorff, *NASA TN* D-99, Jan. 1960, 30 pp.

Exploratory Investigation of Several Coated and Uncoated Metal, Refractory, and Graphite Models in a 3,800°F Stagnation Temperature Air Jet, by Otto F. Trout Jr., *NASA TN* D-190, Feb. 1960, 73 pp.

Development of High-temperature Iron-base Alloys, by A. Kasak, V. K. Chandhok and E. J. Dulis, *Wright Air Dev. Center, Tech. Rep.* 59-353, July 1959, 62 pp.

Continued Study of Advanced-temperature Nickel-base Alloys to Investigate Vanadium Additives, by John C. Freche, Thomas J. Riley and William J. Waters, *NASA TN* D-260, Feb. 1960, 34 pp.

Predicted Behavior of Rapidly Heated Metals in Compression, by Elbridge Z. Stowell and George J. Heimerl, *NASA Tech. Rep.* R-59, 1960, 11 pp.

Review of Design Information on Buckling of Unstiffened Thin Walled Circular Cylindrical Shells, by Bertram Klein, ARS JOURNAL, vol. 30, Jan. 1960, pp. 7-13.

Calculation of Orthotropic Conical Shell for Arbitrary External Load, Using the Method of V. Z. Vlasov, by V. A. Sibirya-

kov, ARS JOURNAL, vol. 30, Jan. 1960, pp. 78–82.

Radiation-resistant Fluids and Lubricants, by William L. R. Rice, David A. Kirk and William B. Cheney Jr., *Nucleonics*, vol. 18, Feb. 1960, pp. 67–71.

Structural Considerations of Manned Space Vehicles, by Anthony P. Coppa, ARS JOURNAL, vol. 30, Jan. 1960, pp. 34–40.

The Kinetics of Polymer Chain Degradation, by Henry L. Friedman, *General Electric Co., Missile & Space Vehicle Dept.*, T.I.S. R59SD384, June 19, 1959, 14 pp. (Aerophys. Res. Memo. 36.)

The Thermal Degradation of Reinforced Plastics During Hypersonic Re-Entry, by Sinclaire M. Scala, *General Electric Co., Missile & Space Vehicle Dept.*, T.I.S. no. R59SD401, July 1959, 49 pp.

Vacuum Induction, Vacuum-arc, and Air-induction Melting of a Complex Heat-resistant Alloy, by R. F. Decker, John P. Rowe and J. W. Freeman, *NASA TN* D-6, Aug. 1959, 43 pp.

Relationship of Polymer Structures to Thermal Deterioration of Adhesive Bonds in Metal Joints, by J. M. Black and R. F. Blomquist, Forest Products Lab., *NASA TN* D-108, Aug. 1959, 35 pp.

Determination of the Free Surface Energy of Metals and Polymers, by James Haygood, Robert Ullman and Seymour Z. Lewin, *Wright Air Devel. Center*, TR 59–147, April 1959, 78 pp. (*ASTIA AD* 211, 923).

The Erosion of Tungsten in Electronic Torch Discharges, by H. Friedman, *General Electric Co., Missile & Space Vehicle Dept.*, T.I.S. R59SD375, May 14, 1959, 49 pp. (Aerophys. Res. Memo. 31.)

Solders for Nuclear and Space Environments, by A. B. Kaufman, *Electronics*, vol. 32, Sept. 4, 1959, pp. 50–51.

Pressing R&D on Refractory Metals, by S. David Pursglove, *Missiles and Rockets*, vol. 5, no. 36, Aug. 31, 1959, pp. 13–15.

The High-temperature Properties of Ceramics and Cermets, by E. Glenny and T. A. Taylor, *Powder Metallurgy* (Powder Metallurgy Joint Group, London), no. 1–2, 1958, pp. 189–226.

Materials for Re-entry Protection of Satellites, by L. Steg, *General Electric Co., Missile & Space Vehicle Dept., Aero-Sci. Lab. Summary of Tech. Repts.*, Jan.–June 1959, *Vol. I, Gas Dynamics, Paper*, no. 1, 30 pp., 16 figs.

Fluid Dynamics, Heat Transfer and MHD

Magnetohydrodynamic-hypersonic Flow Past a Blunt Body, by William B. Bush, *Space Tech. Labs., Inc., Phys. Res. Lab.*, 1959, 24 pp.

Effects of a Magnetic Field on the Hypervelocity Flow About a Blunt Body, by Richard W. Ziemer, *Space Tech. Labs., Inc., Phys. Res. Lab., GM-TR*-0165-00464, Aug. 1958, 22 pp.

An Investigation of a Wall Jet in a Free Stream, by Albert R. George, *Princeton Univ., Dept. Aeron. Engng. Rep.* 479, Sept. 1959, 28 pp.

On the Laminar Compressible Boundary Layer in the Presence of An Applied Magnetic Field, by William B. Bush, *Space Tech. Labs. Inc., Phys. Res. Lab., TR*-59-0000-00668, Oct. 1959, 41 pp.

On the Stable Shape of Slender Ablating Graphite Body, by George W. Sutton, *General Electric Co., Missile & Space Vehicle Dept., TIS* R59SD352, March 1959, 9 pp.

A Literature Survey on the Applicability of Steady-state Heat-transfer Coefficients to Transients in Power or in Flow with Single-phase Flow and with Two-phase Flow, by R. H. Norris, *General Electric Co., General Engng. Lab., Rep.* 57 GL 346, Nov. 1957, 15 pp.

Nucleate Boiling Literature Search, by J. J. Jocha and E. J. Lemanski, *The Martin Co., Rep.* MND-1, April 1957, 51 pp.

Heat Transfer Fluids for Nuclear Power Generation; Literature Abstracts, 1947-1957, by *North Carolina State College, Dept. Engng. Res.*, Jan. 15, 1958, 168 pp.

Equilibrium Hydrodynamic Variables Behind a Reflected Shock Wave in Hydrogen, by Eugene B. Turner, *Space Tech. Labs., Inc., Phys. Res. Lab., TR*-59-0000-00744, June 1959, 17 pp.

Equilibrium Hydrodynamic Variables Behind a Normal Shock Wave in Hydrogen, by Eugene B. Turner, *Space Tech. Labs., Inc., Phys. Res. Lab., GM-TR*-0165-00560, Aug. 1958, 27 pp.

Magnetohydrodynamic Hypersonic Flow in the Quasi-Newtonian Approximation, by Rudolf X. Meyer, *Space Tech. Labs., Inc., Phys. Res. Lab. TR*-59-0000-00690, May 1959, 12 pp.

High Temperature Gasdynamics Phenomena in Hypersonic Flight, by W. H. Wurster and C. E. Treanor, *Cornell Aeron. Lab., Inc., Cornell Univ.*, March 1958, 11 pp.

Remarks on Rocket and Aerodynamic Applications of Magnetohydrodynamic Channel Flow, by Theodore A. Wilson, *Cornell Univ., Grad. School Aeron. Engng.*, Dec. 1958, 55 pp.

An Electromagnetic Shock Tube for Aerodynamic Research, by Richard W. Ziemer, *Space Tech. Labs., Inc., Phys. Res. Lab., GM-TR*-0127-00419, June 1958, 11 pp.

Tables of Thermodynamic Properties of Air Including Dissociation and Ionization from 1,500° K to 15,000° K, by Joseph Hilsenrath, Max Klein and Harold W. Woolley, *Nat. Bur. Standards, Thermodynamics Section*, Dec. 1959, 148 pp.

Plasma Oscillations of a Confined Electron Gas, by Erich S. Wibel, *Space Tech. Labs., Inc., Phys. Res. Lab., TR*-59-0000-00769, July 1959, 18 pp.

Conductivity Measurement of Deuterium Plasma at Magnetic Reynolds Numbers Greater than Unity, by Eugene B. Turner and John E. Eastmond, *Space Tech. Labs., Inc., Phys. Res. Lab., GM-TR*-0165-00514, Dec. 1959, 37 pp.

Diffusion of a Fully Ionized Gas Confined in a Strong Magnetic Field, by Toyoki Koga, *Southern Calif. Univ., Engng. Center, USCEC Rep.* 56-209, Dec. 1959, 33 pp.

Spontaneously Growing Transverse Waves in a Plasma Due to an Anisotropic Velocity Distribution, by Erich S. Weibel, *Space Tech. Labs., Inc, Phys. Res. Lab., PRL* 8-17, Dec. 1958, 4 pp.

Longitudinal Plasma Oscillations in an Electric Field, by B. D. Fried, M. Gell-Mann, J. D. Jackson and H. W. Wyld, *Space Tech. Labs., Inc., Phys. Res. Lab., TR*-59-0000-00760, June 1959, 29 pp.

Elementary Dynamics of the Non-adiabatic Transverse Pinch, by Burton D. Fried, *Space Tech. Labs., Inc., Phys. Res. Lab., TR*-59-0000-00561, Jan. 1959, 22 pp.

On the Mechanism for Instability of Transverse Plasma Waves, by Burton D. Fried, *Space Tech. Labs., Inc., Phys. Res. Lab., TN*-59-0000-00235, Feb. 1959, 4 pp.

Stable Orbits of Charged Particles in an Oscillating Electromagnetic Field, by Erich S. Weibel, *Space Tech. Labs., Inc., Phys. Res. Lab., GM-TR*-0165-00481, Sept. 1958, 12 pp.

Effects of Diffusion and Chemical Reaction on Convective Heat Transfer, by Daniel E. Rosner, ARS JOURNAL, vol. 30, Jan. 1960, p. 114.

Transient and Steady-state Behavior of an Idealized Solar Powered Heat Exchanger, by J. W. Tatom, ARS JOURNAL, vol. 30, Jan. 1960, pp. 116–117.

Thermodynamic Properties of Air in the Temperature Interval from 1000 to 12,000 K and the Pressure Intervals from 0.001 to 1000 atm, by E. V. Stupochenko, I. P. Stakhanov, E. V. Samuilov, A. S. Pleshanov and I. B. Rozhdestvenskii, ARS JOURNAL, vol. 30, Jan. 1960, pp. 98–112.

Shock Waves in Magneto-gasdynamics, by M. N. Kogan, *PMM: J. Appl. Math. and Mech.* (*trans. of Prikladnaya Matematika i Mekhanika*), vol. 23, no. 3, 1959, pp. 785–792.

The Thermal Conductivity of Water: An Investigation of a Reported Anomaly, by R. W. Powell and A. R. Challoner, *Phil. Mag.*, vol. 4, Oct. 1959, pp. 1183–1186.

Transport Phenomena in Slightly Ionized Gases: Low Electric Fields, by Mahendra Singh Sodha, *Phys. Rev.*, vol. 116, Nov. 1, 1959, pp. 486–488.

An Implicit, Numerical Method for Solving the Two-dimensional Heat Equation, by G. A. Baker Jr. and T. A. Oliphant, *Quart. Appl. Math.*, vol. 17, Jan. 1960, pp. 361–374.

An Implicit, Numerical Method for Solving the n-Dimensional Heat Equation, by G. A. Baker Jr., *Quart. Appl. Math.*, vol. 17, Jan. 1960, pp. 440–442.

Spectroscopic Investigation of an Intense Pulsed Discharge in Hydrogen, III: Determination of the Parameters of a High-temperature Plasma, by S. Yu. Luk'yanov and V. I. Sinitsyn, *Soviet Phys.-JETP*, vol. 36, no. 6, Dec. 1959, pp. 1155–1157.

Motion of a Plasma Loop in an Axially Symmetric Magnetic Field, by L. M. Kovrizhnykh, *Soviet Phys.-JETP*, vol. 36, no. 6, Dec. 1959, pp. 1308–1311.

Acceleration of Plasmoids by High-frequency Electric Fields, by M. A. Miller, *Soviet Phys.-JETP*, vol. 36, no. 6, Dec. 1959, pp. 1358–1363.

Combustion and Propulsion, Third AGARD Colloquium (Palermo, 1958); **Noise—Shock Tubes—Magnetic Effects—Instability and Mixing,** Pergamon Press, N. Y., 1958, 614 pp.

Radiation Heat Transfer to Hypersonic Vehicles, by R. E. Meyerott, pp. 431–447.

Convective Heat Transfer with Mass Addition and Chemical Reactions, by L. Lees, pp. 451–497.

High Temperature Shock Waves, by O. Laporte, pp. 499–521.

On Magneto-fluid-dynamics, by A. Schluter, pp. 525–531.

Graphical Method on Problems of Gasdynamic Mixing, by O. Litz, pp. 598–610.

Dependence of Electron Mobility on Magnetic Field in a Fully Ionized Gas, by M. S. Sodha and Y. P. Varshni, *Phys. Rev.*, vol. 114, May 15, 1959, pp. 946–947.

Ionic Theory of Plasmas and Magnetohydrodynamics, by H. S. Green, *Phys. Fluids*, vol. 2, no. 4, July-Aug. 1959, pp. 341–349.

Propagation of Weak Hydrodynamic Discontinuities, by J. Bazer and O. Fleischman, *Phys. Fluids*, vol. 2, no. 4, July-Aug. 1959, pp. 366–378.

Rayleigh's Problem in Magnetohydrodynamics, by C. C. Chang and J. T. Yen, *Phys. Fluids*, vol. 2, no. 4, July-Aug. 1959, pp. 393–403.

Laminar Steady-state Magnetohydrodynamic Flow in an Annular Channel, by Samuel Globe, *Phys. Fluids*, vol. 2, no. 4, July-Aug. 1959, pp. 404–407.

Radiative Transport within an Ablating Body, by Leo P. Kadanoff, *Avco-Everett Res. Lab.*, July 1959, 37 pp.

Aerothermodynamic and Electrical Properties of Some Gas Mixtures to Mach 20, by W. Chinitz, C. L. Eisen and R. A. Gross, ARS JOURNAL, vol. 29, Aug. 1959, pp. 573–578.

Meteoric Ablation through Interfacial Instability, by Sin-I Cheng, ARS JOURNAL, vol. 29, Aug. 1959, pp. 579–587.

Graphical Computation of Shock and Detonation Waves in Real Gases, by George H. Markstein, ARS JOURNAL, vol. 29, Aug. 1959, pp. 588–590.

Magnetic Boundary Layers, by H. F. Ludloff, ARS JOURNAL, vol. 29, Aug. 1959, pp. 590–591.

Optimum Magnetic Field for Stagnation Heat Transfer Reduction at Hypersonic Velocities, by Robert Goulard, ARS JOURNAL, vol. 29, Aug. 1959, pp. 604–605.

Analysis of the Aerodynamic Heating for a Re-entrant Space Vehicle, by M. J. Brunner, *J. Heat Transfer (ASME Trans.)*, vol. 81, Series C, Aug. 1959, pp. 223–229.

A Photographic Study of Boiling in the Absence of Gravity, by R. Siegel and C. Usiskin, *J. Heat Transfer (ASME Trans.)*, vol. 81, Series C, Aug. 1959, pp. 230–236.

A Note on Magnetohydrodynamic-hypersonic Flow Past a Blunt Body, by William A. Bush, *J. Aero/Space Sci.*, vol. 26, Aug. 1959, pp. 536–537.

The Effect of Vehicle Deceleration on a Melting Surface, by D. M. Tellep, *J. Aero/Space Sci.*, vol. 26, Aug. 1959, pp. 537–538.

Solutions of the Laminar Compressible Boundary-Layer Equations with Transpiration which are Applicable to the Stagnation Regions of Axisymmetric Blunt Bodies, by John T. Howe and William A. Mersman, *NASA TN* D-12, Aug. 1959, 73 pp.

Turbulent Boundary Layer Equations with Binary Diffusion, by N. Mess and H. G. Lew, *Gen. Electric Co., Missile & Space Vehicle Dept.*, T.I.S. R59SD310, May 1958, 35 pp. (*Aerophys. Res. Memo.* 23).

Compressible Flow Tables k = 1.40; Stagnation Temperature Change Without Friction, by C. Hoebich, *Army Rocket and Guided Missile Agency, Ordnance Missile Labs. Division, Design and Development Lab., ARGMA TN*-1H1N-5, June 1959, 89 pp.

On the Stability of a Shear Layer, by J. Mankes, *Calif. Inst. Tech., Jet Propulsion Lab.*, Prog. Rep. 30–10, April 20, 1959, 9 pp.

The Electric Conductivity of a Partially Ionized Gas, by A. C. Pipkin, *Maryland Univ., Inst. for Fluid Dynamics and Appl. Math, TN* BM-170, April 1959, 30 pp.

On Series Expansions in Magnetic Reynolds Number, by Vernon J. Rossow, *NASA TN* D-10, Aug. 1959, 44 pp.

A Contribution to the Theory of Meteor Ablation, by George W. Sutton, *General Electric Co., Missile and Space Vehicle Dept.*, T.I.S. R59SD331, March 1959, 23 pp. (Aerophys. Res. Memo. 28.)

Transient Temperature With and Without Ablation in the Skin of a Ballistic Missile Entering the Earth's Atmosphere, by Shih-Yuan Chen, *Boeing Airplane Co., Document* D7–1138, June 1959, 40 pp.

On Some Problems in Radiative Heat Transfer, by Saul S. Abarbanel, *Mass. Inst. Tech., Fluid Dynamics Res. Group, Rep.* no. 59–1, April 1959, 217 pp. (*AF OSR TN* 59–531; *ASTIA AD* 216,538.)

Heat Transfer to a Vaporizing, Ablating Surface, by Richard G. Fledderman, *J. Aero/Space Sci.*, vol. 26, Sept. 1959, pp. 604–605.

How Far Are We on Re-entry Cooling? by Kurt R. Stehling, *Space Aeron.*, vol. 32, no. 3, Sept. 1959, pp. 43–45.

A Shallow-liquid Theory in Magnetohydrodynamics, by L. E. Fraenkel, *Calif. Inst. Tech., Guggenheim Aeron. Lab.*, June 1959, 74 pp. (*AFOSR TN*-59-563; *ASTIA AD*-216,758.)

On the Mechanism of Sub-cooled Nucleate Boiling, by S. G. Bankoff, *Calif. Inst. Tech., Jet Prop. Lab., Memo.*, 30–8, Feb. 5, 1959, 50 pp.

Experimental Studies on Heat Transfer and Fluid Flow (Liquid Hydrogen), by M. E. Ellion, E. L. Geery, L. Green Jr. and W. R. Thompson, *Aerojet General Corp., Rep.* 1520, vol. II, Nov. 1958, 38 pp. (*WADC TR*-58-610, vol. II.)

Selected Topics from the Theory of Gas Flow at High Temperatures, VI: Some Aspects of Particle Interaction in Gases, by J. M. Burgers, *Maryland Univ., Inst. Fluid Dynam. and Appl. Math., TN* BN 176, June 1959, 40 pp.

Heat Transfer from Non-isothermal Surfaces, by Helmut Wolf, *Princeton Univ., Proj. Squid Tech. Rep.* PUR-38-0 (*ASTIA AD* 215,140), April 1959, 25 pp. (Available only on microcards.)

A Study of the Mean Thickness of the Liquid Film and the Characteristics of the Interfacial Surface in Annular, Two-phase Flow in a Vertical Pipe, by D. A. Charvonia, *Proj. Squid Tech. Rep.* PUR-39-T-R (*ASTIA AD* 216,823), May 1959, 253 pp. (Available only on microcards.)

Entropy Production and Pressure Waves, by Gerald Rosen, *Princeton Univ., Proj. Squid Tech. Rep.* PR-90-P (*ASTIA AD* 217,238), June 1959, 11 pp. (Available only on microcards.)

Hydrodynamic Studies on the Effect of Entrained Gases on Injection and Atomization, by R. W. Mascolo, *North American Aviation, Inc., Rocketdyne Div., Rep.* R-1466, June 5, 1959, 69 pp., 38 refs.

Use of the Revolving Arm Method for the Determination of the Stagnation Temperature in an Ionized Gas, by F. Marcel Devienne, André F. Roustan, Henri L. Bosc, Robert G. Clapier and Raymond F. Meslet, *Lab. Mediterranéen de Recherches Thermodynamiques*, Feb. 1959, 21 pp. (*ASTIA AD* 211,473.)

The Large High Pressure Arc Plasma Generator: A Facility for Simulating Missile and Satellite Re-entry, by P. H. Rose, W. E. Powers and D. Hritzay, *Avco-Everett Research Lab., Res. Rep.* 56, June 1959, 30 pp.

Interaction of Two-dimensional Inviscid Incompressible Jet Facing a Hypersonic Stream, by S. H. Lam, *Princeton Univ., Dept. Aeron. Engng., Rep.* 447, March 1959, 23 pp. (*AFOSR-TN*-59-274; *ASTIA AD* 212,708.)

An Experimental and Theoretical Study of Quartz Ablation at the Stagnation Point, by Mac C. Adams, William E. Powers and Steven Georgiev, *Avco-Everett Research Lab., Res. Rep.* 57, June 1959, 28 pp.

Experimental Investigation of Coaxial Jet Mixing of Two Subsonic Streams at Various Temperatures, Mach Number, and Diameter Ratios for Three Configurations, by Richard R. Burley and Lively Bryant, *NASA Memo* 12–21–58E, Feb. 1959, 29 pp.

The Application of Constant Property Solutions to Mass Transfer Cooling Calculations, by C. J. Scott, *Minnesota Univ. Rosemount Aeron. Labs. Engng. Mem.* 76, Dec. 1958, 31 pp. (*AFOSR-TN*-59-201; *ASTIA AD* 211,521.)

Impact of High Speed Particles with Solids and Gases, by M. C. Kells and D. D. Keough, *Stanford Res. Inst., Poulter Labs. Tech. Rep.* 017–58, Dec. 15, 1958, 42 pp.

Burnout of Heating Surfaces in Water, by R. L. Menegus, *AEC*, DP-363, March 1959, 52 pp.

Nitrogen at High Temperatures (Presented at ASME High Temperature Symposium, Purdue Univ., Feb. 1959), by Frank Martinek, *General Electric Co., Flight Propulsion Lab., Cincinnati, Ohio*, 1959, 50 pp. (*AFOSR-TN*-59-264; *ASTIA AD* 212,467.)

Radio-frequency Circuits for Plasma Physics, by R. L. Gamblin, *Electronics*, vol. 32, July 3, 1959, pp. 50–52.

Entrance Effects and Prediction of Turbulence in Non-Newtonian Flow, by D. C. Bogue, *Ind. Engng. Chem.*, vol. 51, July 1959, pp. 874–878.

Heat Transfer to Turbulent Non-Newtonian Fluids, by A. B. Metzner and P. S. Friend, *Ind. Engng. Chem.*, vol. 51, July 1959, pp. 879–884.

Laminar Heat Transfer Around Blunt Bodies in Dissociated Air, by Nelson H. Kemp, Peter H. Rose and Ralph W. Detra, *J. Aero/Space Sci.*, vol. 26, July 1959, pp. 421–430.

Experimental Verification of Boundary Layer Corrections in Hypersonic Nozzles, by Donald L. Baradell, *J. Aero/Space Sci.*, vol. 26, July 1959, pp. 454–455.

A Total-temperature Probe for High-temperature Boundary-layer Measurements, by M. Sibulkin, *J. Aero/Space Sci.*, vol. 26, July 1959, pp. 458–459.

Transport Phenomena in a Fluid Composed of Diatomic Molecules, by John S. Dahler, *J. Chem. Phys.*, vol. 30, June 1959, pp. 1447–1475.

The Kinetic Radiation Equilibrium of Air, by P. Harteck, *J. Phys. Chem.*, vol. 63, June 1959, pp. 956–961.

Strong Hydromagnetic Disturbances in a Collision-free Plasma, by J. W. Dungey, *Philosophical Magazine*, vol. 4, May 1959, pp. 585–593.

Stable Orbits of Charged Particles in an Oscillating Electromagnetic Field, by Erich S. Weibel, *Phys. Rev.*, vol. 114, April 1, 1959, pp. 18–23.

Theory of Spatially Growing Plasma Waves, by Masao Sumi, *Phys. Soc. Japan, J.*, vol. 14, May 1959, pp. 653–663.

Flash X-ray Radiography for the Density Measurement in a Hypersonic Air Flow, by Fumio Tamaki and Chol-Soo Kim, *Phys. Soc. Japan, J.*, vol. 14, May 1959, pp. 664–677.

A Visualizing Method of Electron Temperature and Plasma Density, by Hajime Tamagawa and Junji Fujita, *Phys. Soc. Japan, J.*, vol. 14, May 1959, pp. 678–686.

Relativistic Hydrodynamics for a Charged Nonviscous Fluid, by Chau-Chin Wei, *Phys. Rev.*, vol. 113, March 15, 1959, pp. 1414–1419.

Flight Mechanics

Trajectory Design Methods, *Calif. Inst. Tech., Jet Prop. Lab., Pub.* 30-18, Nov. 1959, 28 pp.

The Approximate Analysis of Zero-lift Trajectories, by C. P. Hoult, *Air Force, Cambridge Res. Center, Geophys. Res. Directorate, GRD Res. Notes* 17, *AFCRC-TN*-59-404, Aug. 1959, 19 pp.

Effects of Small Changes in Position and Velocity at Burnout on the Orbit of a Ballistic Missile, by Edouard E. Perret and John C. Corbin Jr., *Wright Air Dev. Center, TN* 59-336, Oct. 1959, 25 pp.

Trajectory Problems in Cislunar Space, *Westinghouse Electric Corp., Air Arm Div., TN*, Dec. 1959, 42 pp. (*AF OSR TN* 59-1284.)

Orbits of Cosmic Rockets Toward the Moon, by L. I. Sedov, ARS JOURNAL, vol. 30, Jan. 1960, pp. 14–21.

An Approximation to the Re-entry Trajectory, by Mildred M. Moe, ARS JOURNAL, vol. 30, Jan. 1960, pp. 50–53.

Analytical Estimates for Optimum Transfer Paths, by H. Munick and R. McGill, ARS JOURNAL, vol. 30, Jan. 1960, pp. 120–121.

Projected Orbits of 24-hour Earth Satellites, by Louis B. Wadel, ARS JOURNAL, vol. 30, Jan. 1960, pp. 122–123.

Satellite Librations of Large Amplitude, by W. B. Klemperer, ARS JOURNAL, vol. 30, Jan. 1960, pp. 123–124.

Librations on a Slightly Eccentric Orbit, by Robert M. L. Baker Jr., ARS JOURNAL, vol. 30, Jan. 1960, pp. 124–126.

Plane Libration of a Prolate Ellipsoidal Shell, by Robert M. L. Baker Jr., ARS JOURNAL, vol. 30, Jan. 1960, pp. 126–128.

Rendezvous Compatible Orbits, by Norman V. Petersen and Robert S. Swanson, *Astron. Sci. Rev.*, vol. 1, Oct.-Dec. 1959, pp. 13–14, 20.

An Orbital Rendezvous Simulator, by E. Levin and J. Ward, *Astron. Sci. Rev.*, vol. 1, Oct.-Dec. 1959, pp. 15–16, 21.

Orbital Plane-change Maneuver, by Daniel B. DeBra, *Astron. Sci. Rev.*, vol. 1, Oct.-Dec. 1959, pp. 19–20.

On an Aspect of the Relations Between Mechanics and Artificial Earth Satellites, by Maurice Roy, *La Recherche Aéronautique*, no. 73, Nov.-Dec. 1959, pp. 1–7. (In French.)

Motion of a Satellite in the Earth's Gravitational Field, by G. V. Groves, *Proc. Roy. Soc., London*, vol. 254, no. 1276, Jan. 19, 1960, pp. 48–65.

A Method for Simulating the Atmospheric Entry of Long-range Ballistic Missiles, by A. J. Eggers Jr., *NACA Rep.* 1378, 1958, 7 pp.

Experimental Investigation of the Simulation of Atmospheric Entry of Ballistic Missiles, by Stanford E. Neice, James A. Carson and Bernard E. Gunningham, *NACA Res. Mem.* A57126, Dec. 1957, 32 pp. (Declassified from Confidential by authority *NASA TPA* 8, 7-22-59.)

Lagrange Multipliers and Quasi-steady Flight Mechanics, by Angelo Miele, *J. Aero/Space Sci.*, vol. 26, Sept. 1959, pp. 592–598.

Steady-state Circular Pitching and Yawing Motion of Symmetric Missiles, by Charles H. Murphy Jr., *J. Aero./Space Sci.*, vol. 26. Sept. 1959, pp. 600–601.

Similitude of Hypersonic Real-gas Flows over Slender Bodies with Blunted Noses, by Hsien K. Cheng, *J. Aero/Space Sci.*, vol. 26, Sept. 1959, pp. 575–585.

Stability of a Globular Cluster in the Oblate Earth's Equatorial Plane, by Marvin H. Hewitt, ARS JOURNAL, vol. 29, Aug. 1959, pp. 595–596.

Ogive Having Minimum Drag in Two-dimensional Hypersonic Flow, by E. Mattioli, *Aerotecnica*, vol. 29, no. 1, Feb. 1959, pp. 16–24. (In Italian.)

Optimum Staging Techniques, by Leon Weisbord, ARS JOURNAL, vol. 29, June 1959, pp. 445–446.

Some Design Aspects of an Interplanetary Exploratory Vehicle, by Henry K. Hebeler and Richard D. White, *Astronautical Sci. Rev.*, vol. 1, no. 2, April-June, 1959, pp. 11–15.

Graphic Determination of the Main Influences and Design Parameters of Missiles, by O. Scholze, *Raketentechnik und Raumfahrtforschung*, vol. 3, no. 2, April 1959, pp. 36–44. (In German.)

Design of Missile Bodies for Minimum Drag at Very High Speeds—Thickness Ratio, Lift, and Center of Pressure Given, by T. Strand, *J. Aero/Space Sci.*, vol. 26, Sept. 1959, pp. 568–570.

On a Class of Variational Problems in Rocket Flight, by G. Leitmann, *J. Aero/-Space Sci.*, vol. 26, Sept. 1959, pp. 586–591.

Theoretical Principles of Guided Missile Systems, by E. G. C. Burt, *J. Roy. Aero. Soc.*, vol. 63, Aug. 1959, pp. 455–464.

Vehicle Design, Testing and Performance

Static Stability and Separation Characteristics of a Two-stage Rocket Configuration at Mach Numbers from 1.57 to 4.50, by Kenneth L. Turner, David S. Shaw and Lawrence W. Enderson Jr., *NASA TN-D*-188, Jan. 1960, 35 pp.

Proposal for Standard Weight Definitions for Space Vehicles, by H. H. Koelle, *Army Ballistic Missile Agency, Redstone Arsenal, Rep.* DSP-TR-6-59, Dec. 1959, 27 pp.

Booster Design for a 20,000 lb. Satellite, by S. B. Kramer and R. A. Byers, *Space Aeron.*, vol. 31, June 1959, pp. 52–55.

Atlas, Carrier Rocket for Important Space Flight Projects, by D. E. Kölle, *Raketentechnik und Raumfahrtforschung*, vol. 3, no. 2, April 1959, pp. 50–52. (In German.)

The First Artificial Planetoid Mechta, by D. E. Kölle, *Raketentechnik und Raumfahrtforschung*, vol. 3, no. 2, April 1959, pp. 50–53. (In German.)

Satellite Vanguard II with Infrared Detectors, *Raketentechnik und Raumfahrtforschung*, vol. 3, no. 2, April 1959, pp. 55–56. (In German.)

Space Sound Juno II, by D. E. Kölle, *Raketentechnik und Raumfahrtforschung*, vol. 3, no. 2, April 1959, pp. 57–59. (In German.)

Designing an ICBM Nose-cone Liner, by Bernard H. Gerberg, ASTRONAUTICS, vol. 4, Sept. 1959, pp. 38–39, 97.

Launcher for Honest John, by Arnold A. Kester, *Ordnance*, vol. 43, May-June 1959, p. 1008.

Rocket Readiness, by J. W. Wiggins, *Ordnance*, vol. 43, May-June 1959, p. 1010.

The Explorers, by W. von Braun, *Astronautica Acta*, vol. 5, no. 2, 1959, pp. 126–143.

Lockheed X-17 Rocket Test Vehicle and Its Applications, by Ronald Smelt, ARS JOURNAL, vol. 29, Aug. 1959, pp. 565–572.

Guidance and Control

Some Considerations Concerning Magnetohydrodynamic Exhaust Control for Rocket Guidance, by Wulf B. Kunkel, *Space Tech. Labs., Inc., Phys. Res. Lab., TR*-59-0000-00608, Feb. 1959, 12 pp.

Requirements of Trajectory Corrective Impulses During the Approach Phase of an Interplanetary Mission, by Alan L. Friedlander and David P. Harry III, *NASA TN* D-255, Jan. 1960, 53 pp.

A Study of the Guidance of Space Vehicle Returning to a Braking Ellipse About the Earth, by Jack A. White, *NASA TN*-D-191, Jan. 1960, 65 pp.

Midcourse Guidance Problem in Satellite Interception, I, by Angelo J. Skalafuris and Donald H. Schiller, ARS JOURNAL, vol. 30, Jan. 1960, pp. 41–45.

Missile Orientation Errors in Command Guidance Systems, by Kenneth C. Mathews, ARS JOURNAL, vol. 30, Jan. 1960, pp. 46–49.

Steady-state Behavior of Extended Surfaces in Space, by J. W. Tatom, ARS JOURNAL, vol. 30, Jan. 1960, pp. 118–119.

Transients in Optimal Control Systems, by O. M. Kryzhanovski and V. M. Kuntsevich, ARS JOURNAL, vol. 30, Jan. 1960, pp. 86–92.

Contribution to the Theory of Inertial Damped Systems with Arbitrary Period, Invariant with Respect to Maneuver of the Object, by V. A. Bodner, V. P. Seleznov and V. E. Ovcharov, ARS JOURNAL, vol. 30, Jan. 1960, pp. 93–97.

Effect of Thrust Misalignment on Gyrostabilized Vehicles, by Russell P. Nagorski, ARS JOURNAL, vol. 30, Jan. 1960, pp. 128–129.

Terminal Guidance for Rendezvous, by Raymond S. Wiltshire, *Astron. Sci. Rev.*, vol. 1, Oct.-Dec. 1959, pp. 9–10.

Multifrequency Pulse Devices for Telecontrol, by F. A. Katkov, *Automation and Remote Control* (*trans. of Avtomatika i Telemekhanika*), vol. 20, Jan. 1959, pp. 49–55.

Auto-oscillations in a Single-loop Automatic Control System Containing Two Symmetric Relays, by Tu Syui-Yan' and Tei Lui-Vy, *Automation and Remote Control* (*trans. of Avtomatika i Telemekhanika*), vol. 20, Jan. 1959, pp. 83–88.

The Behavior of a Vibration Servo in an Electrical Autopilot, by I. N. Drutova, *Automation and Remote Control* (*trans. of Avtomatika i Telemekhanika*), vol. 20, Feb. 1959, pp. 113–121.

The Stability of a Nonlinear Control System with a Neutral Object, by L. I. Kupriyanova, *Automation and Remote Control* (*trans. of Avtomatika i Telemekhanika*), vol. 20, Feb. 1959, pp. 122–129.

Unified Twin-drive Servosystems, by P. F. Klubnikin, *Automation and Remote Control* (*trans. of Avtomatika i Telemekhanika*), vol. 20, Feb. 1959, pp. 154–168.

Choice of an Optimum Amplification Factor for a Self-aligning Control System, by I. I. Perel'man, *Automation and Remote Control* (*trans. of Avtomatika i Telemekhanika*), vol. 20, Feb. 1959, pp. 177–184.

Synthesis of the Control Unit of a Servosystem Optimum from the Point of View of Speed of Response, by Sung Chien,

Automation and Remote Control (*trans. of Avtomatika i Telemkhanika*), vol. 20, March 1959, pp. 261–275.

Concerning the Realization of Optimum Weighting Functions of Pulse Servosystems, by V. P. Perov, *Automation and Remote Control* (*trans. of Avtomatika i Telemekhanika*), vol. 20, March 1959, pp. 276–284.

A Fast Transistorized Magnetic Push-pull Amplifier for a Servo Drive, by V. S. Volodin, E. D. Larin, M. A. Rozenblat, and G. V. Subbotina, *Automation and Remote Control* (*trans. Avtomatika i Telemekhanika*), vol. 20, March 1959, pp. 307–313.

Choice of Characteristic for Nonlinear-rate Feedback in Position Servos, by B. N. Naumov, *Automation and Remote Control* (*trans. of Avtomatika i Telemekhanika*), vol. 20, March 1959, pp. 319 329.

Use of an Integral Square Estimate to Determine the Optimal Parameters of an Autopilot with Rate Feedback, by V. D. Matytsin and V. A. Ryapolov, *Automation and Remote Control* (*trans. of Avtomatika i Telemekhanika*), vol. 20, April 1959, pp. 403–408.

The Dynamics of a Vibration Loop in an Electrical Servo During Free Oscillations. by I. N. Krutova, *Automation and Remote Control* (*trans. of Avtomatika i Telemekhanika*), vol. 20, April 1959, pp. 409–420.

Compensation of a Continuous Automatic Control System by Means of a Delay-Element Filter, by Wang Sin-Min, *Automation and Remote Control* (*trans. of Avtomatika i Telemekhanika*), vol. 20, April 1959, pp. 453–464.

Stability of Nonlinear Automatic Control Systems, by O. I. Komarnitskaia, *PMM: Journal of Appl. Math. and Mech.* (*trans. of Prikladnaya Matematika i Mekhanika*), vol. 23, no. 3, 1959, pp. 716–729.

The Stability of Motion of a Gyroscope, by Chzhan Sy-In, *PMM: J. Appl. Math. and Mech.* (*trans. of Prikladnaya Matematika i Mekhanika*), vol. 23, no. 3, 1959, p. 860.

The Stability of Unperturbed Motion of a Gyroscope, by Chzhan Sy-In, *PMM: J. Appl. Math. and Mech.* (*trans. of Prikladnaya Matematika i Mekhanika*), vol. 23, no. 3, 1959, pp. 860–863.

Reliability in Inertial Systems, by A. M. Voutsas and W. T. Chow, *Interavia*, vol. 14, July 1959, p. 823.

LINS—Lightweight Inertial Navigation System, *Interavia*, vol. 14, July 1959, p. 824.

Comparison Study Between a Microwave Interferometer and an Electrical Contact System for Following the Motion of High-Speed Projectile, by Z. I. Slawsky, A. E. Siegel, L. T. Ho, H. J. Kopp and J. T. Vanderslice, *Rev. Sci. Instr.*, vol. 30, Aug. 1959, pp. 679–683.

MIG Platform Extends Inertial System Use (Design Digest), by Bernard Kovit, *Space/Aeron.*, vol. 32, July 1959, pp. 128–129.

Precision Gyroscopics—New Demands on an Old Art, by Roland E. Barnaby Jr., *Sperry Engineering Review*, vol. 12, June 1959, pp. 2–7.

Determining Lunar Mission Guidance Requirements, by Benjamin M. Rosen, *Sperry Engineering Review*, vol. 12, June 1959, pp. 27–33.

Trade-Off Considerations in the Design of Guidance Equipment for Space Flight, by Charles J. Mundo Jr., *Aero/Space Engng.*, vol. 18, June 1958, pp. 31–34.

The Radar Appearance of a Rotating Corner Reflector, by R. J. Davis, *Astronautica Acta*, vol. 5, no. 1, 1959, pp. 1–14.

Design Digest: Astro Compass Brings Space Navigation Closer, by Bernard Kovit, *Space/Aeron.*, vol. 31, June 1959, pp. 127–129.

The Performance of Inertial Components on an Unstabilized Base, by Henry F. Blazek, *ARS Preprint*, 775–59, April 30-May 1, 1959, 12 pp.

Tracking and Recovery of the Jupiter Rocket Nose, *Raketentechnik und Raumfahrtforschung*, vol. 3, no. 1, Jan.-March, 1959, pp. 25–26. (In German.)

Instrumentation and Communications

Theory of the Stagnation Point Langmuir Probe, by L. Talbot, *Univ. of Calif., Inst. Engng. Res., Tech. Rep.* HE-150-168, March 30, 1959, 26 pp. (*AFOSR-TN*-59-474; *ASTIA AD* 215,717.)

Commutators for Airbourne Multiplex Telemetering, by M. M. Kranzler, *Electronics*, vol. 32, July 3, 1959, pp. 46–47.

Six Rules for Evaluating CFVS Generators, by F. T. DeWolf, E. A. Erdely, E. E. Kolatorowicz and W. R. Miller, *Space/Aeron.*, vol. 32, July 1959, pp. 93–94, 96, 98, 102–103.

The Payoff of Missile Design: Elec-

RESEARCH SCIENTISTS

ARMOUR RESEARCH FOUNDATION has professionally challenging openings for high calibre research engineers and scientists to do theoretical and experimental research in the fields of:

Shock and Detonation Wave Phenomena
Hypersonic Flow
Rarefied Gas Phenomena
Transport Phenomena

The Foundation encourages original research and publication of papers. These positions offer stimulating associations with other leading scientists in these fields.

Applicants must have an M.S. or Ph.D. degree in Engineering or Science, and have experience in one or more of these areas. In addition to the many cultural opportunities in Chicago, we offer the advantage of being located on a university campus. We have an excellent benefit program which includes a liberal vacation policy of up to four weeks each year.

We invite you to send your resume to:

E. P. Bloch
ARMOUR RESEARCH FOUNDATION
of Illinois Institute of Technology
10 West 35th Street
Chicago 16, Illinois

SOUTHWEST
"Monoball"®
SELF-ALIGNING BEARINGS

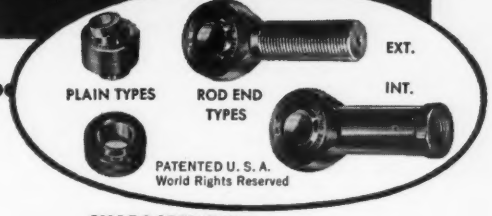

CHARACTERISTICS

	ANALYSIS	RECOMMENDED USE
1	Stainless Steel Ball and Race	For types operating under high temperature (800-1200 degrees F.).
2	Chrome Alloy Steel Ball and Race	For types operating under high radial ultimate loads (3000-893,000 lbs.).
3	Bronze Race and Chrome Steel Ball	For types operating under normal loads with minimum friction requirements.

Thousands in use. Backed by years of service life. Wide variety of Plain Types in bore sizes 3/16" to 6" Dia. Rod end types in similar size range with externally or internally threaded shanks. Our Engineers welcome an opportunity of studying individual requirements and prescribing a type or types which will serve under your demanding conditions. Southwest can design special types to fit individual specifications. As a result of thorough study of different operating conditions, various steel alloys have been used to meet specific needs. Write for Engineering Manual No. 551. Address Dept. ARS-60.

SOUTHWEST PRODUCTS CO.
1705 SO. MOUNTAIN AVE., MONROVIA, CALIFORNIA

tronic Fuzing, by William H. Doty, *Space/Aeron.*, vol. 32, July 1959, pp. 120–123.

A Device for Dynamical Measurements of Pressure, by P. Bassi, R. Cano, S. Focardi, C. Rubbia, A. Micheline and F. Saporetti, *Nuovo Cimento*, vol. II, no. 4, Feb. 16, 1959, pp. 589–594.

Reliable Optical Window for Cells Subjected to Widely Cycling Temperatures and Pressures, by W. C. Waggener and A. M. Tripp, *Rev. Sci. Instr.*, vol. 30, Aug. 1959, pp. 677–680.

Pressure Sensing Probes for Detecting Shock Waves, by Adolph B. Amster and Raymond L. Beauregard, *Rev. Sci. Instr.*, vol. 39, Oct. 1959, pp. 942–944.

High-sensitivity Pressure Gauge Coupling Two Spoon Gauges, by R. R. Monchamp, E. Bannister and F. A. Cotton, *Rev. Sci. Instr.*, vol. 39, Oct. 1959, pp. 945–946.

Basic Principles of Radar with Particular Reference to Aircraft and Missile Applications, by F. D. Boardman, *J. Roy. Aeron. Soc.*, vol. 63, Oct. 1959, pp. 581–596.

Photographic Pyrometry of Rocket Exhaust Jets, by Fredrick S. Simmons and Arthur G. DeBell, *Aircr. Engng.*, vol. 31, May 1959, pp. 144–149.

Low Frequency Vibrating Table for the Dynamic Calibration of Accelerometers, by L. Lemoine, *La Recherche Aéronautique*, no. 69, March-April 1959, pp. 27–37.

Liquid Nitrogen Liquid Level Controller, by Rodger L. Gamblin, Ernest Goldberg and Dane T. Seag, *Rev. of Sci. Instr.*, vol. 30, May 1959, pp. 371–373.

What the Designer Faces in Active Satellite Communications, *Space/Aeron.*, vol. 31, June 1959, pp. 122–125.

Representation and Analysis of Signals, Part I: The Use of Orthogonalized Exponentials, by W. H. Huggins, *Air Force Cambridge Res. Center, Tech. Rep. AFCRC TR* 57-357, Sept. 30, 1957, 76 pp.

Temperature Response of a Hot-wire Anemometer to Shock and Rarefaction Waves, by S. G. Datar, *Inst. Aerophys., Univ. Toronto, UTIA TN* 28, June 1959, 20 pp.

Study of a Phosphor Light Pulser, by M. R. Zatzick, *Air Force Cambridge Res. Center, Geophys. Res. Directorate, AFCRC-TR*-58-274, Sept. 1959, 19 pp.

Study of a Pulsed Logarithmic Photometer, by M. R. Zatzick, *Air Force Cambridge Res. Center, Geophys. Res. Directorate,* Sept. 1959, 25 pp.

General Model of a Semi-infinite Transmission Line with Mutual Inductance, by Richard H. Huddlestone, *Space Tech. Labs., Inc., Phys. Res. Lab., TR*-59-0000-00786, Oct. 1959, 16 pp.

Survey of Analog Cross-spectral Analyzers, by Lester J. Seltzer and Duane T. McRuer, *Wright Air Dev. Center, Tech. Rep.* 59-241, Oct.1959, 72 pp.

The Optimal Parameters for Noise Stability in a Telemetry System, by V. A. Kashirin, *Automation and Remote Control* (*trans. of Avtomatika i Telemekhanika*), vol. 20, Feb. 1959, pp. 216–225.

Noise Stability in Pulse-width and Pulse-time Telemetry Subject to Strong Fluctuation Noise, by N. V. Pozin, *Automation and Remote Control* (*trans. of Avtomatika i Telemekhanika*), vol. 20, Feb. 1959, pp. 227–235.

Investigation of the Characteristics of Pneumatic Jet Elements, by L. A. Zalmonzon and A. I. Semikova, *Automation and Remote Control* (*trans. of Avtomatika i Telemekhanika*), vol. 20, April 1959, pp. 431–448.

Strain Gauge with High Sensitivity Made of Semiconductor Material, *Aviation Week*, vol. 72, Feb. 1, 1960, pp. 74–75.

Sensitive Method for the Measurement of Small Rotations, by J. King and J. W. Gates, *J. Sci. Instr.*, vol. 36, Dec. 1959, pp. 507–508.

Simple Method for the Control of the Liquid Level in a Manometer, by J. G. Cunningham, *J. Sci. Instr.*, vol. 36, Dec. 1959, pp. 509.

Effect of Antenna Size on Gain, Bandwidth, and Efficiency, by Roger F. Harrington, *J. Res. Nat. Bur. Standards, D. Radio Propagation*, vol. 64D, no. 1, Jan.-Feb. 1960, pp. 1–12.

A Very-low-frequency Antenna for Investigating the Ionosphere with Horizontally Polarized Radio Waves, by R. S. Macmillan, W. V. T. Rusch and R. M. Golden, *J. Res., Nat. Bur. Standards, D. Radio Propagation*, vol. 64D, no. 1, Jan.-Feb. 1960, pp. 27–36.

Sampling Oscilloscope for Millimicrosecond Pulses at a 30-Mc Repetition Rate, by Arnold S. Farber, *Rev. Sci. Instr.*, vol. 31, Jan. 1960, pp. 15–17.

Precise Measurement of Density and Surface Tension at Temperatures up to 1000°C in One Apparatus, by George J. Janz and Max R. Lorenz, *Rev. Sci. Instr.*, vol. 31, Jan. 1960, pp. 18–22.

Fluctuation Noise in Frequency-modulated Radio Lines Transmitting a Multichannel Signal with Pulse-phase Modulation, by G. A. Malolepshii, *Radio Engng.* (*trans. of Radiotekhnika*), vol. 13, no. 7, Nov. 1959, pp. 12–30.

Some Problems of Magnetic Pulse Recording, by R. G. Ofengenden, *Radio Engng.* (*trans. of Radiotekhnika*), vol. 13, no. 7, Nov. 1959, pp. 95–102.

Atmospheric and Space Physics

Atmospheric Refraction of Infrared Radiation, by T. P. Condron, *Air Force Cambridge Research Center, Geophys. Res. Directorate, GRD Res. Notes* 23, *AFCRC-TN*-59-617, Oct. 1959, 15 pp.

Results of Scientific Investigations Made by Soviet Sputniks and Cosmic Rockets, by V. I. Krasovskii, ARS Journal, vol. 30, Jan. 1960, pp. 27–33.

Summary of Rawinsonde Measurements of Temperatures, Pressure Heights, and Winds Above 50,000 Feet Along a Flight-test Range in the Southwestern United States, by Terry J. Larson and Harold P. Washington, *NASA TN* D-192, Jan. 1960, 80 pp.

Interplanetary Gas, I: Hydrogen Radiation in the Night Sky, by John C. Brandt and Joseph W. Chamberlain, *Astrophys. J.*, vol. 130, no. 2, Sept. 1959, pp. 670–676.

Carbon Thermonuclear Reactions and the Formation of Heavy Elements, by A. G. W. Cameron, *Astrophys. J.*, vol. 130, no. 2, Sept. 1959, pp. 429–434.

Advances in Astron. Sci., vol. 4 (*Proc., 5th Annual Meet., American Astron. Soc., Nov. 1958*), Plenum Press, N. Y., 1959:

Some Aspects of the Electrical Properties of the Upper Atmosphere, by P. A. Goldberg, pp. 37–50.

On Gravitation, by Vjekoslav Gradecak, pp. 98–113.

Corpuscular Radiation Around the Earth, by James A. Van Allen, pp. 329–334.

Artificial Modification of the Earth's Radiation Belt, by S. Fred Singer, pp. 335–354.

Interplanetary Dust Distribution and Erosion Effects, by David B. Beard, *Advances in Astron. Sci., vol. 3* (*Proc. Western Regional Meet., American Astron. Soc., Aug. 1958*), Plenum Press, N. Y., 1958, *Paper* 23, 6 pp.

Advances in Astron. Sci., vol. 2 (*Proc., 4th Annual Meet., American Astron. Soc., Dec. 1957*), Plenum Press, N. Y., 1958:

A Recoverable Emulsion Package for Extra-atmospheric Study of Cosmic Rays, by Robert A. Webster, *Paper* 32, 12 pp.

Plastic Balloons for Planetary Research, by Malcolm D. Ross, *Paper* 42, 13 pp.

A Preliminary Determination of the Positions of Some First, Second, and Third Magnitude Stars on Mars' Celestial Sphere, by Frederick West Jr., *Paper* 44, 31 pp.

Meteor Trains, by Robert F. Hughes, *Smithsonian Contribs. to Astrophys.*, vol. 3, no. 8, 1959, pp. 79–94.

Exploring the Depth of the Surface Layer of the Moon from a Radar Space Observatory, by W. E. Fensler and K. M. Siegel, *Aero/Space Engng.*, vol. 18, Nov. 1959, pp. 38–41.

Should the Laws of Gravitation be Reconsidered? Part II: Experiments in Connection with the Abnormalities Noted in the Motion of the Paraconical Pendulum with an Anisotropic Support, by Maurice F. C. Allais, *Aero/Space Engng.*, vol. 18, Oct. 1959, pp. 51–55.

The Study of the Terrestrial Corpsucular Radiation and Cosmic Rays During the Flight of a Cosmic Rocket, by S. N. Vernov, A. E. Chudakov, P. V. Vakulov and Yu. I. Logachev, *Soviet Physics-Doklady*, vol. 4, no. 2, Oct. 1959, pp. 338–342.

A Nonlinear Vacuum Effect in Gravitation Theory, by N. V. Mitskevich, *Soviet Physics-JETP*, vol. 36(9), no. 4, Oct. 1959, pp. 859–861.

Atomospheric Diffusion, by A. S. Monin, *Soviet Physics-Uspekhi*, vol. 2(67), no. 1, Jan.-Feb. 1959, pp. 50–58.

Cosmic Ray Detection by Visual Scintillations, by Herman Yagoda, *Inst. Aeron. Sci., Rep.* 59–45, Jan. 1959, 8 pp.

Infra-red Spectroscopy from Balloons and the Possibility of Some Observations on the Biosphere, by David M. Gate, *Inst. Aeron. Sci., Rep.* 59–47, Jan. 1959 5 pp.

Vistas in Astronautics, vol. 2 (*2nd Annual Astron. Symposium*), Pergamon Press, N. Y., 1959, 318 pp:

How High the Moon, by C. C. Furnas, pp. 9–17.

Cosmic Debris of Interplanetary Space, by Maurice Dubin, pp. 39–45.

The Scientific and Engineering Exploration of the Moon, by John L. Barnes, pp. 255–260.

Dust on the Moon, by Thomas Gold, pp. 261–266.

On the Lunar Dust Layer, by Fred L. Whipple, pp. 267–272.

The Exploration of the Moon, by Gerald P. Kuiper, pp. 273–313.

High-energy Neutrons in Cosmic Rays, by G. N. Flerov, V. I. Kalashnikova, A. V. Podgurskaya, E. D. Vorob'ev and G. A. Stolyarov, *Soviet Physics-JETP*, vol. 36(9), no. 3, Sept. 1959, pp. 511–515.

Should the Laws of Gravitation Be Reconsidered? Part I: Abnormalities in the Motion of a Paraconical Pendulum on an Anisotropic Support, by Maurice F. C. Allais, *Aero/Space Engng., Rev.*, vol. 18, Sept. 1959, pp. 46–52.

The Hund Gravitational Equations and Geons, by Ll. G. Chambers, *Canadian J. Phys.*, vol. 37, Sept. 1959, pp. 1008–1016.

Sidereal Anisotropy of High Energy Cosmic Rays, by I. Escobar, V. N. Nerurkar and R. Weil, *Planetary and Space Sci.*, vol. 1, no. 3, Aug. 1959, pp. 155–160.

Nitric Oxide and Molecular Oxygen in the Earth's Upper Atmosphere, by A. S. Jursa, Y. Tanaka and F. LeBlanc, *Planetary and Space Sci.*, vol. 1, no. 3, Aug. 1959, pp. 161–172.

The Relation Between Lightning Discharges and Whistlers, by Harald Norinder and Edgar Knudsen, *Planetary and Space Sci.*, vol. 1, no. 3, Aug. 1959, pp. 173–183.

Strongly Absorbing Layers Below 50km, by Bengt Hultquist and Johannes Ortner, *Planetary and Space Sci.*, vol. 1, no. 3, Aug. 1959, pp. 193–204.

On Some Characteristics of the E_s-layer, by M. Bossolasco and A. Elena, *Planetary and Space Sci.*, vol. 1, no. 3, Aug. 1959, pp. 205–212.

The Thermal Radiation of the Moon at 1420 Mc/s, by P. G. Mezger and H. Strassl, *Planetary and Space Sci.*, vol. 1, no. 3, Aug. 1959, pp. 213–226.

Artificial Electron Clouds, I: Summary Report on the Creation of Artificial Electron Clouds in the Upper Atmosphere, by F. F. Marmo, L. M. Aschenbrand, and J. Pressman, *Planetary and Space Sci.*, vol. 1, no. 3, Aug. 1959, pp. 227–237.

Determination of Upper-atmosphere Air Density and Scale Height from Satellite Observations, by G. V. Groves, *Proc. Roy. Soc., London*, vol. A 252, Aug. 25, 1959, pp. 16–27.

Determination of Upper-atmosphere Air-density Profile from Satellite Observations, by G. V. Groves, *Proc. Roy. Soc., London*, vol. A 252, Aug. 25, 1959, pp. 28–36.

The Earth's Simple Shadow-Effect on Cosmic Radiation, by J. E. Kasper, *Nuovo Cimento Supplemento*, no. 1, 1959, pp. 1–7.

Penumbra and Simple Shadow Cone of Cosmic Radiation, by M. Schwartz, *Nuovo Cimento Supplemento*, no. 1, 1959, pp. 27–35.

Propagation of Radio Waves along an Inhomogeneous Surface, by E. L. Feinberg, *Nuovo Cimento Supplemento*, no. 1, 1959, pp. 60–66.

Polarization of the Red-oxygen Auroral Line, by R. A. Duncan, *Planetary and Space Sci.*, vol. 1, no. 2, April 1959, pp. 112–114.

Observations of the Russian Satellites and the Structure of the Outer Terrestrial Atmosphere, by H. K. Paetzold, *Planetary and Space Sci.*, vol. 1, no. 2, April 1959, pp. 115–124.

Ambipolar Diffusion of a Meteor Train and its Relation with Height, by E. L. Murray, *Planetary and Space Sci.*, vol. 1, no. 2, April 1959, pp. 125–129.

Absorption and Electron Distribution in the F_2 Layer Determined from Measurements of Transmitted Radio Signals from Earth Satellites, by A. N. Kazantsev, *Planetary and Space Sci.*, vol. 1, no. 2, April 1959, pp. 130–135.

Derivation and Analysis of Atmospheric Density from Observations of Satellite 1958 Epsilon, by G. F. Schilling and C. A. Whitney, *Planetary and Space Sci.*, vol. 1, no. 2, April 1959, pp. 136–145.

Some Remarks on the Nature and Origin of Noctilucent Cloud Particles, by Drian Deirmendjian and E. H. Vestine, *Planetary and Space Sci.*, vol. 1, no. 2, April 1959, pp. 146–153.

Trends in Upper Atmosphere Research, by R. D. Cadle, *SRI J.*, vol. 3, 2nd Quarter, 1959, pp. 41–45.

Rocketsondes for High-altitude Soundings, by I. G. Poppoff, *SRI J.*, vol. 3, 2nd Quarter, 1959, pp. 56–61.

Highly Directional Detector for Cosmic Ray Particles, by G. W. Hutchinson, *Nuovo Cimento*, vol. II, no. 3, Feb. 1, 1959, pp. 377–382.

An Experimental Analysis of Two Large Cosmic Ray Jets, by F. A. Brisbout and C. B. A. McCusker, *Nuovo Cimento*, vol. 11, no. 4, Feb. 16, 1959, pp. 484–490.

Gravitational Motion and Radiation I, by A. Peres, *Nuovo Cimento*, vol. II, no. 5, March 1, 1959, pp. 617–627.

Gravitational Motion and Radiation II, by A. Peres, *Nuovo Cimento*, vol. II, no. 5, March 1, 1959, pp. 644–655.

An Astronomical Telescope in Space, by R. J. Davis, F. L. Whipple and C. A. Whitney, *Astron. Sci. Rev.*, vol. 1, no. 1, Jan.–March, 1959, pp. 9–12, 14.

On the Existence of a Strong Magneto-Ionic Effect Topside of the F Maximum of the Kenelly-heaviside Layer, by P. R. Arendt, *J. Appl. Phys.* vol. 30, no. 5, May 1959, pp. 793–794.

Near Infrared Solar Radiation Measurements by Balloon to an Altitude of 100,000 Feet, by D. M. Gates, D. G. Murcray, C. C. Shaw and R. Herbold, *J. Optical Soc. Amer.*, vol. 48, no. 12, Dec. 1958, pp. 1010–1017.

Scientific Problems in Cislunar Space and Their Exploration with Rocket Vehicles, by S. F. Singer, *Astronautica Acta*, vol. 5, no. 2, 1959, pp. 116–125.

Techniques of Analyzing Terrestrial Radio and Optical Observations of Earth Satellites, by R. H. Merson, *Astronautica Acta*, vol. 5, no. 1, 1959, pp. 26–39.

The Physical Nature of the Surface of the Moon, by Gilbert Fielder, *Brit. Interplanet. Soc., J.*, vol. 17, March-April 1959, pp. 57–58.

The Detection of Planets at Interstellar Distances, by M. H. Briggs, *Brit. Interplanet. Soc., J.*, vol. 17, March-April 1959, pp. 59–60.

Size of Irregularities in the E region of the Ionosphere, by M. Srirama Rao, *Canadian J. Phys.*, vol. 37, May 1959, pp. 557–568.

Transient Decreases in Cosmic Ray Intensity During the Period October 1956 to January 1958, by A. G. Fenton, K. G. McCracken, D. C. Rose and B. G. Wilson, *Canadian J. Phys.*, vol. 27, May 1959, pp. 569–578.

Further Observations from the Russian Satellites, by H. K. Paetzold, *Raketentechnik und Raumfahrtforschung*, vol. 3, no. 2, April 1959, pp. 45–49. (In German.)

Balloon Astronomy, by Martin and Barbara Schwarzchild, *Scientific American*, vol. 200, May 1959, pp. 52–59.

Artificial Satellites and Relativity, by V. L. Ginzburg, *Scientific American*, vol. 200, May 1959, pp. 149–160.

Rocket Astronomy, by Herbert Friedman, *Scientific American*, vol. 200, June 1959, pp. 52–59.

Artificial Modification of the Earth's Radiation Belt, by S. F. Singer, *J. Astron. Sci.*, vol. 6, no. 1, Spring 1959, pp. 1–10.

The Sun and the Upper Atmosphere, by Herbert Friedman, ASTRONAUTICS, vol. 4, July 1959, pp. 20–22, 55–56.

Density and Temperature of the Upper Atmosphere, by Robert Jastrow, ASTRONAUTICS, vol. 4, July 1959, pp. 24–25.

13 Noted Scientists Present A SPACE AGE SYMPOSIUM...

Robert Jastrow
Fred L. Whipple
Thomas Gold
Eugene Parker
James A. Van Allen
N. C. Christofilos
Homer E. Newell
Gerard P. Kuiper
Harold C. Urey
G. de Vaucouleurs
Herbert Friedman
Leo Goldberg
J. W. Townsend, Jr.

THE EXPLORATION OF SPACE

edited by Robert Jastrow

illustrated, $5.50

Van Allen discusses the geomagnetically trapped corpuscular radiation; Christofilos reports on "The Argus Experiment;" de Vaucouleurs, on Mars and Venus; Goldberg, on astronomy from satellites and space vehicles; Whipple, on solid particles in the solar system. Other vital topics include rocket astronomy, plasma and magnetic fields in the solar system, the U.S. space-exploration program, and the U.S.S.R. report of an active volcano on the moon.

Order Today From Your Nearest Bookstore Or Write Dept. ARS-1.

The Macmillan Company

60 FIFTH AVENUE, NEW YORK 11, N.Y.

Princeton
Aeronautical
Paperbacks

New paperbacks—published in response to a growing demand for the most essential sections of the HIGH SPEED AERODYNAMIC AND JET PROPULSION series—bring to the student and research engineer directly useful information, at prices they can easily afford.

1. LIQUID PROPELLANT ROCKETS
David Altman, James M. Carter, S. S. Penner, Martin Summerfield. 196 pp. $2.95

2. SOLID PROPELLANT ROCKETS
Clayton Huggett, C. E. Bartley and Mark M. Mills. 176 pp. $2.45

3. GASDYNAMIC DISCONTINUITIES
Wallace D. Hayes. 76 pp. $1.45

4. SMALL PERTURBATION THEORY
W. R. Sears. 72 pp. $1.45

5. HIGHER APPROXIMATIONS IN AERODYNAMIC THEORY
M. J. Lighthill. 156 pp. $1.95

6. HIGH SPEED WING THEORY
Robert T. Jones and Doris Cohen. 248 pp. $2.95

At your bookstore
Princeton University Press
Princeton, New Jersey

Approach to the Ionosphere, by Warren W. Berning, ASTRONAUTICS, vol. 4, July 1959, pp. 26–27, 116–117.

Measuring Upper-air Structure, by Leslie M. Jones, ASTRONAUTICS, vol. 4, July 1959, pp. 28–29, 50.

Positive Ions in the Ionosphere, by Julian C. Holmes and Charles Y. Johnson, ASTRONAUTICS, vol. 4, July 1959, pp. 30–31.

Pioneer's Radiation-detection Instrument, by Conrad Josias, ASTRONAUTICS, vol. 4, July 1959, pp. 32–33, 114–115.

Mechta Radiation Data, by S. N. Vernov, A. Ye. Chudakov, P. V. Vakulov and Yu. I. Logachev, ASTRONAUTICS, vol. 4, July 1959, pp. 23, 84.

Artificial Modification of the Upper Atmosphere, by Murray Zelikoff, ASTRONAUTICS, vol. 4, July 1959, pp. 46, 118–119.

Far Ultra-violet Radiation in the Night Sky, by J. E. Kupperian Jr., E. T. Byram, T. A. Chubb and H. Friedman, *Planetary and Space Sci.*, vol. 1, no. 1, Jan. 1959, pp. 3–6.

Spectroscopic Study of the Afterglows of N_2 and (N_2 + O_2) in the Vacuum Region, by Y. Tanaka, A. S. Jursa, F. J. Leblanc and E. C. Y. Inn, *Planetary and Space Sci.*, vol. 1, no. 1, Jan. 1959, pp. 7–13.

Energy Sources of the Upper Atmosphere, by V. I. Krassovsky, *Planetary and Space Sci.*, vol. 1, no. 1, Jan. 1959, pp. 14–19.

An Interim Atmosphere Derived From Rocket and Satellite Data, by I. Harris and R. Jastrow, *Planetary and Space Sci.*, vol. 1, no. 1, Jan. 1959, pp. 20–26.

Micrometeorite Measurements from 1958 Alpha and Gamma Satellites, by Edward R. Manring, *Planetary and Space Sci.*, vol. 1, no. 1, Jan. 1959, pp. 27–31.

The Airglow of Venus, by Gordon Newkirk Jr., *Planetary and Space Sci.*, vol. 1, no. 1, Jan. 1959, pp. 32–36.

A Short Duration Afterglow of Nitrogen, Survey of Afterglows, by O. Oldenberg, *Planetary and Space Sci.*, vol. 1, no. 1, Jan. 1959, pp. 40–42.

Decay of Spin in Sputnik I, by J. W. Warwick, *Planetary and Space Sci.*, vol. 1, no. 1, Jan. 1959, pp. 43–49.

Absorption Refraction and Scintillation Measurements at 4700 Mc/s with a Travelling-wave Tube Radiometer, by John P. Castelli, Jules Aarons, Carl Ferioli and Joseph Casey, *Planetary and Space Sci.*, vol. 1, no. 1, Jan. 1959, pp. 50–56.

Hydrogen Emission and Two Types of Auroral Spectra, by G. I. Galperin, *Planetary and Space Sci.*, vol. 1, no. 1, Jan. 1959, pp. 57–62.

On Hydrogen Emission in the Night Glow, by I. S. Shklovsky, *Planetary and Space Sci.*, vol. 1, no. 1, Jan. 1959, pp. 63–65.

Current Systems in the Vestigial Geomagnetic Field: Explorer VI, by C. P. Sonett, E. J. Smith, D. L. Judge, and P. J. Coleman Jr., *Phys. Rev. Letters*, vol. 4, Feb. 1960, pp. 161–162.

Recent Trends in the Theory of the Ionosphere, by J. A. Ratcliffe, *Proc. Phys. Soc., London*, vol. 75, Jan. 1960, pp. 2–3.

Excitation of O_2 Atmospheric Bands in the Aurora, by L. Wallace and J. W. Chamberlain, *Planetary and Space Sci.*, vol. 2, no. 1, Oct. 1959, pp. 60–70.

On the Polarization of the Oxygen Red Line in Aurorae, by J. W. Chamberlain, *Planetary and Space Sci.*, vol. 2, no. 1, Oct. 1959, pp. 73–74.

Micrometeorite Impacts to an Altitude of 135 km, by J. F. Lovering, *Planetary and Space Sci.*, vol. 2, no. 1, Oct. 1959, p. 75.

Relative Intensities of Na Lines in the Emission of Sodium Ejected from Rockets, by A. and E. Vassey, *Planetary and Space Sci.*, vol. 2, no. 1, Oct. 1959, pp. 71–72.

The Distribution of Helium-3 in the Grant Meteorite and a Determination of the Original Mass, by E. L. Fireman, *Planetary and Space Sci.*, vol. 1, no. 1, Jan. 1959, pp. 66–70.

A Study of Winds Between 80 and 100 km in Medium Latitudes, by W. G. Elford, *Planetary and Space Sci.*, vol. 1, no. 2, April 1959, pp. 94–101.

An Example of Heavy Absorption in the VHF-Band in the Arctic Ionosphere, by L. Harang and J. Tröim, *Planetary and Space Sci.*, vol. 1, no. 2, April 1959, pp. 102–104.

Cerenkov Radiation in the Atmosphere, by J. V. Jelley, *Planetary and Space Sci.*, vol. 1, no. 2, April 1959, pp. 105–111.

Human Factors and Bioastronautics

Vistas in Astronautics, vol. 2 (2nd Annual Astron. Symposium), Pergamon Press, N. Y., 1959, 318 pp:

The Importance of High Vacuum in Space Environment Simulation, by R. A. Roche, pp. 22–27.

Experiments from a Lunar Vehicle, by M. H. Johnson, pp. 28–31.

Space Flight Simulators, by Otto Schveller, pp. 46–59.

Project Skyball: A Proposed Primary Satellite Trainer System for Space Flight Operation, by Norman V. Petersen, *Advances in Astron. Sci., vol. 2 (Proc., 4th Annual Meet., American Astron. Soc., Dec. 1957)*, Plenum Press, N. Y., 1958, *Paper* 43, 19 pp.

Man's Operational Environment in Space, by George W. Hoover, *Advances in Astron. Sci., vol. 3 (Proc., Western Regional Meet., American Astron. Soc., Aug. 1958)*, Plenum Press, N. Y., 1958, *Paper* 4, pp. 1–12.

Environmental Testing of Spacemen, by M. Traite, W. Welkowitz, J. Kilduff and G. Purpuro, *Electronics*, vol. 32, Oct. 16, 1959, pp. 65–71.

Rocket Powered Capsule for Aeromedical Research and Space Crew Indoctrination, by N. V. Petersen, *Inst. Aeron. Sci., Paper* 59–126, June 1959, 20 pp.

The Pilot's Role in Space Flight, by Charles B. Westbrook, *Aero/Space Engng.*, vol. 18, Nov. 1959, pp. 51–54.

Project MIA (Mouse-in-Able), Experiments on Physiological Response to Space-Flight, by F. L. van der Wal and V. D. Young, ARS JOURNAL, vol. 29, Oct. 1959, pp. 716–720.

Law, Sociology and Education

An Aeronautical Engineering Educator's Viewpoint on the Challenge of Space Technology to Aeronautical Engineering Education, by G. L. Von Eschen, *Inst. Aeron. Sci., Rep.* 59–74, Jan. 1959, 10 pp.

International Control of Outer Space, Hearings before the *Committee on Science and Astronautics, 86th U.S. Congress, 1st Session, House* (no.7), March 5, 6 and 11, 1959, 108 pp.

Satellites for World Communication, Hearings before the *Committee on Science and Astronautics, 86th U.S. Congress, 1st Session, House* (no. 9), March 3 and 4, 1959, 122 pp.

Index to Advertisers

AEROJET-GENERAL CORP. . . . . Back cover
D'Arcy Advertising Co., Los Angeles, Calif.

ALLIED CHEMICAL CORP., GENERAL CHEMICAL DIV. . . 521
Kastor, Hilton, Chesley, Clifford & Atherton, Inc., New York, N. Y.

ARMOUR RESEARCH FOUNDATION OF ILLINOIS INSTITUTE OF TECHNOLOGY 585

CONVAIR, A DIV. OF GENERAL DYNAMICS CORP. . . . Third Cover
Lennen & Newell, Inc., Beverley Hills, Calif.

EXCELCO DEVELOPMENTS 520
Melvin F. Hall Advertising Agency, Inc., Buffalo, N. Y.

FOOD MACHINERY & CHEMICAL CORP., CHLOR-ALKALI DIV. 522
James J. McMahon, Inc., New York, N. Y.

LOS ALAMOS SCIENTIFIC LABORATORY 519
Ward Hicks Advertising, Albuquerque, N. Mex.

THE MACMILLAN CO. 587
J. M. Hickerson, Inc., New York, N. Y.

THE MARTIN CO., DENVER DIV. . . . . Second Cover
E. M. Halvorson Co., Denver, Colo.

PRINCETON UNIVERSITY PRESS 587
Franklin Spier, Inc., New York, N. Y.

SOUTHWEST PRODUCTS CO. . . . 585
O. K. Fagan Advertising Agency, Los Angeles, Calif.

UNITED AIRCRAFT CORP., RESEARCH LABORATORIES 517
B. E. Burrell & Associates, Hartford, Conn.

JOHN WILEY & SONS, INC. . . . 518
Needham & Grohmann Inc., New York, N. Y.